PLEASE RETURN TO EDEZ
SEAFORD

Saturn

D5-15796-1

SATURN V AEROTHERMODYNAMICS FLIGHT EVALUATION SUMMARY - AS-501 THROUGH AS-503

JUNE 19, 1969

THE BOEING COMPANY · AEROSPACE GROUP
SOUTHEAST DIVISION

DOCUMENT NO. D5-15796-1

TITLE SATURN V AEROTHERMODYNAMICS FLIGHT EVALUATION SUMMARY - AS-501 THROUGH AS-503

MODEL NO. SATURN V. CONTRACT NO. NAS8-5608, Paragraph 8.1.6, Schedule II, Part IIA, Exhibit CC, DRL 049, Line Item 100

Prepared by: AEROPHYSICS GROUP

June 19, 1969

S. C. KRAUSSE, MANAGER
FLIGHT SYSTEMS ANALYSIS

ISSUE NO. ISSUED TO

THE BOEING COMPANY SPACE DIVISION LAUNCH SYSTEMS BRANCH

REVISIONS

REV. SYM	DESCRIPTION	DATE	APPROVED

ABSTRACT AND LIST OF KEY WORDS

A summary of measured Aerothermodynamic flight environments are presented for the first three flights of the Saturn V (AS-501 through AS-503). Flight data are compared to show the relative variation from flight to flight and also compared with predicted environments. The environments include vehicle internal compartment pressures, acoustics, base pressures, axial force characteristics, aerodynamic heating, base heating and stage separation heating and pressures. The S-IC stage, S-II stage, S-IVB stage, and Instrument Unit environments are analyzed.

Flight Evaluation
Aerothermodynamics
Pressure
Aerodynamic Heating
Base Heating
Acoustics
Stage Separation Heating

CONTENTS

ILLUSTRATIONS

ILLUSTRATIONS (Continued)

ILLUSTRATIONS (Continued)

ILLUSTRATIONS (Continued)

ILLUSTRATIONS (Continued)

ILLUSTRATIONS (Continued)

ILLUSTRATIONS (Continued)

ILLUSTRATIONS (Continued)

TABLES

REFERENCES

1. Boeing Document D5-15556-1, "Aerothermodynamic Flight Evaluation Saturn V, AS-501," January 30, 1968.

2. Boeing Document D5-15556-2, "Aerothermodynamic Flight Evaluation Saturn V, AS-502," July 3, 1968.

3. Boeing Document D5-15556-3, "Aerothermodynamic Flight Evaluation Saturn V, AS-503," March 6, 1969.

4. MSFC Document MPR-SAT-FE-68-1, "Saturn V Launch Vehicle Flight Evaluation Report - AS-501, Apollo 4 Mission," January 15, 1968.

5. MSFC Document MPR-SAT-FE-68-3, "Saturn V Launch Vehicle Flight Evaluation Report - AS-502, Apollo 6 Mission," June 25, 1968.

6. MSFC Document MPR-SAT-FE-69-1, "Saturn V Launch Vehicle Flight Evaluation Report - AS-503, Apollo 8 Mission," February 20, 1969.

7. North American Rockwell Document SD 67-1136, "S-II-1 Flight Final Test Report," January 16, 1968.

8. North American Rockwell Document SD 68-381, "S-II-2 Flight Final Test Report," June 18, 1968.

9. North American Rockwell Document SD 69-76, "S-II-3 Flight Final Test Report," March 5, 1969.

SOURCE DATA PAGE

The following listed government-furnished documentation was used in the preparation of this document.

Exhibit FF Line Item Number	GFD Title	Date of Issue	Revision Date
R-AERO-P-27	S-IC, S-II, S-IVB, IU Post Flight Data Analysis Reports Covering Aerothermodynamics Data	3/21/69 (L + 90)	

NOMENCLATURE

A_{ref}	Reference area, $\pi D_{ref}^2/4$
A_v	Compartment vent area
C_{A_F}	Forebody axial force coefficient
D_{ref}	Reference diameter (10.06 meters)
DB	Decibel
F_A	Axial force
F_{A_b}	Base axial force
F_{A_f}	Forebody axial force
HZ	Hertz
M_∞	Freestream Mach number
P	Static pressure
P_b	Base pressure
P_{int}	Compartment pressure
P_∞	Ambient pressure
q	Dynamic pressure, $\frac{\gamma}{2} P_\infty M_\infty^2$
Re	Reynolds number
α_p	Pitch angle of attack
α_y	Yaw angle of attack

SECTION 1

INTRODUCTION

Apollo 4, 6, and 8 missions were launched successfully at 0700 hours EST November 9, 1967; April 4, 1968; and December 21, 1968, respectively, from Cape Kennedy, Florida. These missions were the first three flights of the Saturn V launch vehicle and the primary objectives were qualification of the vehicle and spacecraft for the Lunar Landing Mission. Apollo 8 was the first manned Saturn V Apollo flight.

The Saturn V flight measurements of the aerothermodynamic environments, which includes aerodynamics, vehicle acoustics, base heating, stage separation, and aerodynamic heating environments are analyzed in this report. Evaluation of the flight data following individual flights (reported in References 1 through 9) showed that flight environments were generally below design levels. For this reason, the content of this report concentrates on comparisons of AS-501, AS-502, and AS-503 flight data and post-flight predictions. The predictions were made using previous flight data, wind tunnel test data, and theoretical and analytical methods.

Changes in vehicle configuration and flight operating procedures from flight-to-flight affected the aerothermodynamic environments. Significant changes on the S-IC stage include removal of the base region flow deflectors from the AS-502 and AS-503 vehicles, 2 degree outboard cant on the AS-503 F-1 control engines, and earlier AS-503 inboard engine cutoff. Changes on the S-II stage include removal of four of the eight S-II ullage motors after AS-501 flight, variations in times of J-2 programmed mixture ratio (PMR) step-down, J-2 engines 2 and 3 early shutdown on AS-502, and AS-502 longer burn time. Only moderate variations in flight trajectories were experienced. These changes and variations and their effects on the environments are discussed in the following sections.

(THIS PAGE INTENTIONALLY LEFT BLANK)

SECTION 2

AERODYNAMICS

2.0 INTRODUCTION

This section contains a summary of the aerodynamic flight evaluation of the first three Apollo/Saturn V missions. Presented in this section are the flight trajectories, axial force characteristics, base pressure environments, and vehicle compartment internal pressure environments. The vehicle aerodynamic static stability characteristics are not presented. The first three missions flew wind biased trajectories resulting in low angles of attack and engine deflections. This rendered static stability calculations very unreliable.

2.1 VEHICLE PRESSURE INSTRUMENTATION

The instrumentation utilized in the aerodynamics analysis consists of pressure transducers in the base region and various compartments along the vehicle. In the S-IC base region there were eight static pressure measurements and two differential pressure measurements on the heat shield. The locations of these instruments are described in Table 2-I and shown graphically in Figure 2-1. There were two internal pressure measurements in each of the S-IC aft, intertank, and forward skirt compartments. The S-IVB forward skirt compartment and the S-II/S-IVB interstage compartment each had one measurement. The locations of these instruments are described in Table 2-II and illustrated in Figure 2-2.

2.2 TRAJECTORY AERODYNAMIC PARAMETERS

The dynamic pressure, atmospheric pressure, altitude, and Mach number are shown as a function of flight time for the three flights in Figure 2-3. There were no significant deviations in these parameters between flights. However, time of maximum dynamic pressure was slightly different. On AS-501 maximum dynamic pressure occurred at 78 seconds, on AS-502 at 75 seconds, and on AS-503 at 79 seconds. The vehicle Reynolds number based on the first stage reference diameter, is shown in Figure 2-4. The maximum Reynolds number and flight time at which it occurred varied on all three flights. On AS-501 the maximum Reynolds number was 113.9 million and occurred 57.5 seconds into flight, on AS-502 maximum Reynolds number was 118.7 million and occurred at 67.5 seconds, and on AS-503 maximum was 113.6 million at 71 seconds into flight.

The pitch and yaw angles of attack that the vehicle encountered during first stage boost are shown in Figures 2-5 and 2-6, respectively. The differences between flights present no problem since the magnitude of the angle is small. The higher values at times less than 40 seconds are due to winds at launch. These angles of attack were calculated using Q-Ball differential pressure data.

2.3 AXIAL FORCE CHARACTERISTICS

The vehicle base axial force characteristics are shown in two parts in Figure 2-7. Experience with data from the first three flights has proven that S-IC base pressures, from which base axial force is obtained, are more a function of altitude than Mach number. This is true over a major portion of typical Saturn V S-IC boost trajectories. During liftoff and up to approximately one kilometer altitude the base pressures remain a function of range time. This is shown in the first part of Figure 2-7 and is intended for use in liftoff studies. The second part of Figure 2-7 contains an average base differential pressure which can be used to calculate base axial force throughout the remainder of S-IC boost. The data show fair agreement. The small differences that do exist are attributed to a combination of the outboard engine cant on AS-503 (2 degrees after 20 seconds) and base flow deflectors on AS-501. The S-IC base flow deflectors were removed after the AS-501 flight.

The predicted forebody axial force coefficients for each flight are shown as a function of Mach number in Figure 2-8 and are based on wind tunnel data. The AS-501 coefficient is greater because of the S-IC stage base flow deflectors.

The total aerodynamic axial force (F_A) is the sum of the forces calculated from the base differential pressure and the forebody coefficient.

$$F_A = F_{A_b} + F_{A_f}$$

where $$F_{A_b} = -0.798\ (P_b - P_\infty)\ A_{ref}$$

and $$F_{A_f} = C_{A_f}\ A_{ref}\ q$$

2.4 S-IC BASE PRESSURE ENVIRONMENT

S-IC base pressure differentials (base pressure minus ambient pressure) are shown in Figure 2-9 as a function of altitude. In general, good agreement exists between flights. The differences in magnitude between AS-501 and the other flights is attributed to the base flow deflectors being flown on AS-501.

2.5 VEHICLE COMPARTMENT INTERNAL PRESSURE ENVIRONMENT

A summary of the vehicle compartment internal pressure histories is presented in the following paragraphs. Pressure differentials are presented for the S-IC aft compartment, the S-IC intertank compartment, the S-IC forward skirt compartment, the S-IC shroud compartment, the S-II/S-IVB interstage compartment, and the S-IVB forward skirt compartment.

2.5.1 S-IC Compartment Pressure History

The S-IC aft compartment internal pressure differential is shown in Figure 2-10 as a function of range time and altitude. Inflight venting of the S-IC compartments was accomplished by a series of vent ports located in the interstage and intertank areas. The aft compartment is vented into the shroud base by four ducts which are located in the shrouds. The AS-502 compartment pressures are less than AS-501 throughout first stage flight due to the removal of the base flow deflectors after AS-501 flight. The AS-503 data are less than AS-502 throughout most of the first stage flight. This probably results from the removal of the F-1 engine fuel line boots on AS-503.

The S-IC intertank and forward skirt pressure differentials are shown in Figures 2-11 and 2-12, respectively. Data agreement between the flights is good. The S-IC intertank and forward skirt pressure differentials show a characteristic drop associated with the vehicle passing through Mach 1.0 between 60 and 62 seconds for all three flights.

A typical S-IC shroud compartment pressure differential is shown in Figure 2-13. There are no significant deviations in the data between flights. This compartment vents into the shroud base through leakage area only.

2.5.2 S-II and S-IVB Compartment Pressure Histories

Pressure differentials for the S-II/S-IVB interstage and S-IVB forward skirt compartments are shown in Figure 2-14. Inflight venting of the S-II/S-IVB interstage compartment and S-IVB forward skirt compartment was accomplished by a series of vent ports located around the vehicle in these compartments. The comparison of the S-II/S-IVB interstage compartment data is good for all three flights. The AS-502 and AS-503 S-IVB forward skirt compartment pressures were higher than those experienced during AS-501 flight as a result of a decrease in the compartment vent area. The venting area of 0.129 square meters (200 square inches) on AS-501 was decreased to 0.097 square meters (150 square inches) on subsequent flights.

TABLE 2-I. S-IC BASE HEAT SHIELD PRESSURE INSTRUMENTATION

MEASUREMENT NUMBER	INSTRUMENT TYPE	RANGE N/cm^2	LOCATION
D0035-106	Static Pressure	0-13.79	Station 112, 166 Inch Radius, Position II
D0036-106*	Static Pressure	0-13.79	Station 112, 120 Inch Radius, Position II
D0037-106	Static Pressure	0-13.79	Station 112, 91 Inch Radius, Fin C Centerline
D0038-106	Static Pressure	0-13.79	Station 112, 220 Inch Radius, 80 Inches from Fin B Centerline toward Position II
D0042-106	Static Pressure	0-13.79	Station 112, 260 Inch Radius, 40° from Position II toward Fin B Centerline
D0043-106	Static Pressure	0-13.79	Station 112, 80 Inch Radius, Position II
D0044-106	Static Pressure	0-13.79	Station 112, 150 Inch Radius, 25° from Fin A Centerline toward Position II
D0045-106	Static Pressure	0-13.79	Station 112, 80 Inch Radius, 25° from Fin A Centerline toward Position II
D0046-106	Differential Pressure	± 2.07	Station 112, 120 Inch Radius, Position IV
D0047-106	Differential Pressure	± 2.07	Station 112, 91 Inch Radius, Fin D Centerline

* Instrument not on AS-503

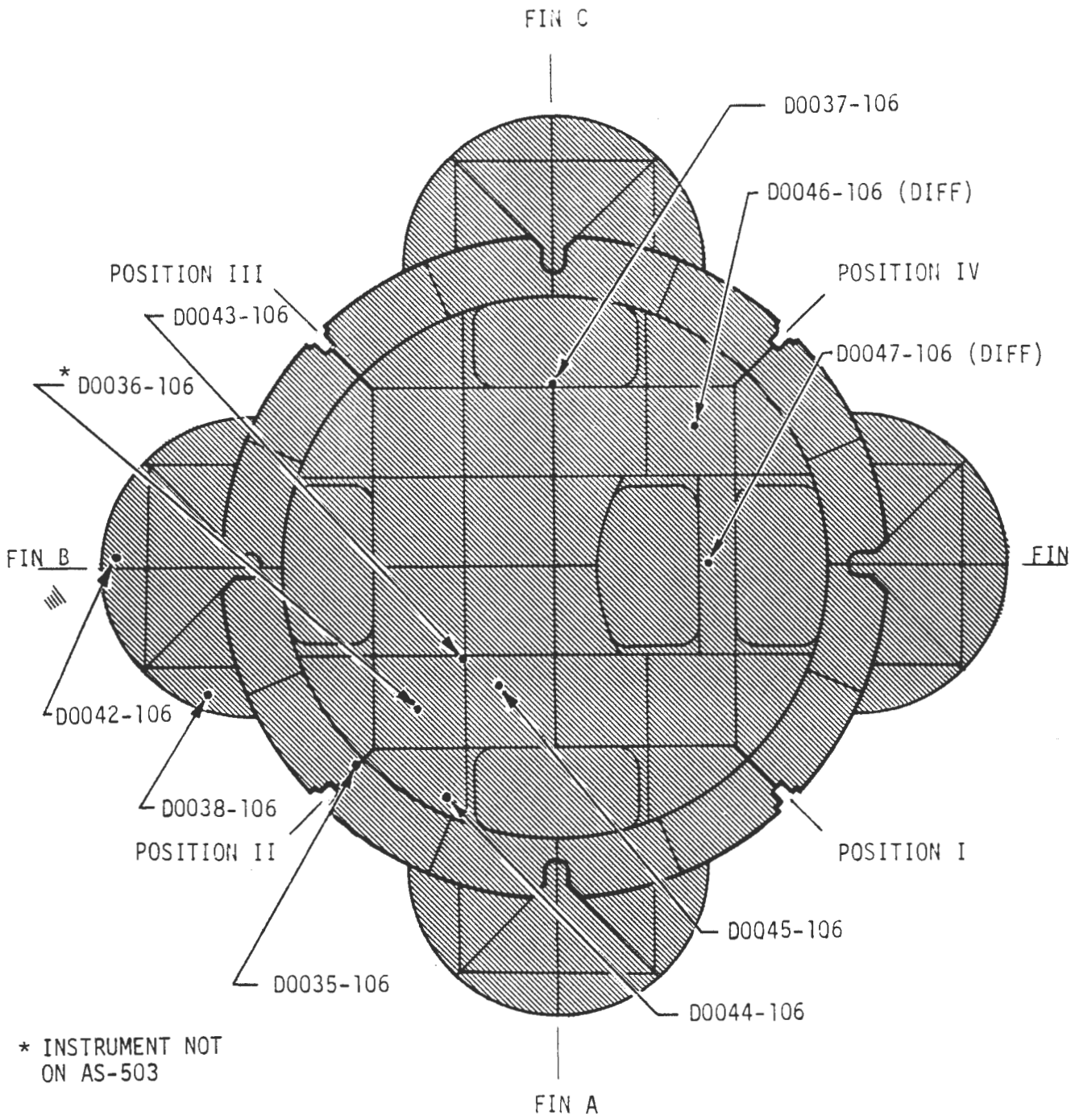

FIGURE 2-1. S-IC BASE PRESSURE INSTRUMENTATION

TABLE 2-II. SATURN V COMPARTMENT INTERNAL PRESSURE INSTRUMENTATION

MEASUREMENT NUMBER	INSTRUMENT TYPE	RANGE N/cm^2	LOCATION
D0081-115	Static Pressure	0-13.79	S-IC Aft Compartment, Station 173, Position II, 84 Inches from Vehicle Centerline
D0082-115	Static Pressure	0-13.79	S-IC Aft Compartment, Station 173, Position IV, 84 Inches from Vehicle Centerline
D0092-118	Static Pressure	0-13.79	S-IC Intertank Compartment, Station 730, 15° from Fin A toward Fin D
D0093-118	Static Pressure	0-13.79	S-IC Intertank Compartment, Station 727, 52° from Fin C toward Fin B
D0098-120	Static Pressure	0-13.79	S-IC Forward Skirt Compartment, Station 1513, 65° from Fin C toward Fin B
D0099-120	Static Pressure	0-13.79	S-IC Forward Skirt Compartment, Station 1513, Fin D
D0052-404	Static Pressure	0-10.34	S-II/S-IVB Interstage Compartment, Station 2771, 68° from Position IV toward Position I
D0051-411	Static Pressure	0-10.34	S-IVB Forward Compartment, Station 3214, 78° from Position I toward Position II

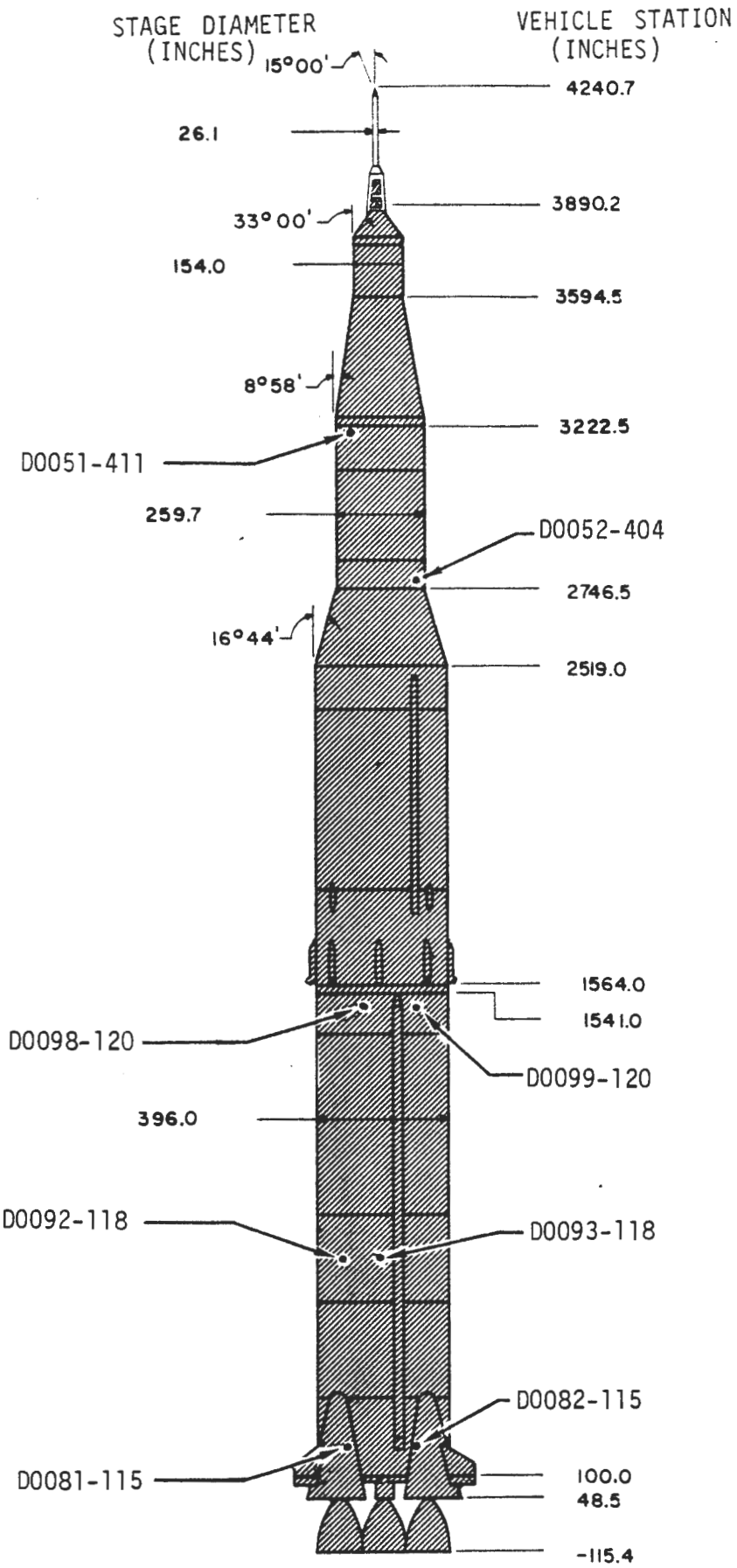

FIGURE 2-2. SATURN V COMPARTMENT INTERNAL PRESSURE INSTRUMENTATION

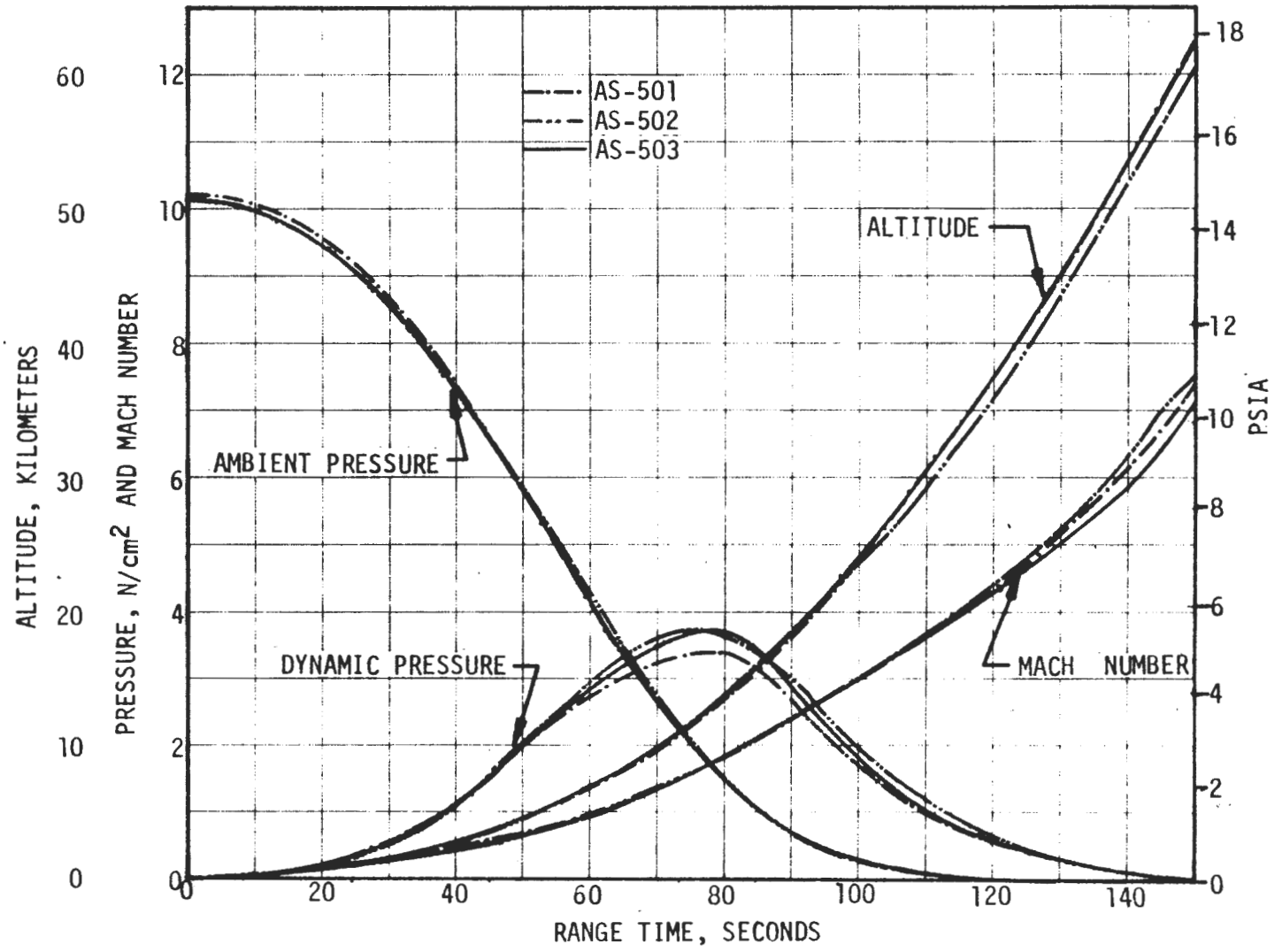

FIGURE 2-3. APOLLO SATURN V TRAJECTORIES

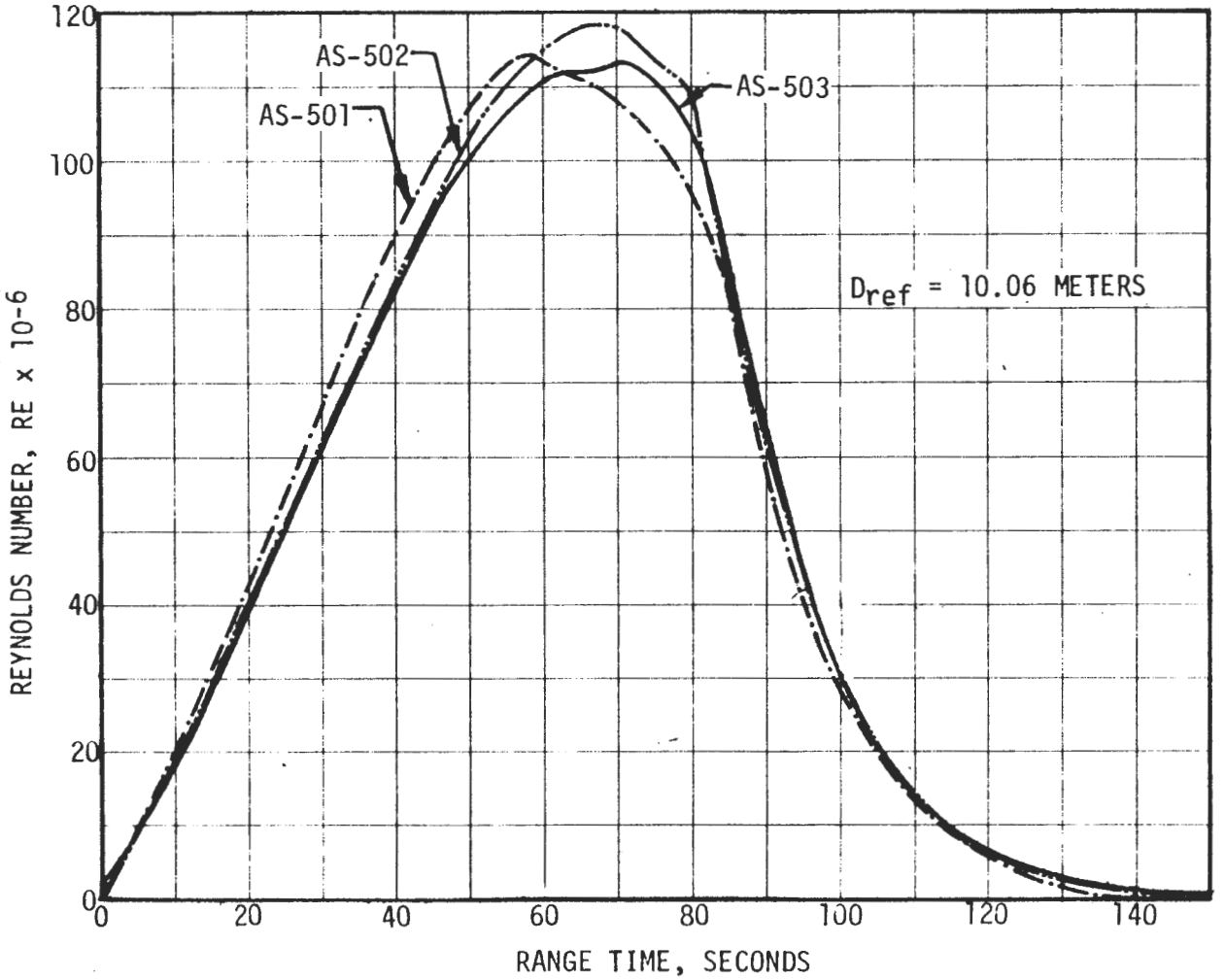

FIGURE 2-4. APOLLO SATURN V REYNOLDS NUMBER

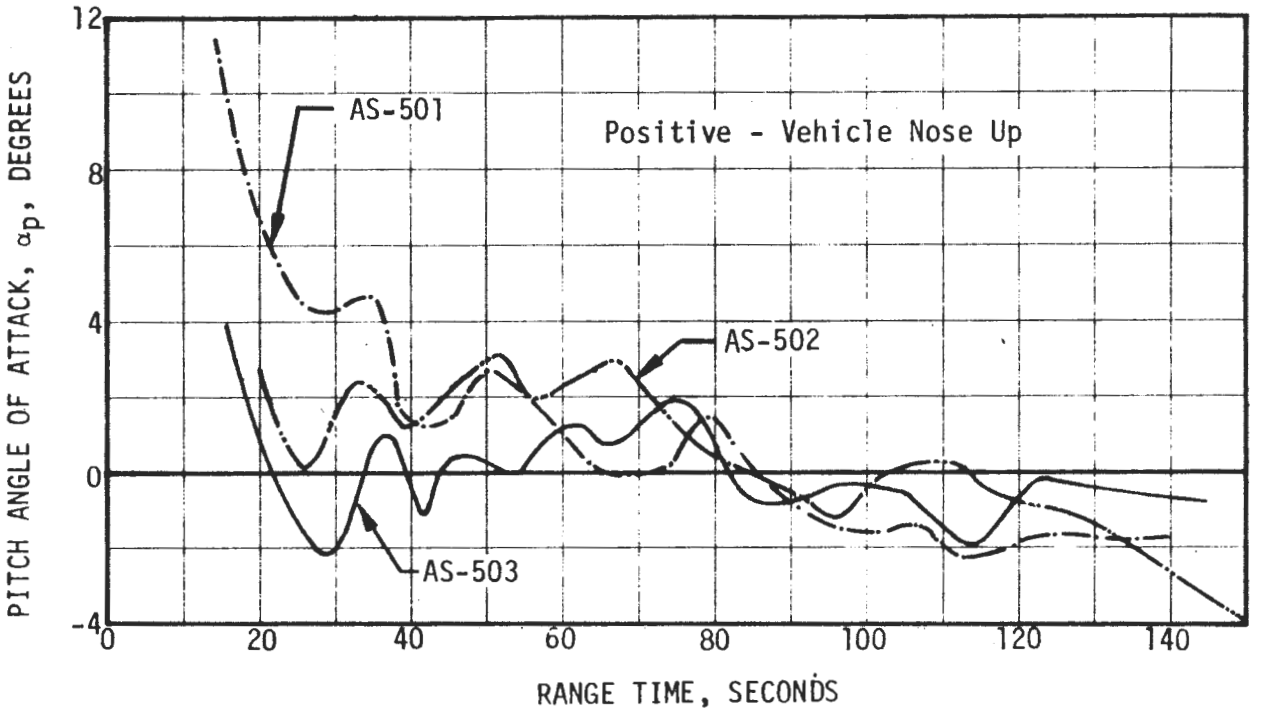

FIGURE 2-5. APOLLO SATURN V PITCH ANGLE OF ATTACK

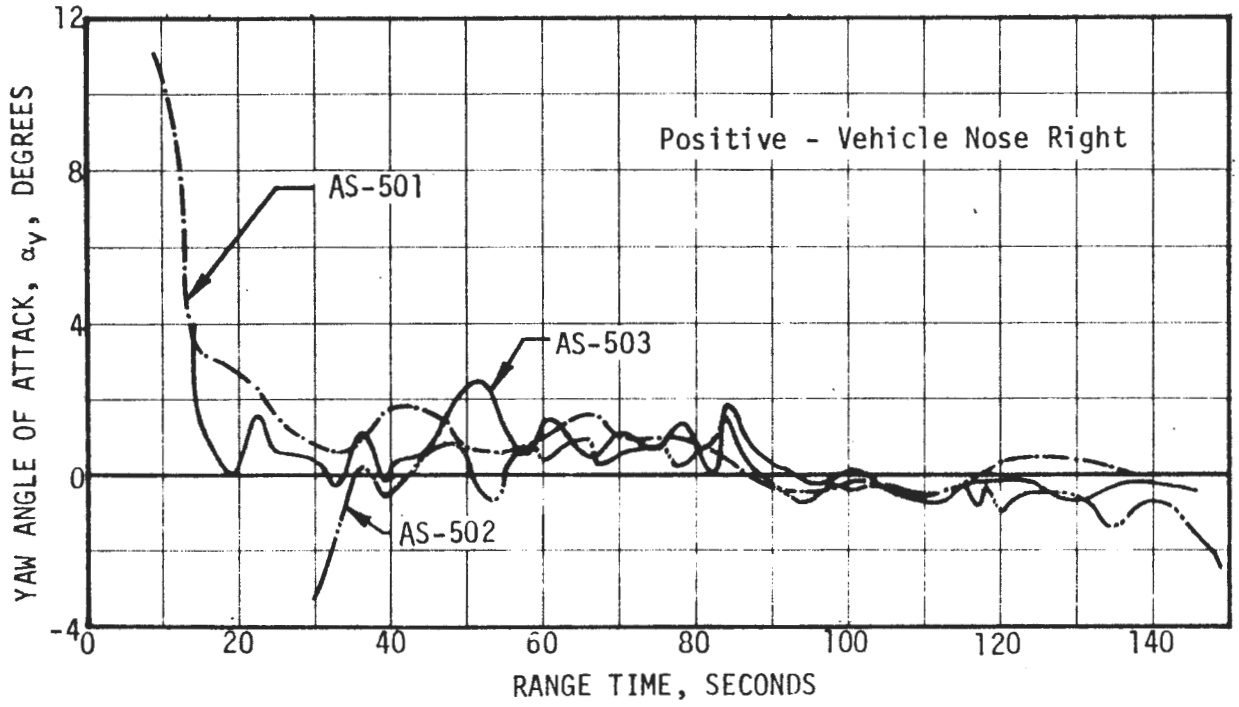

FIGURE 2-6. APOLLO SATURN V YAW ANGLE OF ATTACK

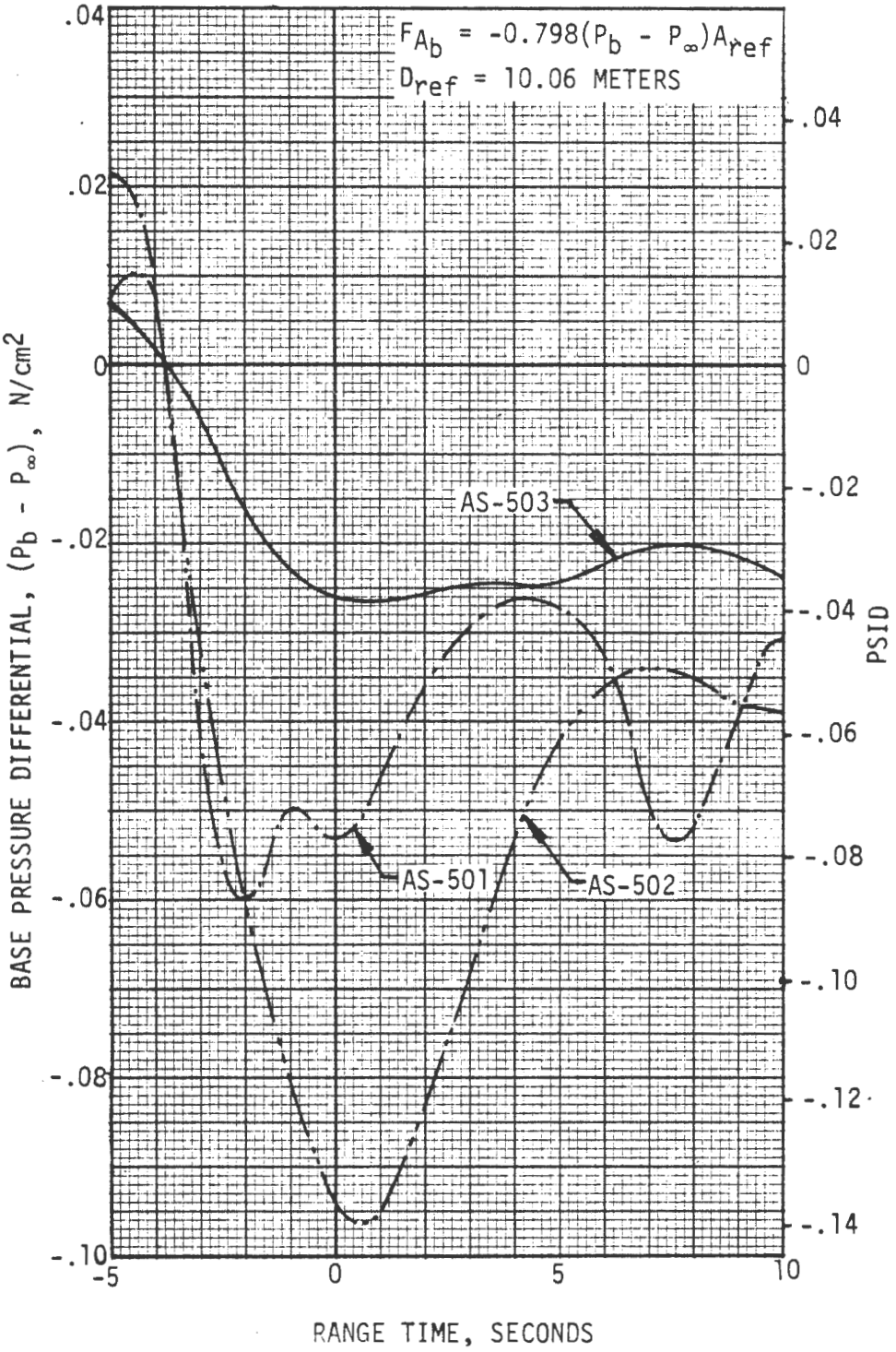

FIGURE 2-7. S-IC BASE AVERAGE PRESSURE DIFFERENTIAL

(CONTINUED ON NEXT PAGE)

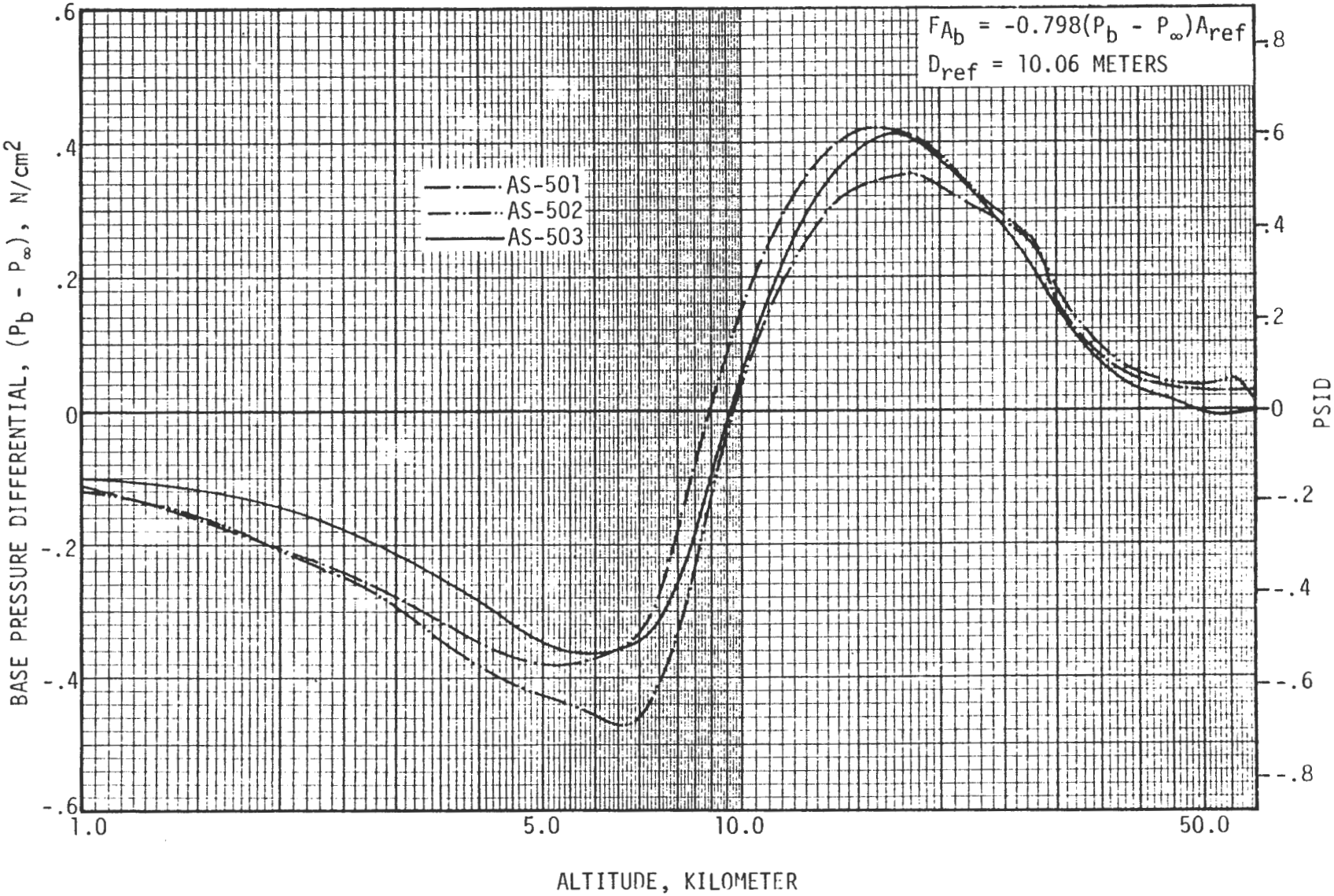

FIGURE 2-7. S-IC BASE AVERAGE PRESSURE DIFFERENTIAL (CONCLUDED)

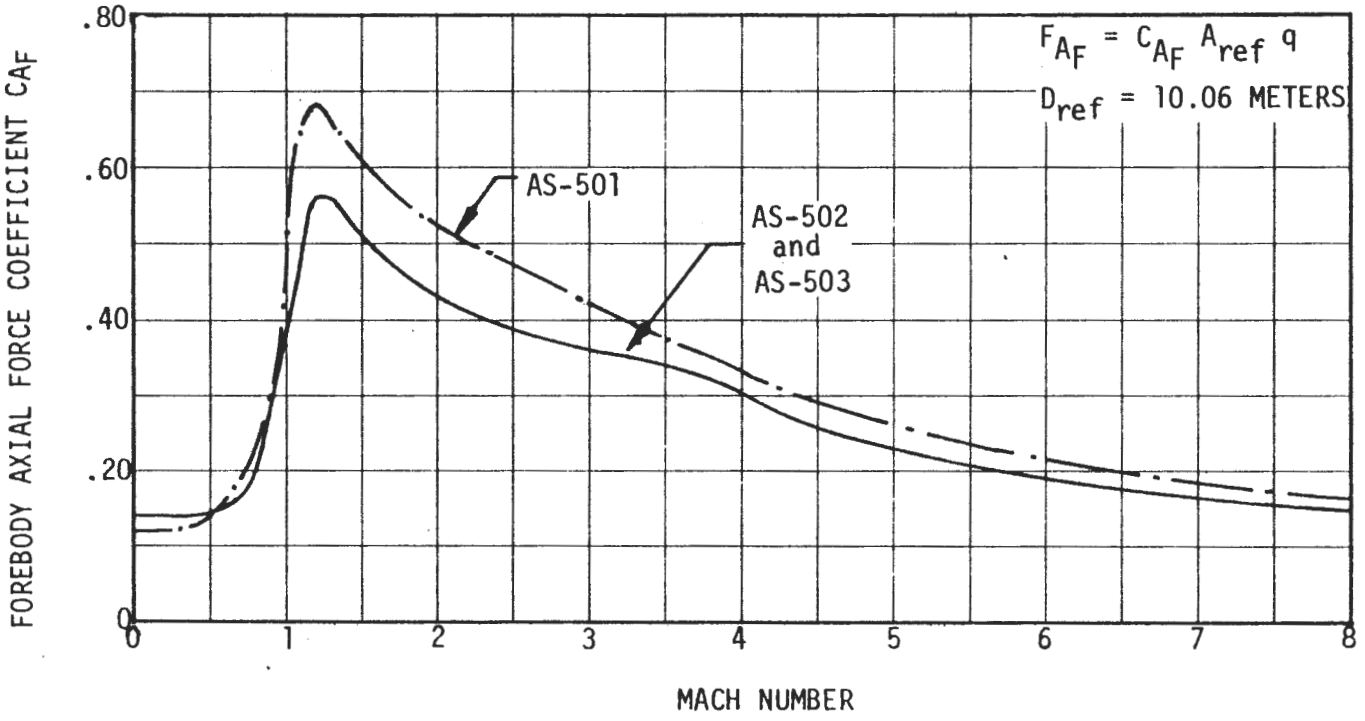

FIGURE 2-8. APOLLO SATURN V FOREBODY AXIAL FORCE COEFFICIENT

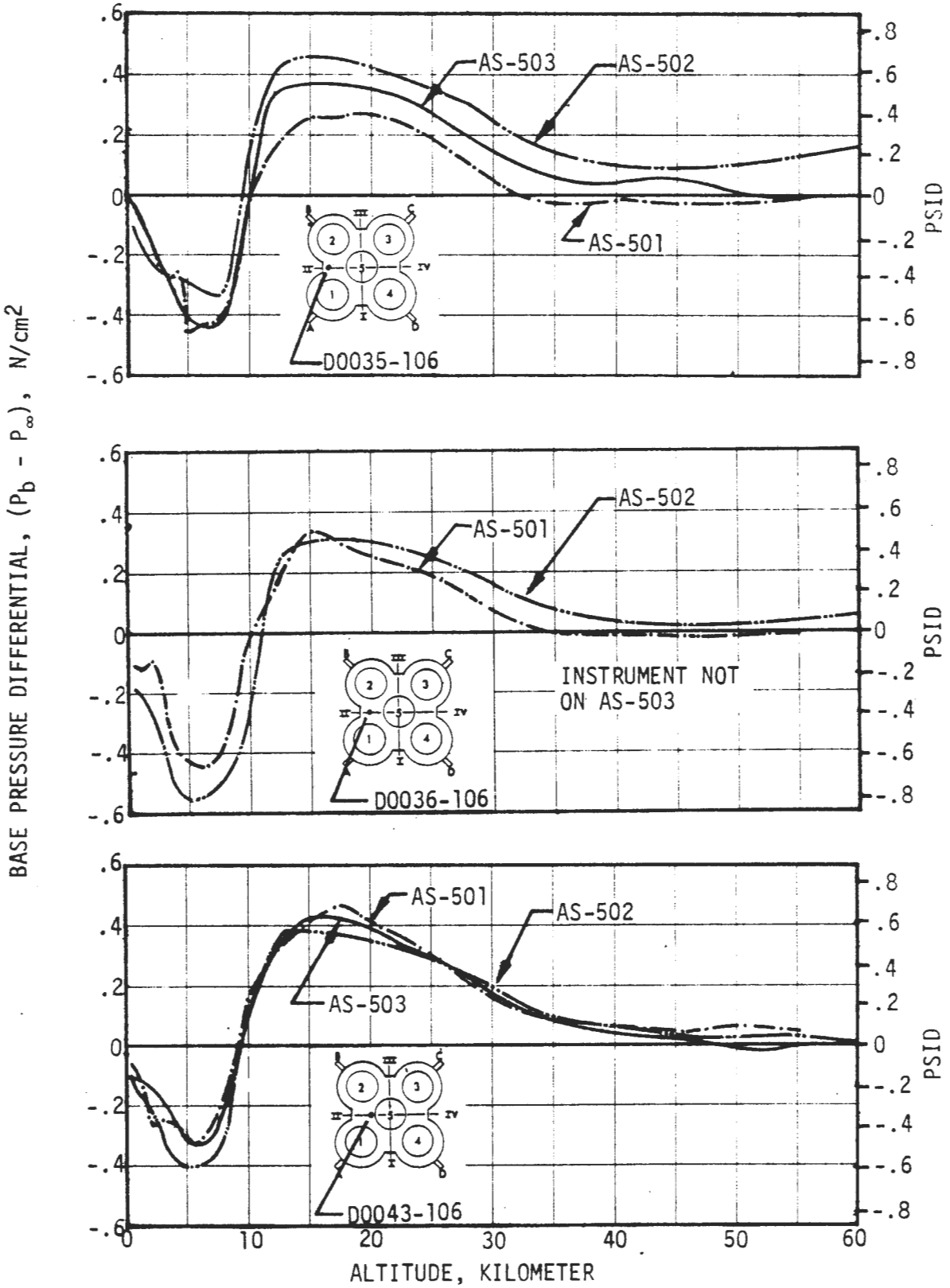

FIGURE 2-9. S-IC BASE PRESSURE DIFFERENTIAL

(CONTINUED ON NEXT PAGE)

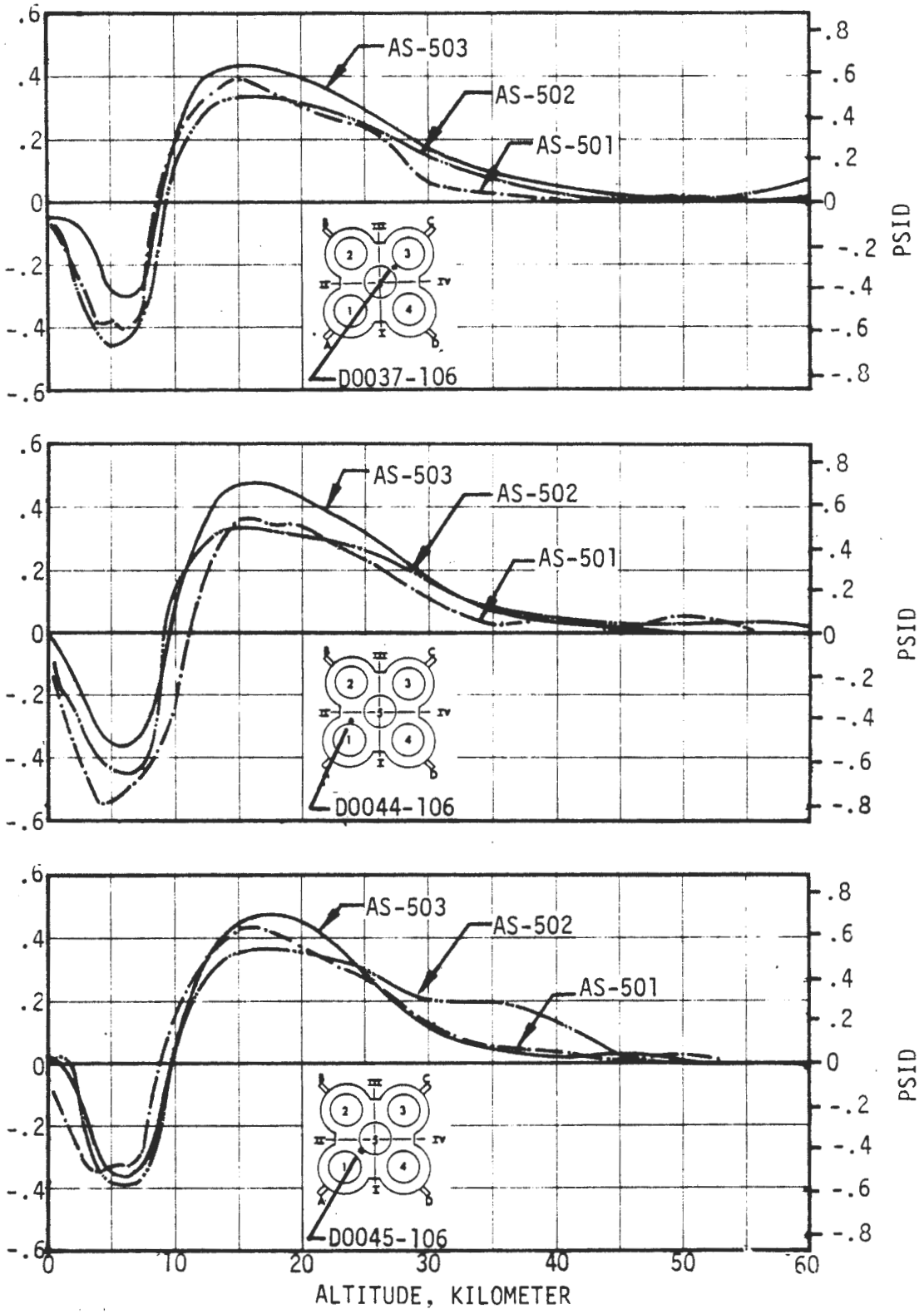

FIGURE 2-9. S-IC BASE PRESSURE DIFFERENTIAL

(CONTINUED ON NEXT PAGE)

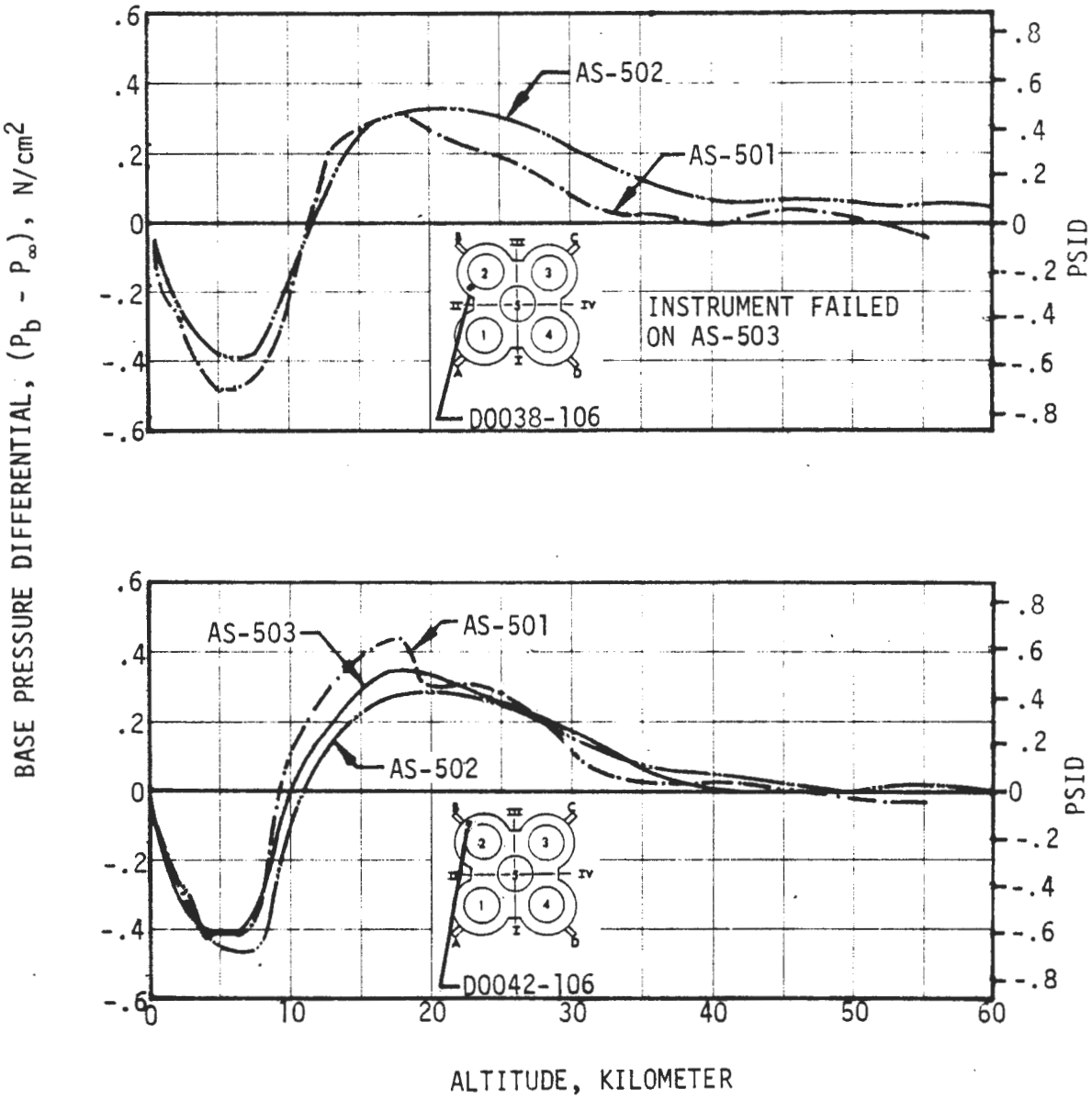

FIGURE 2-9. S-IC BASE PRESSURE DIFFERENTIAL (CONCLUDED)

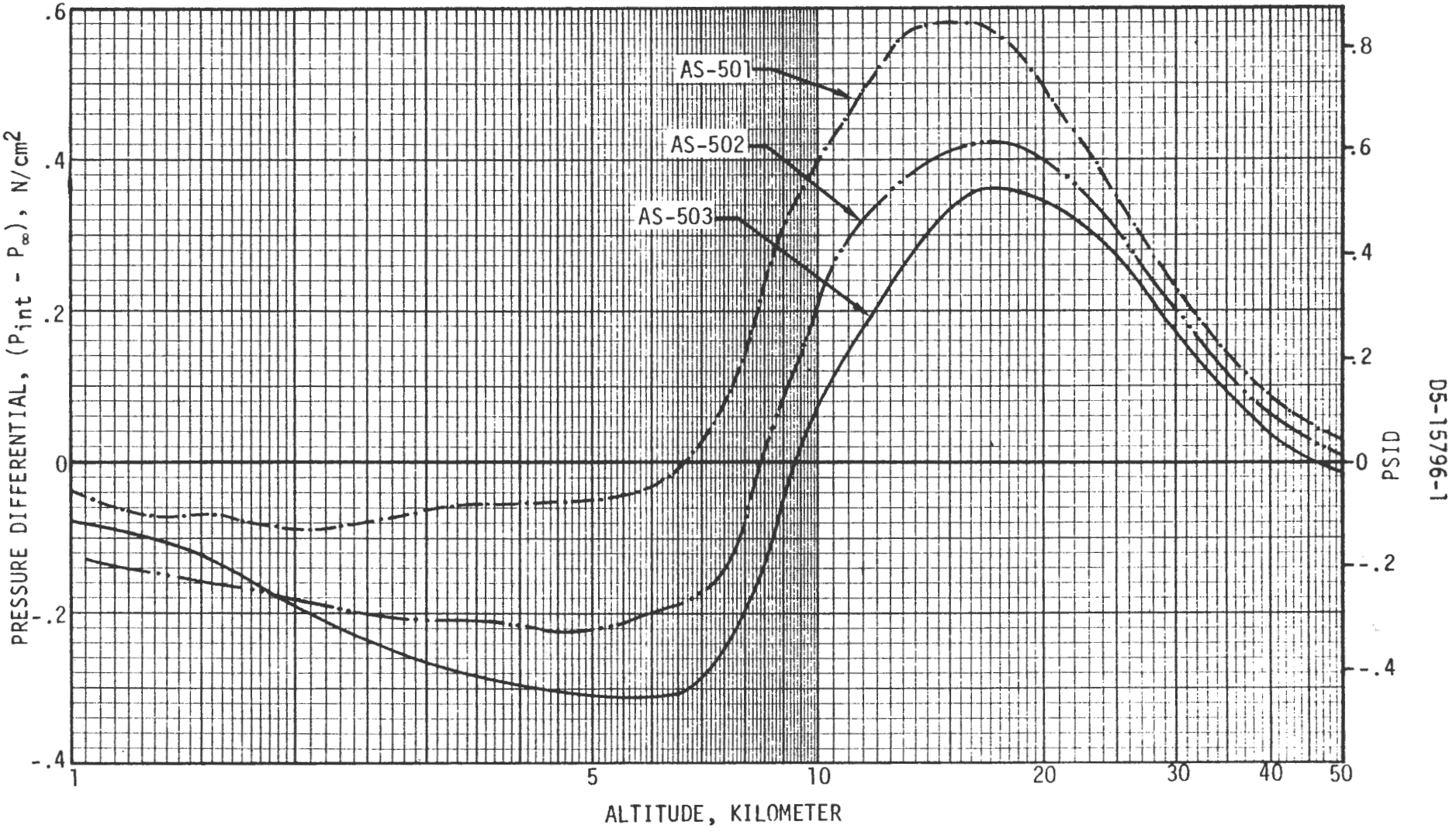

FIGURE 2-10. S-IC AFT COMPARTMENT PRESSURE DIFFERENTIAL (CONTINUED ON NEXT PAGE)

05-15796-1

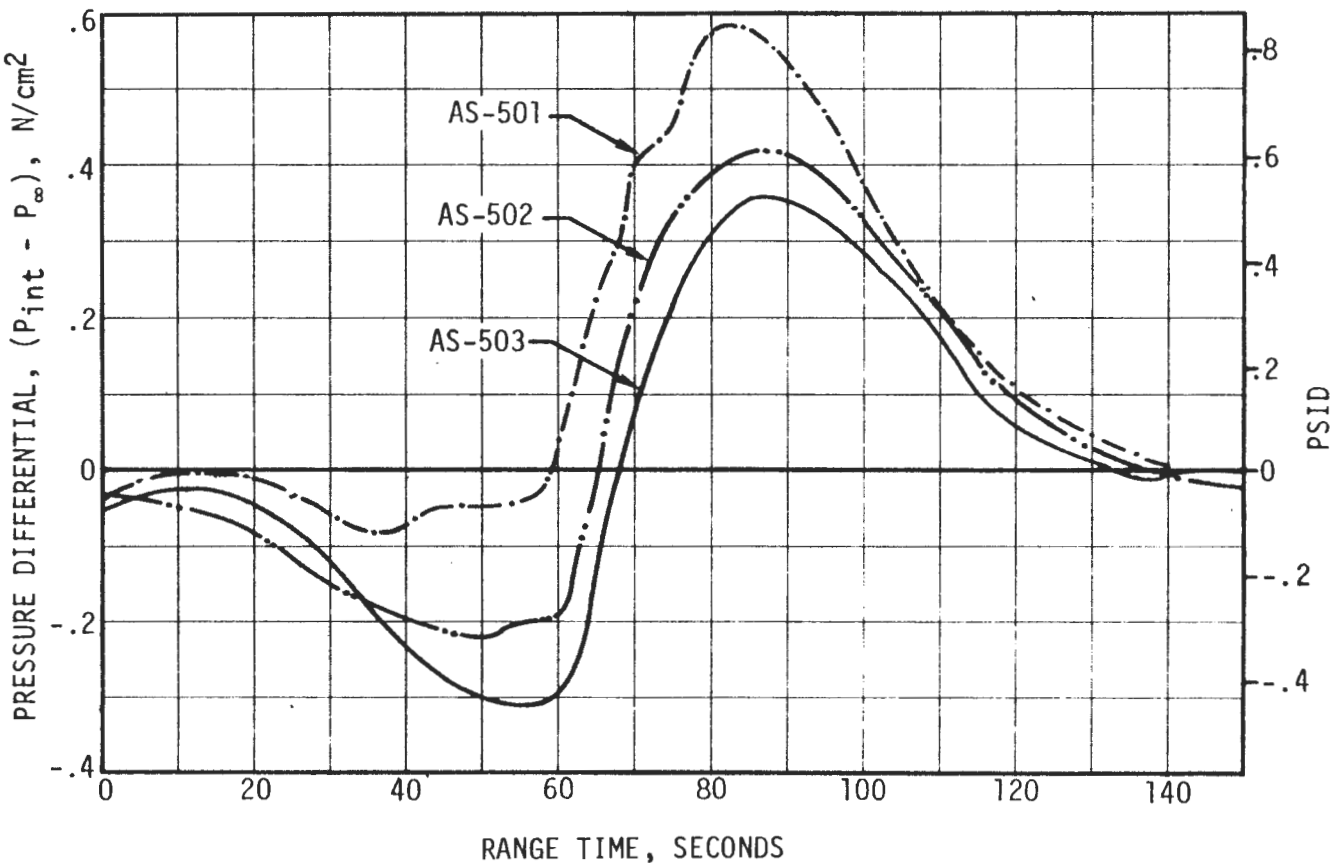

FIGURE 2-10. S-IC AFT COMPARTMENT PRESSURE DIFFERENTIAL (CONCLUDED)

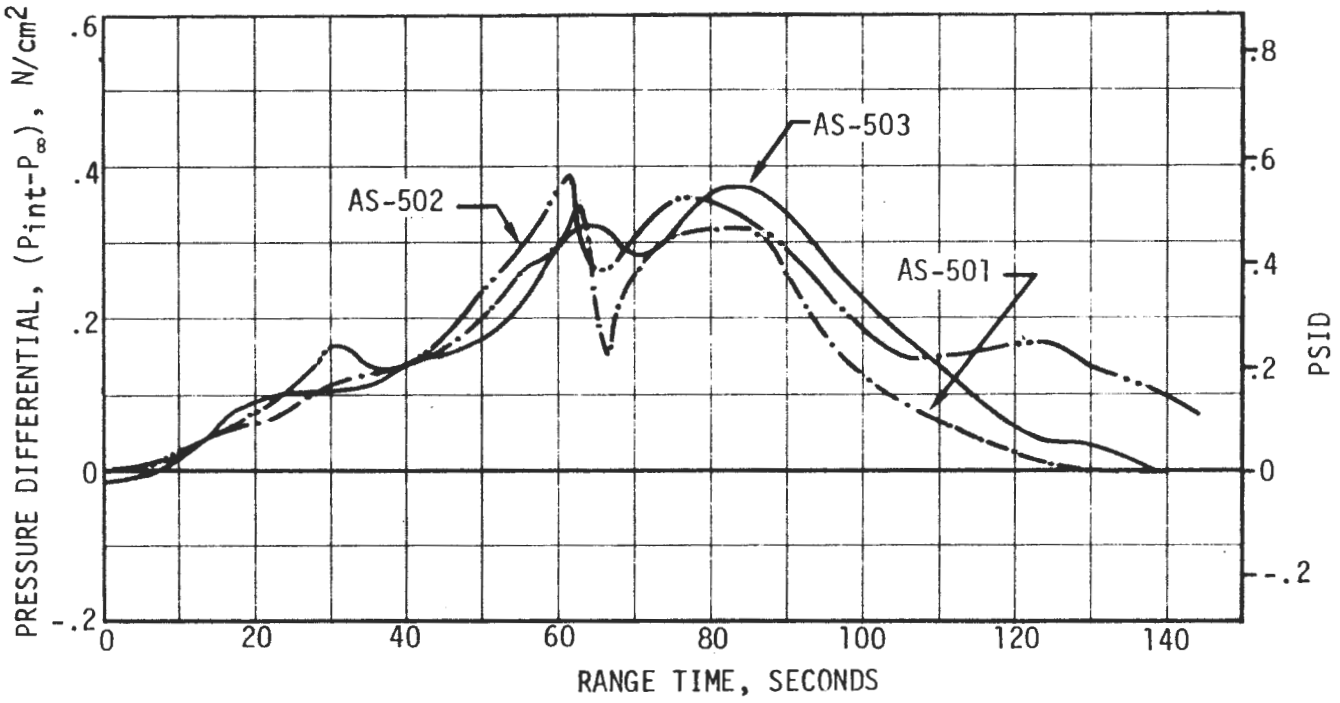

FIGURE 2-11. S-IC INTERTANK COMPARTMENT PRESSURE DIFFERENTIAL

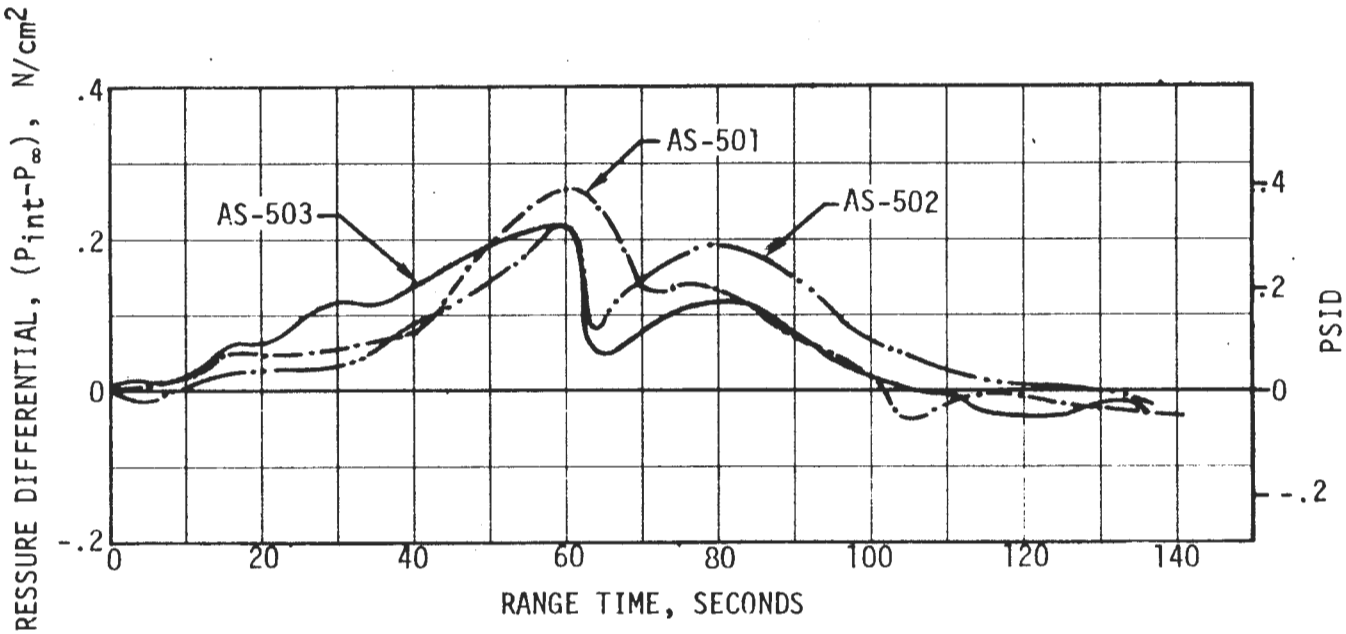

FIGURE 2-12. S-IC FORWARD SKIRT COMPARTMENT PRESSURE DIFFERENTIAL

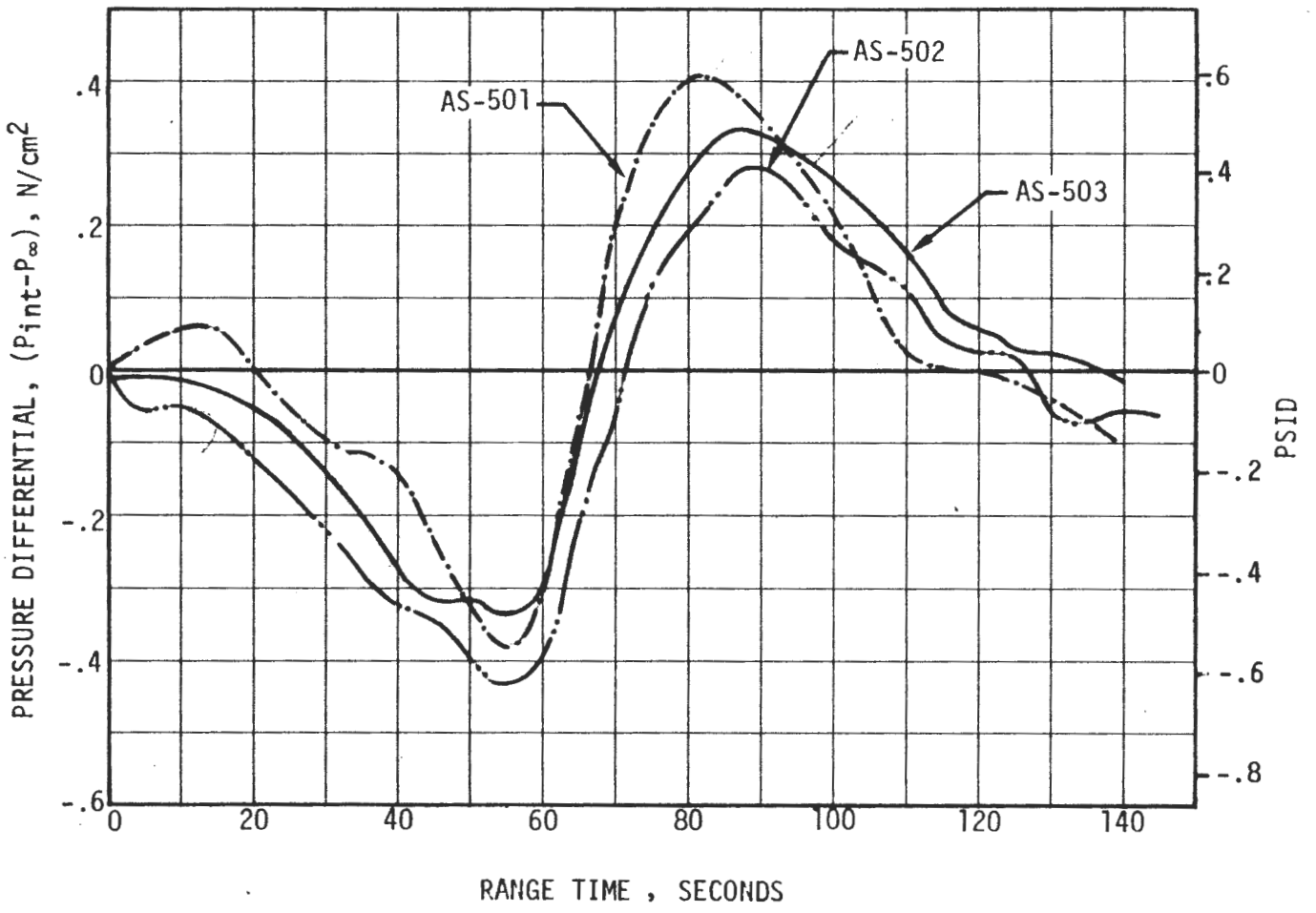

FIGURE 2-13. S-IC SHROUD COMPARTMENT PRESSURE DIFFERENTIAL

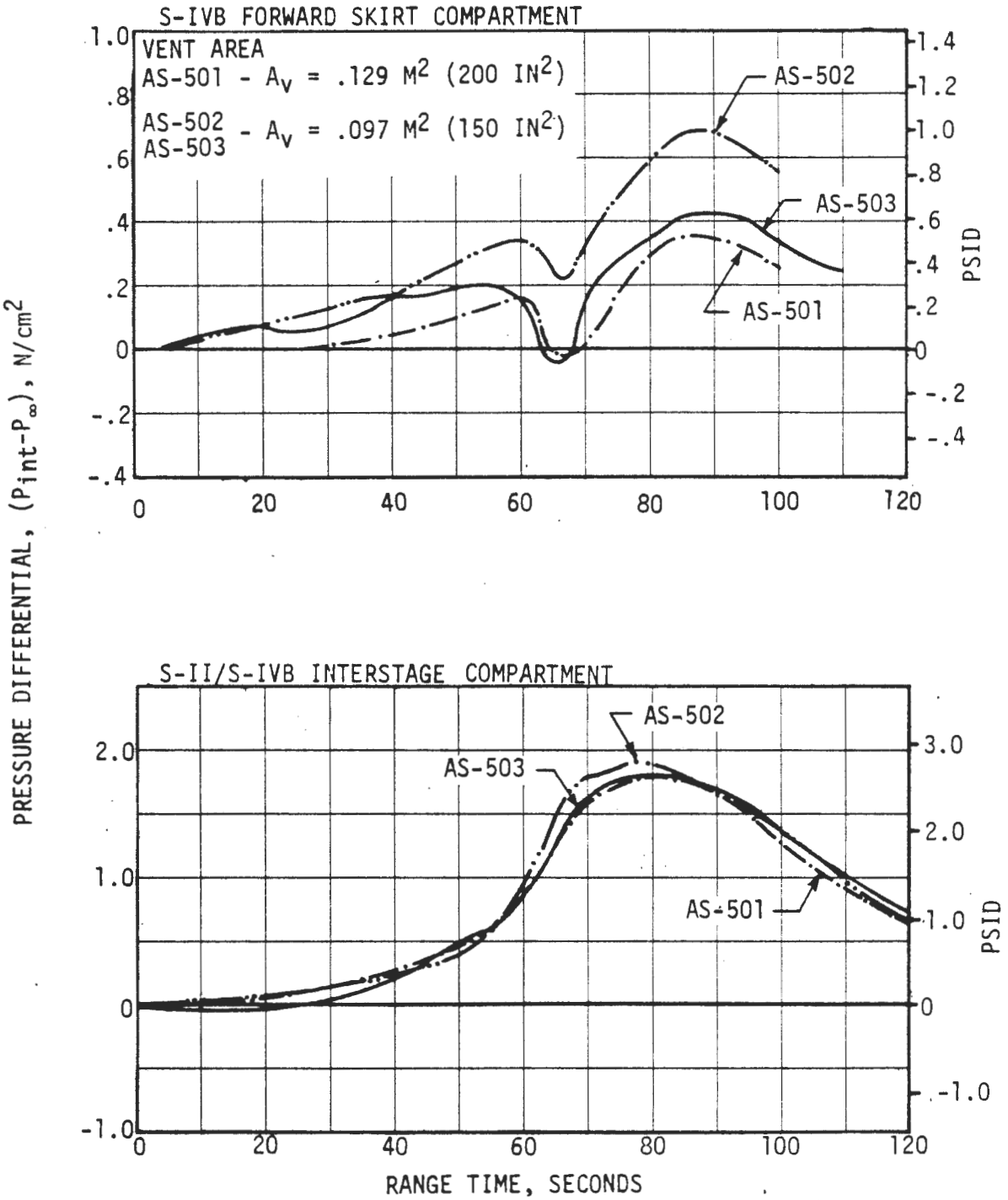

FIGURE 2-14. S-II AND S-IVB COMPARTMENT PRESSURE DIFFERENTIALS

(THIS PAGE INTENTIONALLY LEFT BLANK)

SECTION 3

VEHICLE LAUNCH AND INFLIGHT ACOUSTICS

3.0 INTRODUCTION

This section contains a summary of the external acoustic environments for the first three Saturn V flights. Presented in this section are the vehicle external overall sound pressure level at liftoff, external sound pressure spectral densities at liftoff, external overall fluctuating pressure level, and external fluctuating pressure spectral densities.

3.1 VEHICLE ACOUSTIC INSTRUMENTATION

The instrumentation used to measure fluctuating pressures were piezoelectric pressure transducers. These instruments were located on the instrument unit, S-IVB forward and aft skirts, S-II forward and aft skirts, S-IC intertank, aft skirt and Fin D. The angular locations of some of the instruments were changed between flights. The acoustic instrumentation is tabulated in Table 3-I and shown graphically in Figure 3-1.

3.2 VEHICLE EXTERNAL ACOUSTICS

In this section the vehicle external acoustics are presented in two parts; liftoff environment and inflight environment. Flight data are not shown for all flights on some figures due to instrumentation failure and/or removal.

3.2.1 Liftoff Environment

The vehicle external overall sound pressure levels at liftoff are shown in Figure 3-2. Instrument B0019-427, located on the AS-503 S-IVB aft skirt, experienced a data dropout from -1 to 2 seconds and, consequently, AS-503 liftoff data are not shown for this instrument. The spread noted in the data of the S-II forward skirt and aft skirt may be caused by instrument position changes between flights at fixed vehicle stations. The data indicate that up to a 6 DB circumferential variation exists at these vehicle stations with the lower levels from measurements located on the LUT side of the vehicle (Position II).

S-IC aft skirt measurement (B0002-115) for AS-502 and AS-503 show an approximate 8 DB level increase from AS-501. These levels are more representative of expected levels. The fin and S-IC aft skirt measurements for all three flights have been corrected by -3 DB to account for RACS (Remote Automatic Calibration System) error.

3.2.1 (Continued)

Liftoff sound pressure spectral densities are compared in Figure 3-3. Frequency characteristics generally appear similar for all flights. S-II instrument data from the AS-503 flight show some changes in spectrum shape, but these instruments were moved 90 degrees from the corresponding AS-501 and AS-502 measurements.

3.2.2 Inflight Environment

Overall fluctuating pressure time histories to 140 seconds are shown in Figure 3-4. The peak in the S-IC intertank data after 110 seconds may be caused by flow separation and exhaust gas recirculation due to the expanded exhaust plume. The majority of time-histories show reasonable agreement between all flights. However, B0037-200 (S-II aft skirt) for AS-503 shows consistently higher overall levels. The cause appears to be a strong narrow band random or sinusoidal component in the 600 to 700 cps frequency range which was observed in power spectral data after 20 seconds. B0038-200 (S-II aft skirt) overall levels show good agreement for all flights, however, available power spectral data indicates the 600 to 700 cps component is present only at 80 seconds on AS-503. The difference in data on the instrument unit (B0001-601) between the AS-501 and the other two flights is noted but the cause is unknown.

Pressure spectral densities at maximum aerodynamic noise are shown in Figure 3-5. On AS-503 the 600 to 700 cps peak is evident in the spectra for B0037-200 and B0038-200. All other spectra show good agreement in trend between flights.

TABLE 3-I. SATURN V EXTERNAL FLUCTUATING PRESSURE INSTRUMENTATION

MEASUREMENT NUMBER	VEHICLE	RANGE DB	LOCATION
B0002-115	AS-501 AS-502 AS-503	155-175 155-175 150-170	S-IC Aft Skirt Station 120, Position I
B0003-118	AS-501 AS-502 AS-503	145-165 145-165 140-160	S-IC Intertank Station 750, Position I
B0004-114	AS-501 AS-502 AS-503	155-175 155-175 155-175	S-IC Fin D Base Station 81
B0003-219	AS-501 AS-502	130-160 160 Max.	S-II Forward Skirt Station 2494, Position III
B0016-219	AS-503	160 Max.	S-II Forward Skirt Station 2494, Position IV
B0004-200	AS-501 AS-502	130-160 160 Max.	S-II Aft Skirt Station 1664, Position I
B0037-200	AS-503	160 Max.	S-II Aft Skirt Station 1664, Position II
B0005-200	AS-501 AS-502	130-160 160 Max.	S-II Aft Skirt Station 1664, Position III
B0038-200	AS-503	160 Max.	S-II Aft Skirt Station 1664, Position IV
B0013-426	AS-501	120-150	S-IVB Forward Skirt Station 3213, 78° from Position I toward Position II
B0025-426	AS-502 AS-503	120-160 163 Max.	S-IVB Forward Skirt Station 3213, 68° from Position IV toward Position I
B0019-427	AS-501 AS-502 AS-503	120-150 120-160 163 Max.	S-IVB Aft Skirt Station 2776, 68° from Position IV toward Position I
B0001-601	AS-501 AS-502 AS-503	145-165 145-165 145-165	Instrument Unit Station 3244, 23° from Position I toward Position IV

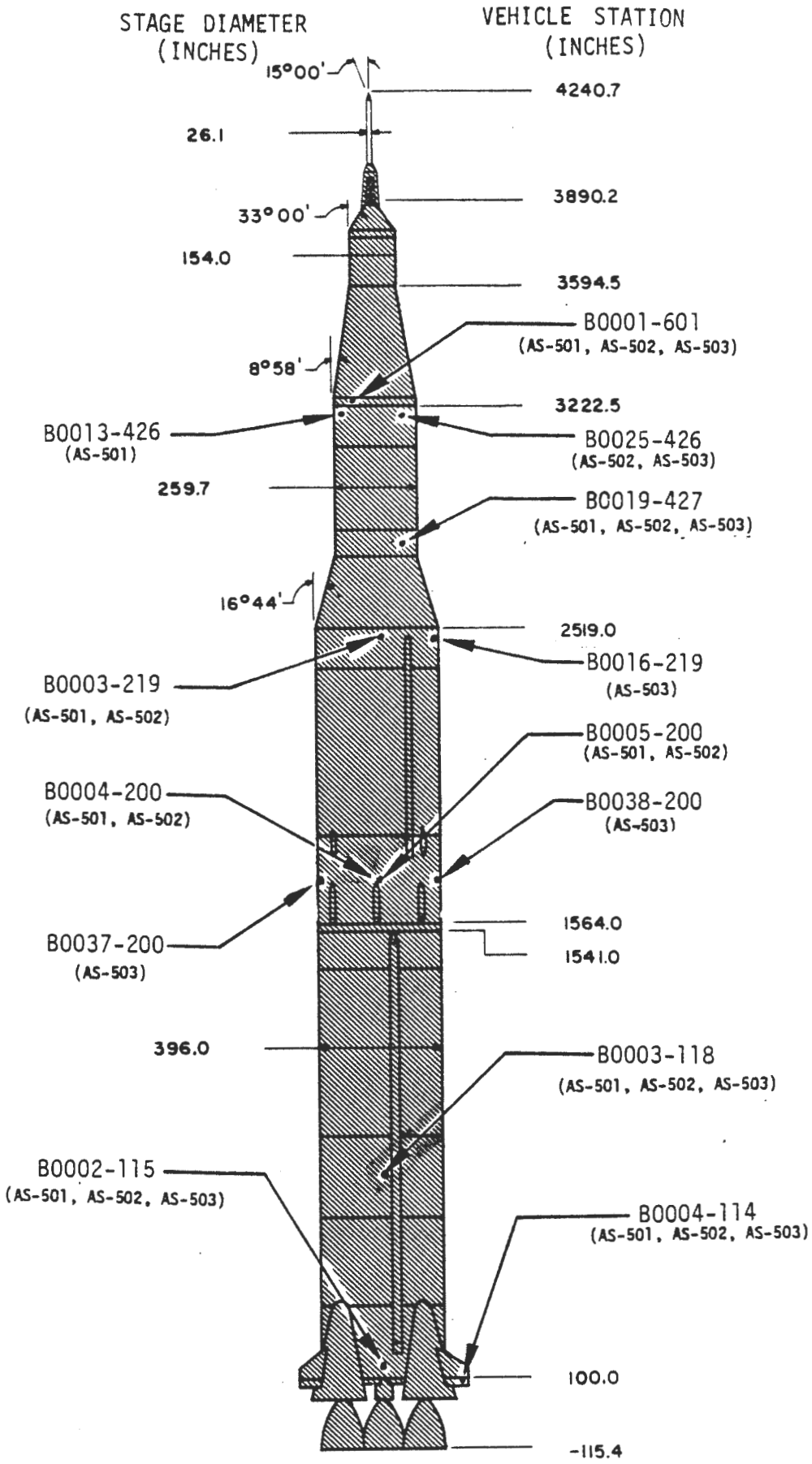

FIGURE 3-1. SATURN V EXTERNAL FLUCTUATING PRESSURE INSTRUMENTATION

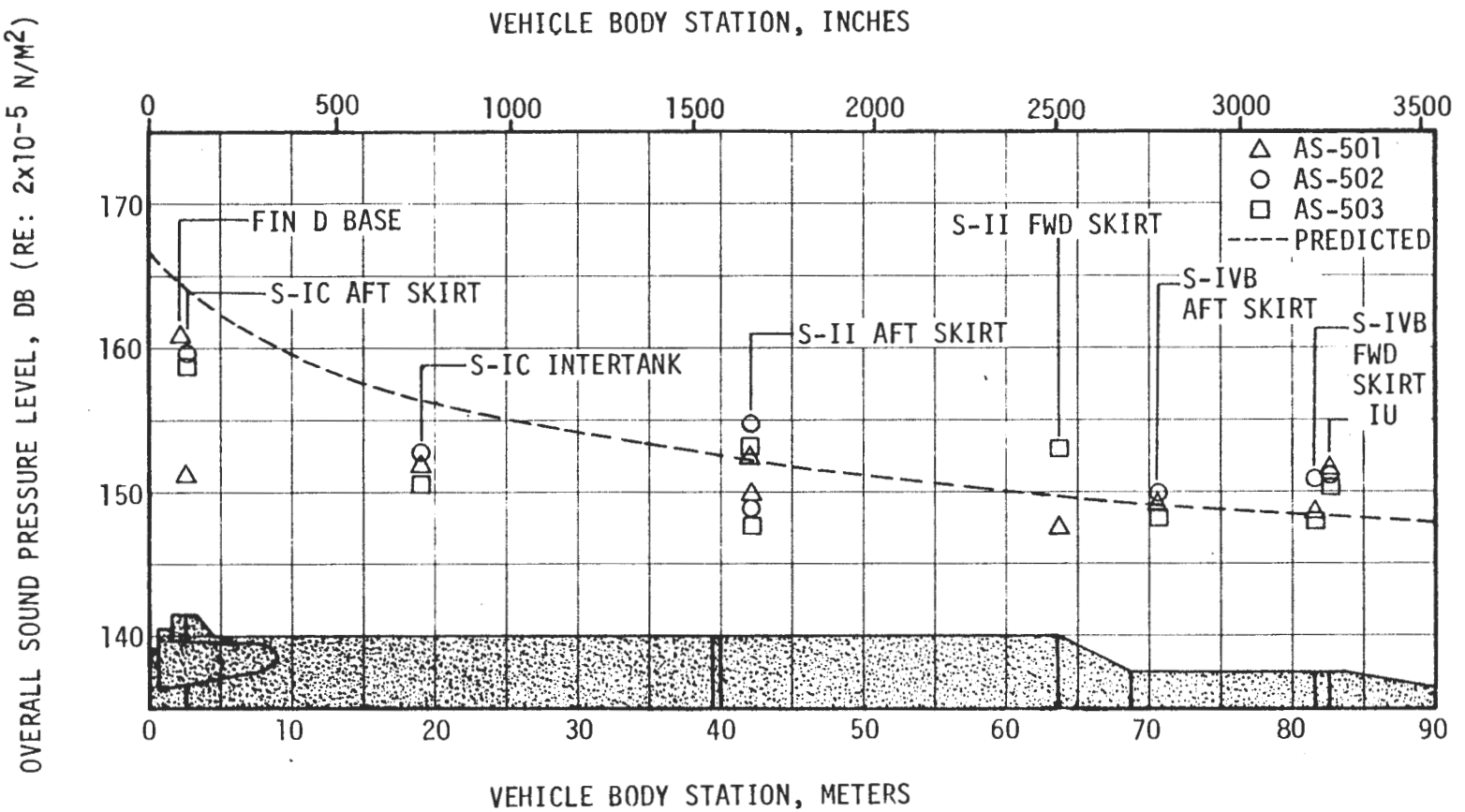

FIGURE 3-2. SATURN V EXTERNAL OVERALL SOUND PRESSURE LEVEL AT LIFTOFF

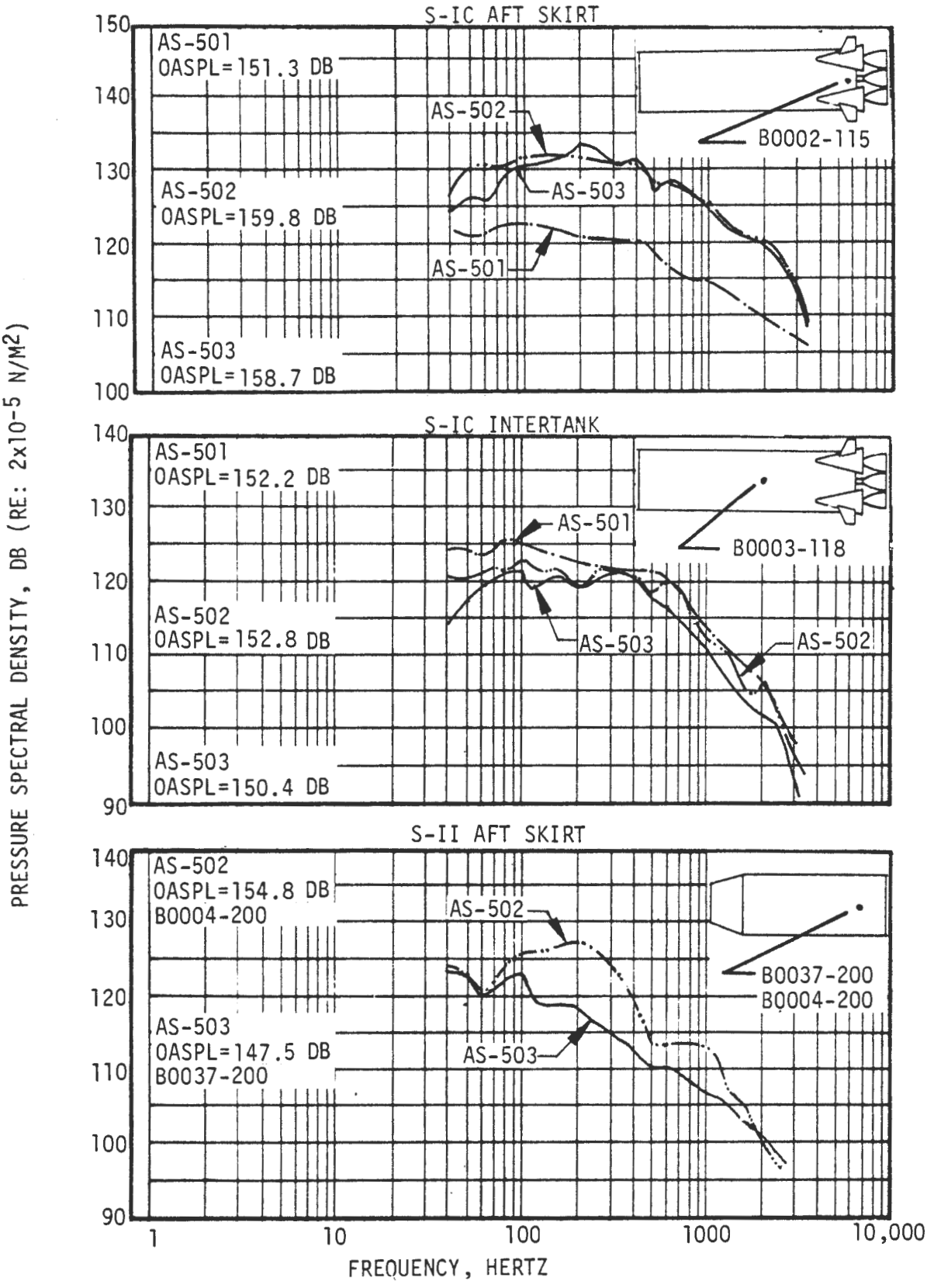

FIGURE 3-3. SATURN V EXTERNAL SOUND PRESSURE SPECTRAL DENSITIES AT LIFTOFF

(CONTINUED ON NEXT PAGE)

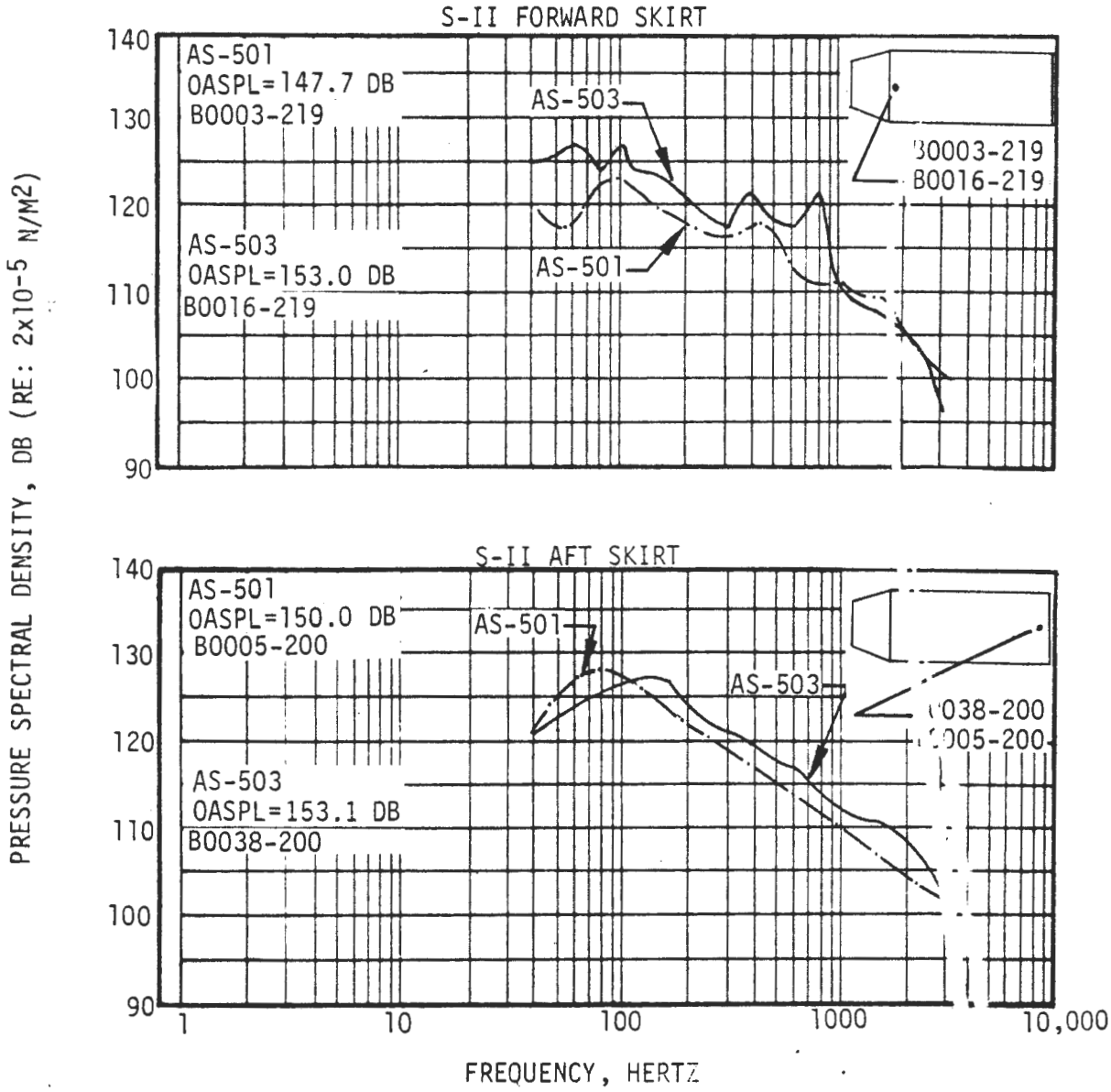

FIGURE 3-3. SATURN V EXTERNAL SOUND PRESSURE SPECTRAL DENSITIES AT LIFTOFF

(CONTINUED ON NEXT PAGE)

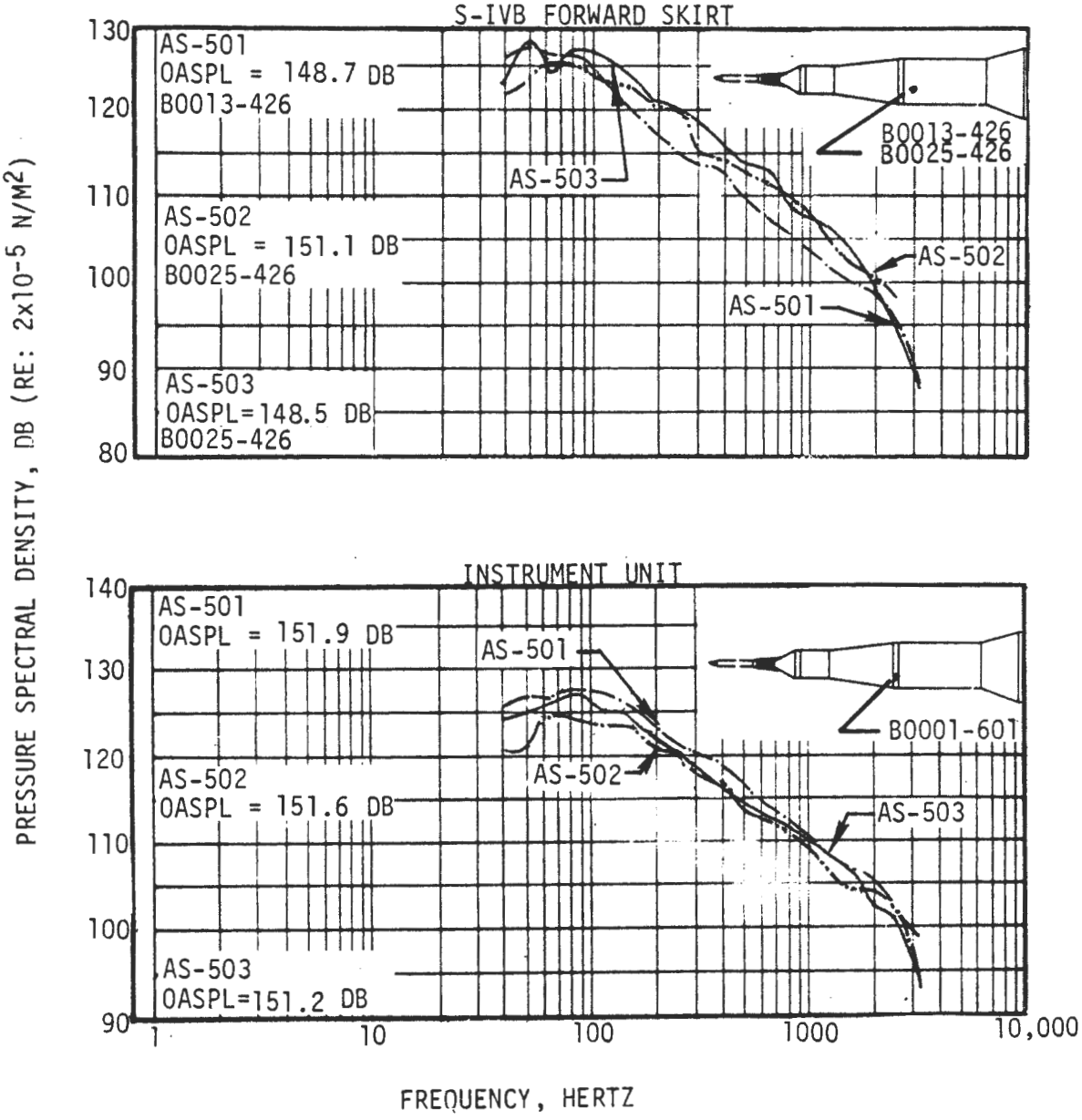

FIGURE 3-3. SATURN V EXTERNAL SOUND PRESSURE SPECTRAL DENSITIES AT LIFTOFF (CONCLUDED)

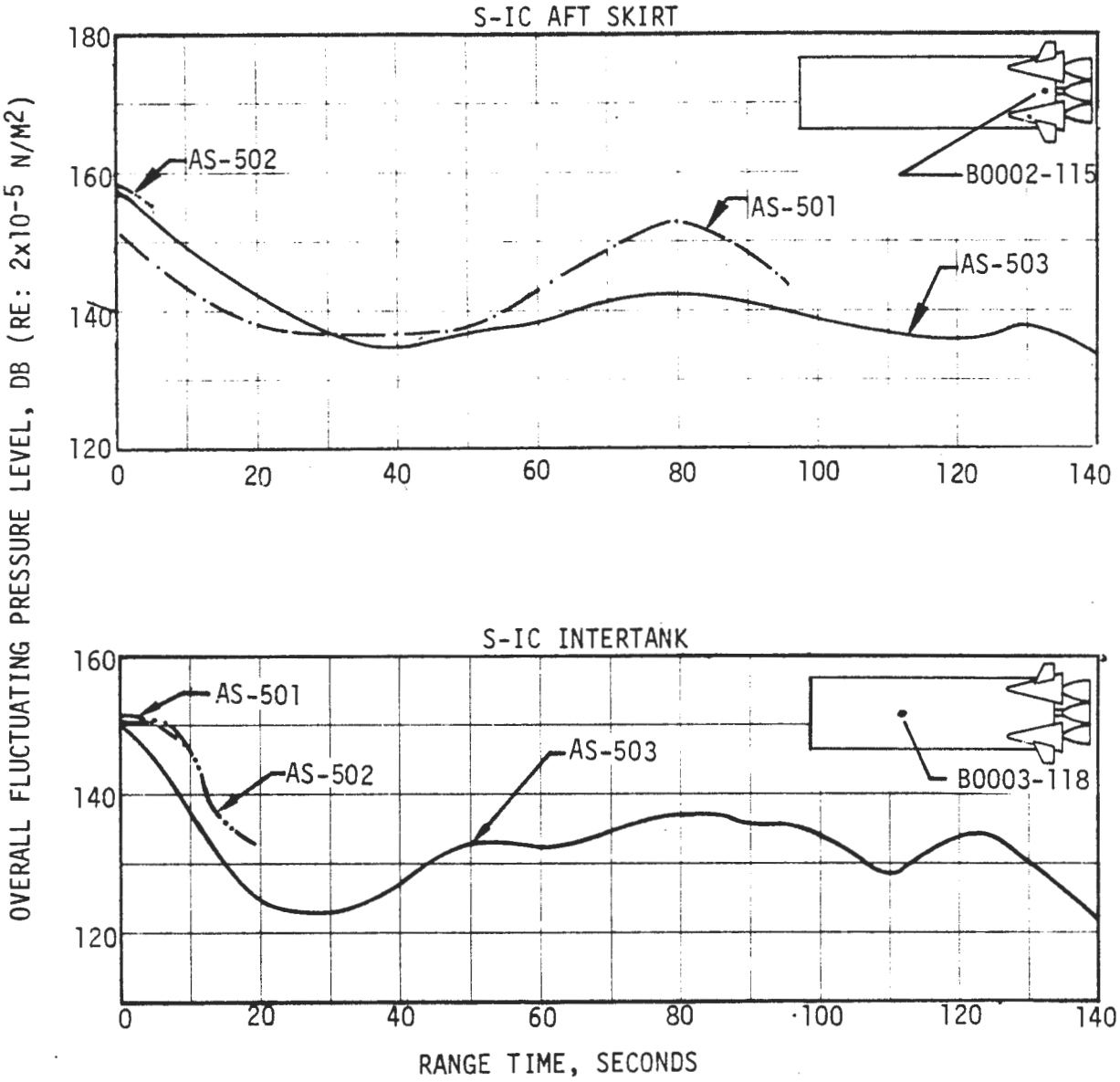

FIGURE 3-4. SATURN V EXTERNAL OVERALL FLUCTUATING PRESSURE LEVEL

(CONTINUED ON NEXT PAGE)

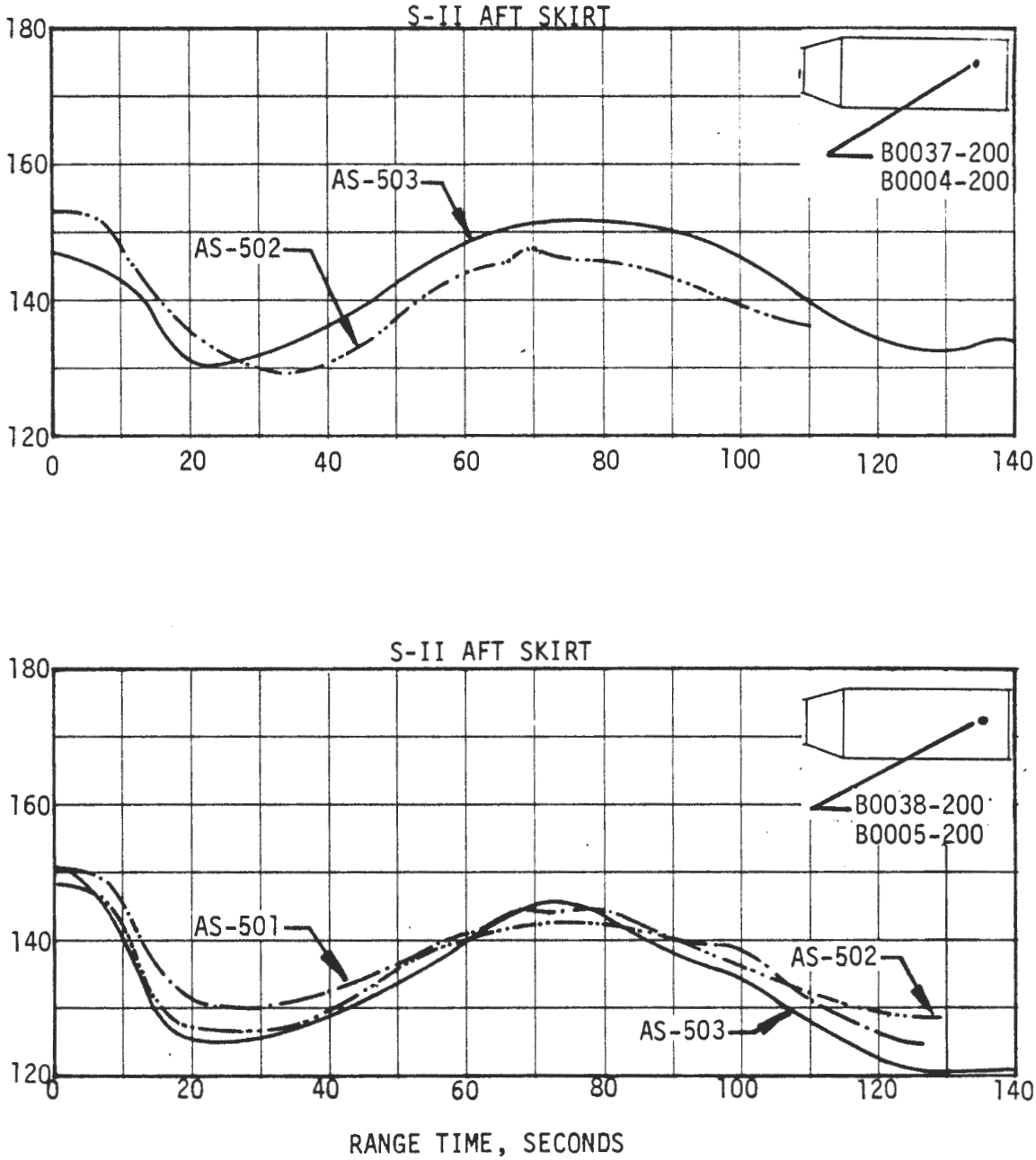

FIGURE 3-4. SATURN V EXTERNAL OVERALL FLUCTUATING PRESSURE LEVEL

(CONTINUED ON NEXT PAGE)

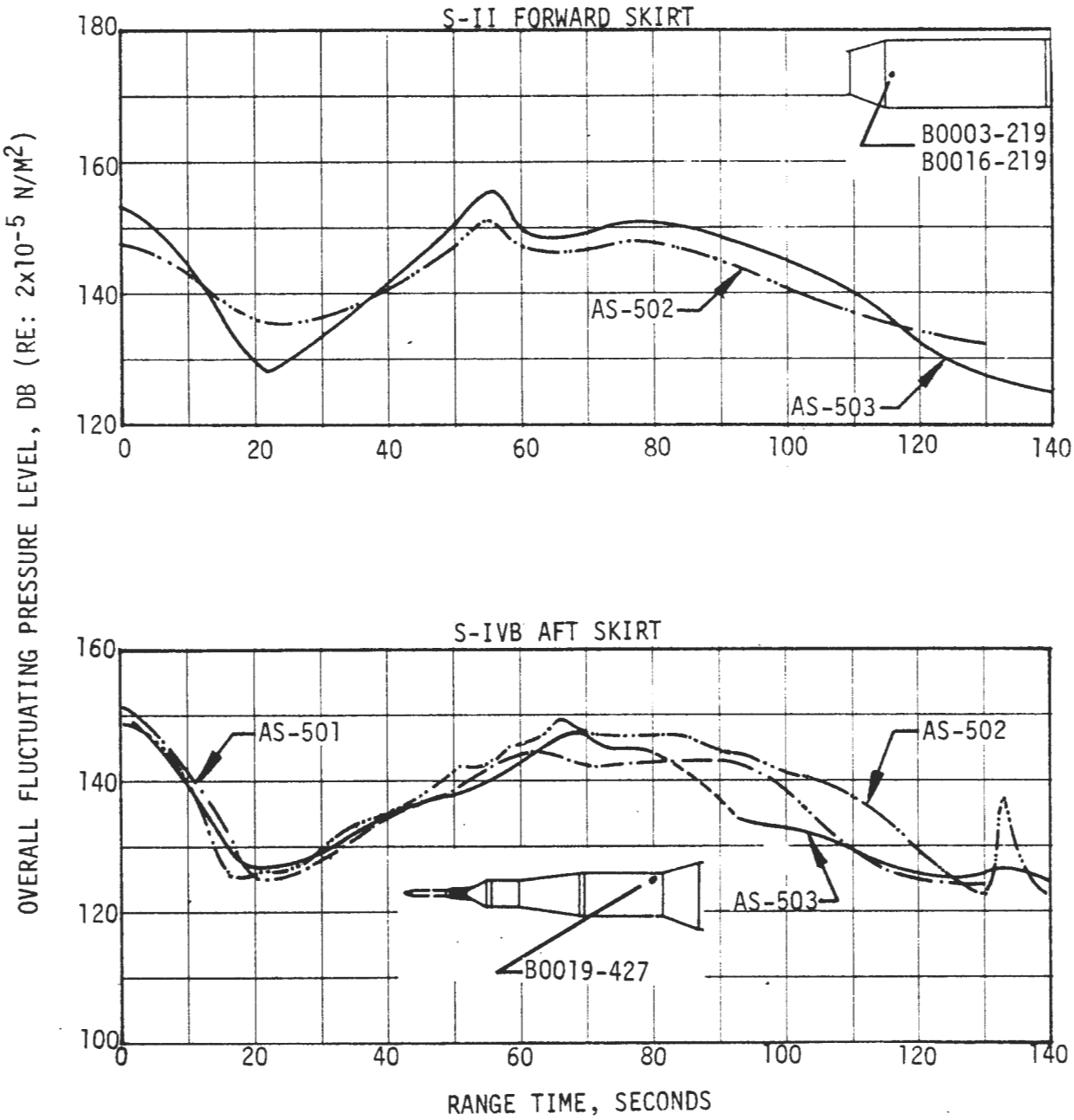

FIGURE 3-4. SATURN V EXTERNAL OVERALL FLUCTUATING PRESSURE LEVEL

(CONTINUED ON NEXT PAGE)

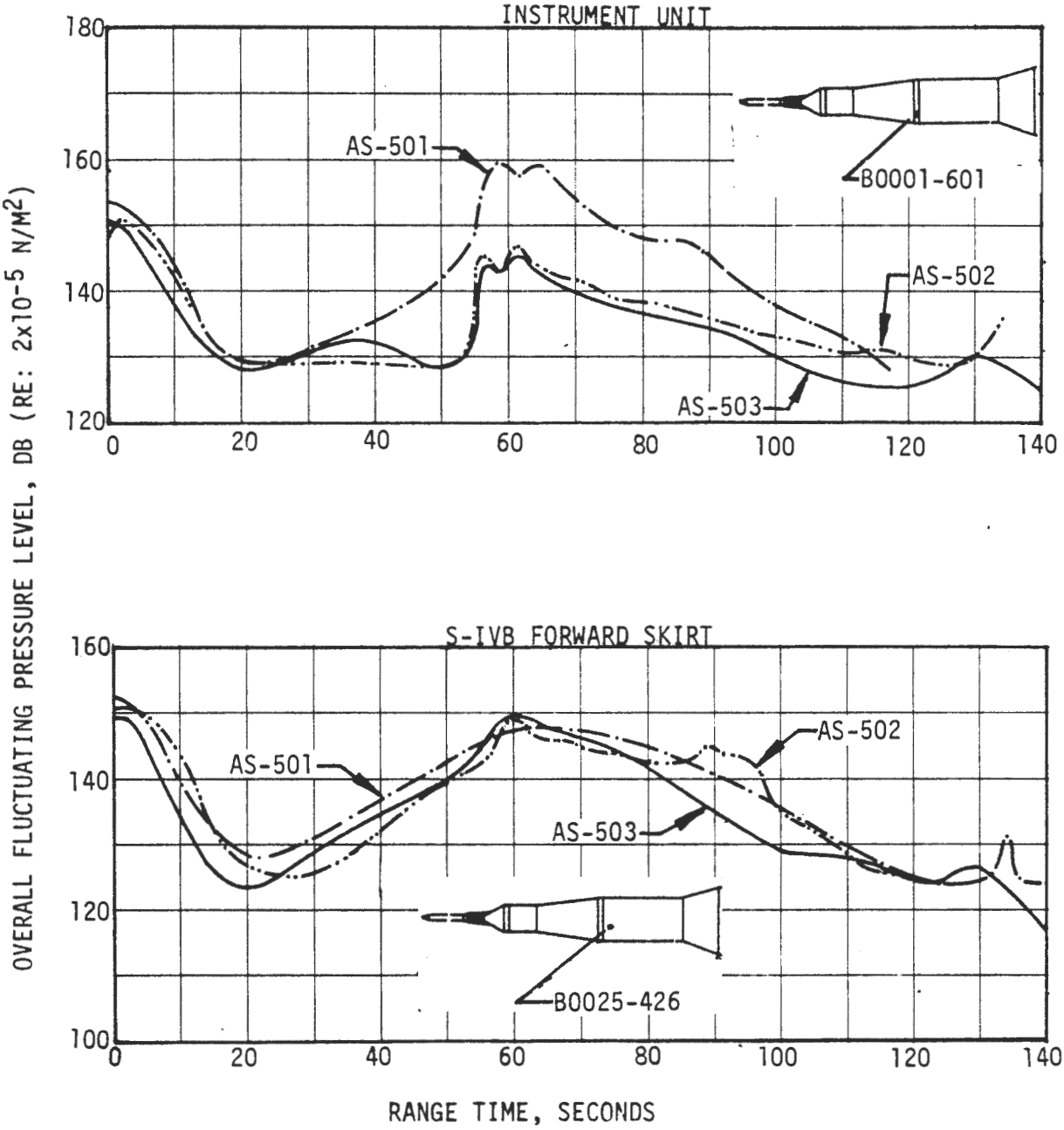

FIGURE 3-4. SATURN V EXTERNAL OVERALL FLUCTUATING PRESSURE LEVEL (CONCLUDED)

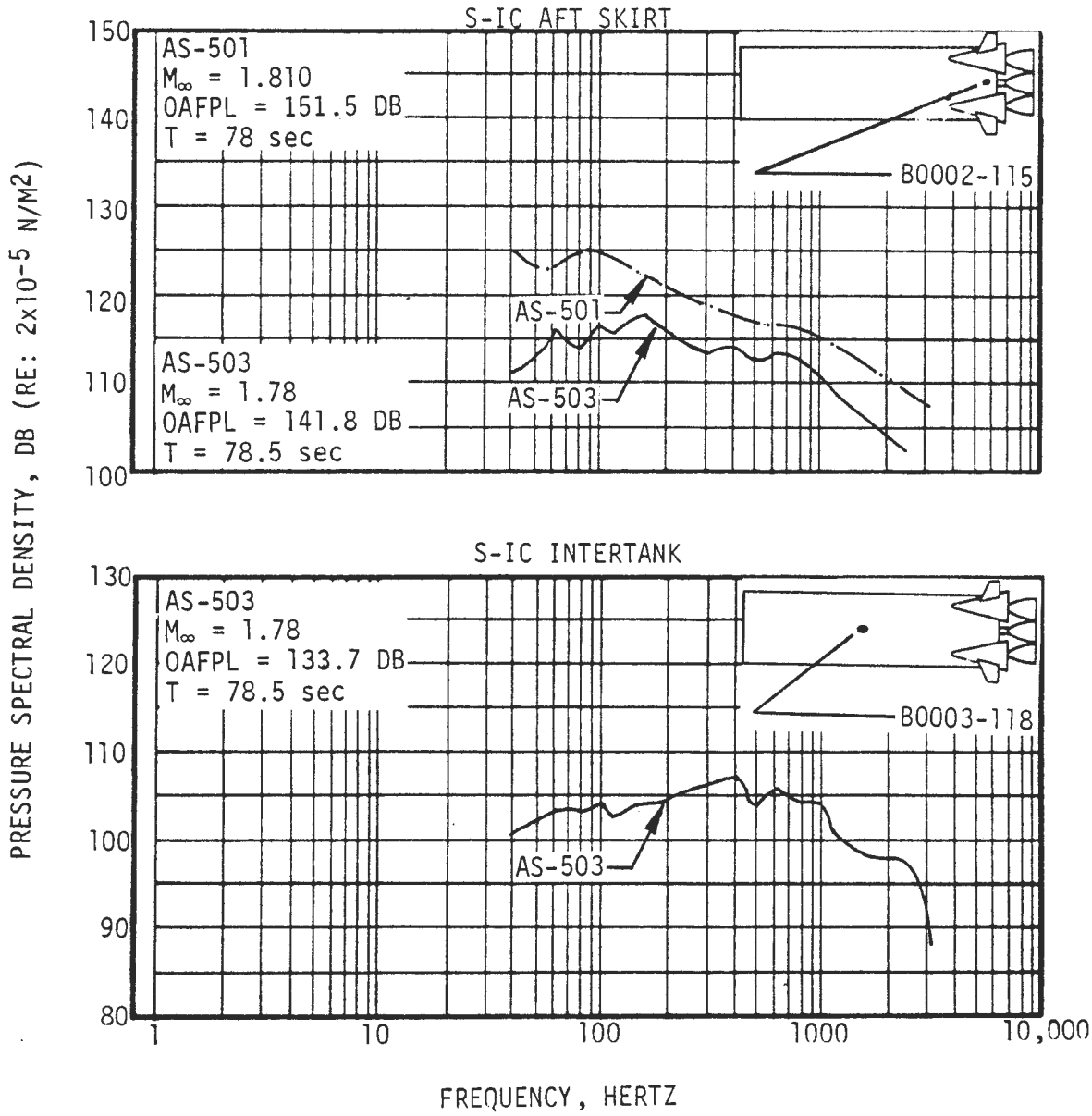

FIGURE 3-5. SATURN V EXTERNAL FLUCTUATING PRESSURE SPECTRAL DENSITIES (CONTINUED ON NEXT PAGE)

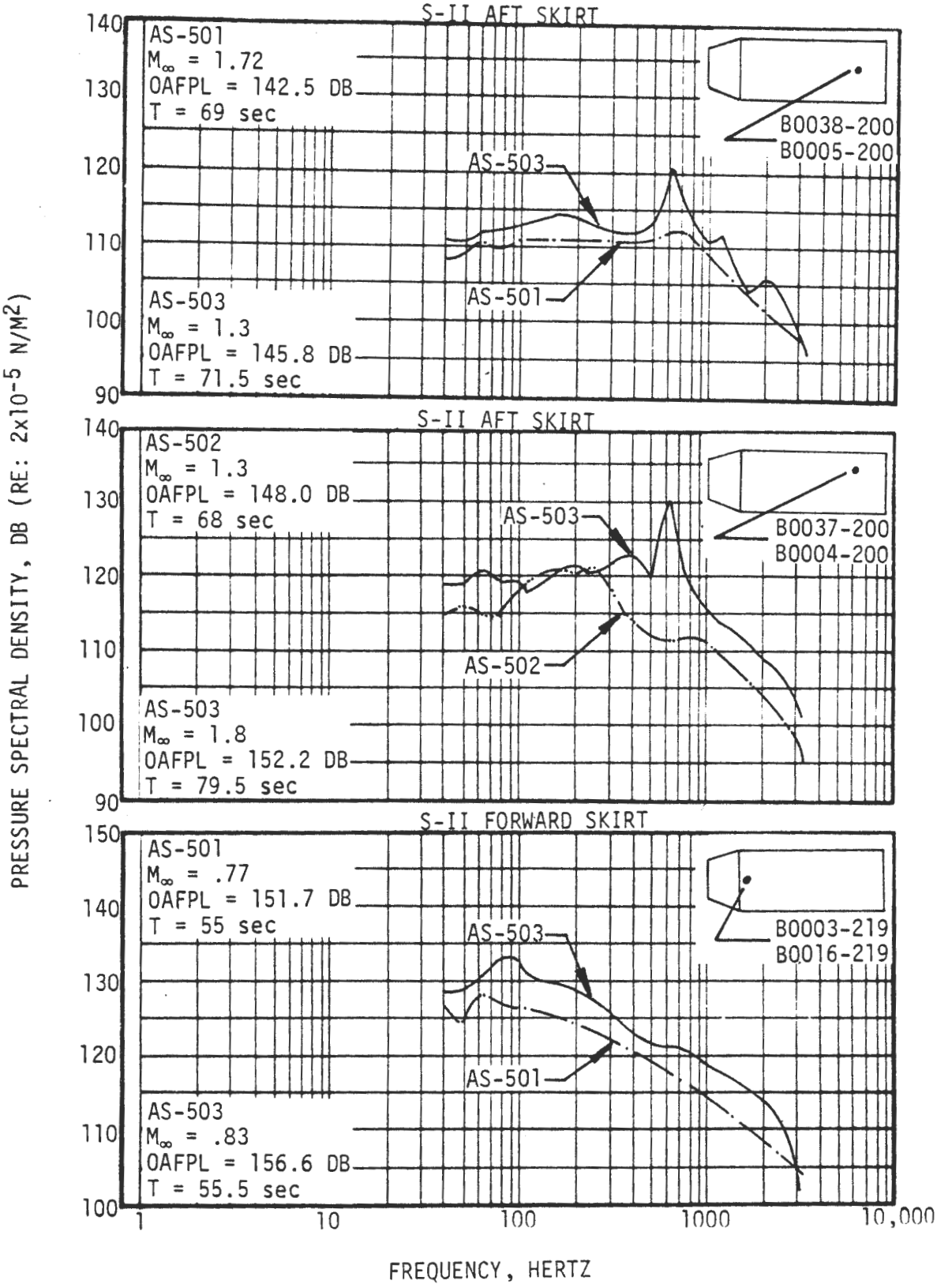

FIGURE 3-5. SATURN V EXTERNAL FLUCTUATING PRESSURE SPECTRAL DENSITIES (CONTINUED ON NEXT PAGE)

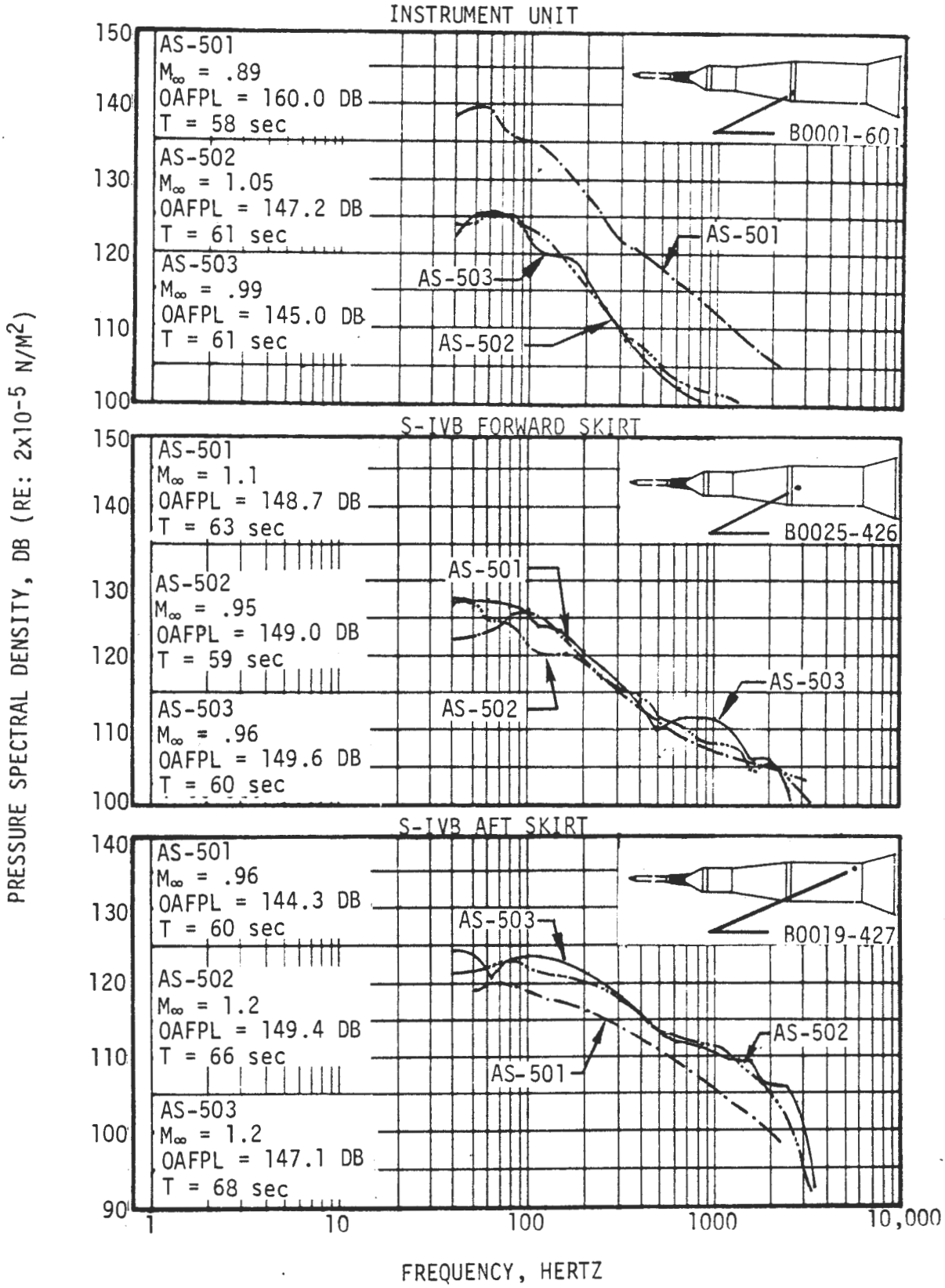

FIGURE 3-5. SATURN V EXTERNAL FLUCTUATING PRESSURE SPECTRAL DENSITIES (CONCLUDED)

(THIS PAGE INTENTIONALLY LEFT BLANK)

SECTION 4

BASE REGION ENVIRONMENTS

4.0 INTRODUCTION

This section contains the base region flight data analysis for the S-IC stage, S-II stage, and S-IVB stage of the AS-501, AS-502, and AS-503 launch vehicles. Flight-to-flight data comparisons are presented and discussions of data variations and trends are included where applicable. The total heating rates consist of radiation and convective heating. The convective heating component is based on the calorimeter wall temperature and must be corrected for wall temperature effects for application to heat shield and engine surfaces. Flight instrumentation is described and locations are given. In general, all base region thermal environments were lower than design, and heat shield and engine insulation were adequate to maintain structural temperatures below design limits.

4.1 S-IC BASE REGION

4.1.1 Flight Conditions and Base Region Flow Fields

The thermal environment of the S-IC stage base region was not influenced significantly by slight changes in the performance of the F-1 engines or by the small deflections of the engines. However, the AS-501 S-IC stage base region flow deflectors and the two degree outboard cant of the AS-503 S-IC stage control engines did affect the thermal environment. The base region thermal environment was a strong function of altitude. Variations in the flight time-altitude histories during S-IC boost appreciably changed the time and magnitude of peak values of heating rates, gas temperatures, and static pressures. Consequently, the S-IC base region environments are presented as a function of altitude. The trajectories have previously been discussed in Section 2.0.

During liftoff, the flow fields near the base region were erratic due to the disrupting influence of the launch complex. The Saturn V AS-501 sea level flow field is shown in Figure 4-1. The reflected flame resulting from the F-1 engine exhaust being turned by the trench flame deflector and the steam resulting from the flame and LUT water quench influenced the base and engine environment until the vehicle cleared the launch complex.

Afterburning of exhaust gases was clearly evident in flight tracking films at the lower altitudes for all three vehicles. Dark fuel-rich exhaust gases were noted at the F-1 nozzle exit plane followed by a flame front approximately three-fourths of a nozzle diameter downstream. Radiation from these high temperature exhaust plumes was the major contributor to the thermal environment during the early part of flight. Exhaust gas recirculation was noted on the engine nozzle extensions.

4.1.1 (Continued)

As altitude increases, the exhaust plumes expanded until they interacted with each other. The plume photograph at 108 seconds (29 KM) of Figure 4-2 illustrates this expansion. The exhaust plume interactions created high pressure regions in the exhaust flow field, forcing low energy exhaust gases forward into the base region. It was noted in the review of flight film that the plumes remain highly luminous until 25 to 28 KM of altitude. A gradual graying of the plumes was then observed from 28 to 40 KM of altitude, and the plumes were totally gray and virtually indistinguishable from 40 KM to the end of S-IC stage boost.

Exhaust flow reversal was not clearly indicated by pressure probes located in the S-IC base region of AS-501, AS-502, or AS-503. Neither the pitot pressure probes located on the three vehicles nor the pitot-static pressure probes located on AS-503 indicated significant changes in flow directions or velocities. Refer to Tables 4-I and 4-II for a description of the location of these instruments.

Television cameras were mounted on the S-IC heat shield of AS-502 and AS-503 vehicles. The flow field visualization provided by the TV cameras were extremely important because of the correlations which were possible with flight data from the heat shield and engine instrumentation. A comparison of AS-503 heat shield radiation heating rates and events observed by the base region TV cameras is presented in Figure 4-3. The TV camera data showed recirculated gases were first present in the base region near the heat shield at 12.2 kilometers for AS-502 and at 12.7 kilometers for AS-503. The recirculated exhaust flow appeared fully established at 18.5 and 20.1 kilometers for AS-502 and AS-503, respectively. The arrival of recirculated gases in the base area was accompanied by radiation increases on all base and engine calorimeters.

The flight data and TV data also showed that flow field changes occurred at center engine cutoff. Center engine cutoff was characterized by a momentary brightening of the base area. The effects of center engine cutoff on base heating levels are described in Paragraphs 4.1.3 and 4.1.4.

4.1.2 Instrumentation

Thermal environment measurements were made in the S-IC stage base region by instruments located on the base heat shield, engines, and fin trailing edge. The S-IC stage base configuration is shown in Figure 4-4.

4.1.2 (Continued)

The S-IC base heat shield thermal instrumentation consisted of radiation calorimeters, total calorimeters, and gas temperature probes. The instruments were located on the heat shield as shown in Figures 4-5 and 4-6. These instruments are described and summarized in Table 4-I. Base heat shield pressure instrumentation consisted of static pressure taps, pitot-static pressure probes, and differential pressure gages. The pitot-static pressure probe locations are shown in Figure 4-7 and are also described and summarized in Table 4-I. The remaining S-IC base heat shield pressure instrumentation are discussed in Section 2.

The total and radiation calorimeter sensing surfaces were 0.17 inches and 0.55 inches in diameter, respectively. They were mounted such that the sensing surfaces of the total calorimeters and the sapphire windows of the radiation calorimeters were flush with the heat shield surface. The calorimeters were asymptotic instruments which maintain a low wall temperature. These calorimeters are discussed in more detail in References 1 through 3. The instrument temperatures were monitored at the sensing surface edge during flight. An "effective" sensing surface temperature, which is used with the indicated heating rate, was determined by techniques discussed in Reference 1.

The heat shield gas temperature probes consisted of a platinum-platinum rhodium thermocouple with a 0.25 inch diameter molybdenum single shield. Gases were admitted to the sensing surface through four equally spaced openings facing parallel to the heat shield. Gas temperature probe installations were used with the sensing surface mounted at distances aft of the heat shield surface of 0.25, 0.50, 1.00, and 2.50 inches. Typical heat shield instrumentation installations are shown in Figure 4-8.

The F-1 engine instrumentation consisted of radiation calorimeters, total calorimeters, gas temperature probes, static pressure taps and pitot-static pressure probes. The instruments were located on the engines as shown in Figures 4-9 through 4-14 and are described and summarized in Table 4-II.

Each F-1 engine was enclosed in an insulated "cocoon" which consisted of fibrous silica insulation enclosed in inconel foil, except for the nozzle extension which was insulated by wire-reinforced asbestos. The center engine with the insulation "cocoon" installed is shown in Figure 4-15. Engine instrumentation protruded above the surfaces of the engine and the cocoon insulation was contoured to enclose the transducers and fitted flush with the sensing surfaces of the instruments. Typical engine instrumentation installation is shown in Figure 4-16. The engine calorimeters were of the same type as that used on the heat shield. The engine gas temperature probes consisted of a platinum-platinum rhodium thermocouple enclosed in a double platinum shield. Gases were admitted to the thermocouple through offset openings in both the inner and outer shields.

4.1.2 (Continued)

The raw data used in the aerothermodynamic analysis of the S-IC stage were transmitted on PAM/FM/FM and PCM/FM telemetry channels. The majority of the data were transmitted on PAM/FM/FM. The data were sampled 12 times per second for both telemetry channels. Boeing/Michoud calibrated, time edited and interpolated the raw data to 10 samples per second (SPS). Boeing/Huntsville edited the 10 SPS raw data when required and reworked some of the data dropout line fills. The data edit routine replaced data values which differed more than 2.5 standard deviations from the data set. The edited data were then filtered with a low band pass filter. The means of the data were preserved during the filtering process. Typical S-IC base region flight data before and after conditioning is shown in Figure 4-17.

4.1.3 S-IC Heat Shield Thermal Environment

The S-IC heat shield thermal environments monitored during all three flights were lower than design limits. The AS-501 vehicle which had base flow deflectors experienced a significantly less severe environment than AS-502 and AS-503. The flow deflectors were removed from these vehicles. The AS-503 S-IC stage outboard engines were canted two degrees outboard and produced only slight differences in the base heat shield environment from that monitored on AS-502. A sudden increase followed by a sharp decrease in the environment was noted at inboard engine cutoff (IECO) for all these flights. The stable environment following IECO had approximately the same magnitudes and trends as the environment before IECO. The heating environment was principally radiation with peak heating rates occurring at approximately 30 kilometers for AS-501 and approximately 21 kilometers for AS-502 and AS-503.

Radiation heating rates monitored on the heat shield are presented in Figures 4-18 through 4-21. Radiation heating to the heat shield showed a characteristic middle altitude "hump" on all flights. A similar "hump" was noted on the Saturn I and IB flights. Typical radiation data from Saturn I are compared with AS-501 heat shield radiation flight data in Figure 4-22. The radiation "hump" is believed to be caused by hot exhaust gases recirculating into the base region.

Gas temperatures measured on the S-IC heat shield are shown in Figures 4-18 through 4-20. The delay in the initial rise in radiation and the slightly lower peak values recorded on AS-503, when compared with AS-502, is also evident in the heat shield gas temperature data in the inboard locations. This effect is attributed to the outboard engine cant on AS-503, which delayed the altitude of initial plume impingement and allowed cooler gases to be recirculated around the center engine. Gas temperatures near the periphery of the base heat shield were not greatly affected by the 2 degree cant and were in close agreement with AS-502 flight data.

4.1.3 (Continued)

As noted on previous flights and seen in Figure 4-23, large gradients exist in gas temperature with distance off the heat shield surface. However, gas temperatures are approximately the same at the base locations shown in Figure 4-23 when the probe distances off the heat shield are similar.

The total heating environment monitored on all flights are shown in Figures 4-18 through 4-21. The principal component of total heating was radiation and the shapes and trends of the total calorimeter data are similar to those previously discussed for radiation heating. Removal of the base region flow deflectors and the 2° outboard engine cant had approximately the same effect upon the total heating environment as upon the radiation environment previously discussed. Total and radiation heating was approximately the same at all heat shield locations along a radial line between engines as seen in Figure 4-24.

Total heating and gas temperature data on the heat shield between an outboard engine and engine fairing, and on the fairing near the heat shield are shown in Figures 4-25 and 4-26. The environment in these areas are less severe than that recorded along a radial line between engines. These areas were not significantly influenced by the 2° engine cant, but were slightly affected by the removal of the flow deflectors.

The total heating rate measured on the base of Fin D is shown in Figure 4-27. It is evident that fin total heating measurements for all three flights are approximately the same. The initial rise in heating occurs at 15 kilometers which correlates with the recirculated exhaust gases reaching the heat shield as observed by TV cameras. The second rise in the total heating environment occurs shortly after flow separation is first observed on all three vehicles. Boundary layer flow separation is discussed in Section 6.

Flight data and TV data show that base region flow field changes occur at inboard engine cutoff (IECO). A spike in the calorimeter and gas temperature data is coincident with a momentary brightening in the base region observed by the TV camera coverage. This brightening is probably caused by the high concentration of residual exhaust products and carbon particles from the center engine residual fuel which could raise the emissivity of the base gases and therefore the radiation. As the residual exhaust products are depleted, a reduction in emissivity and radiation would occur. The magnitudes and duration of the data spikes were approximately the same for all three flights, although IECO occurs at different flight times and significantly different altitudes for each flight. IECO occurred at 135.5 seconds (49.64 kilometers), 144.72 seconds (56.07 kilometers), and 125.88 seconds (41.5 kilometers) on flights AS-501, AS-502, and AS-503, respectively. Typical S-IC heat shield environment during IECO is shown in Figure 4-28. A detailed discussion of this phenomena is presented in Reference 3.

4.1.3 (Continued)

On several heat shield panels both the radiation and total calorimeters as well as gas temperature probes were installed at approximately the same location. A complete analysis of the individual components of the thermal environment can be made with flight data obtained at these locations. Typical AS-503 flight data of this type showing radiation and total heating rates plus gas temperatures and calorimeter wall temperatures at one heat shield location are shown in Figure 4-29. During the first 40 seconds of boost, the radiation and total calorimeters on the heat shield recorded nearly equal heating rates with a general trend of radiation data slightly exceeding the total heating data. This heating rate comparison indicates a small convective cooling rate to the calorimeter. The comparison of gas temperature and calorimeter temperature during this same period of flight shows that the gas temperature is higher than the calorimeter body temperature and a small convective heating rate would be expected. At approximately 40 seconds, a sudden rise in both radiation and total heating occurs which is then followed by a gradual decrease in radiation heating and a sharp reduction in total heating to 70 seconds. The decrease in radiation heating is about as expected since slight pressure amd emissivity decreases occur in the plumes which would gradually reduce radiation. The response of the total calorimeters is much more difficult to explain. It should be noted that the data dropoff is not a unique phenomena to instrument C26-106. It was repeated at other total calorimeters on AS-503, and was evident to a lesser degree of flights AS-501 and AS-502. A comparison of gas temperature and effective calorimeter temperature indicates that a slight convective heating potential existed from 40 to 70 seconds. However, the effective calorimeter temperature drops to the value of the calorimeter body temperature indicating that the sensor was suddenly cooled during this time period. This phenomena is presently unexplainable.

The S-IC base heat shield pressure data are discussed in Section 2.0. Data from the pitot-static probes which face inboard and outboard on the heat shield are shown in Figure 4-30. These data are inconclusive. Noise in the transducer causes erratic readings and no discernible trends were evident. Significant velocities across the heat shield are not indicated by these data, and flow direction could not be determined.

4.1.4 F-1 Engine Thermal Environment

In general, the F-1 engine thermal environment flight data exhibited similar trends throughout flight as the S-IC heat shield data. The removal of the base region flow deflectors from AS-502 and AS-503 allowed exhaust gas recirculation to occur earlier and, consequently, the thermal environment was generally more severe. The 2 degree cant of the outboard AS-501 F-1 engines resulted in slightly reduced engine heating rates with peak heating occurring at a slightly higher altitude than AS-502.

4.1.4 (Continued)

The F-1 engine radiation heating flight data from all flights is presented in Figures 4-31 through 4-33. The characteristic middle altitude heating "hump" is evident on the engines as on the heat shield. The heating spike during IECO is also noted on the engines. As can be seen from these figures, radiation heating rates begin to increase at approximately 10 kilometers with peak values occurring at approximately 20 kilometers. Variations are noted in radiation heating to the engines between the exit plane and heat shield.

Gas temperatures measured at approximately the same locations as the radiation calorimeters are shown in Figures 4-31 and 4-32. In general, the engine gas temperatures are higher than the heat shield gas temperatures and correlate with the rise in engine radiation heating for all flights. Gas temperatures monitored at other engine locations are presented in Figures 4-34 through 4-38.

The total heating environments monitored on all three flights are shown in Figures 4-31 through 4-42. The AS-501 engine thermal environment was less severe than AS-502 and AS-503 as a result of the base region flow deflectors. The 2° cant on the AS-503 F-1 engines resulted in the AS-503 heating rates peaking later in flight and at slightly lower magnitudes than on AS-502. In general, the variations in engine total heating rates can be correlated with the engine gas temperatures and radiation heating rates.

Flight-to-flight comparisons of total heating at the engine exit plane are restricted because of erroneous data obtained on AS-503 at instrument C14-101. This instrument, located on engine No. 1 facing the center engine, measured a total heating rate which was approximately two times the rate measured at this location during AS-501 and AS-502 flights. Data from the radiation calorimeter and gas temperature probe at the same engine location did not deviate significantly from the AS-502 flight data indicating that instrument C14-101 gave erroneous readings for AS-503.

Total heating data measured at approximately the same station location and in the same plane drawn through three engines are shown in Figure 4-43. The data are in good agreement and indicate nearly symmetric flow in the base area. Good agreement was also noted for AS-501 and AS-502 flight data.

The effect on engine thermal environment at IECO is similar to that previously discussed for the heat shield. The comparison of AS-503 radiation and total heating rate data, and nearby gas temperature data is shown in Figure 4-44. After the four second spike, radiation heating returned to the same magnitude as before IECO and continued to decrease slightly through the remainder of boost. Gas temperature, although not measured at the same location as the radiation and total calorimeter, had a slight spike and continued to rise slightly throughout boost. Total heating had a spike from 3 to 15 watts/cm^2 of which 3 to 6 watts/cm^2 are

4.1.4 (Continued)

convection, and did not return to the same trend or magnitude after IECO as had been recorded prior to IECO. Instead, total heating became approximately constant at a value of 3 watts/cm^2 greater than the radiation rate.

Flight data from AS-503 which illustrates convective heating to the F-1 engines is shown in Figure 4-45. Radiation and total heating rates are identical through the first 30 seconds of flight. Gas temperature and calorimeter temperature are also identical through this time period. Aspirated air is flowing over the engine at this time and convective heating is essentially zero. As hot gas began to recirculate into the base region and flow over the engine surface, total heating rates increase above radiation. The gas temperature increases steadily as recirculation increases. During this rise in gas temperature from 30 to 80 seconds, a convective heating rate of approximately 4 watts/cm^2 is experienced at the inboard engine total calorimeter. Maximum total heating occurs at the engine location shown in this figure at 83 seconds.

The gas temperature continues to increase but at a reduced rate after 90 seconds. Due to questionable radiation data between 85 and 105 seconds, a definitive statement concerning convective heating through this period of time is not possible. Convective heating spikes at IECO, and is approximately constant at 3 watts/cm^2 from IECO to the end of boost.

F-1 engine pressure data are shown in Figures 4-46 through 4-49. Data from the AS-503 pitot-static probes which face forward and aft on the center engine are shown in Figure 4-46. As with similar heat shield data, the pitot-static probes gave readings of such low magnitude that flow velocity determinations from the data are difficult.

Engine pressure minus ambient pressure, measured near the exit plane on both the center and an outboard engine are shown in Figure 4-47 for all three flights. Axial variation in engine pressure, between the exit plane and the manifold of the inboard and outboard surfaces of the outboard engine, are shown in Figures 4-48 and 4-49. The exit plane pressures began to exceed ambient pressure at 8 to 10 kilometers on both the inboard and outboard surfaces. In general, the pressure readings nearer the heat shield began to exceed ambient at a higher altitude than the instruments near the exit plane.

4.2 S-II BASE REGION

4.2.1 Flight Conditions

The S-II base region thermal environment was strongly influenced by the performance of the five J-2 engines, i.e., propellant mixture ratio, chamber pressure, combustion temperature and engine gimballing, and essentially

4.2.1 (Continued)

independent of altitude or trajectory variations. A complete description of these engine parameters and their effect on the base region thermal environment is presented in References 4 through 9.

In general, the S-II base region thermal environment was significantly affected by two programmed events during S-II stage boost. These events are S-IC/S-II second plane separation and the J-2 engine programmed mixture ratio (PMR) stepdown which provides for minimum propellant residual at S-II flight termination. Range times for these events on each flight are shown below.

EVENT	TIME - SECONDS		
	AS-501	AS-502	AS-503
S-II Ignition	152.14	149.76	155.19
S-IC/S-II Second Plane Separation	181.44	179.06	184.47
PMR Stepdown	429.14	490.76	443.45
S-II Cutoff	519.76	576.33	524.04

After second plane separation, the flow field in the base region was changed significantly. The heating rates and gas temperatures monitored on the thrust structure and in the engine compartment were reduced sharply. However, the heat shield heating rates and gas temperatures were approximately the same as before separation. Static pressure throughout the base region was also reduced after separation.

The J-2 PMR stepdown (from approximately 5.5 to 4.5) altered the base region flow field and its thermodynamic properties. Generally this PMR stepdown reduced the thermal environment throughout the base region. The base pressures were also reduced but this reduction was counteracted by engine gimballing effects.

During AS-502 S-II flight, a sudden performance shift was noted on Engine 2 by thrust decreasing at 319 seconds. The engine continued performance at a reduced level until 412.3 seconds. By 412.9 seconds, the dropout of thrust OK switches indicated Engine 2 cutoff, and at 414.2 seconds Engine 3 also cut off. Consequently, a longer S-II burn time was necessitated. A complete description of these engine anomalies is presented in Reference 5. In general, the base region thermal environment was reduced after Engine 2 and 3 cutoff. However, the heat shield area between Engine 1 and 4 experiences a more severe environment. All static pressure measurements recorded a pressure spike during this time, but returned to near nominal or reduced pressures later in flight.

4.2.2 Instrumentation

Thermal environment measurements were made in the S-II stage base region by instruments located on the heat shield, heat shield curtains, and thrust cone as well as in the engine compartment. Flight data from typical instruments were chosen for presentation.

The S-II heat shield thermal environment instruments consisted of radiation calorimeters, total calorimeters, and gas temperature probes. The S-II stage instrumentation is discussed in References 7 through 9. The instruments chosen for data presentation were located as shown in Figure 4-50. These instruments are described and summarized in Table 4-III. The base heat shield surface pressures were monitored by static pressure probes as located in Figure 4-51. These pressure probes are also described and summarized in Table 4-III.

The thermal environment of the S-II thrust cone engine compartment and S-II engine curtains were monitored by radiation calorimeters, total calorimeters, and gas temperature probes. The location of these instruments are shown in Figures 4-52 and 4-53. These instruments are described and summarized in Table 4-IV. Static pressure was monitored on the S-II thrust cone by one pressure probe as located in Figure 4-52. This instrument is also described in Table 4-IV.

4.2.3 Heat Shield Thermal Environment

The S-II base region thermal environment was, in general, below design data and good agreement between AS-501, AS-502, and AS-503 flight data was experienced. Good agreement was also obtained with post-flight predictions as presented in References 4 through 9.

During S-IC/S-II second plane separation, a momentary increase in the thermal environment was noted in the base region on all three flights. This increase was caused by exhaust plume impingement on the interstage which resulted in a higher reverse mass flow rate, increased pressures and gas temperatures, and hence higher heating rates. Environment increases during separation (184.47 seconds) are depicted in Figure 4-54 for the AS-503 flight. These increases are typical of all three flights. Since these expected environment changes are present only for a short period of time and result from an unsteady flow field, these data spikes have not been included in S-II flight data comparisons. However, these environments are available in References 4 through 9.

The radiation heating rates monitored on the aft surface of the heat shield are shown in Figure 4-55 for the three flights. Good agreement of steady state values is noted from flight to flight. This figure shows that the flight radiative heating rates take a relatively long time to reach a steady state value. This trend is discussed in detail in References 7 through 9.

4.2.3 (Continued)

An appreciable drop in radiation occurs in the vicinity of Engine 2 at the time of Engine 2 shutdown, whereas the calorimeter located between Engines 1 and 4 shows an abrupt decrease followed by a steady rise until PMR stepdown. This rise is probably caused by the engines gimballing approximately 6 degrees outboard at that time.

It should be noted that the radiation heating rates presented in Figures 4-55 and 4-59 have been corrected for the calorimeter view angle.

The total heating rates monitored on the aft surface of the heat shield are shown in Figure 4-56 for the three flights. These figures indicate that the total heating rates are nearly independent of altitude and that the S-IC/S-II interstage has no appreciable effects on the base heat shield heating rates. The heating rates shown have not been normalized to a cold wall heating condition. However, the normalized heating rates are only slightly higher than the flight data because of the large differences between the recovery temperature and the calorimeter sensor effective temperature. These normalized heating rates are presented in References 7 through 9.

Gas temperatures were monitored on the S-II aft heat shield surface of the AS-503 vheicle only. No flight data were obtained on AS-501 or AS-502 because the gas temperature was below the transducer lower range of 1089°K (1500°F). It is noted that the indicated gas probe temperatures are not the gas recovery temperatures but the probe sensor temperatures. It was concluded in Reference 9 that although the indicated probe temperatures vary with location (due to variations of convective heating rates), the gas recovery temperatures remained essentially constant within the base region at a value of 889±56°K (1140± 100°F).

Static pressures monitored on the aft and forward surfaces of the heat shield are presented in Figure 4-57. The pressures show a pronounced drop after second plane separation. This indicates that the flow patterns in the base region change after second plane separation. The base pressures are also reduced slightly after the PMR stepdown. The inboard and outboard deflections of the J-2 control engines slightly influenced the base pressure (References 4 through 9).

The base pressures indicate a sharp spike during second plane separation when the exhaust plumes are confined by the interstage resulting in high impingement pressures and reverse mass flow rates. These spikes occur in a short time period and, consequently, have not been shown in the figures. The pressure spikes are presented in References 4 through 9.

4.2.3 (Continued)

During AS-502 flight, a pressure spike also occurred during J-2 Engine No. 2 shutdown. This sharp increase is probably the result of flow disturbances created by engine curtain curvature reversal caused by the high engine compartment pressure experienced at this time (see Figure 4-57).

The pressure monitored on the aft surface of the AS-502/S-II heat shield between outboard Engines 3 and 4 is shown in Figure 4-57. It should be noted that the abrupt pressure drop after Engine 2 and 3 shutdown indicates that there is no longer reverse-flow direct impingement in this region.

4.2.4 Thrust Cone and Engine Compartment Thermal Environment

The thermal environment monitored on the S-II thrust cone and in the engine compartment demonstrated good agreement between AS-501, AS-502, and AS-503 flights. The same general data trends discussed for the heat shield environments was experienced in these areas. The sharp increase in the environments has not been shown in the data presentation. These short term environments are presented in References 4 through 9.

The radiation heating rates monitored on the S-II thrust cone are shown in Figure 4-58 for AS-502 and AS-503. No measured value was obtained at this location during the AS-501 flight because of apparent instrument malfunction. References 7 through 9 indicate that very good agreement is obtainable between the post-flight predictions and flight data.

The total heating rates monitored on the S-II thrust cone are presented in Figures 4-58 and 4-59 for the three flights. These figures show that the total heating rates are significant only prior to second plane separation. The flight data shows a steady increase from S-II ignition to separation which indicated the thrust cone region is initially cooled by cold purge gases and mix with hot reverse flow gases, thus reducing the heat flux.

The thrust cone total calorimeters C688-708, C666-208, and C821-208 are installed five degrees off Position III toward Position IV at S-II stations 110, 133, and 156, respectively (see Figure 4-59). Post-flight predictions indicate that center calorimeter C666-208 is expected to experience the highest heating rate. This is substantiated by the AS-501 and AS-503. The AS-502 flight data, however, show that the C821-208 calorimeters indicate the maximum heating rate. This apparent discrepancy, as reported in Reference 8, could possibly be caused by flow disturbances originating from the instrumentation wiring located in the vicinity of C666-208 calorimeter.

4.2.4 (Continued)

The AS-502 flight total heating rate calorimeters indicate a gradual heating rate decrease on the thrust cone when compared to the AS-501 and AS-503 data (see Figure 4-59). This decrease begins at approximately 225 seconds flight time. Since no change of the J-2 engine deflection or performance was noted during this time in AS-502 flight, it is believed that the heating rate decrease was caused by a cryogenic leak in the base region (Reference 8).

The gas temperatures monitored on the forward surface of the J-2 engine curtains are shown in Figure 4-60 for AS-501 and AS-502. These instruments are series connected thermocouples which monitored an average temperature and were not installed on the AS-503 vehicle. The indicated gas temperatures are rapidly increasing before second plane separation. After separation, the gas temperatures decrease suddenly. Also, the AS-502 curtain gas temperatures suddenly rise at the time of Engine 2 and 3 cutoff.

The gas temperatures monitored in the J-2 engine compartment are presented in Figure 4-61 for the three flights. The gas temperatures are rapidly increasing before second plane separation which again indicates that equilibrium flow conditions were not established at that time. After separation, the gas temperatures decrease suddenly. The sudden rise of the AS-502 gas temperature is attributed to the cutoff of Engines 2 and 3.

The AS-502 engine compartment gas temperatures are similar to those for the AS-501 and AS-503 for the first 225 seconds of flight. After 225 seconds, temperature transducers located in the engine compartment showed an abnormal cooling trend which has been interpreted as indicating a cryogenic leak near Engine 2. This anomaly is verified by ambient, structural, and component temperature transducers located in the region forward of the heat shield and outboard of Engine 2 and reported in Reference 8.

The static pressure monitored on the S-II thrust cone is presented in Figure 4-62 for the three flights. After second plane separation, the pressure in the thrust cone region drops rapidly. The PMR shift has very little effect on the thrust cone region pressures.

4.3 S-IVB BASE REGION

Prior successful R&D flights of the S-IVB stage severely limited the thermal environment instrumentation in the base region. Consequently only the base region thermal environments during S-II/S-IVB staging are discussed. These environments are presented in Section 5. The S-IVB base region environments are discussed in References 4 through 6.

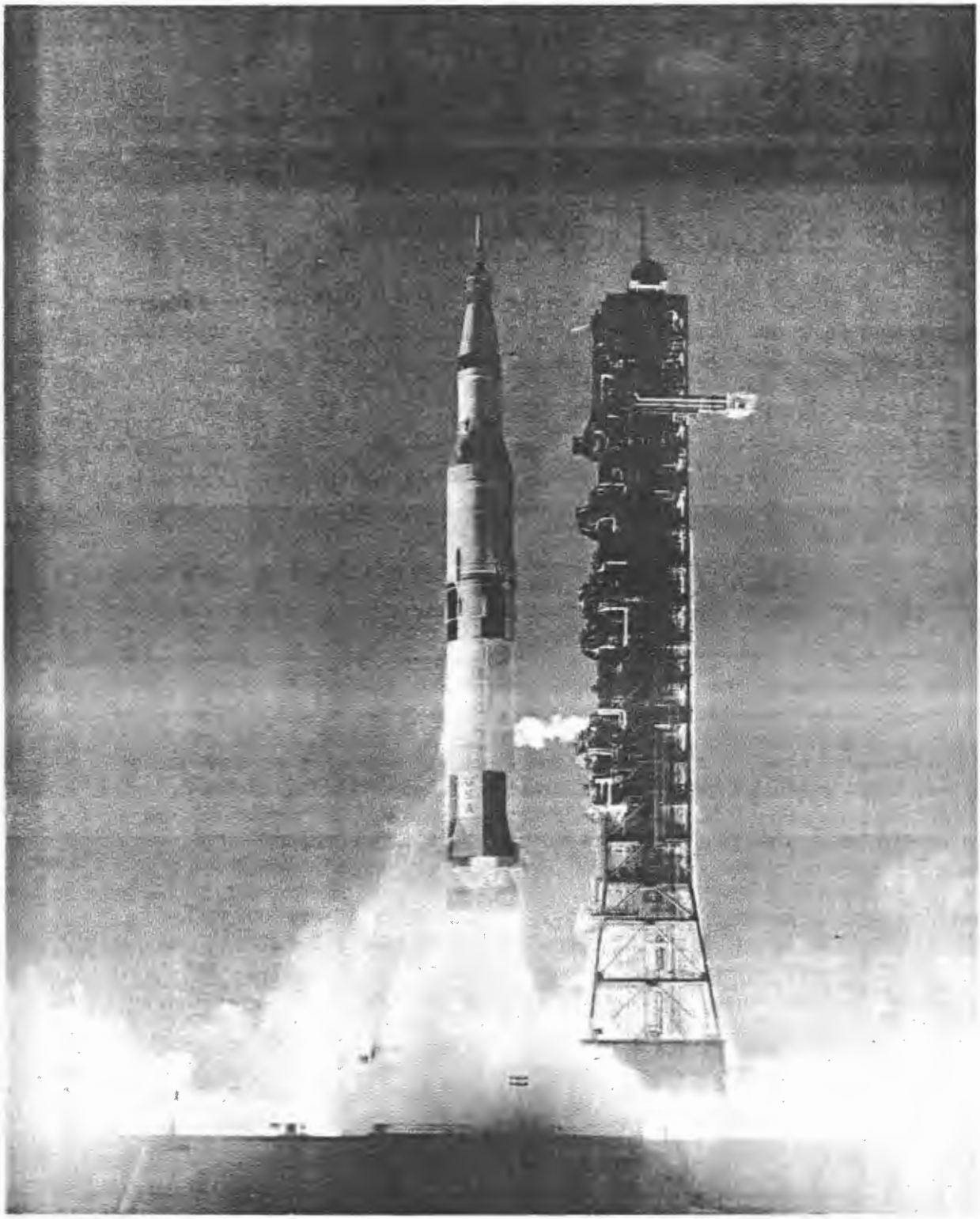

FIGURE 4-1. SATURN V SEA LEVEL EXHAUST FLOW FIELD (AS-501 LIFTOFF)

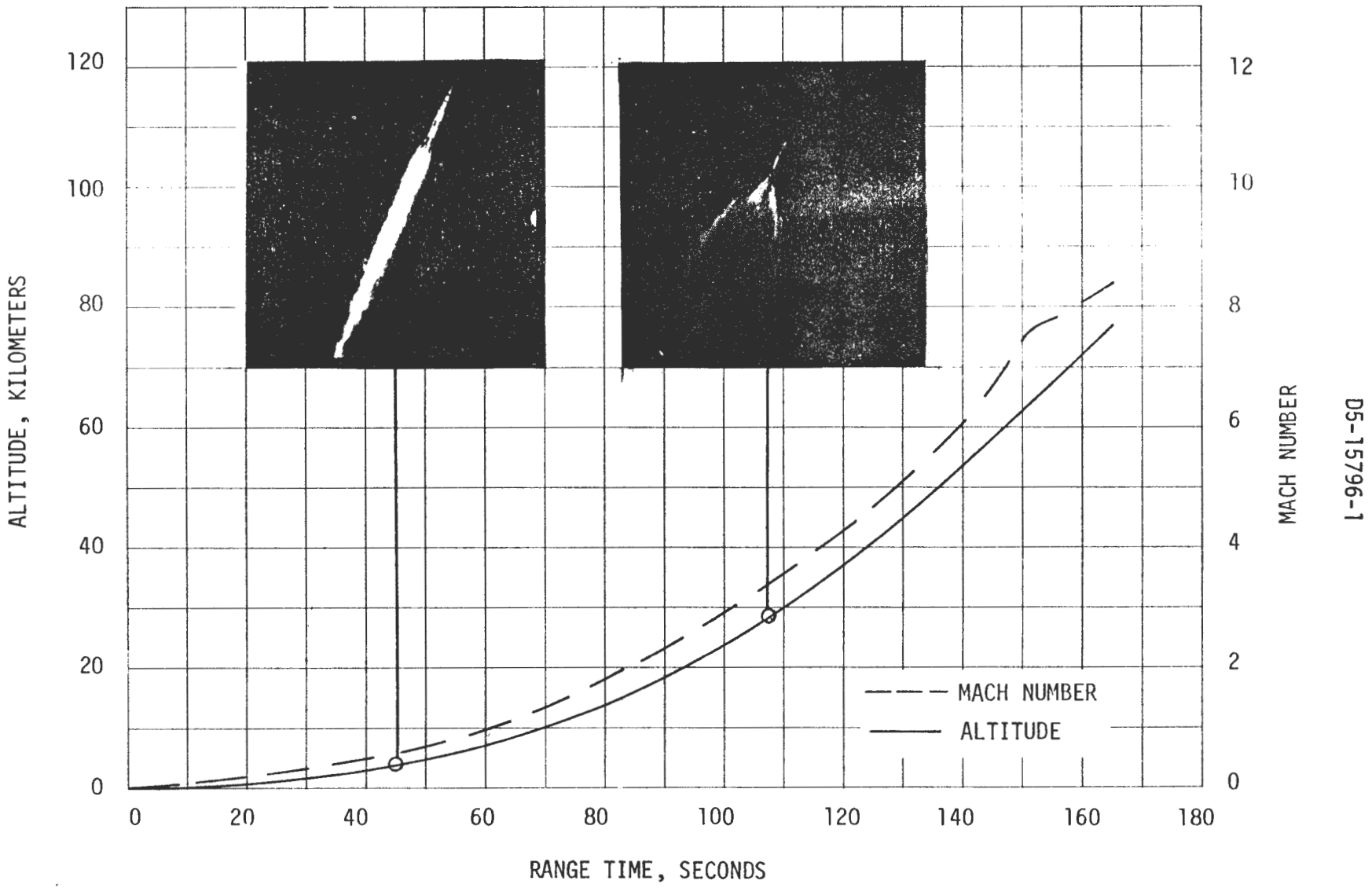

FIGURE 4-2. SATURN V PLUME EXPANSION WITH ALTITUDE (AS-501 TRAJECTORY)

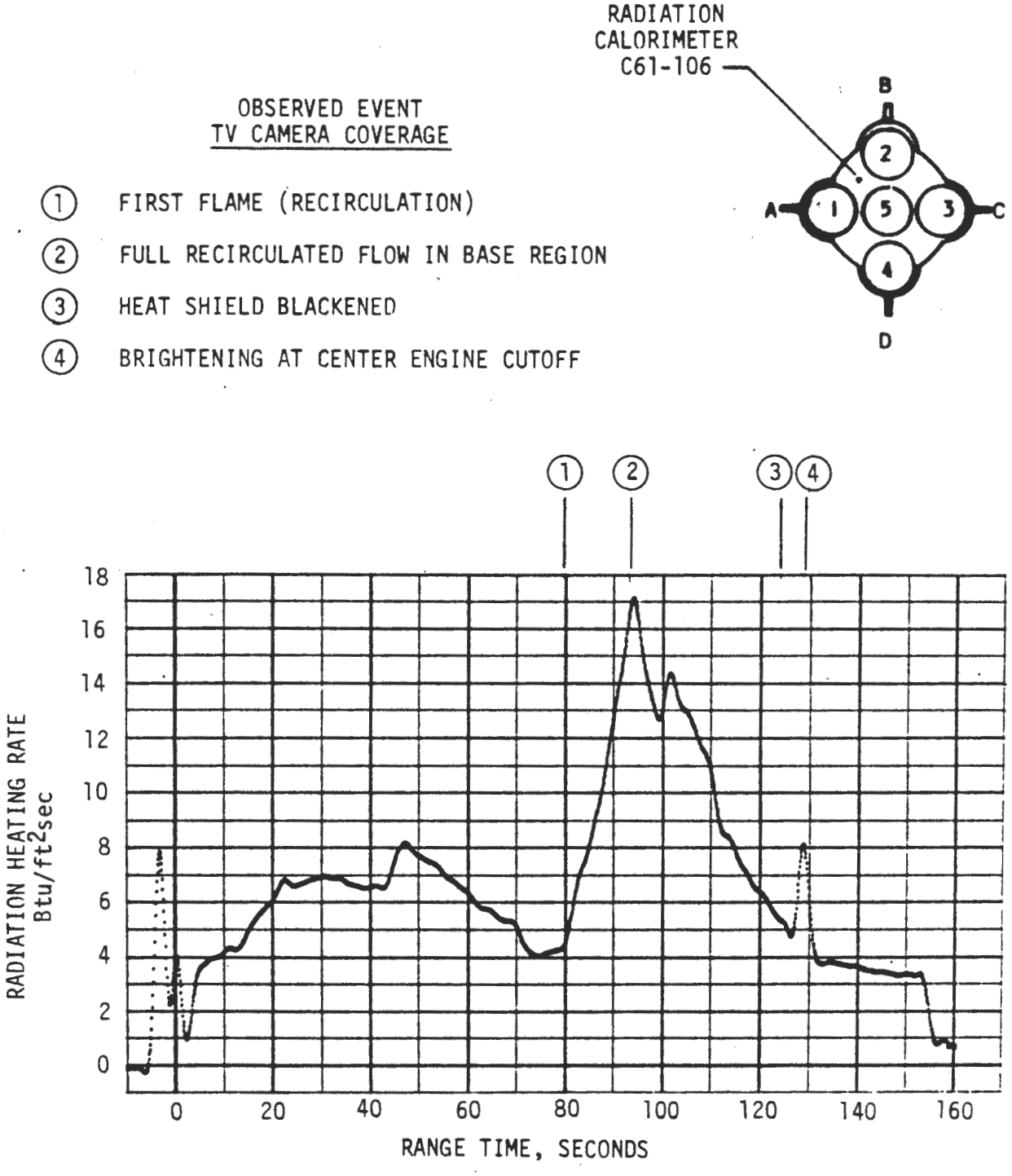

FIGURE 4-3. COMPARISON OF AS-503 HEAT SHIELD RADIATION HEATING RATES AND TV CAMERA DATA

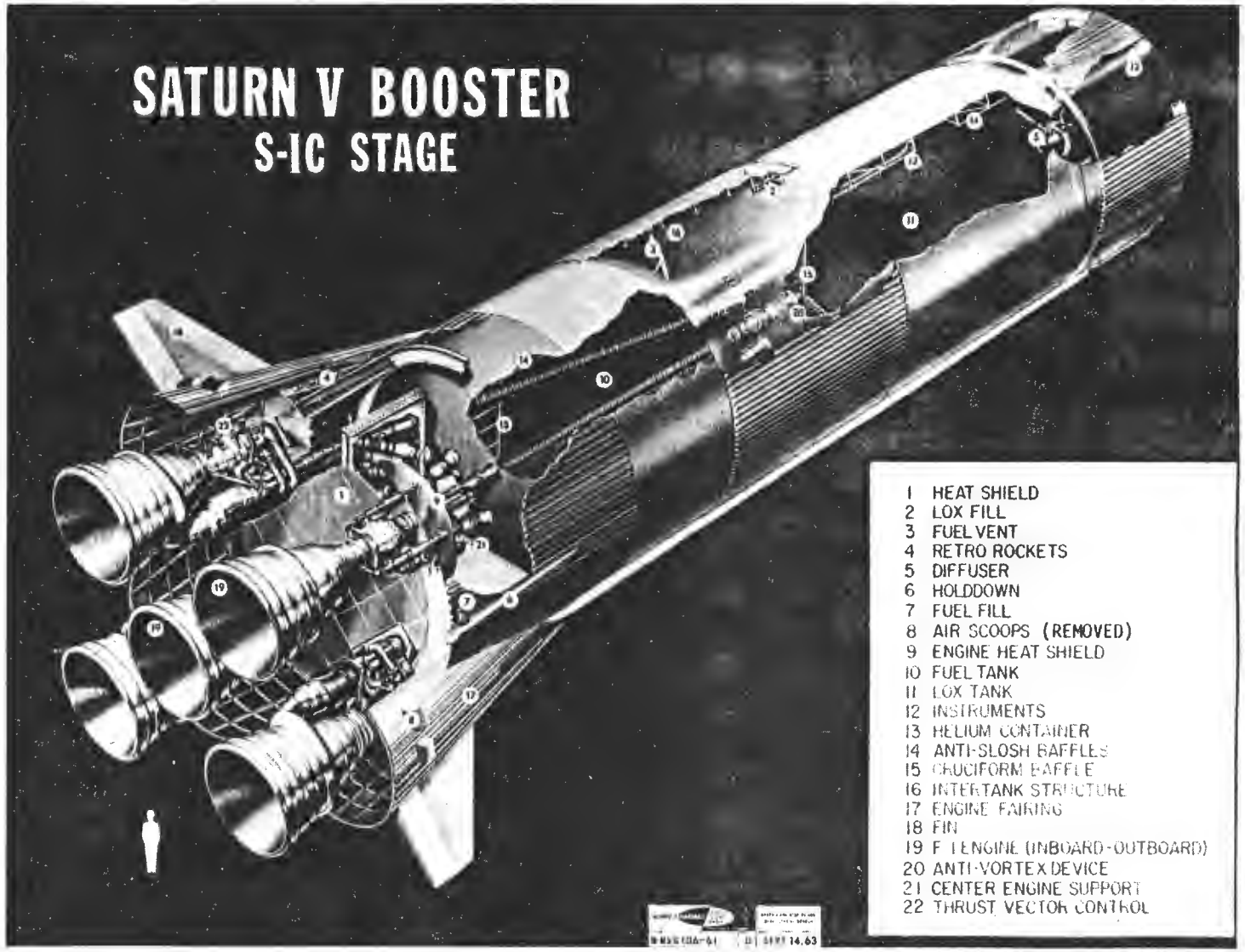

FIGURE 4-4. S-IC STAGE BASE REGION

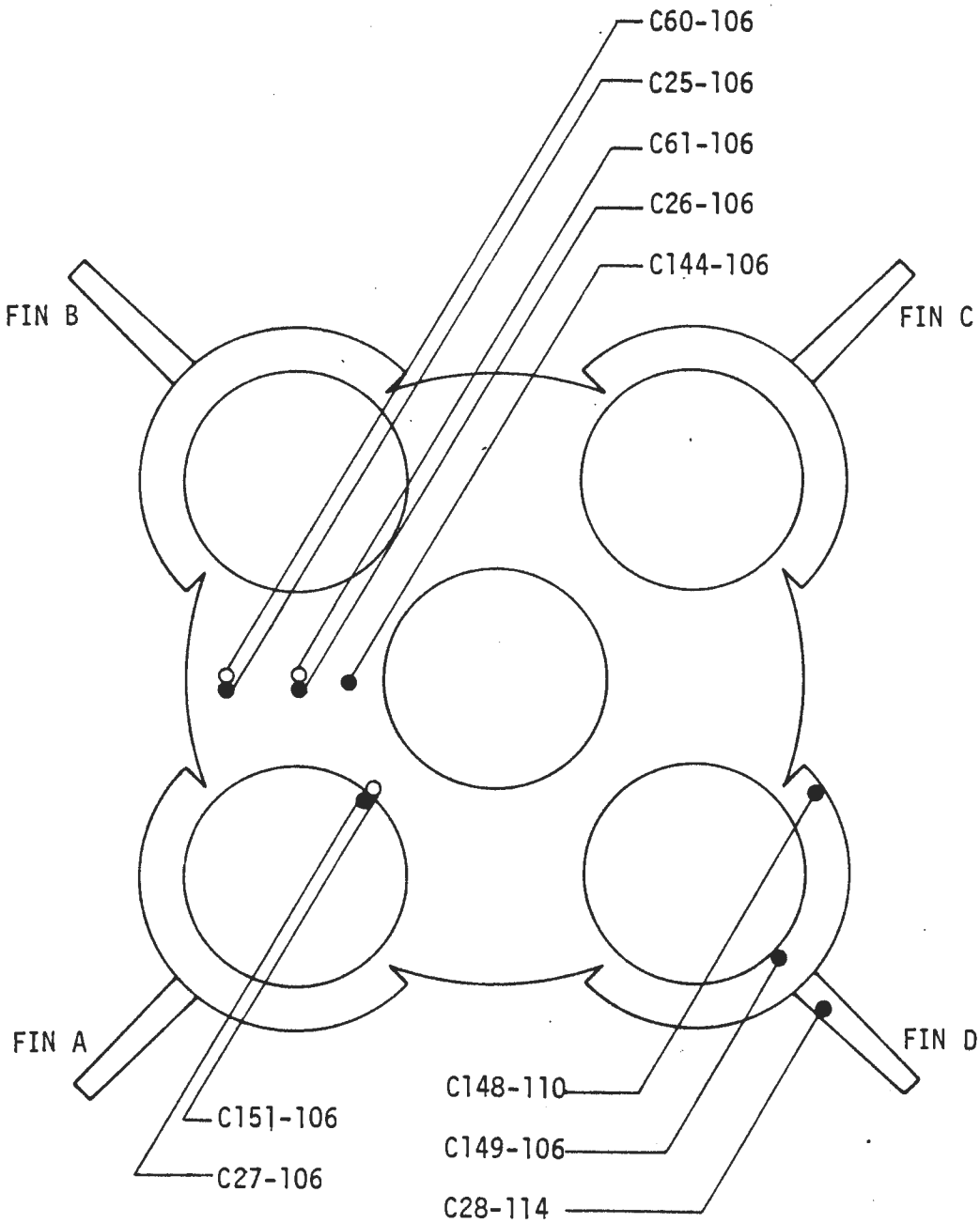

FIGURE 4-5. S-IC BASE HEAT SHIELD HEATING RATE INSTRUMENTATION

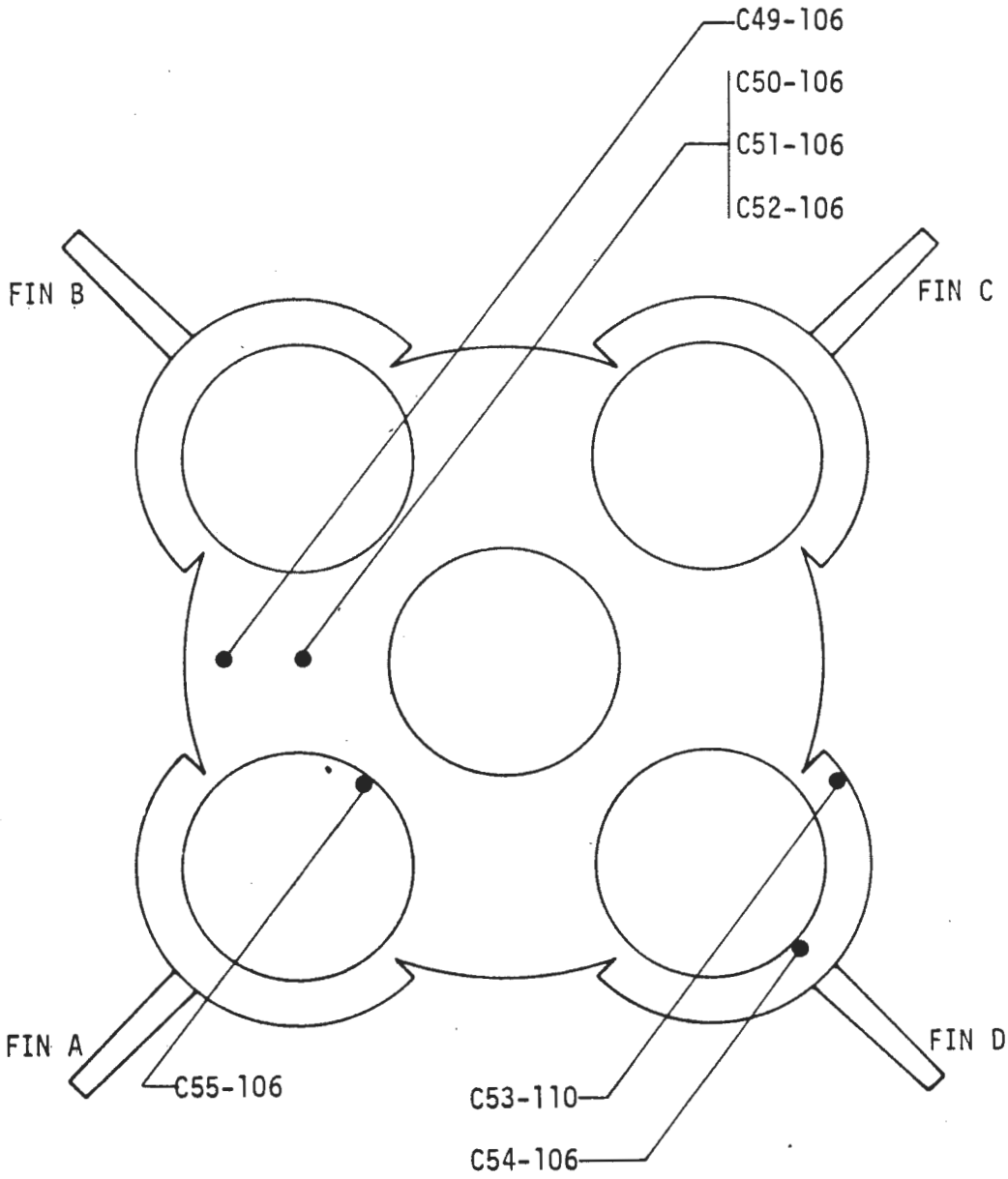

● GAS TEMPERATURE PROBE

FIGURE 4-6. S-IC BASE HEAT SHIELD GAS TEMPERATURE INSTRUMENTATION

TABLE 4-I. S-IC BASE HEAT SHIELD THERMAL ENVIRONMENT INSTRUMENTATION

(CONTINUED ON NEXT PAGE)

MEASUREMENT NUMBER	INSTRUMENT TYPE	RANGE °K	LOCATION		REMARKS
			STATION	RADIAL	
C60-106	Cal., Rad.	0-22.72*	112.0	r/R = 0.84, Pos. II	Facing Aft
C61-106	Cal., Rad.	0-22.72*	112.0	r/R = 0.61, Pos. II	Facing Aft
C151-106	Cal., Rad.	0-22.72*	112.0	r/R = 0.60, Fin A	Facing Aft
C49-106	Gas Temp.**	273-2023	112.0	r/R = 0.84, Pos. II	Mounted 0.25" Off Surface
C50-106	Gas Temp.**	273-2023	112.0	r/R = 0.61, Pos. II	Mounted 0.25" Off Surface
C51-106	Gas Temp.**	273-2023	112.0	r/R = 0.61, Pos. II	Mounted 1.0" Off Surface
C52-106	Gas Temp.**	273-2023	112.0	r/R = 0.61, Pos. II	Mounted 2.5" Off Surface
C53-110	Gas Temp.**	273-2023	97.0	r/R = 1.11 ①	Mounted 1.0" Off Surface
C54-106	Gas Temp.**	273-2023	112.0	r/R = 1.28, Fin D	Mounted 0.50" Off Surface
C55-106	Gas Temp.**	273-2023	112.0	r/R = 0.46, Fin A	Mounted 1.0" Off Surface
C25-106	Cal., Total	0-45.44*	112.0	r/R = 0.84, Pos. II	Facing Aft

① Internal Engine Fairing Fin D

* watts/cm^2

** Platinum - Platinum + 10% Rhodium Thermocouple Probe

TABLE 4-I. S-IC BASE HEAT SHIELD THERMAL ENVIRONMENT INSTRUMENTATION

(CONCLUDED)

MEASUREMENT NUMBER	INSTRUMENT TYPE	RANGE watts/cm^2	LOCATION		REMARKS
			STATION	RADIAL	
C26-106	Cal., Total	0-45.44	112.0	r/R = 0.61, Pos. II	Facing Aft
C27-106	Cal., Total	0-45.44	112.0	r/R = 0.60, Fin A	Facing Aft
C28-114	Cal., Total	0-45.44	81.0	r/R = 1.51, (1)	Facing Aft
C144-106	Cal., Total	0-56.80	112.0	r/R = 0.46, Pos. II	Facing Aft
C148-110	Cal., Total	0-45.44	97.0	r/R = 1.11, Fin C Side of Engine Fairing, Fin D (2)	Facing Engine No. 104
* D36-106	Pitot Pressure	0-13.79	112.0	r/R = 0.61, Pos. II	Facing Aft
* D39-106	Pitot Pressure	0-13.79	112.0	r/R = 0.61, Pos. II	Facing Inboard
* D40-106	Pitot Pressure	0-13.79	112.0	r/R = 0.61, Pos. II	Facing Outboard
** D168-106	Pitot-Static Pressure	0-3.45††	112.0	r/R = 0.61, Pos. II	Facing Inboard
** D169-106	Pitot-Static Pressure	0-3.45††	112.0	r/R = 0.61, Pos. II	Facing Outboard

†† N/cm^2

(1) Trailing Edge of Fin D

(2) Internal Engine Fairing Fin D

* AS-501 and AS-502

** AS-503

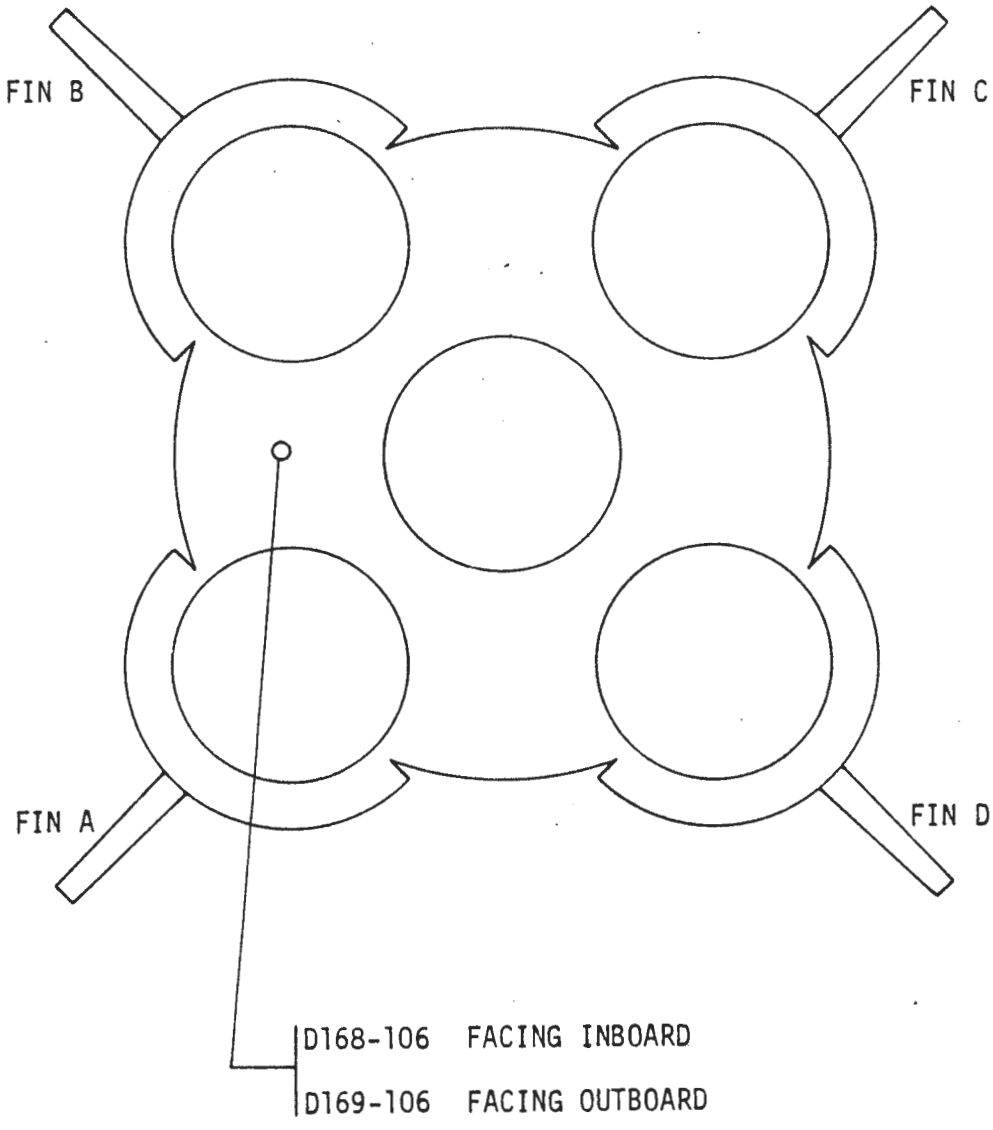

FIGURE 4-7. S-IC BASE HEAT SHIELD PRESSURE INSTRUMENTATION

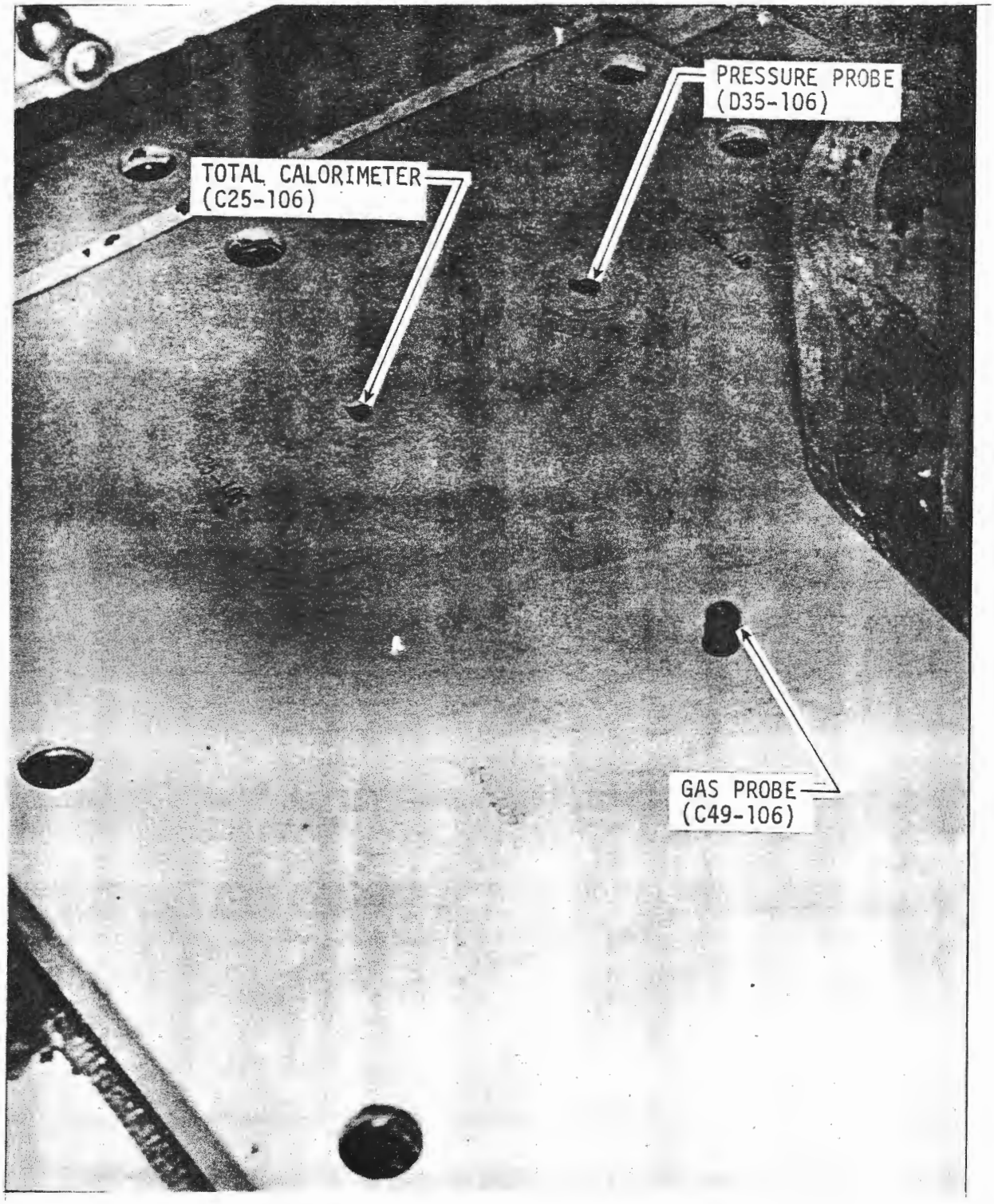

FIGURE 4-8. TYPICAL S-IC HEAT SHIELD INSTRUMENTATION INSTALLATION

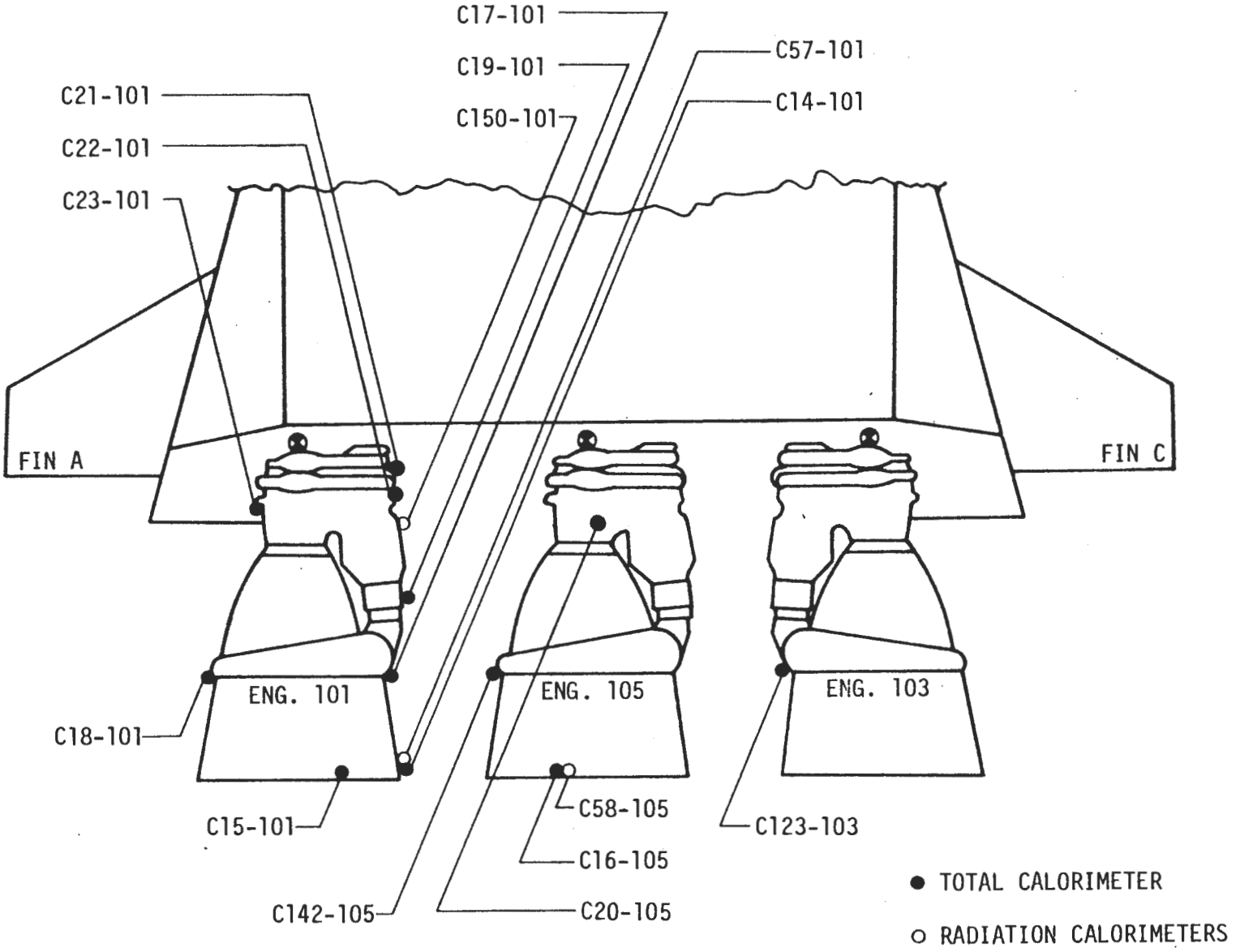

FIGURE 4-9. F-1 ENGINE HEATING RATE INSTRUMENTATION

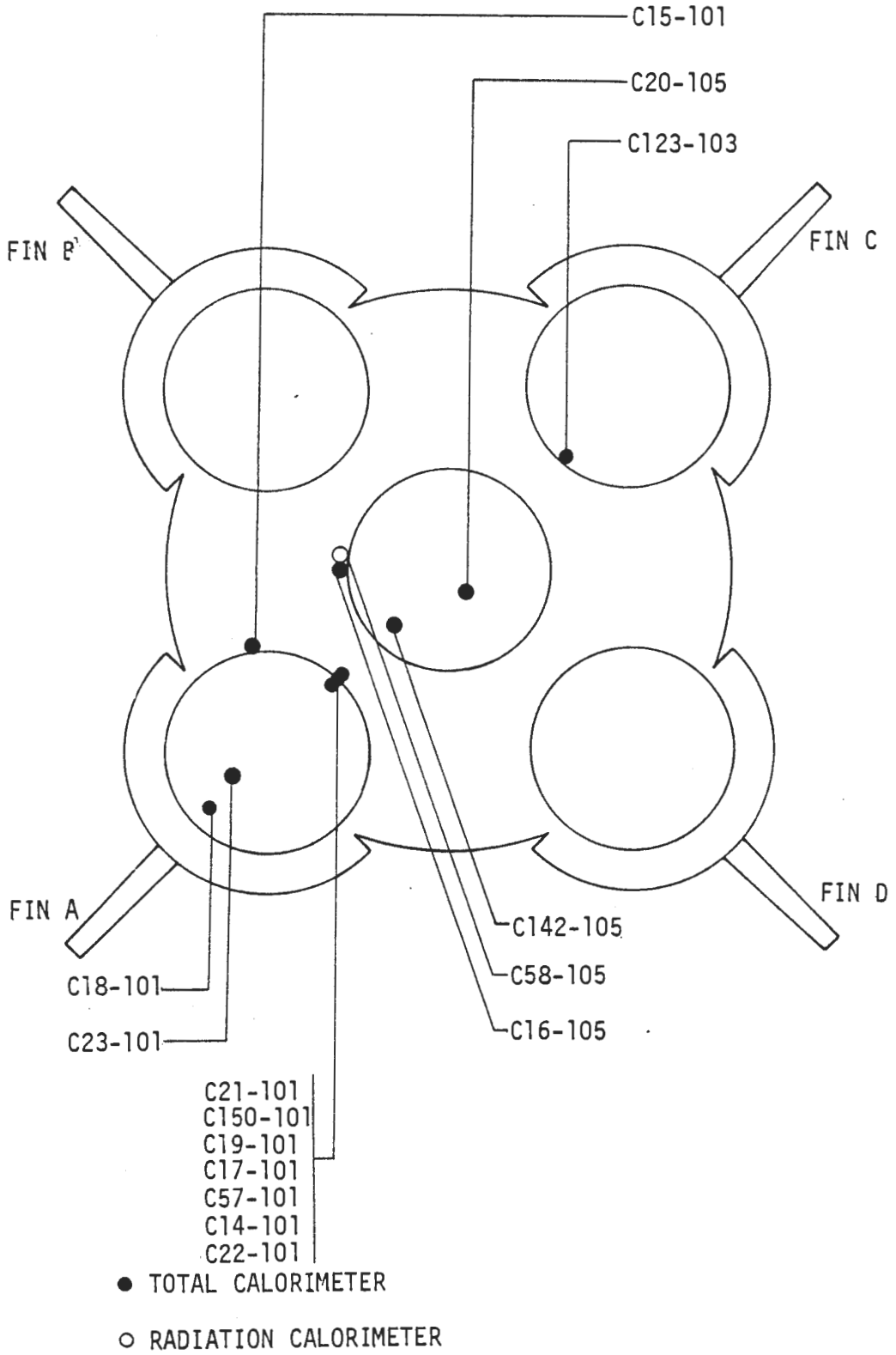

FIGURE 4-10. F-1 ENGINE HEATING RATE INSTRUMENTATION

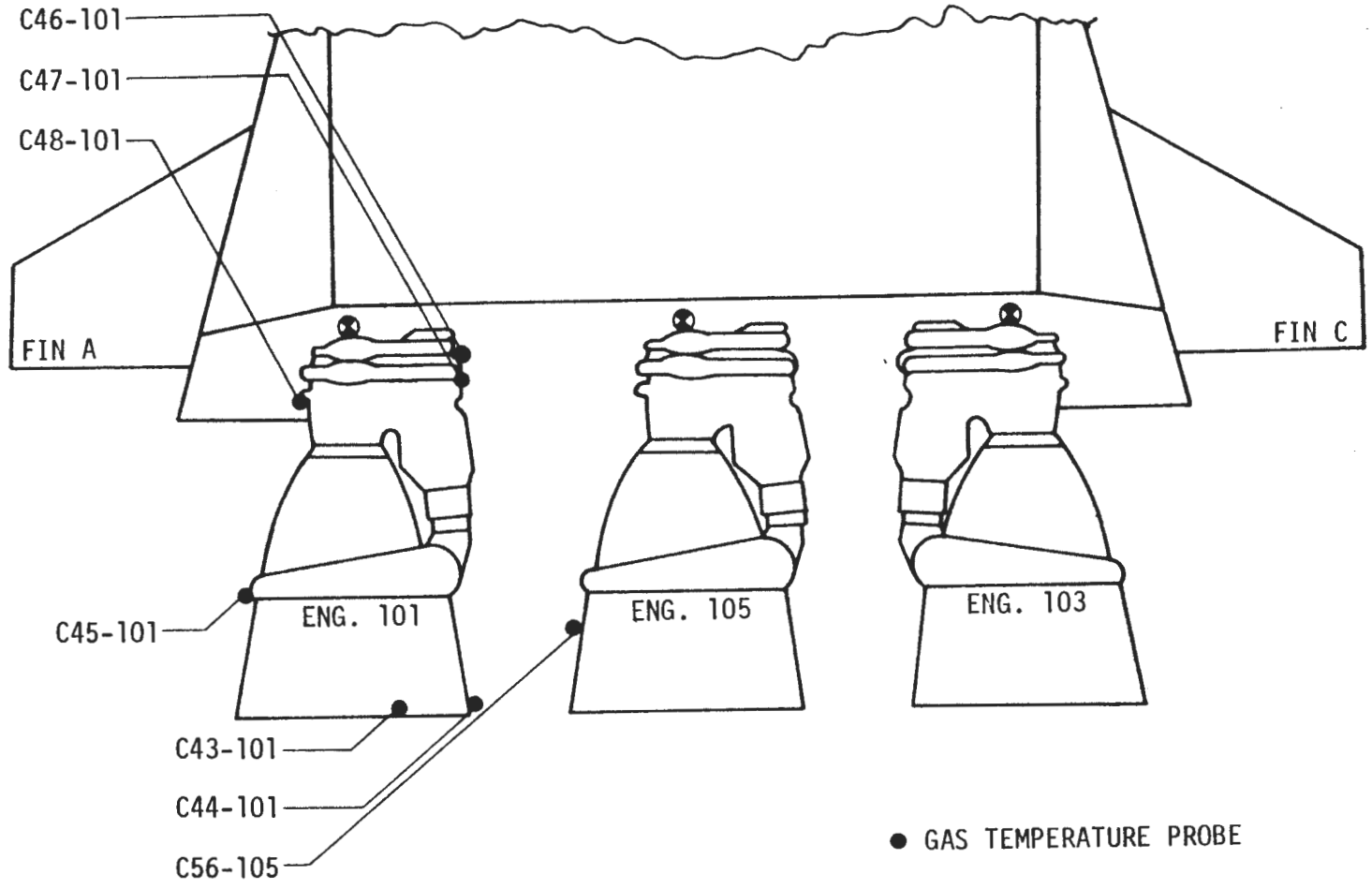

FIGURE 4-11. F-1 ENGINE GAS TEMPERATURE INSTRUMENTATION

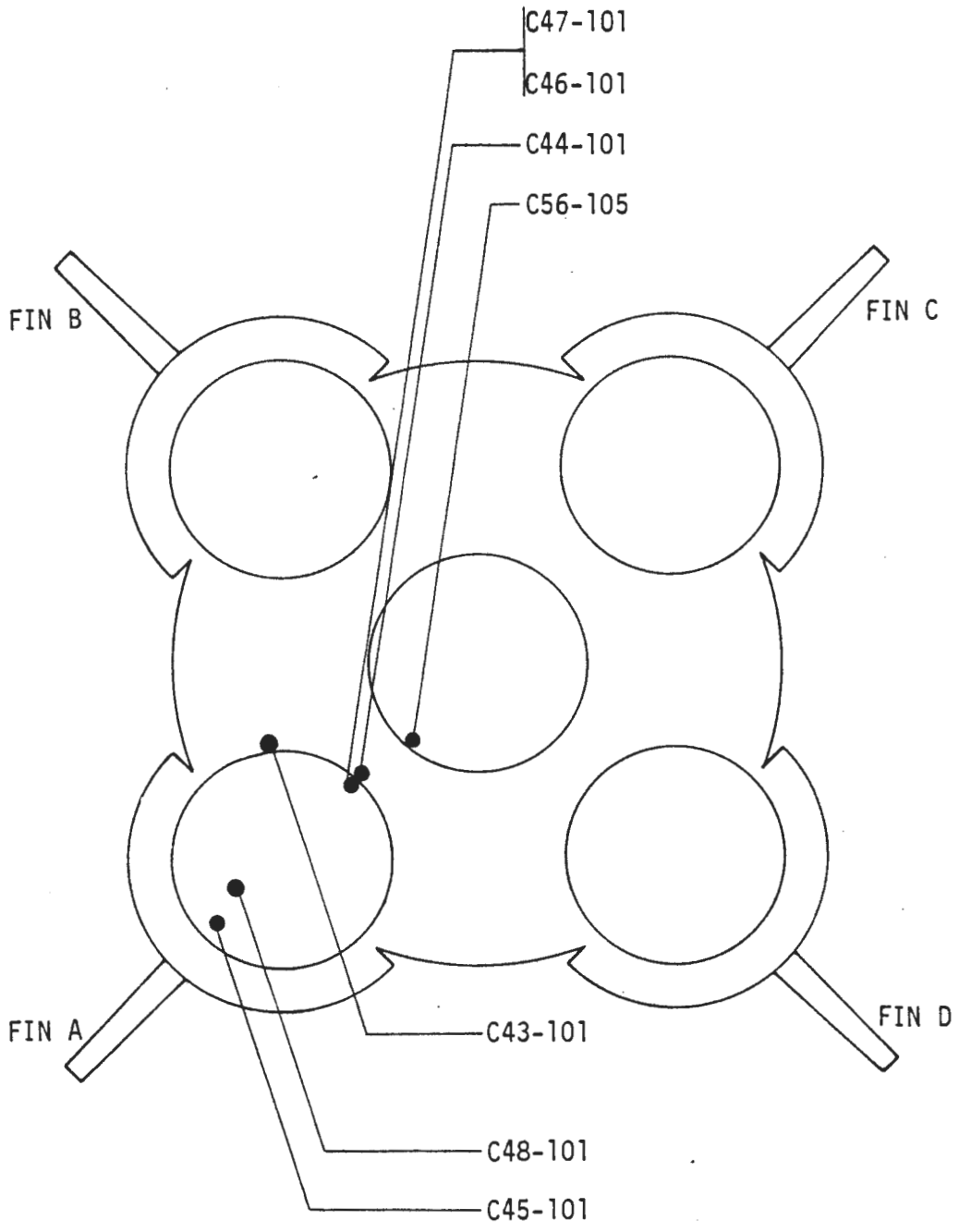

FIGURE 4-12. F-1 ENGINE GAS TEMPERATURE INSTRUMENTATION

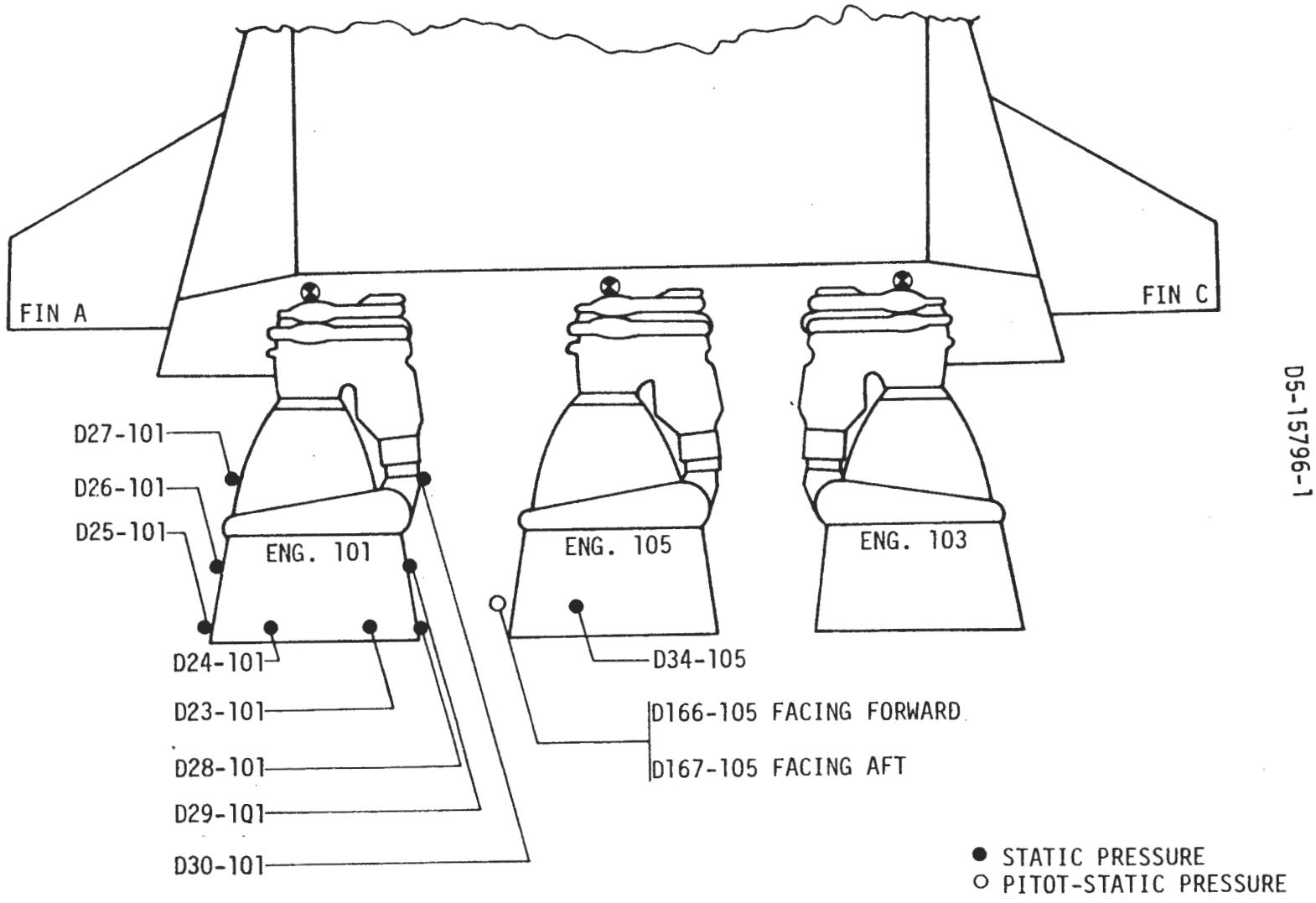

FIGURE 4-13. F-1 ENGINE EXTERNAL PRESSURE INSTRUMENTATION

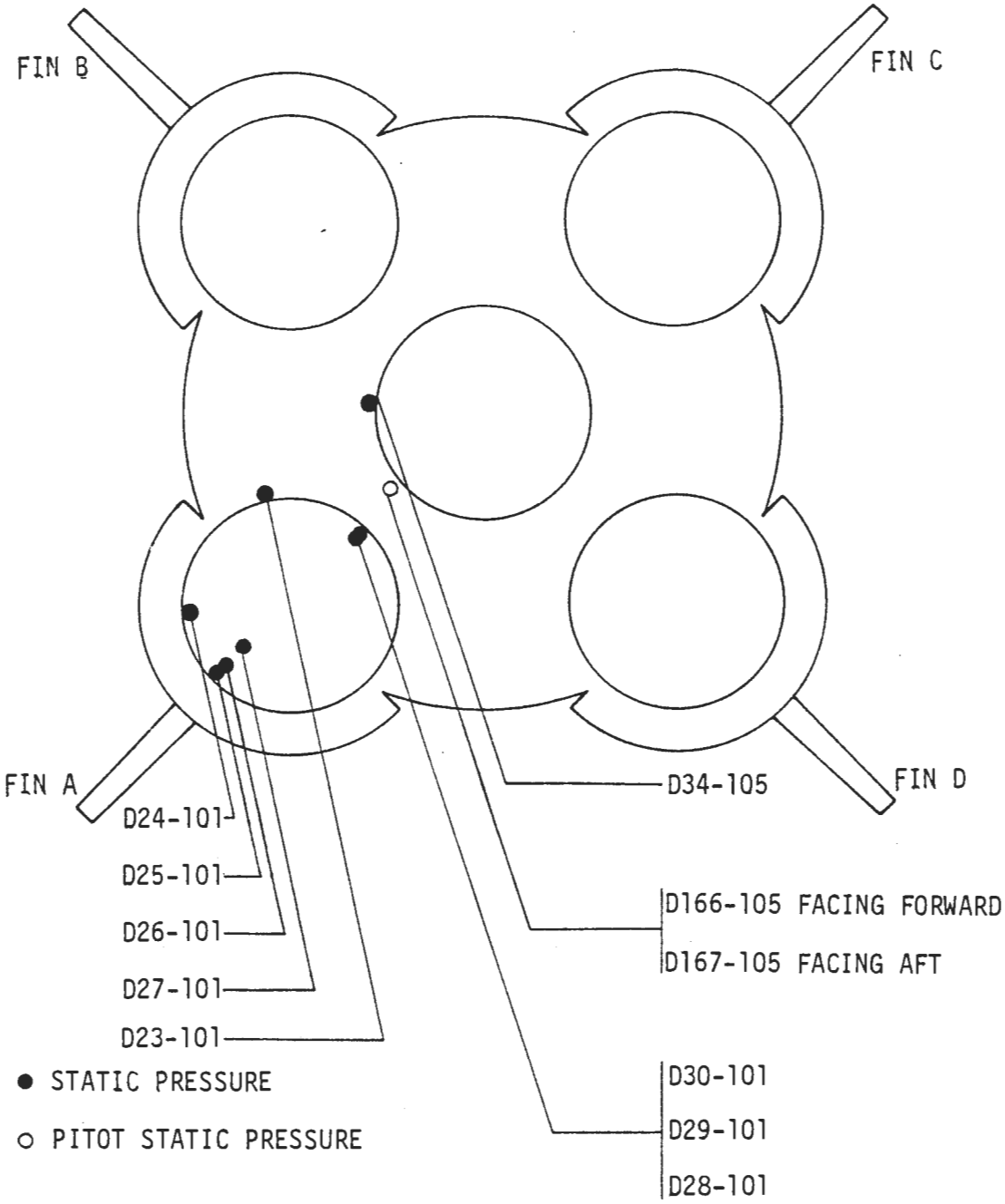

FIGURE 4-14. F-1 ENGINE EXTERNAL PRESSURE INSTRUMENTATION

TABLE 4-II. S-IC STAGE F-1 ENGINE THERMAL ENVIRONMENT INSTRUMENTATION

(CONTINUED ON NEXT PAGE)

MEASUREMENT NUMBER	INSTRUMENT TYPE	RANGE °K	LOCATION		
			STATION	RADIAL	REMARKS
C57-101	Cal., Rad.	0-113.65*	-116.0	Facing Engine No. 105	Engine No. 101
C58-105	Cal., Rad.	0-68.16*	-116.0	Facing Pos. II	Engine No. 105
C150-101	Cal., Rad.	0-68.16*	48.0	Facing Engine No. 105	Engine No. 101
C43-101	Gas Temp.**	273-2023	-116.0	Facing Engine No. 102	Engine No. 101
C44-101	Gas Temp.**	273-2023	-116.0	Facing Engine No. 105	Engine No. 101
C45-101	Gas Temp.**	273-2023	- 48.0	Facing Outboard	Engine No. 101
C46-101	Gas Temp.**	273-2023	70.0	Facing Engine No. 103	Engine No. 101
C47-101	Gas Temp.**	273-2023	59.0	Facing Engine No. 105	Engine No. 101
C48-101	Gas Temp.**	273-2023	56.0	Facing Outboard	Engine No. 101
C56-105	Gas Temp.**	273-2023	- 92.0	Facing Engine No. 101	Engine No. 105
C14-101	Cal., Total	0-113.65*	-116.0	Facing Engine No. 105	Engine No. 101
C15-101	Cal., Total	0-68.16*	-116.0	Facing Engine No. 102	Engine No. 101
C16-105	Cal., Total	0-68.16*	-116.0	Facing Pos. II	Engine No. 105
C17-101	Cal., Total	0-68.16*	- 48.0	Facing Engine No. 105 and Down	Engine No. 101

* watts/cm^2

** Platinum - Platinum + 10% Rhodium Thermocouple Probe

TABLE 4-II. S-IC STAGE F-1 ENGINE THERMAL ENVIRONMENT INSTRUMENTATION

(CONTINUED ON NEXT PAGE)

MEASUREMENT NUMBER	INSTRUMENT TYPE	RANGE watts/cm^2	LOCATION		
			STATION	RADIAL	REMARKS
C18-101	Cal., Total	0-45.44	- 48.0	Facing Outboard and Down	Engine No. 101
C19-101	Cal., Total	0-45.44	0.0	Facing Engine No. 105	Engine No. 101
C20-105	Cal., Total	0-45.44	45.0	Facing Engine No. 104	Engine No. 105
C21-101	Cal., Total	0-45.44	70.0	Facing Engine No. 105	Engine No. 101
C22-101	Cal., Total	0-45.44	59.0	Facing Engine No. 105	Engine No. 101
C23-101	Cal., Total	0-22.72	56.0	Facing Engine Fairing Fin A	Engine No. 101
C123-103	Cal., Total	0-68.16	- 48.0	Facing Engine No. 105 and Down	Engine No. 103
C142-105	Cal., Total	0-56.80	- 48.0	Facing Engine No. 101	Engine No. 105
D23-101	Static Pressure	0-13.79*	-110.0	Facing Engine No. 102	Engine No. 101
D24-101	Static Pressure	0-13.79*	-110.0	45° From Fin A Toward Position II	Engine No. 101
D25-101	Static Pressure	0-13.79*	-110.0	Facing Outboard	Engine No. 101
D26-101	Static Pressure	0-13.79*	- 70.0	Facing Outboard	Engine No. 101

* N/cm^2

TABLE 4-II. S-IC STAGE F-1 ENGINE THERMAL ENVIRONMENT INSTRUMENTATION (CONCLUDED)

MEASUREMENT NUMBER	INSTRUMENT TYPE	RANGE N/cm^2	LOCATION		
			STATION	RADIAL	REMARKS
D27-101	Static Pressure	0-13.79	- 15.0	Facing Outboard	Engine No. 101
D28-101	Static Pressure	0-13.79	-110.0	Facing Engine No. 105	Engine No. 101
D29-101	Static Pressure	0-13.79	- 70.0	Facing Engine No. 105	Engine No. 101
D30-101	Static Pressure	0-13.79	- 15.0	Facing Engine No. 105	Engine No. 101
*D31-105	Pitot Pressure	0-13.79	- 92.0	Facing Forward	①
*D32-105	Pitot Pressure	0-13.79	- 92.0	Facing Aft	①
*D33-105	Static Pressure	0-13.79	- 92.0	Facing Engine No. 101	①
*D34-105	Static Pressure	0-13.79	- 92.0	Facing Position II	Engine No. 105
**D166-105	Pitot-Static Pressure	0-3.45	- 92.0	Facing Forward	①
**D167-105	Pitot-Static Pressure	0-3.45	- 92.0	Facing Aft	①

① Six (6) Inches from Engine No. 105 Toward Engine No. 101

* AS-501 and AS-502

** AS-503

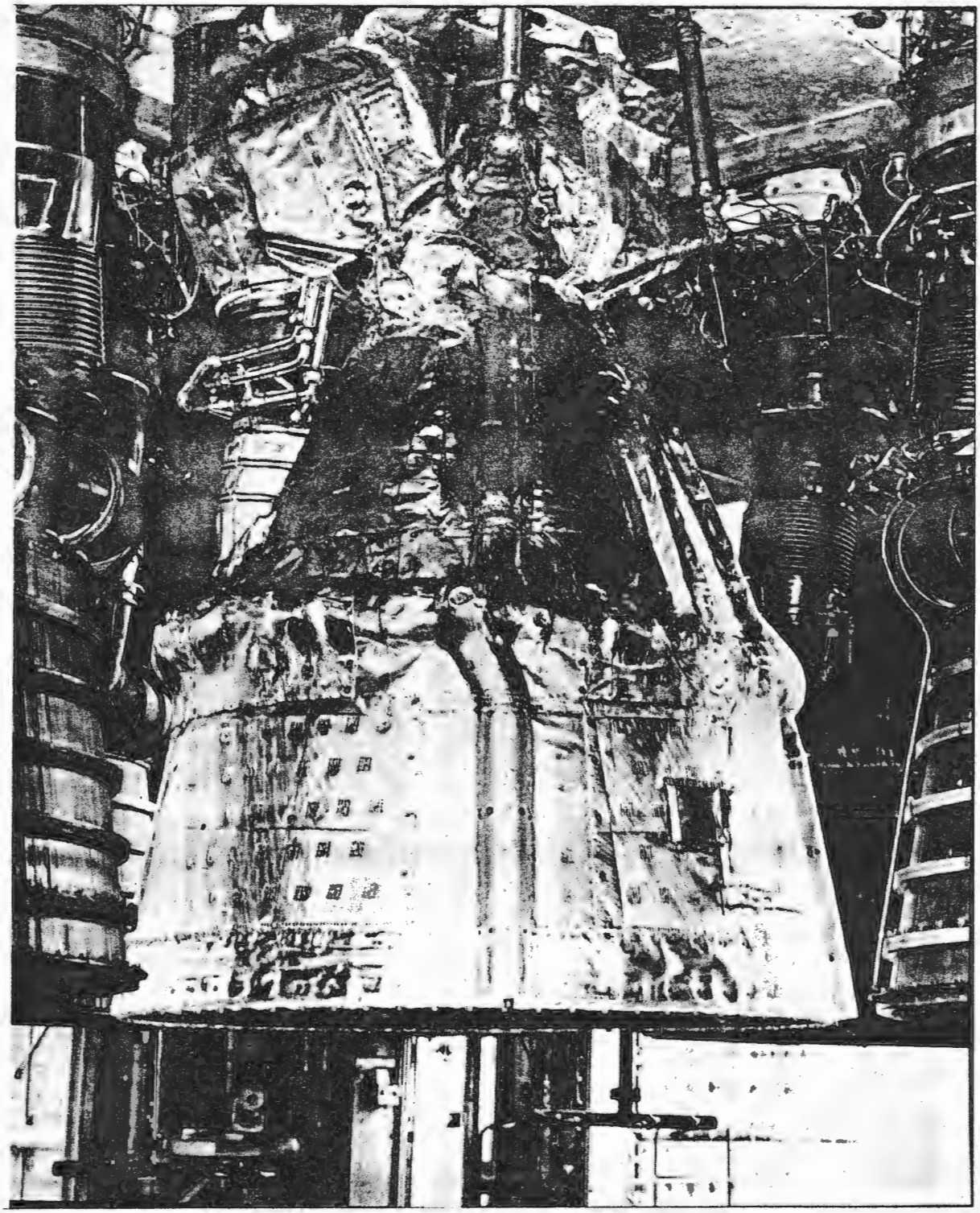

FIGURE 4-15. S-IC STAGE CENTER F-1 ENGINE WITH INSULATION COCOON

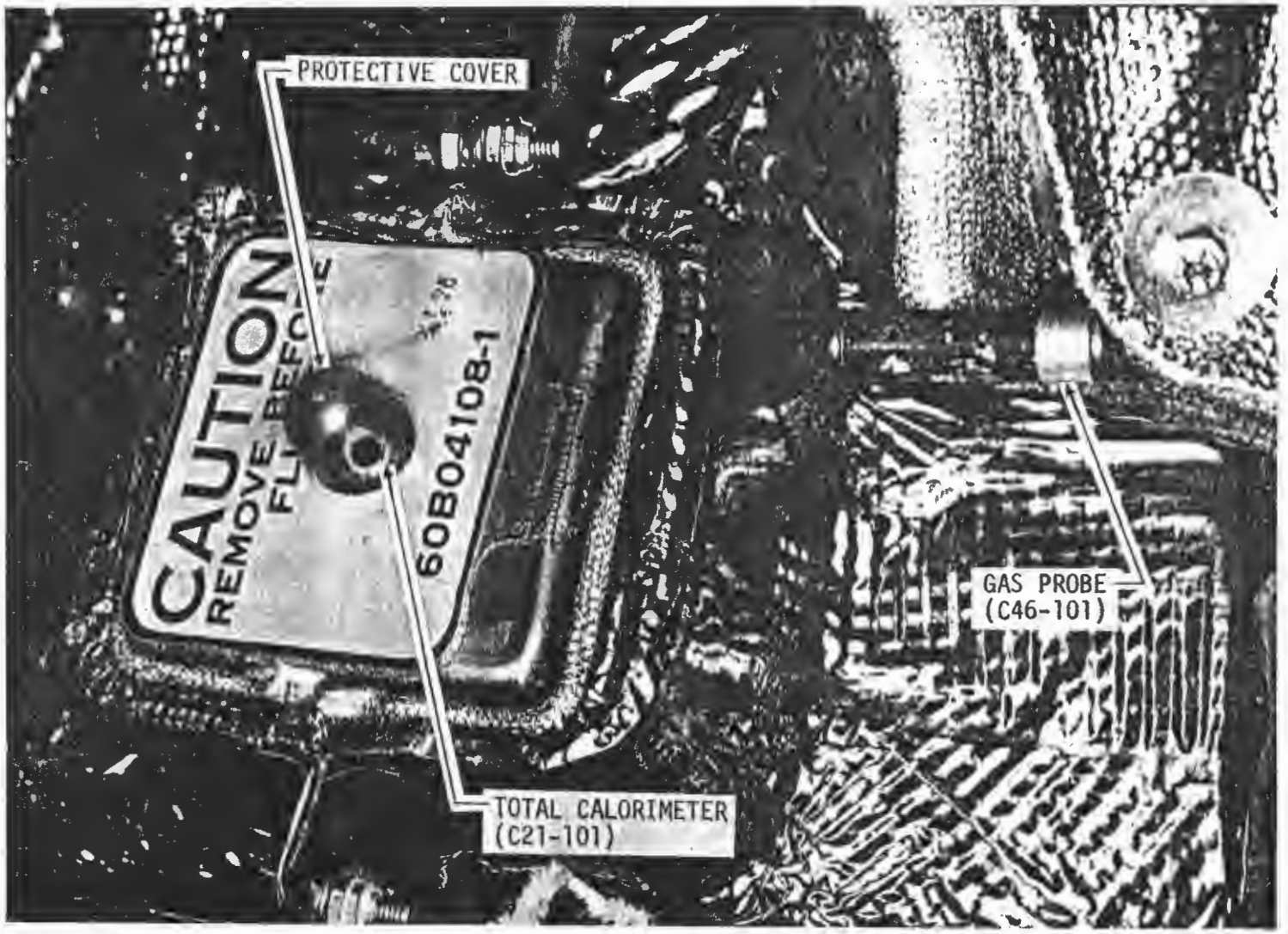

FIGURE 4-16. TYPICAL F-1 ENGINE INSTRUMENTATION INSTALLATION

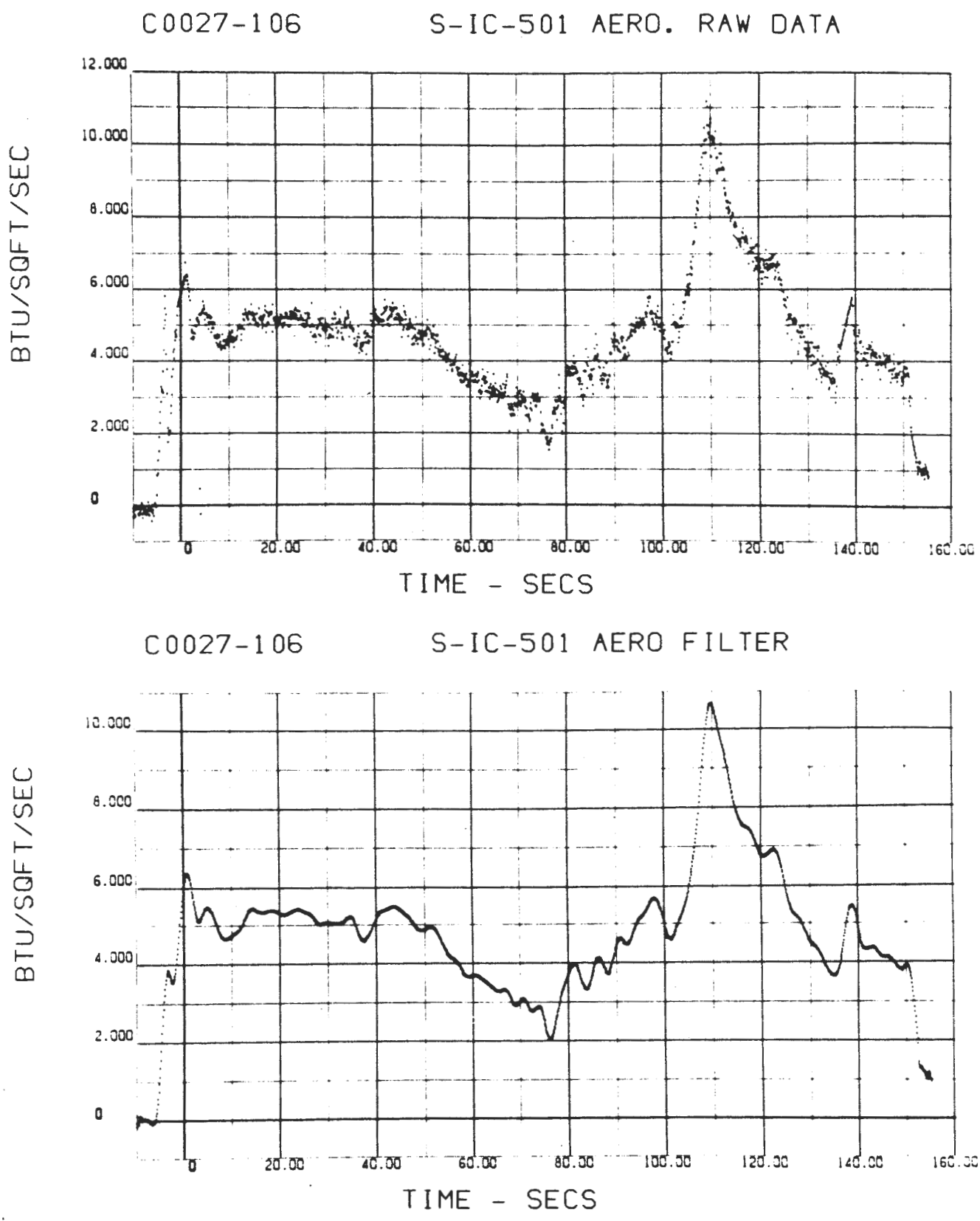

FIGURE 4-17. TYPICAL S-IC HEAT SHIELD RAW AND CONDITIONED FLIGHT DATA

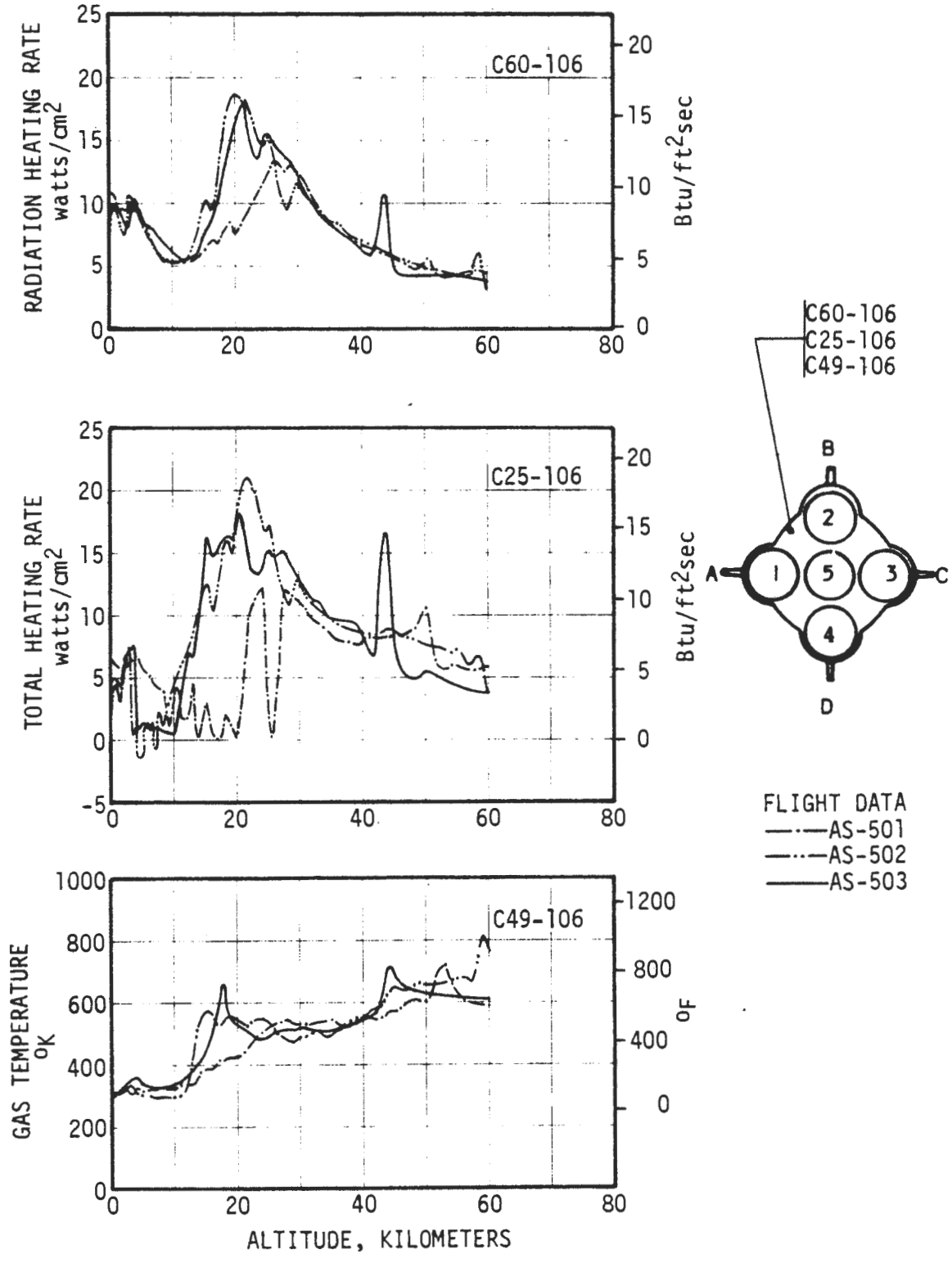

FIGURE 4-18. S-IC HEAT SHIELD ENVIRONMENT - r/R = 0.84 BETWEEN OUTBOARD ENGINES

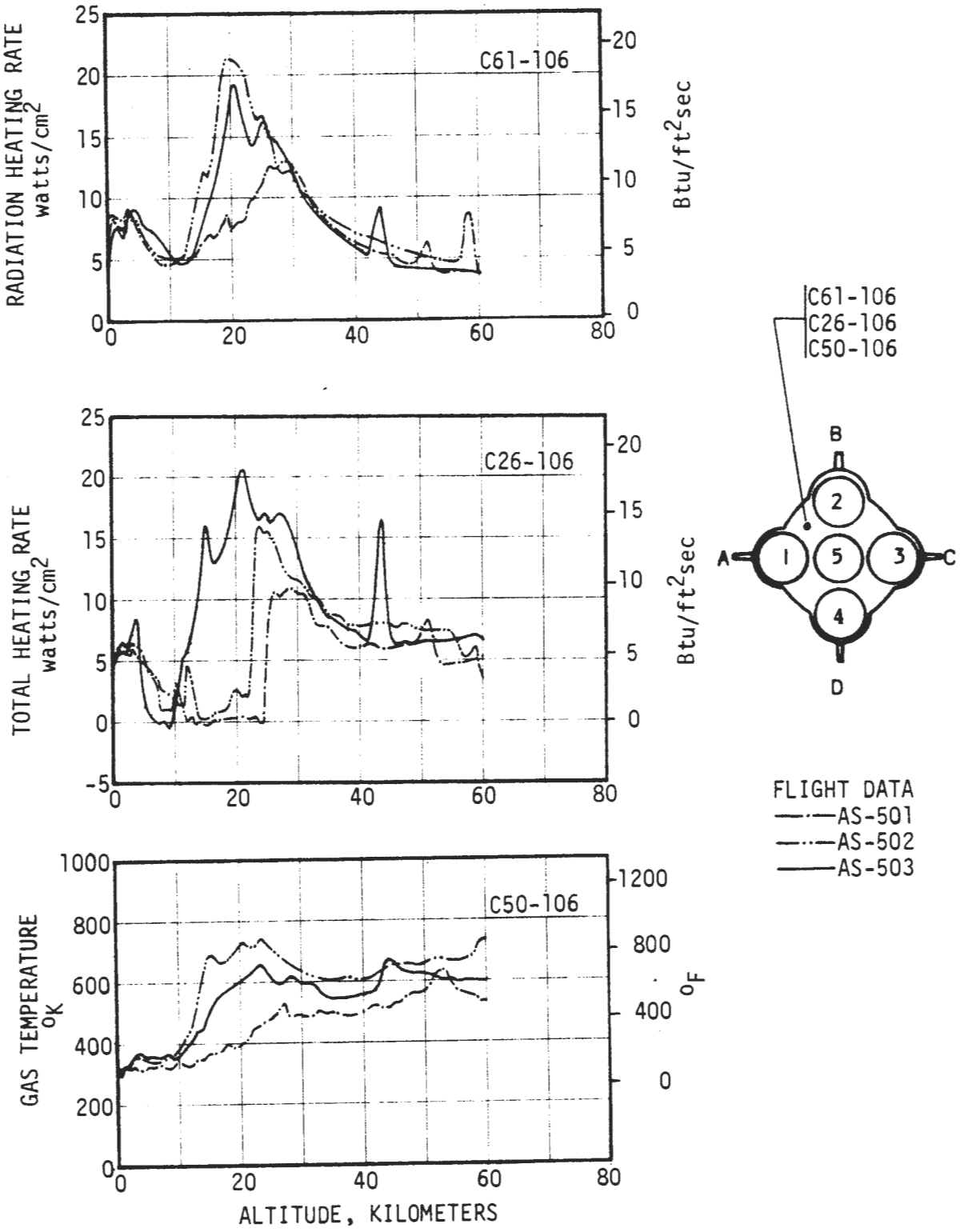

FIGURE 4-19. S-IC HEAT SHIELD ENVIRONMENT - r/R = 0.61 BETWEEN OUTBOARD ENGINES

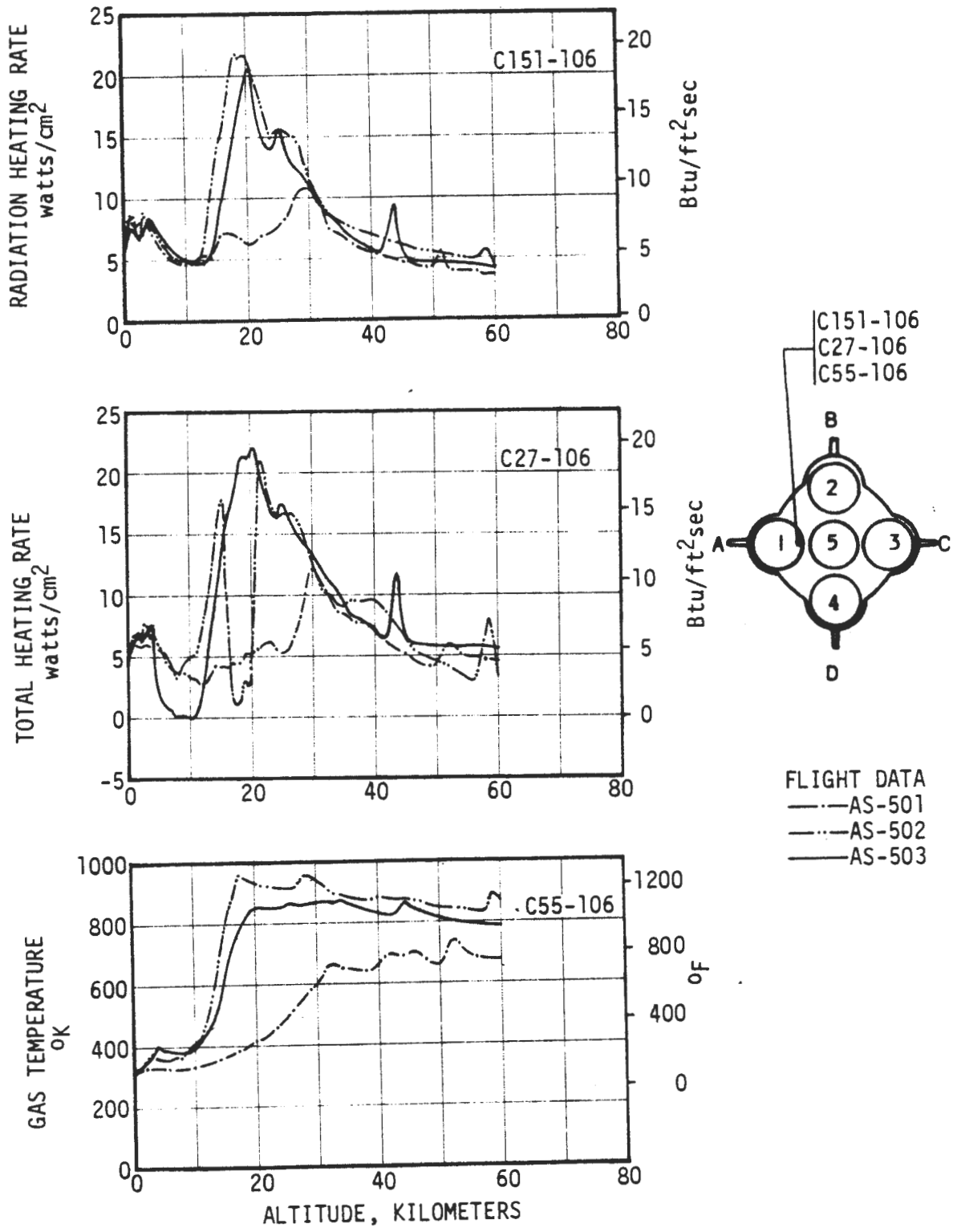

FIGURE 4-20. S-IC HEAT SHIELD ENVIRONMENT - r/R = 0.60 BETWEEN INBOARD AND OUTBOARD ENGINES

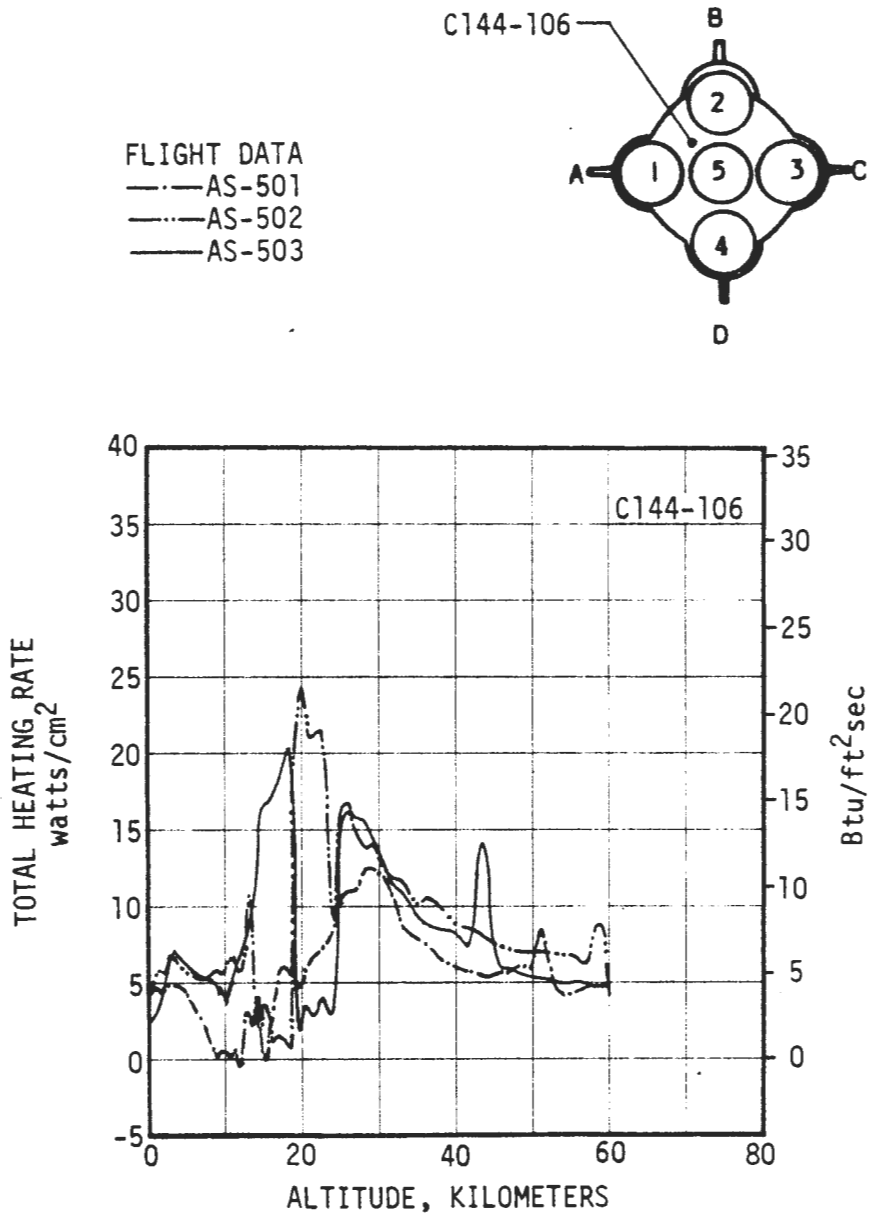

FIGURE 4-21. S-IC HEAT SHIELD TOTAL HEATING RATE - r/R = 0.46 BETWEEN OUTBOARD ENGINES

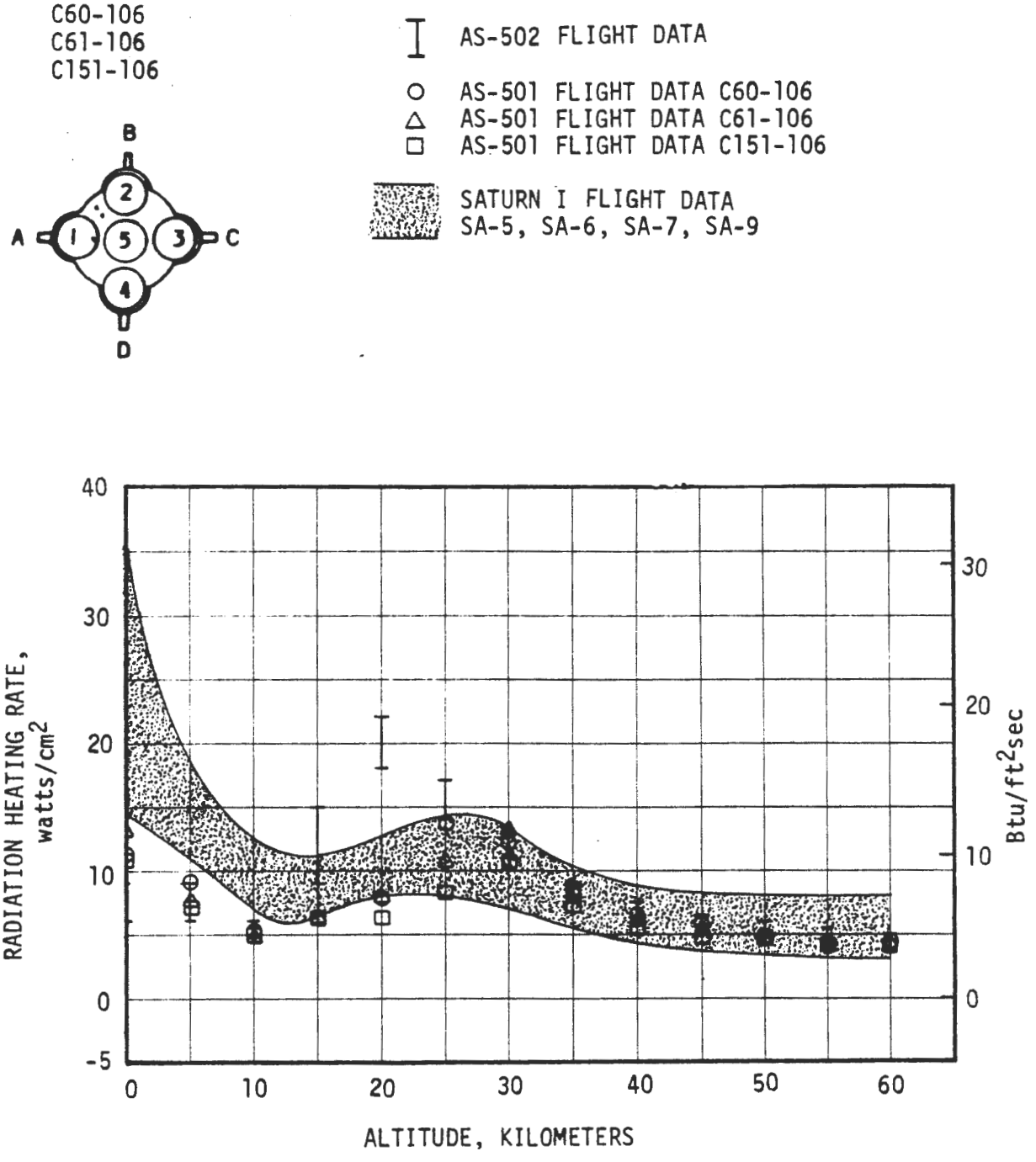

FIGURE 4-22. COMPARISON OF SATURN I AND SATURN V HEAT SHIELD RADIATION HEATING RATE FLIGHT DATA

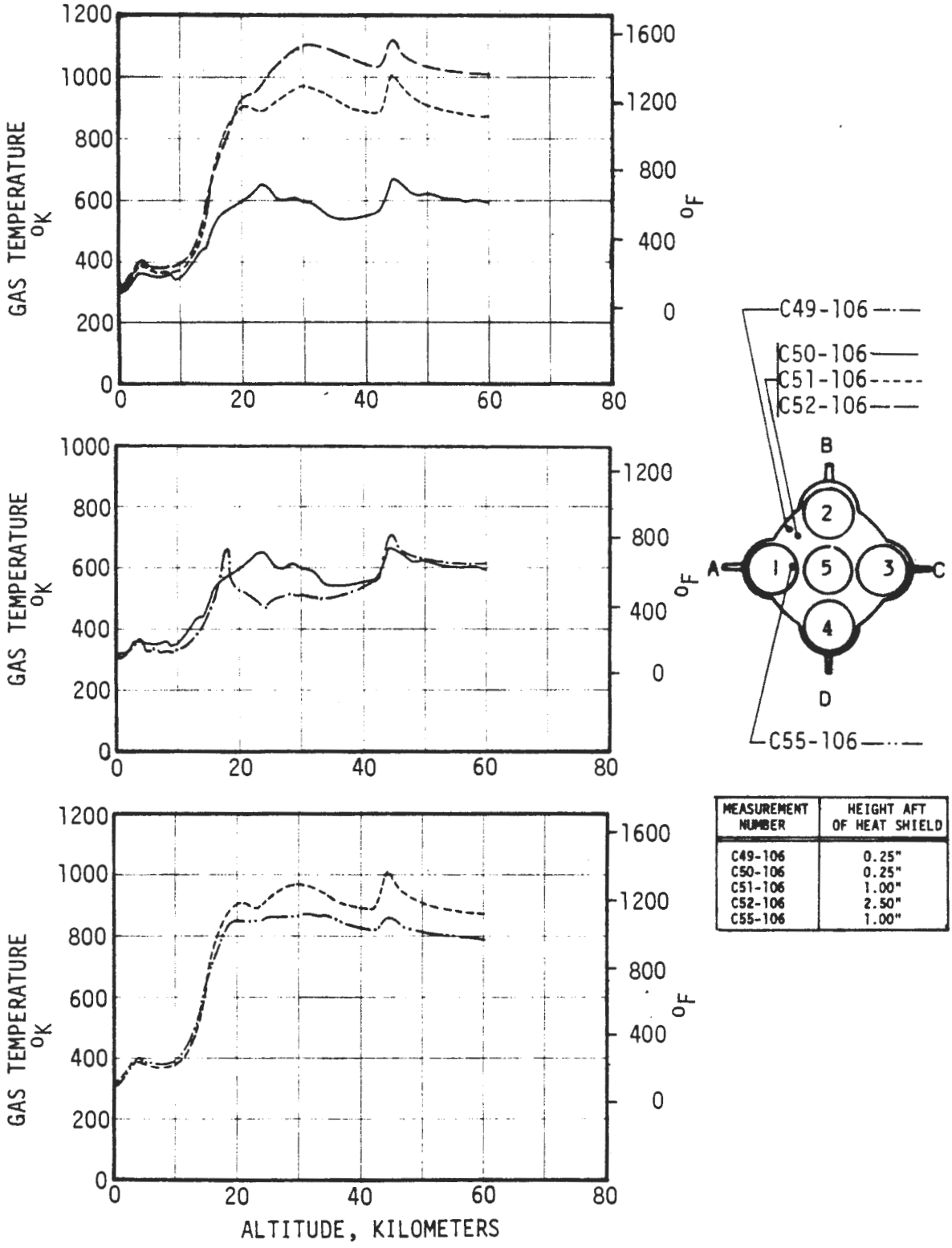

MEASUREMENT NUMBER	HEIGHT AFT OF HEAT SHIELD
C49-106	0.25"
C50-106	0.25"
C51-106	1.00"
C52-106	2.50"
C55-106	1.00"

FIGURE 4-23. S-IC HEAT SHIELD GAS TEMPERATURE, AS-503 FLIGHT DATA

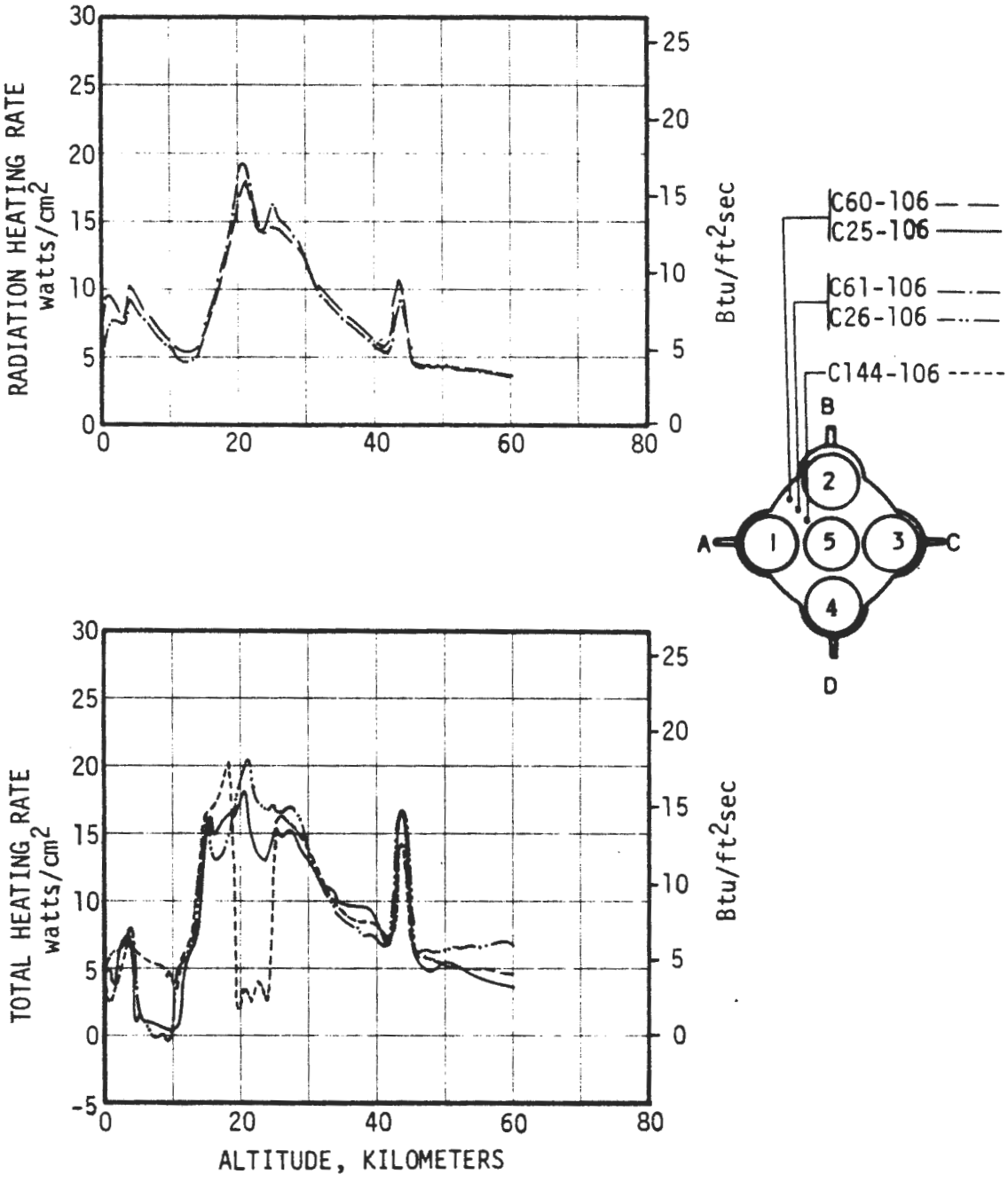

FIGURE 4-24. S-IC HEAT SHIELD HEATING RATES, AS-503 FLIGHT DATA

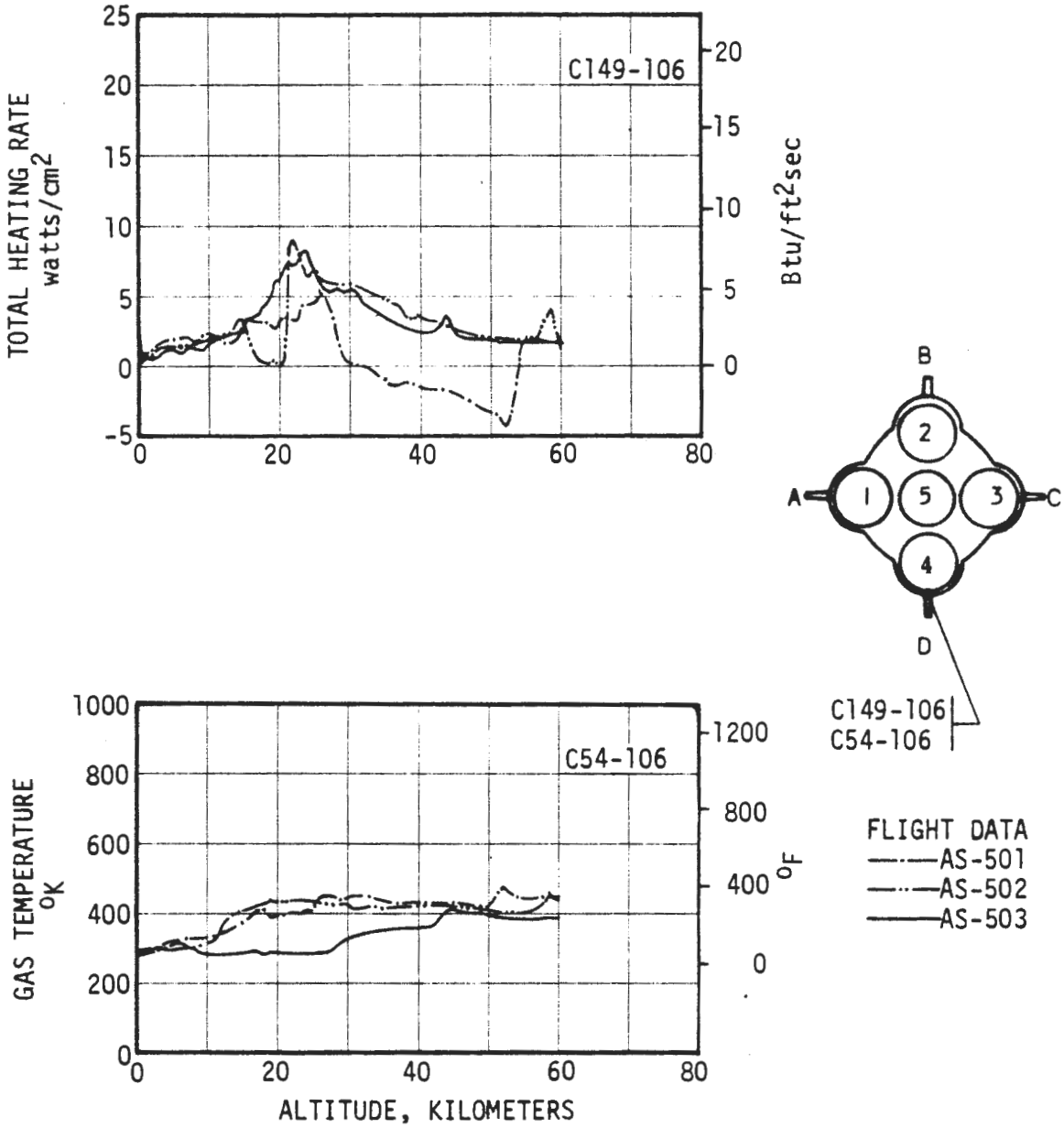

FIGURE 4-25. S-IC HEAT SHIELD ENVIRONMENT - BETWEEN OUTBOARD ENGINE AND ENGINE FAIRING

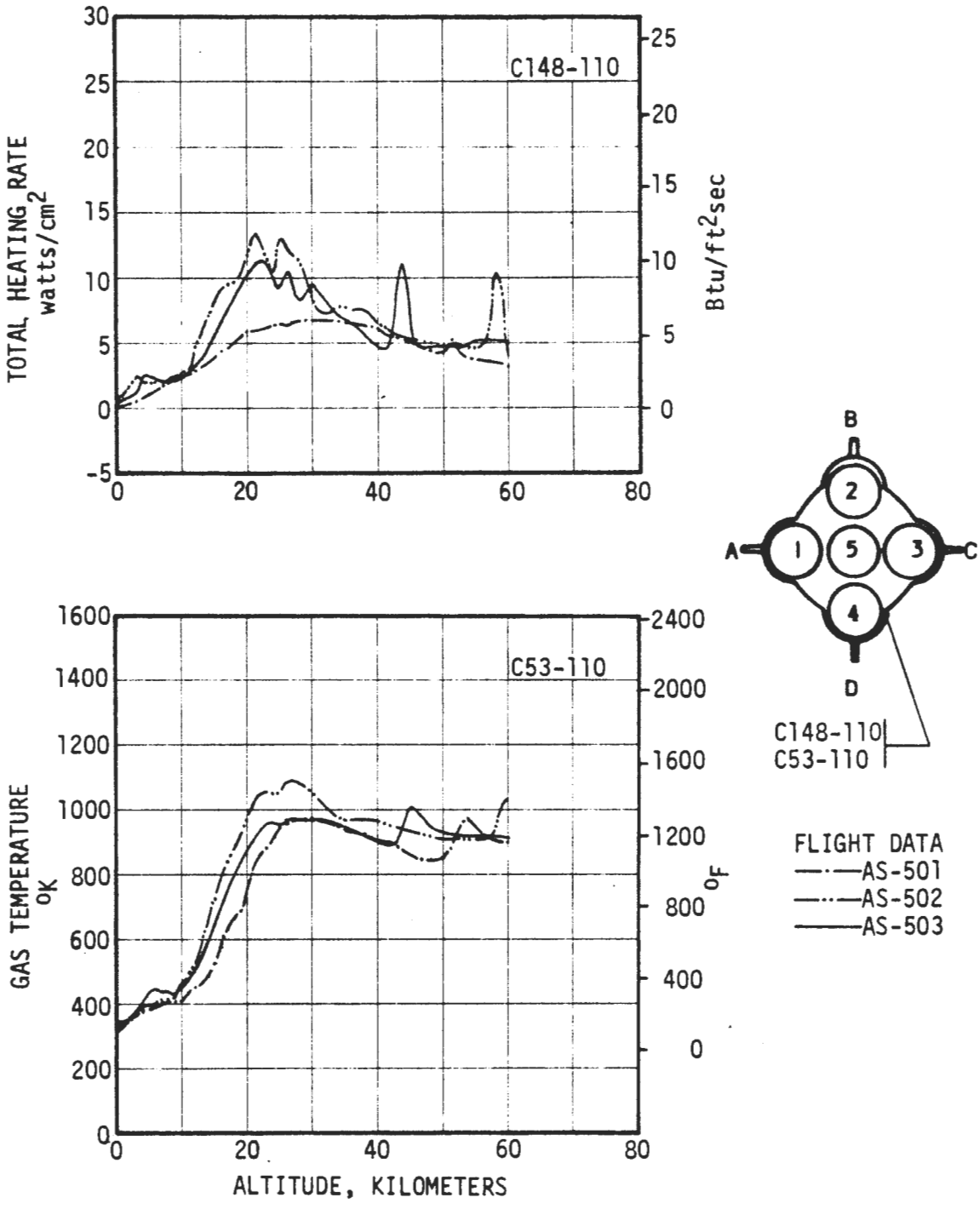

FIGURE 4-26. S-IC ENGINE FAIRING ENVIRONMENT NEAR HEAT SHIELD

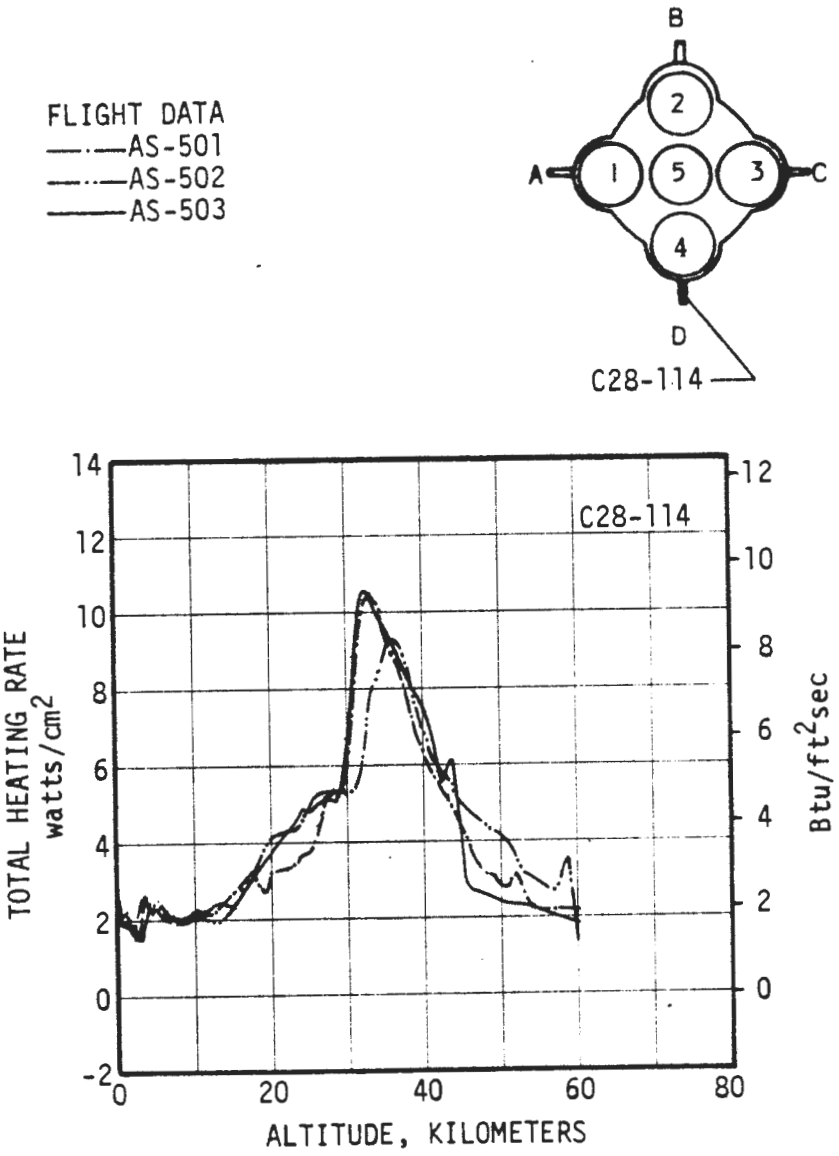

FIGURE 4-27. S-IC FIN TRAILING EDGE ENVIRONMENT

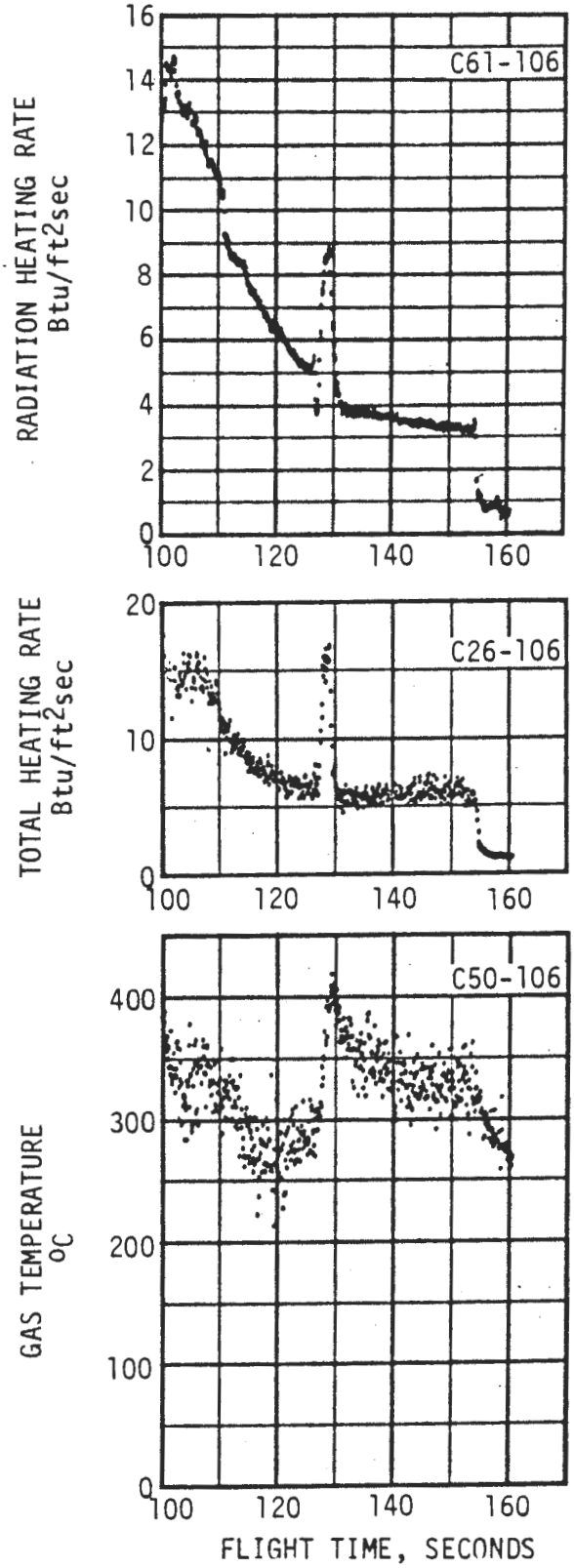

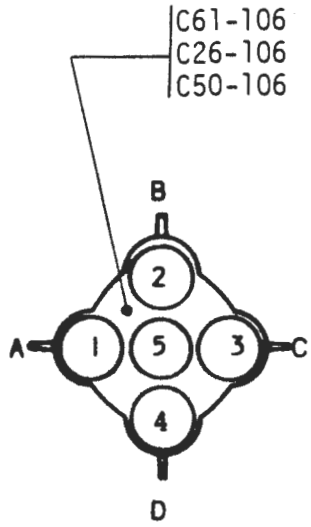

INBOARD ENGINE CUTOFF
AS-503 125.88 SECONDS

FIGURE 4-28. S-IC BASE HEAT SHIELD ENVIRONMENT - INBOARD ENGINE CUTOFF, AS-503 FLIGHT DATA

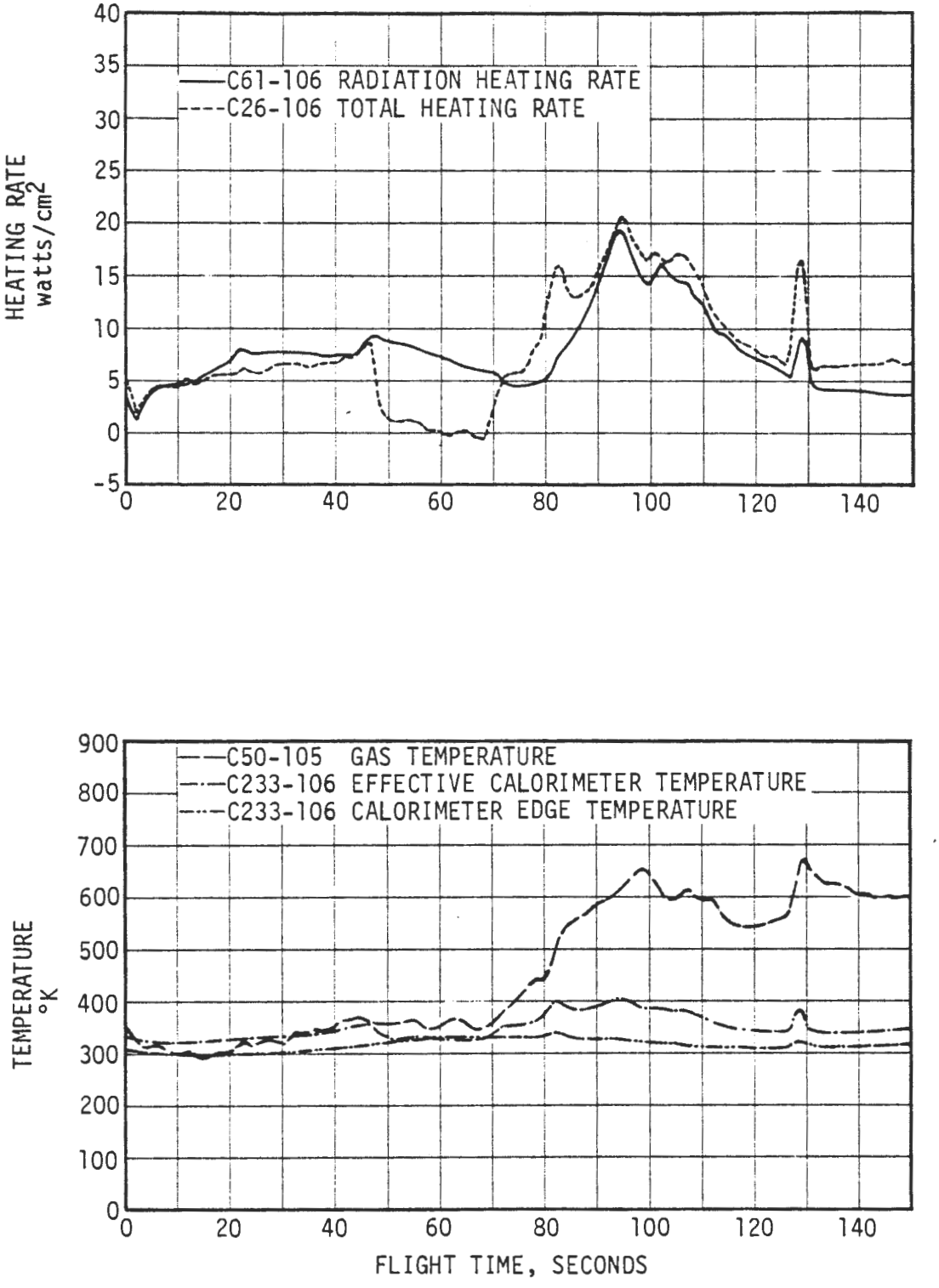

FIGURE 4-29. S-IC BASE HEAT SHIELD ENVIRONMENT - r/R = 0.61 BETWEEN OUTBOARD ENGINES, AS-503 FLIGHT DATA

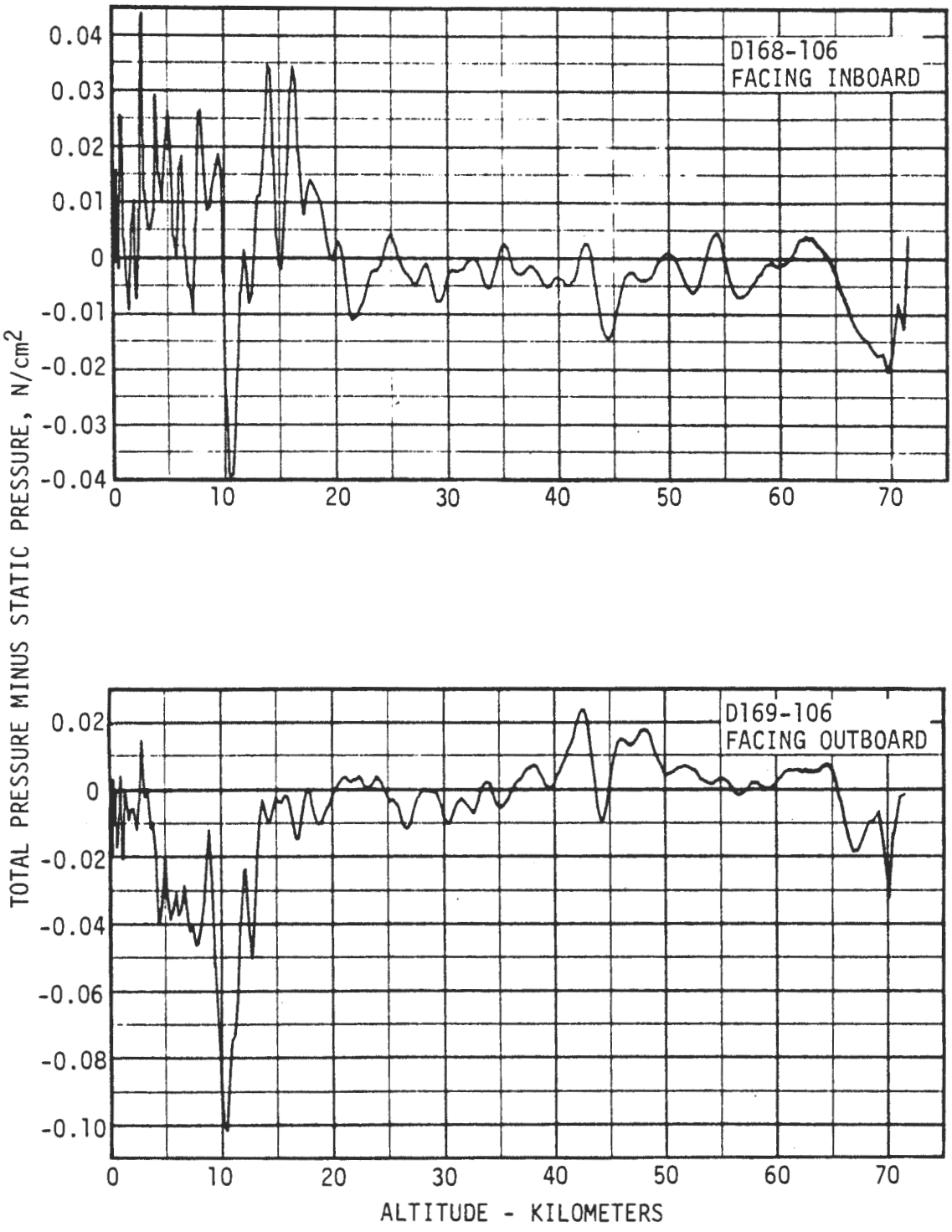

FIGURE 4-30. S-IC BASE HEAT SHIELD PRESSURE ENVIRONMENT, AS-503 FLIGHT DATA

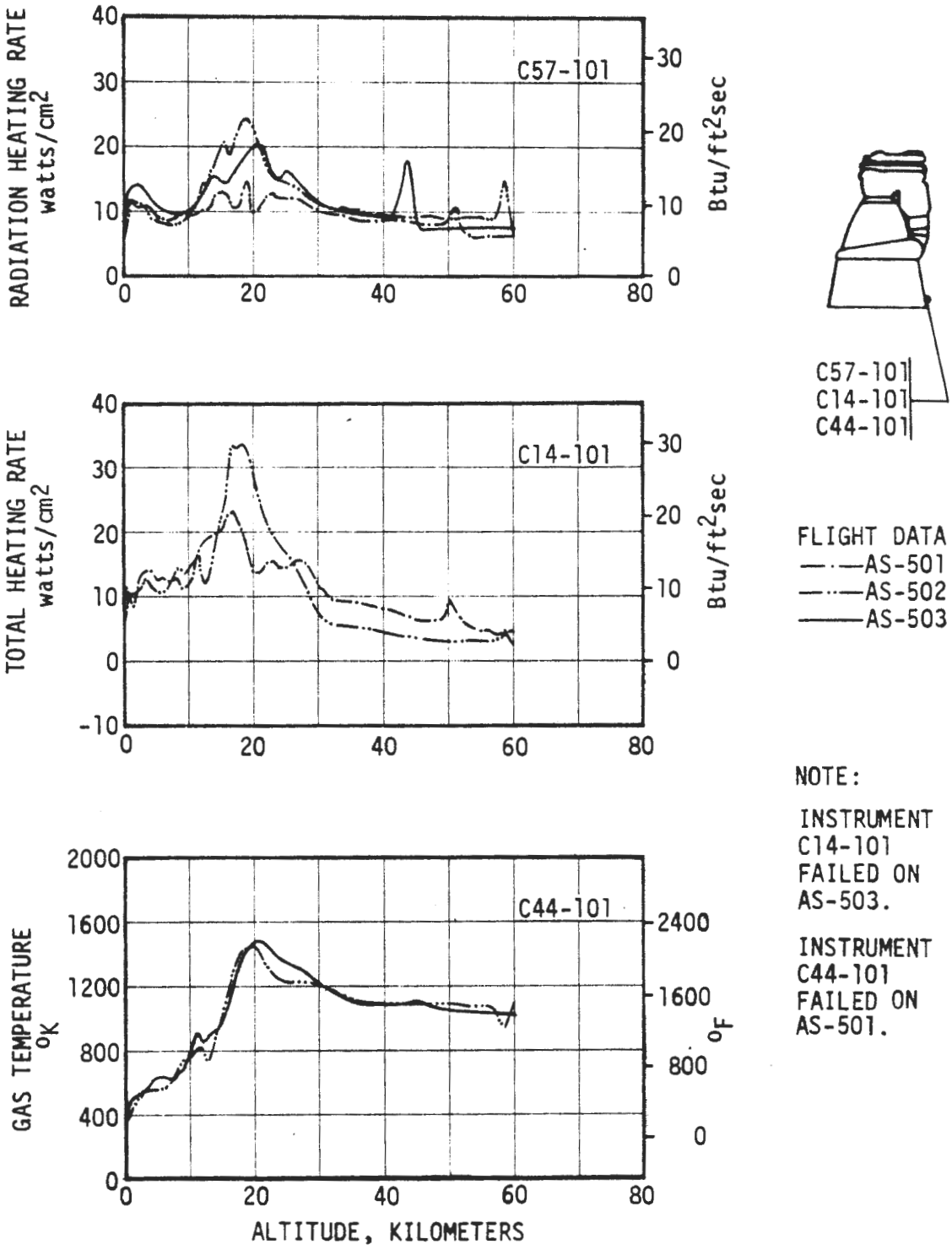

FIGURE 4-31. F-1 ENGINE ENVIRONMENT - OUTBOARD ENGINE EXIT PLANE FACING INBOARD

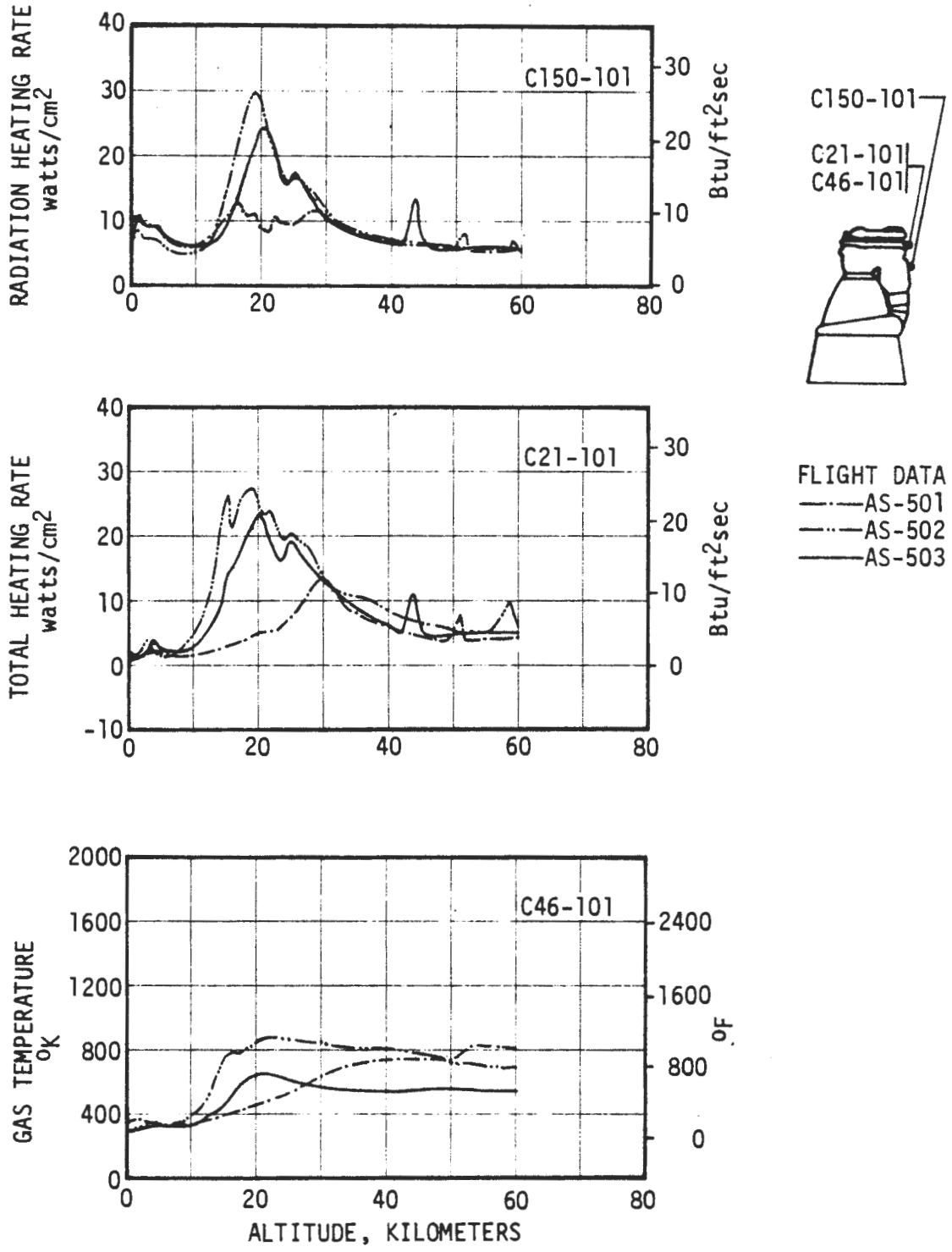

FIGURE 4-32. F-1 ENGINE ENVIRONMENT - OUTBOARD ENGINE NEAR HEAT SHIELD FACING OUTBOARD

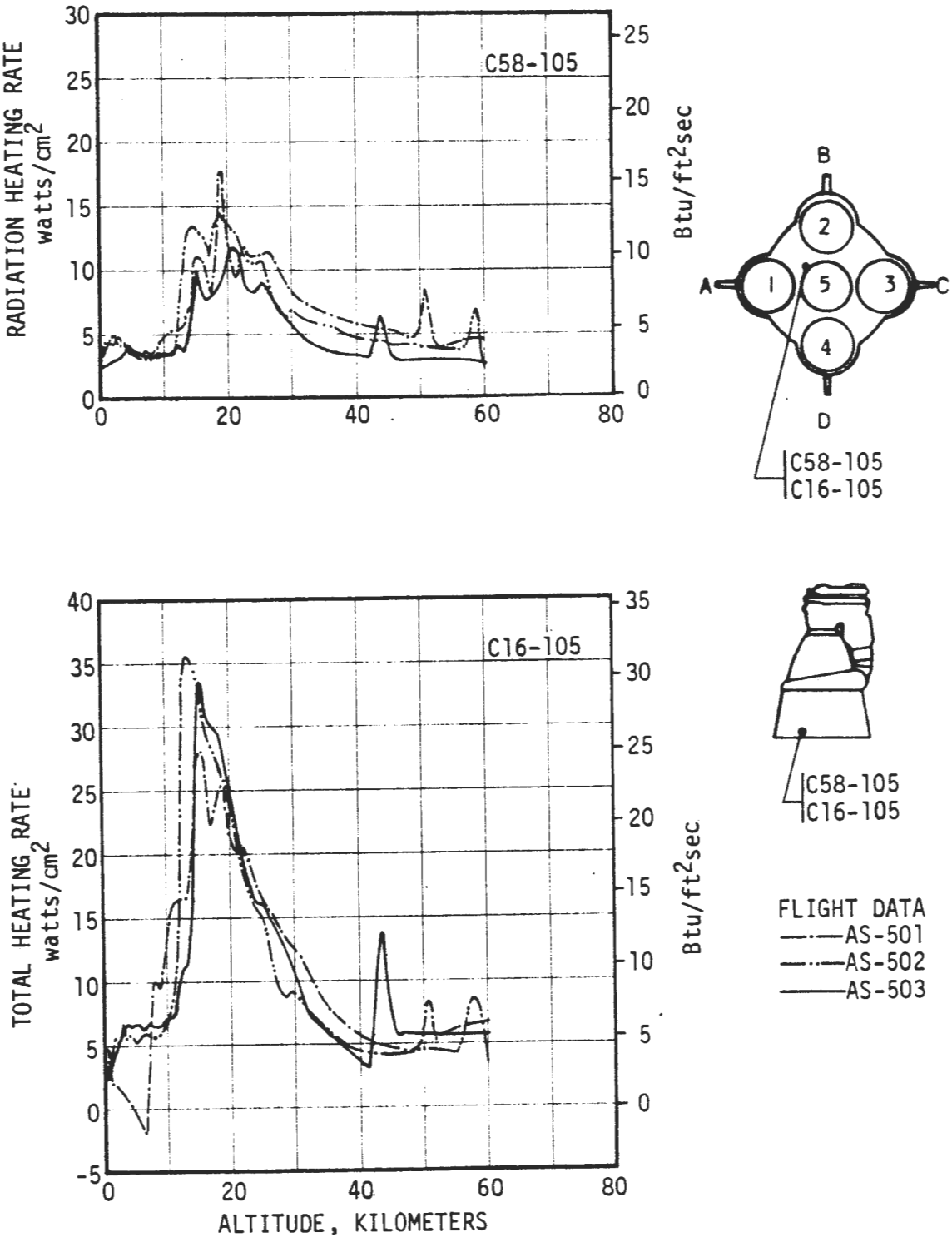

FIGURE 4-33. F-1 ENGINE ENVIRONMENT - INBOARD ENGINE EXIT PLANE FACING OUTBOARD BETWEEN TWO ENGINES

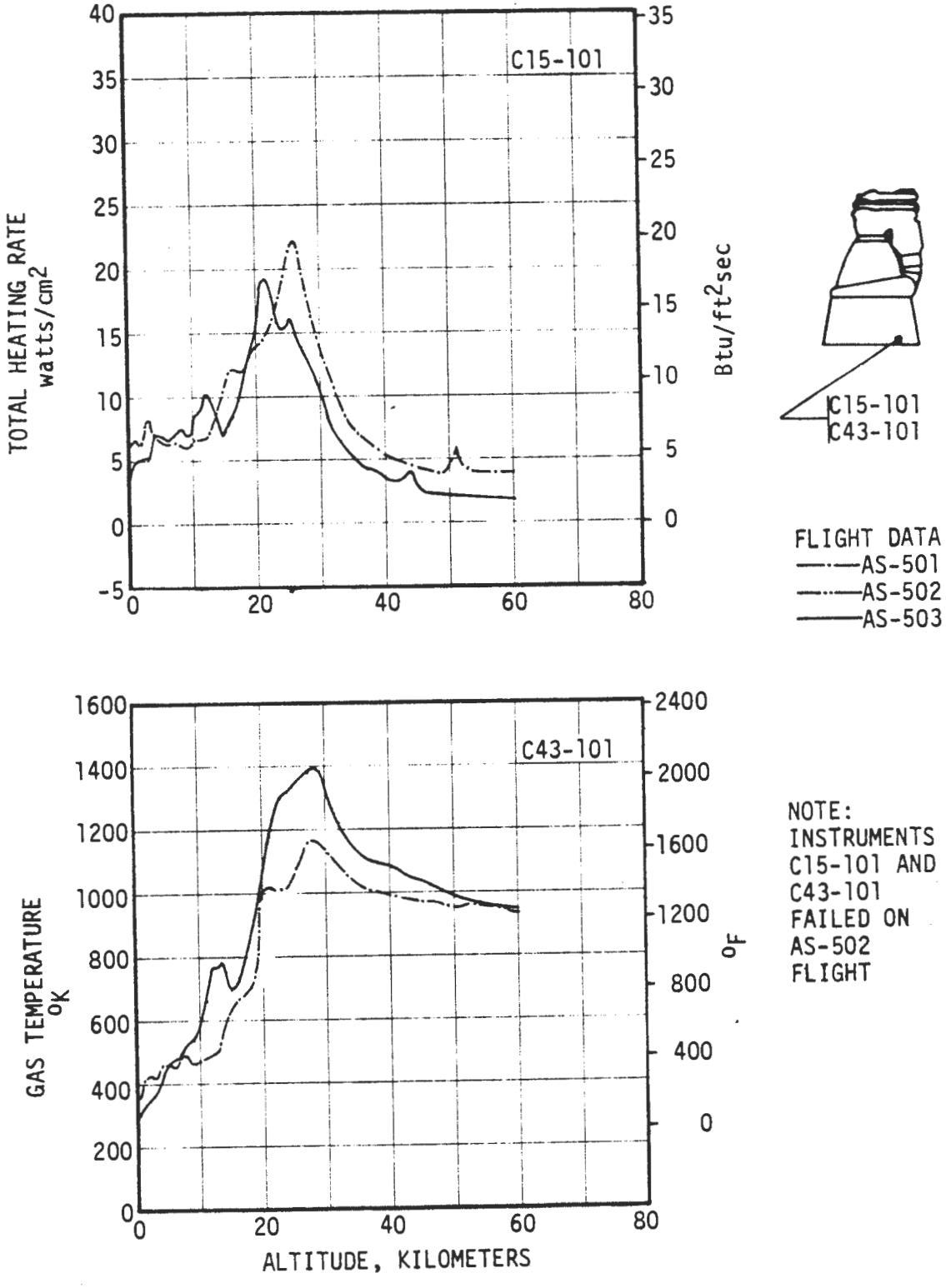

FIGURE 4-34. F-1 ENGINE ENVIRONMENT - OUTBOARD ENGINE EXIT PLANE FACING OUTBOARD ENGINE

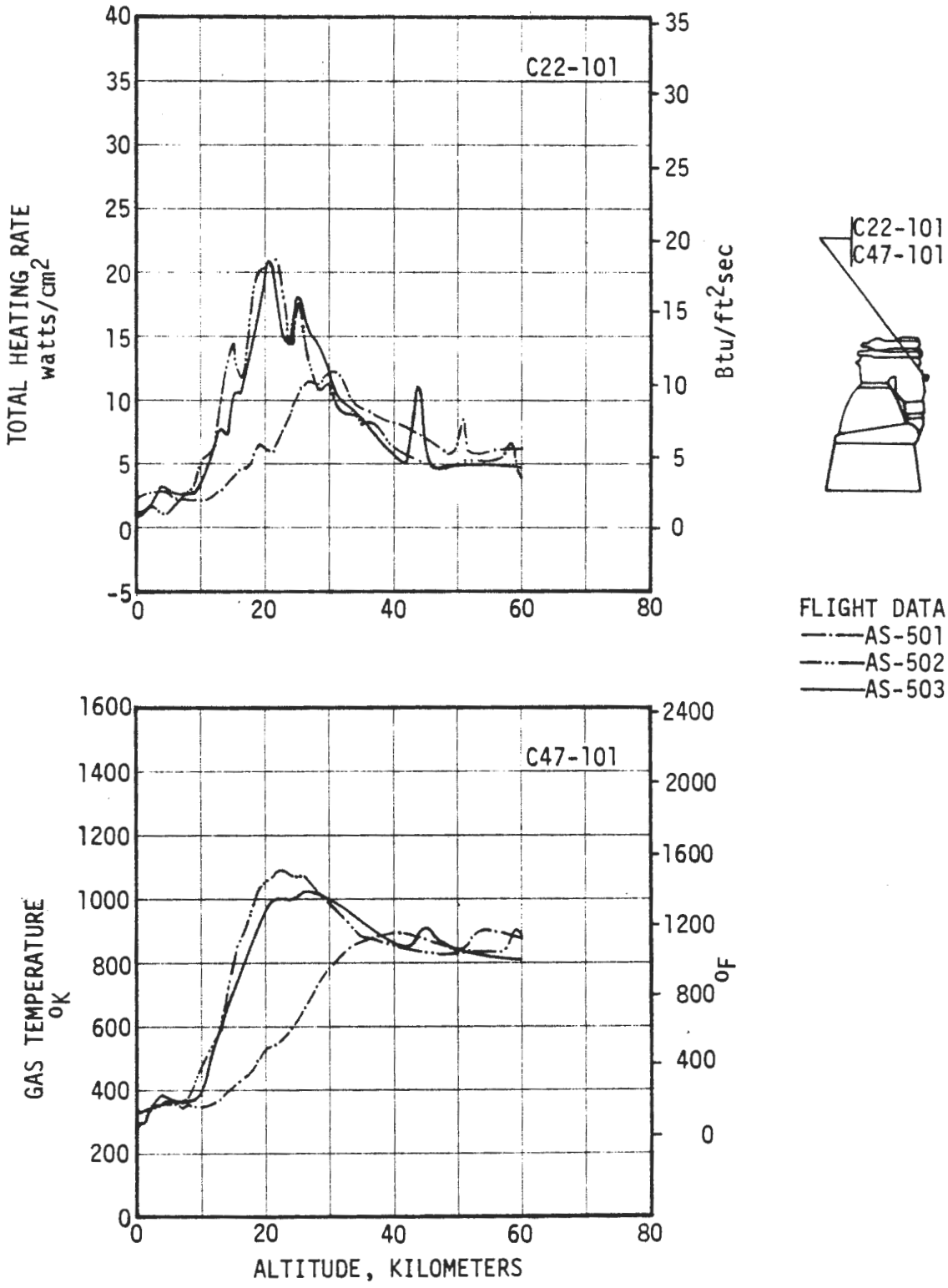

FIGURE 4-35. F-1 ENGINE ENVIRONMENT - OUTBOARD ENGINE NEAR HEAT SHIELD FACING INBOARD ENGINE

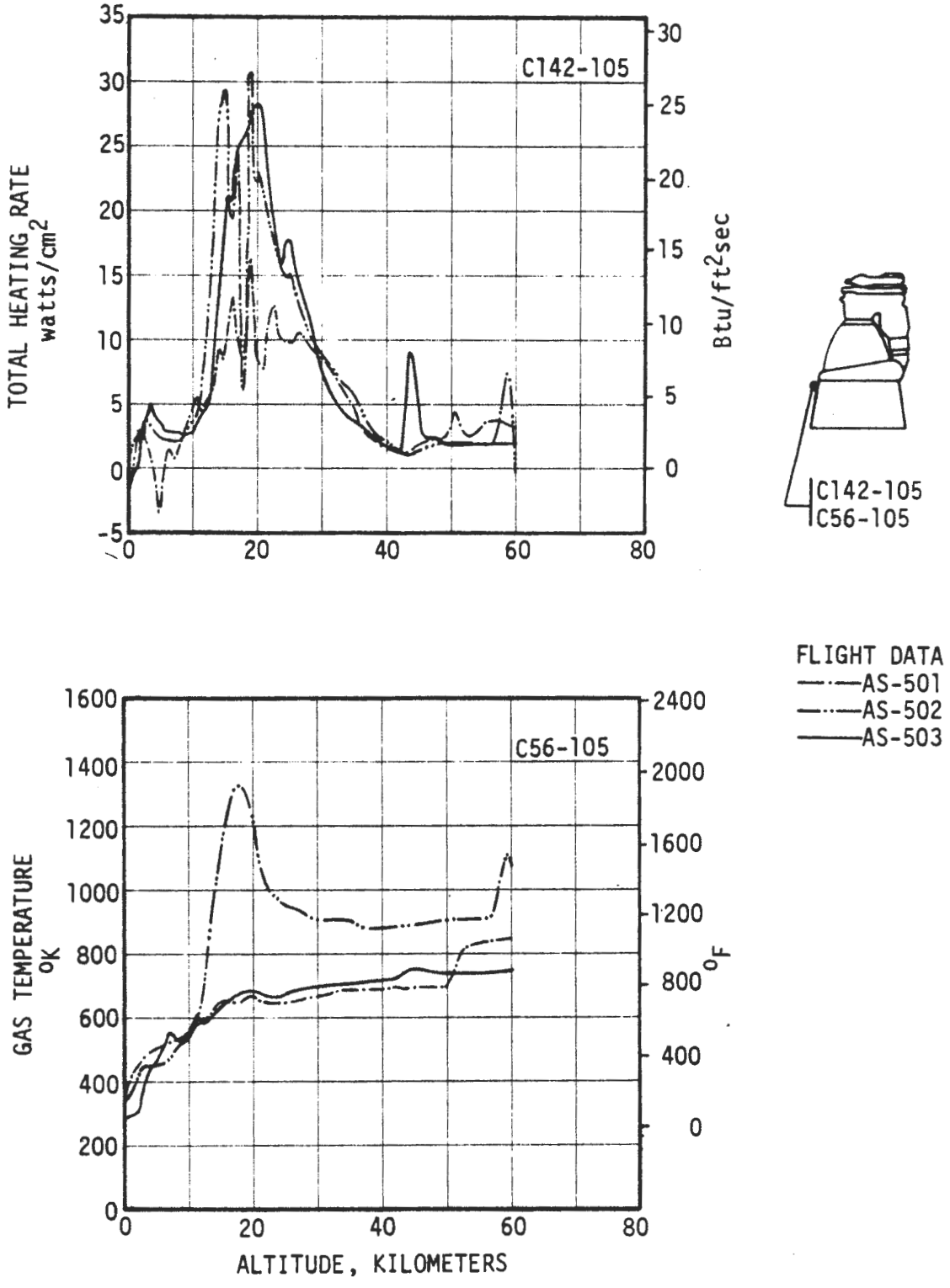

FIGURE 4-36. F-1 ENGINE ENVIRONMENT - INBOARD ENGINE MANIFOLD FACING OUTBOARD ENGINE

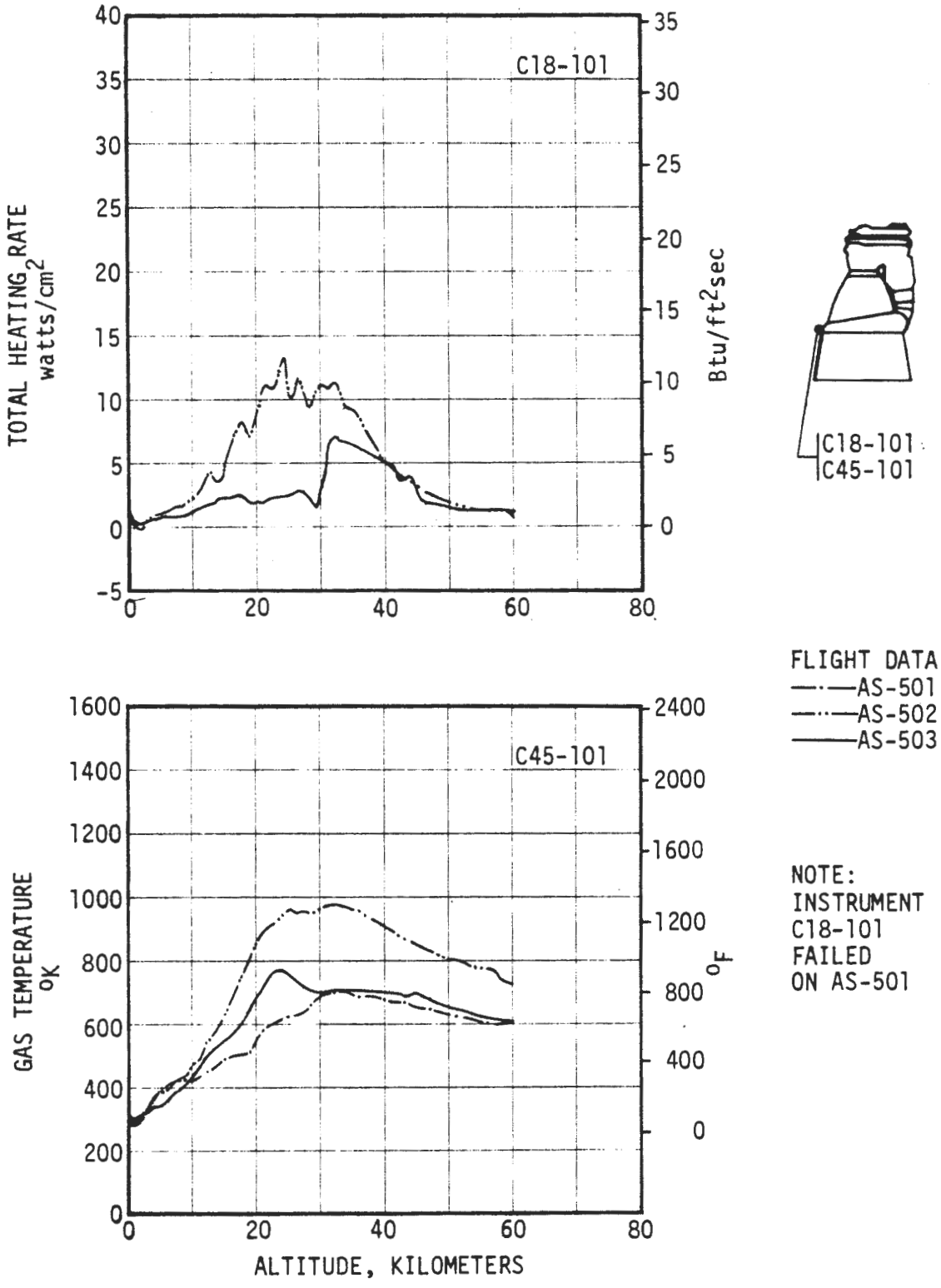

FIGURE 4-37. F-1 ENGINE ENVIRONMENT - OUTBOARD ENGINE MANIFOLD FACING OUTBOARD

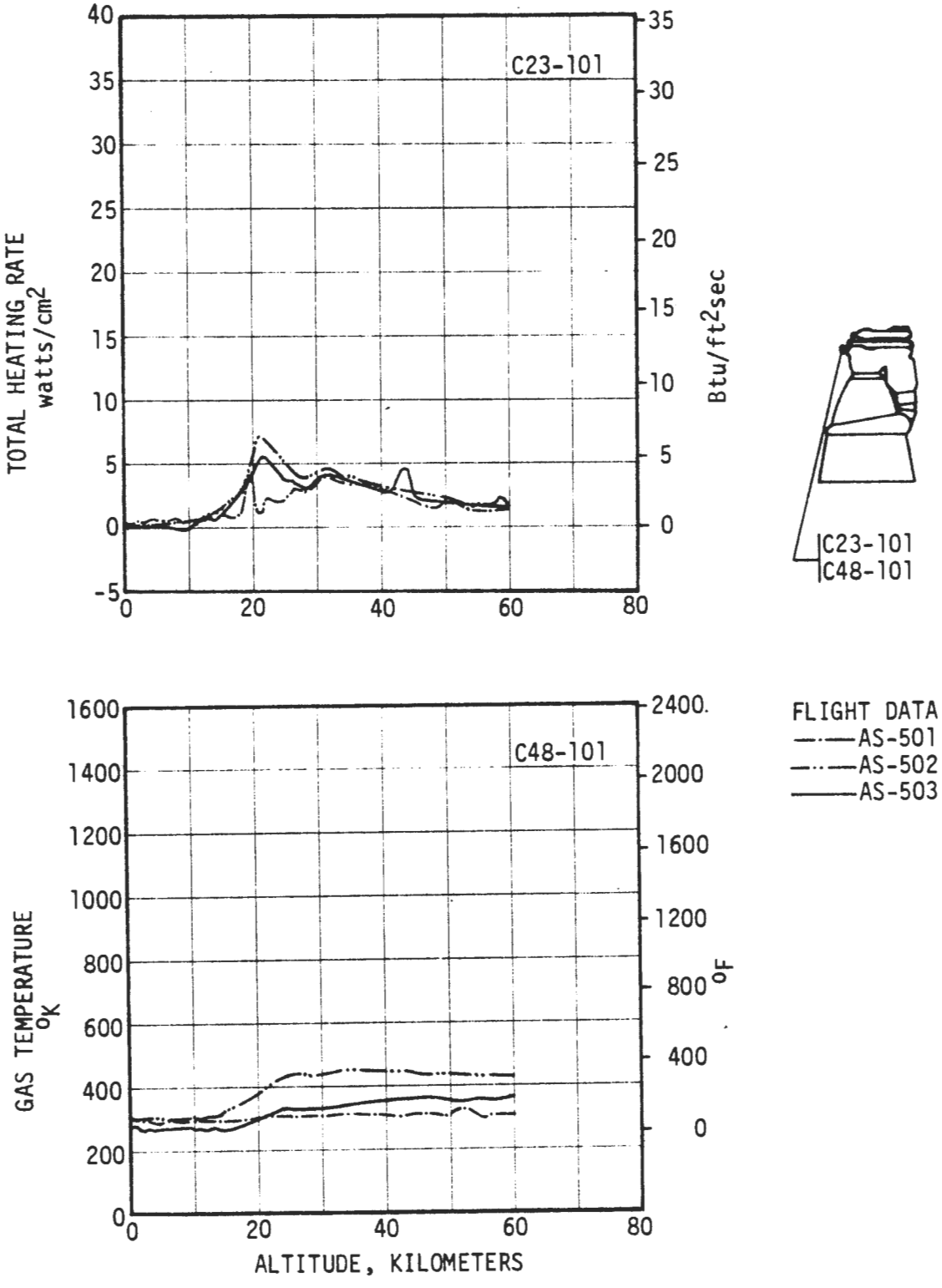

FIGURE 4-38. F-1 ENGINE ENVIRONMENT - OUTBOARD ENGINE NEAR HEAT SHIELD FACING OUTBOARD

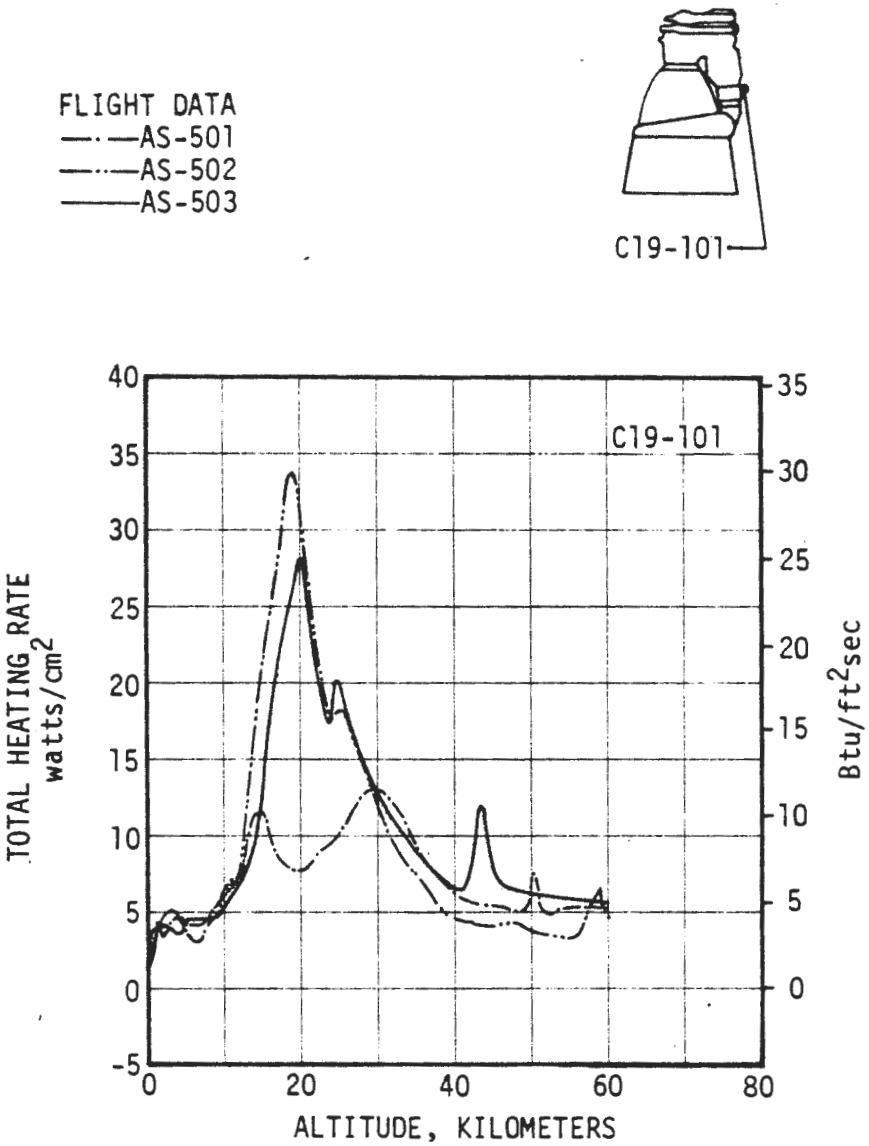

FIGURE 4-39. F-1 ENGINE ENVIRONMENT - OUTBOARD ENGINE FLEXIBLE MANIFOLD FACING INBOARD

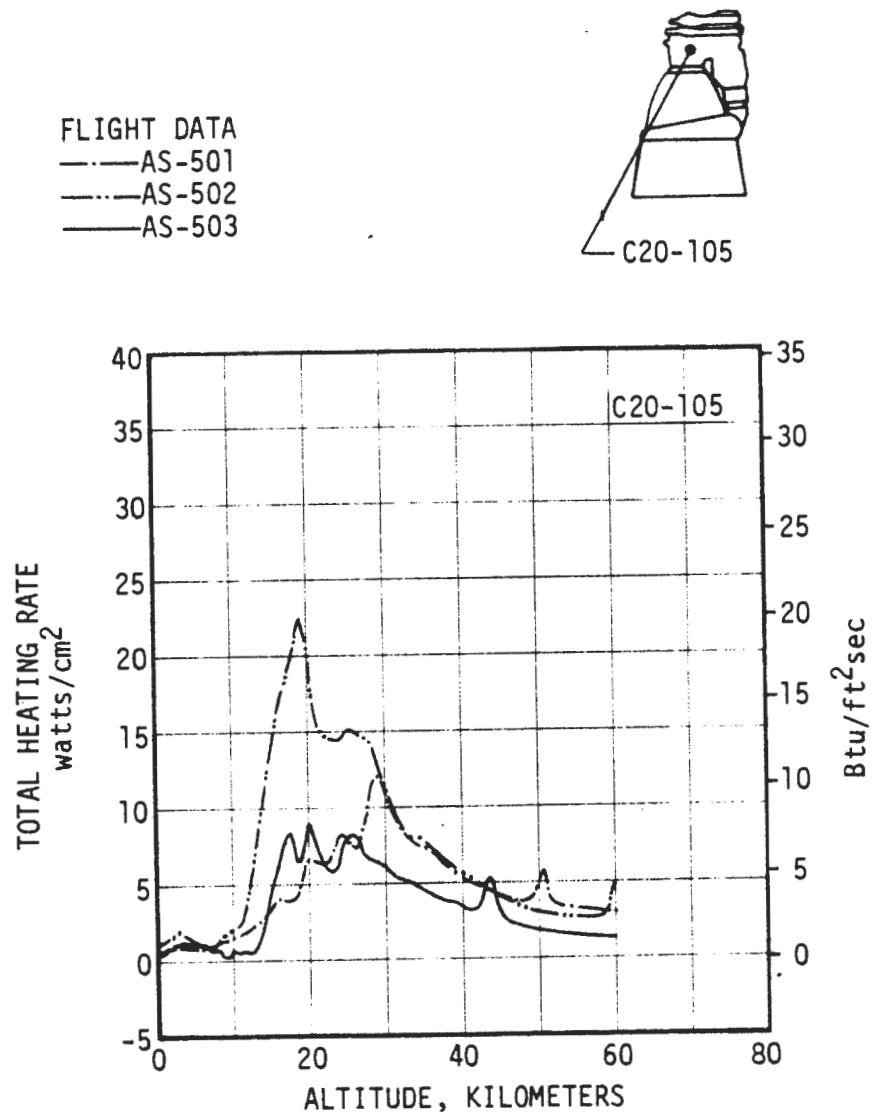

FIGURE 4-40. F-1 ENGINE ENVIRONMENT - INBOARD ENGINE NEAR HEAT SHIELD FACING OUTBOARD ENGINE

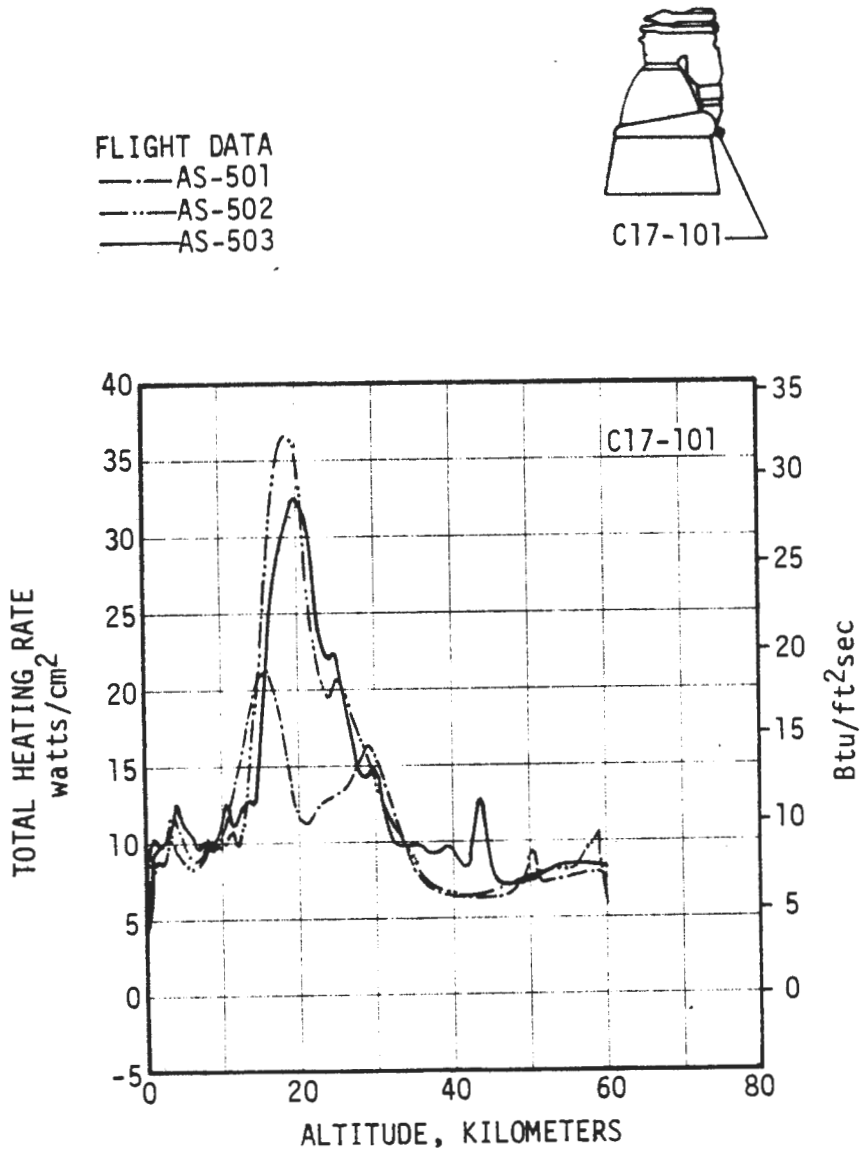

FIGURE 4-41. F-1 ENGINE ENVIRONMENT - OUTBOARD ENGINE MANIFOLD FACING INBOARD

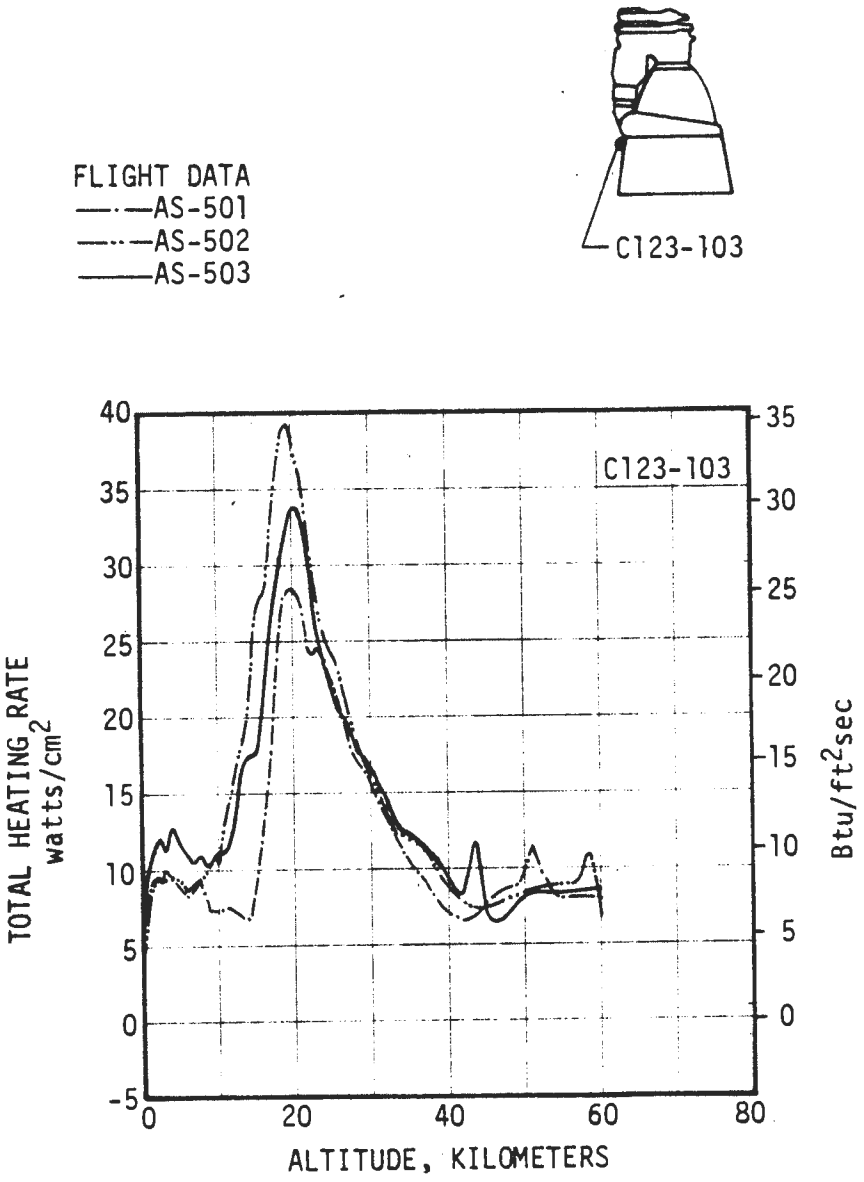

FIGURE 4-42. F-1 ENGINE ENVIRONMENT - OUTBOARD ENGINE MANIFOLD FACING INBOARD

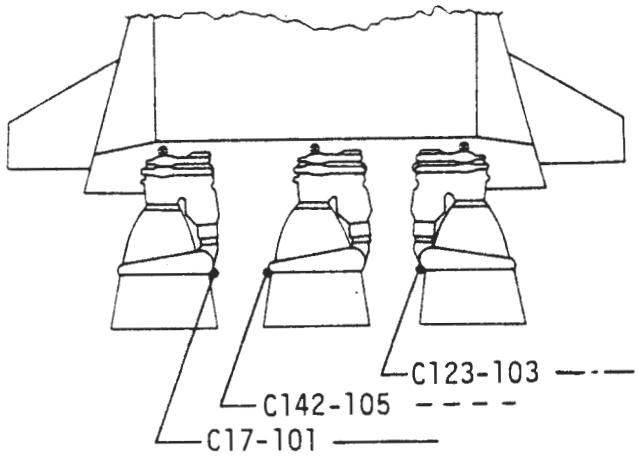

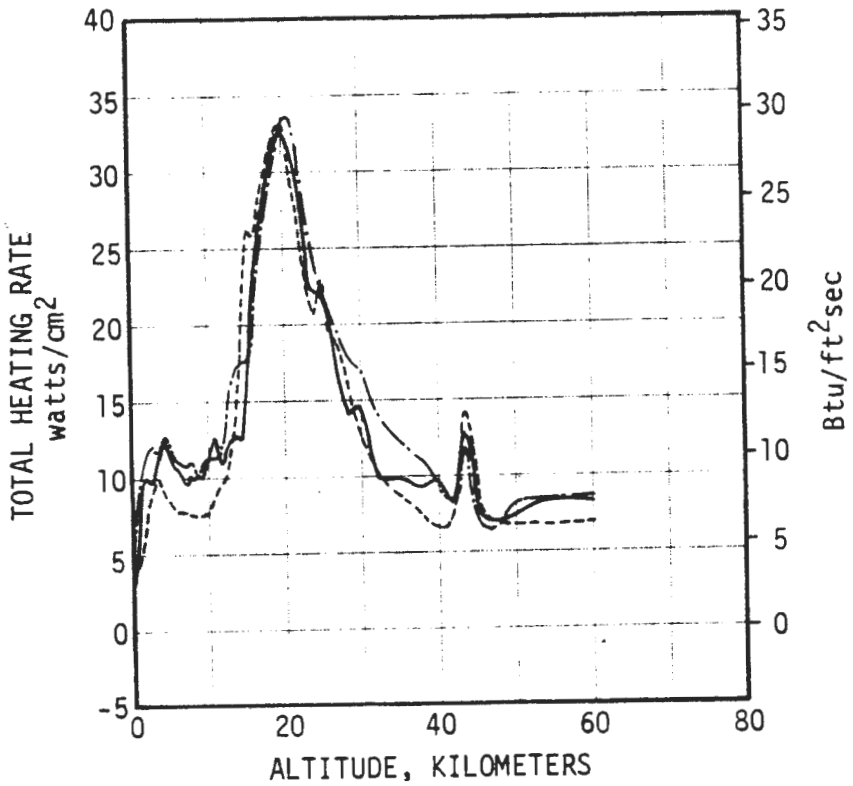

FIGURE 4-43. F-1 ENGINE ENVIRONMENT - FLOW SYMMETRY, AS-503 FLIGHT DATA

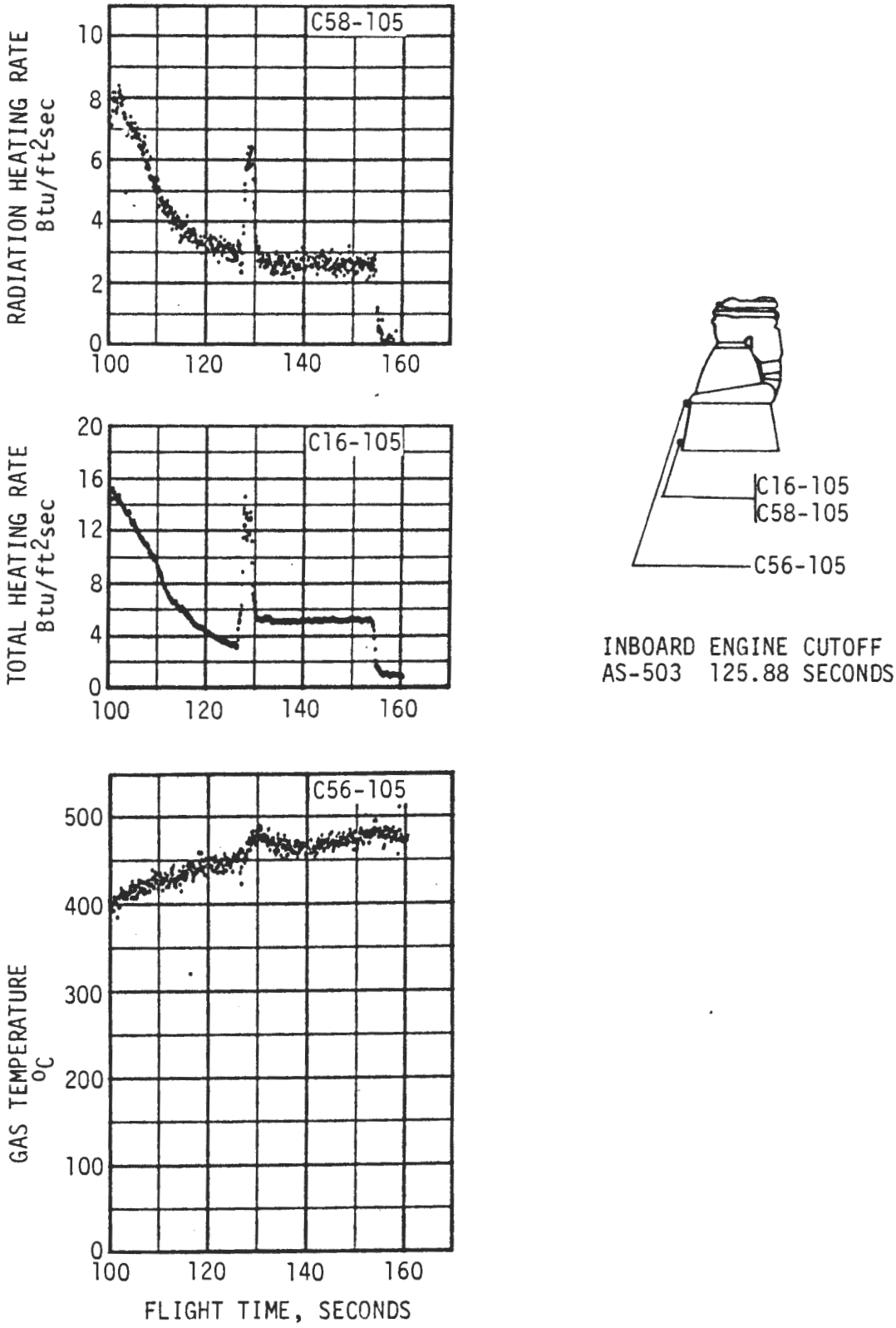

FIGURE 4-44. F-1 ENGINE ENVIRONMENT - INBOARD ENGINE CUTOFF, AS-503 FLIGHT DATA

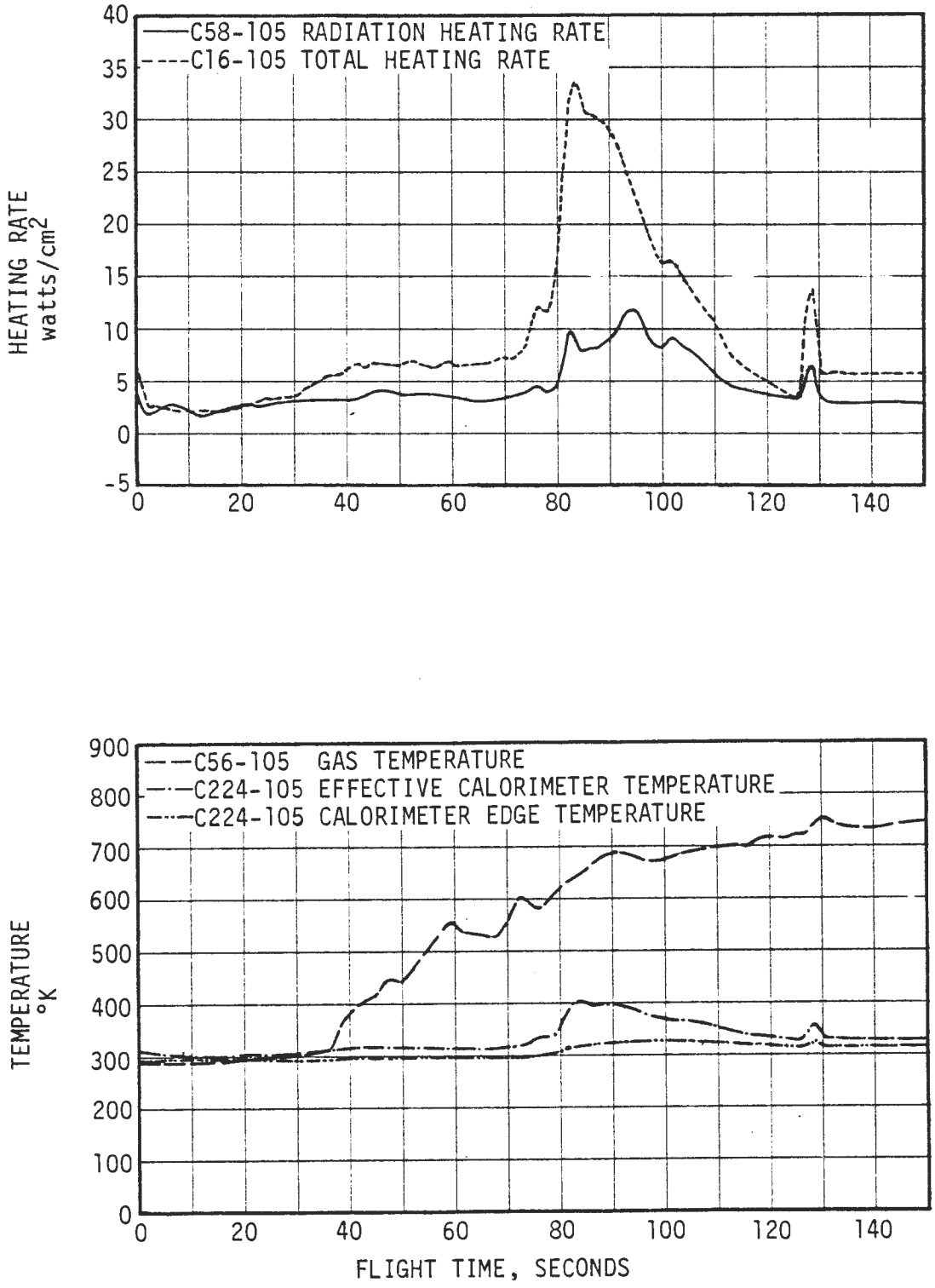

FIGURE 4-45. F-1 ENGINE ENVIRONMENT - INBOARD ENGINE FACING OUTBOARD BETWEEN TWO ENGINES, AS-503 FLIGHT DATA

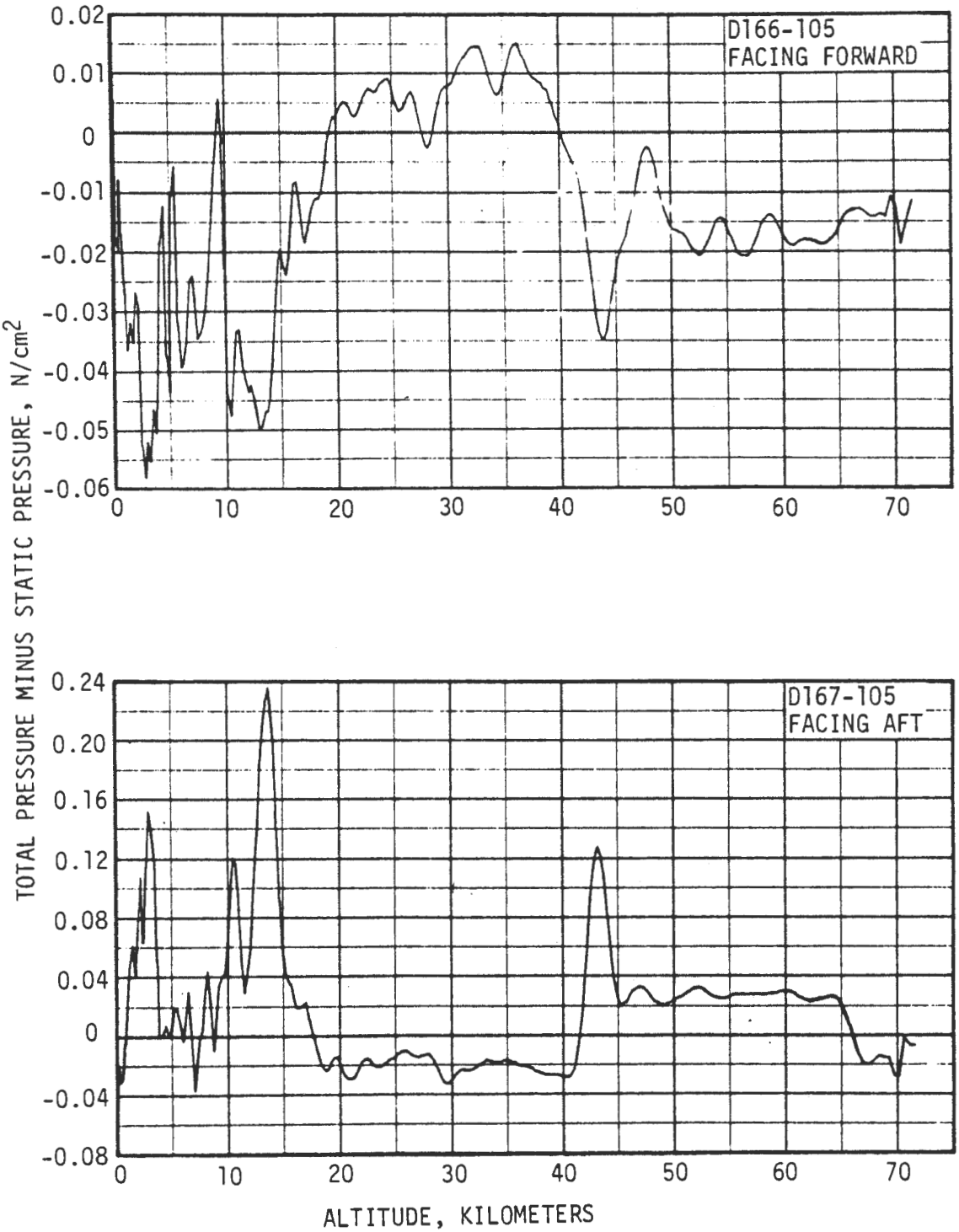

FIGURE 4-46. F-1 ENGINE PRESSURE ENVIRONMENT - INBOARD ENGINE EXIT PLANE, AS-503 FLIGHT DATA

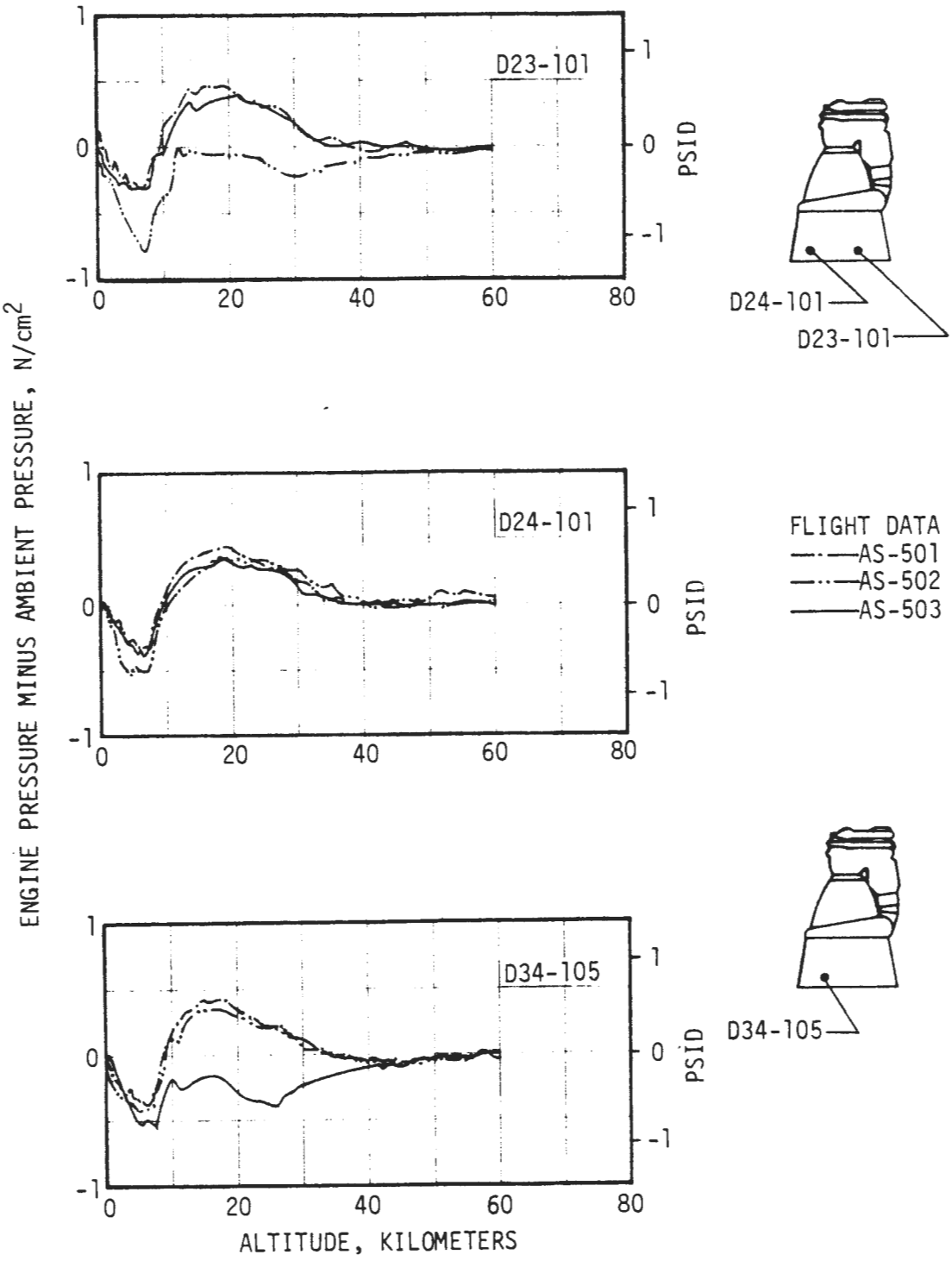

FIGURE 4-47. F-1 ENGINE PRESSURE - INBOARD AND OUTBOARD ENGINE EXIT PLANE

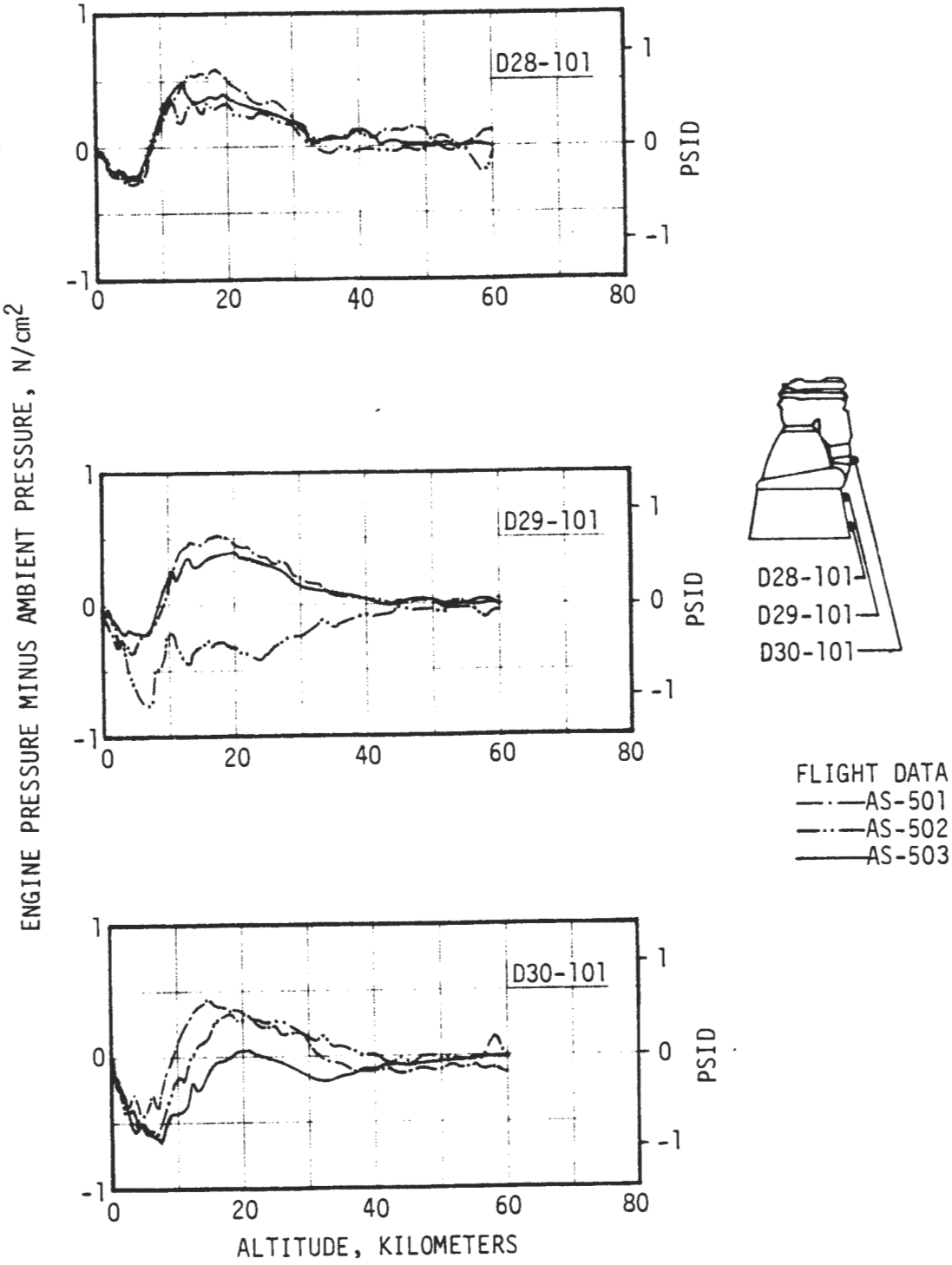

FIGURE 4-48. F-1 ENGINE PRESSURE - AXIAL VARIATION ALONG OUTBOARD ENGINE FACING INBOARD

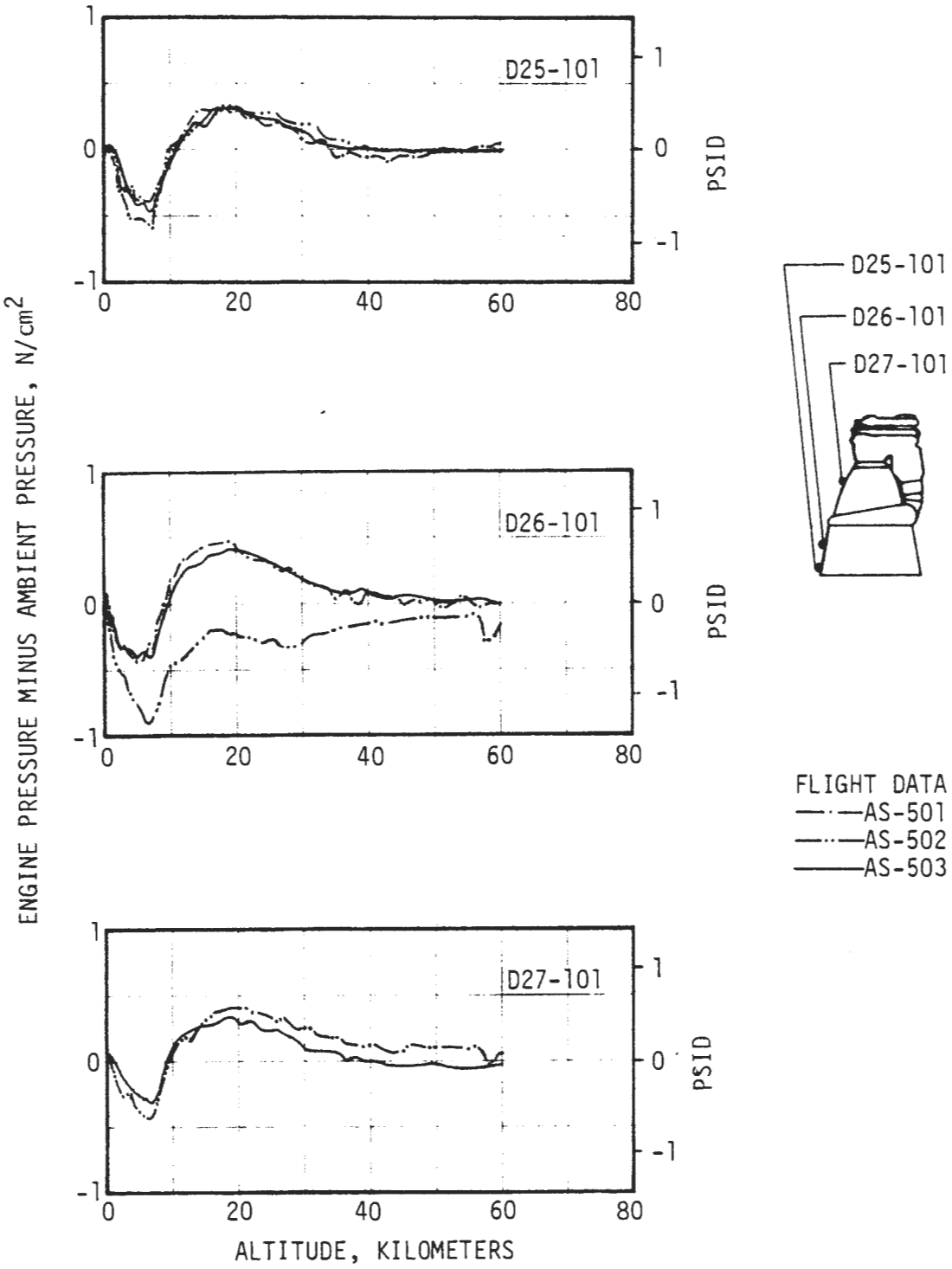

FIGURE 4-49. F-1 ENGINE PRESSURE - AXIAL VARIATION ALONG OUTBOARD ENGINE FACING OUTBOARD

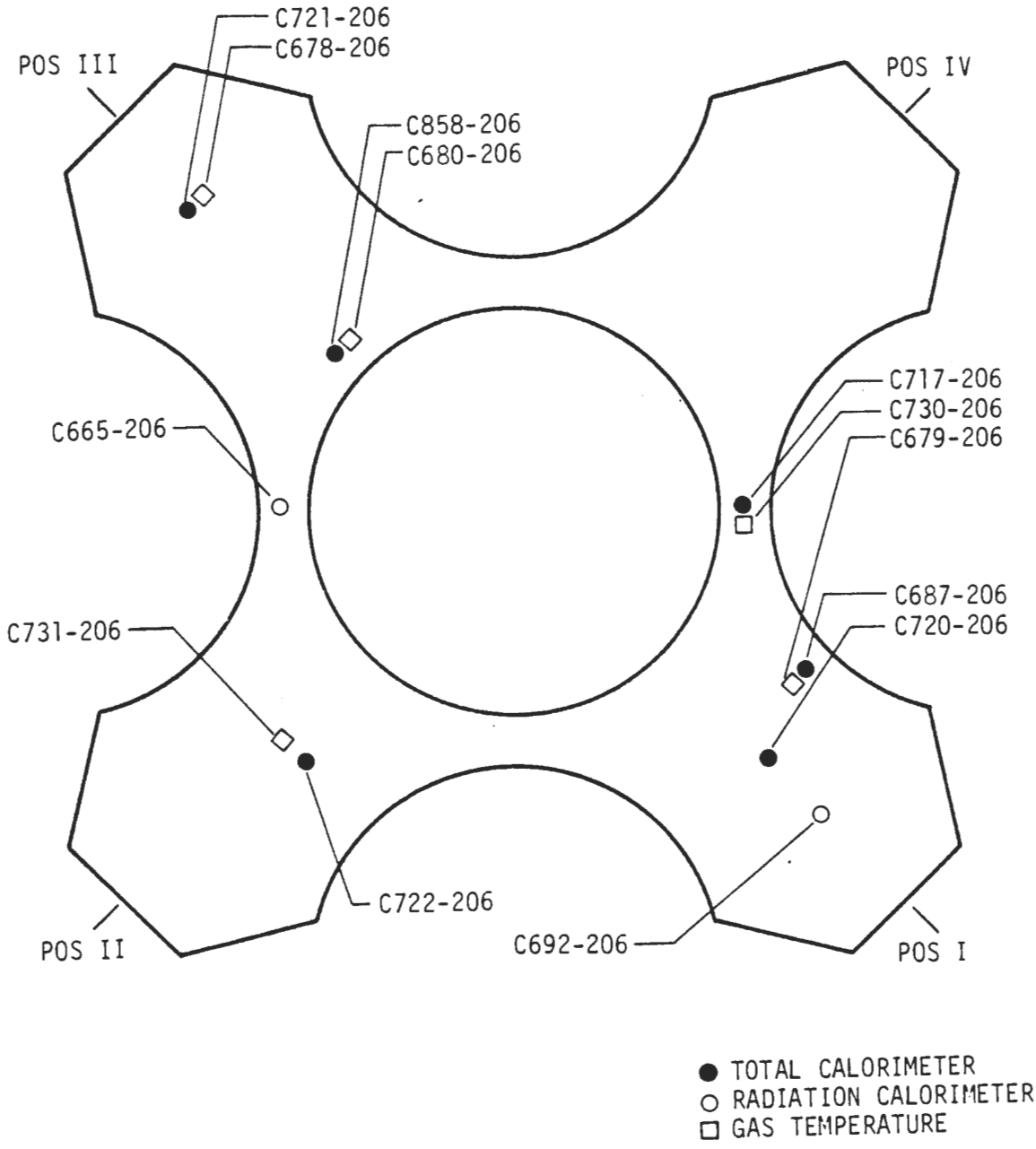

FIGURE 4-50. S-II HEAT SHIELD THERMAL ENVIRONMENT INSTRUMENTATION - AFT SURFACE

TABLE 4-III. S-II BASE HEAT SHIELD THERMAL ENVIRONMENT INSTRUMENTATION
(CONTINUED ON NEXT PAGE)

MEASUREMENT NUMBER	INSTRUMENT TYPE	RANGE watts/cm^2	LOCATION			
			STATION	ANGULAR	RADIAL	REMARKS
C665-206	Cal., Rad.	0-2.27	44	135°	53"	Heat Shield - Aft
C692-206	Cal., Rad.	0-3.41	44	0°	100"	Heat Shield - Aft
C687-206	Cal., Total	0-20.46	44	344°	77"	Heat Shield - Aft
C717-206	Cal., Total	0-20.46	44	315°	53"	Heat Shield - Aft
C720-206	Cal., Total	0.20.46	44	0°	83"	Heat Shield - Aft
C721-206	Cal., Total	0-20.46	44	180°	100"	Heat Shield - Aft
C722-206	Cal., Total	0-20.46	44	83°	75"	Heat Shield - Aft
C858-206	Cal., Total	0-20.46	44	180°	53"	Heat Shield - Aft
C678-206	Gas Temp.	1089-2200*	44	180°	100"	Heat Shield - Aft
C679-206	Gas Temp.	1089-2200*	44	344°	77"	Heat Shield - Aft
C680-206	Gas Temp.	1089-2200*	44	180°	53"	Heat Shield - Aft
C730-206	Gas Temp.	1089-2200*	44	315°	53"	Heat Shield - Aft
C731-206	Gas Temp.	1089-2200*	44	89°	75"	Heat Shield - Aft
D149-206	Pressure	0-0.069**	46	45°	53"	Heat Shield - Forward
D150-206	Pressure	0-0.069**	46	353°	75"	Heat Shield - Forward

* °K
** N/cm^2

TABLE 4-III. S-II BASE HEAT SHIELD THERMAL ENVIRONMENT INSTRUMENTATION (CONCLUDED)

MEASUREMENT NUMBER	INSTRUMENT TYPE	RANGE N/cm^2	LOCATION			
			STATION	ANGULAR	RADIAL	REMARKS
D151-206	Pressure	0-0.069	46	270°	100"	Heat Shield - Forward
D157-206	Pressure	0-0.069	44	45°	53"	Heat Shield - Aft
D158-206	Pressure	0-0.069	44	326°	75"	Heat Shield - Aft
D162-206	Pressure	0-0.069	44	270°	100"	Heat Shield - Aft
D94-206	Pressure	0-0.069	46	90°	85"	Heat Shield - Aft
D95-206	Pressure	0-0.069	46	180°	85"	Heat Shield - Aft
D99-206	Pressure	0-0.069	46	0 °	85"	Heat Shield - Forward
D100-206	Pressure	0-0.069	46	90°	85"	Heat Shield - Forward
D101-206	Pressure	0-0.069	46	180°	85"	Heat Shield - Forward
D102-206	Pressure	0-0.069	46	270°	85"	Heat Shield - Forward

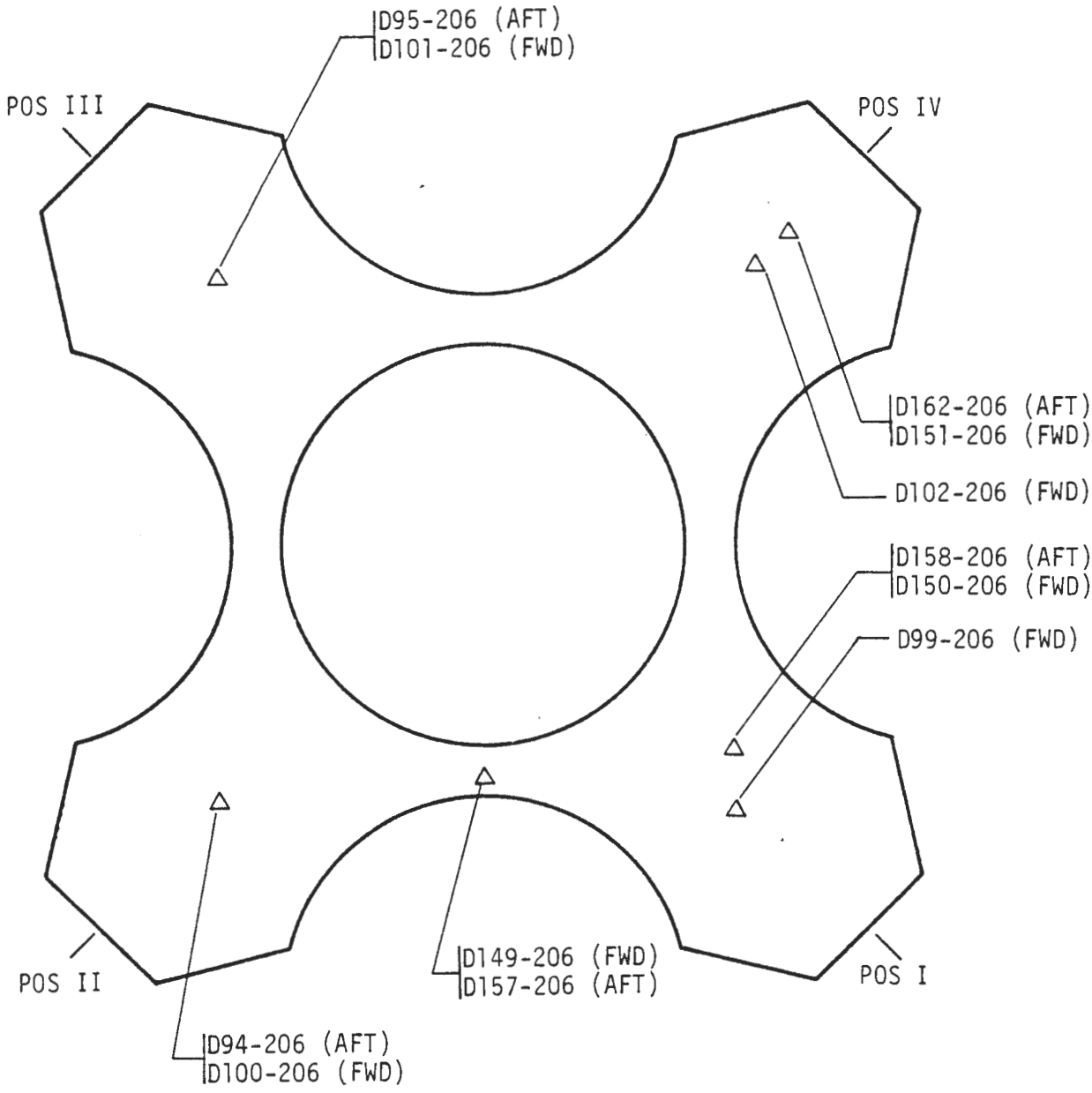

FIGURE 4-51. S-II HEAT SHIELD PRESSURE INSTRUMENTATION - AFT AND FORWARD SURFACES

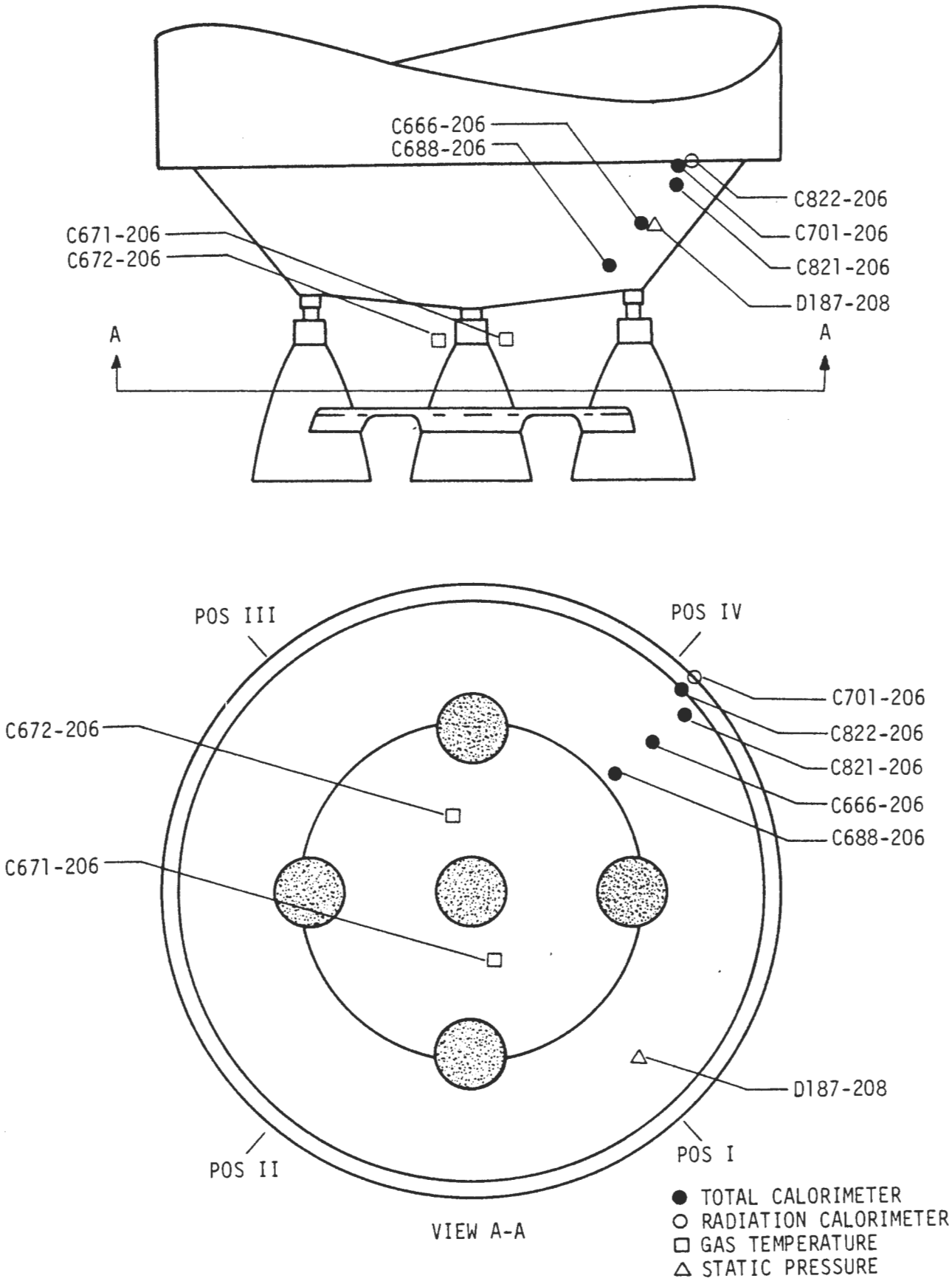

FIGURE 4-52. S-II THRUST CONE AND ENGINE COMPARTMENT INSTRUMENTATIONS

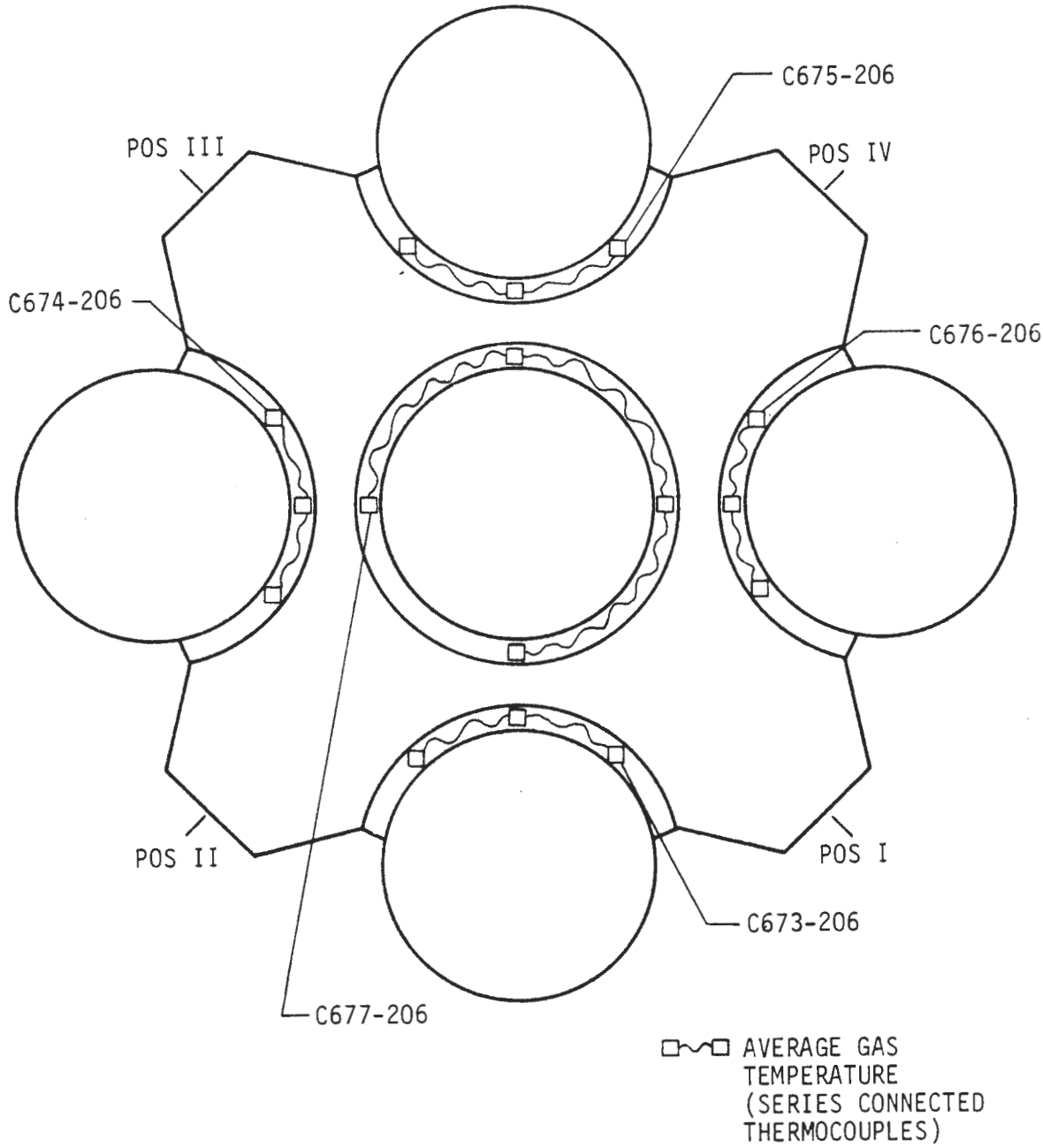

FIGURE 4-53. S-II ENGINE CURTAIN GAS TEMPERATURES

TABLE 4-IV. J-2 ENGINE COMPARTMENT AND THRUST CONE INSTRUMENTATION

(CONTINUED ON NEXT PAGE)

MEASUREMENT NUMBER	INSTRUMENT TYPE	RANGE watts/cm^2	LOCATION			
			STATION	ANGULAR	RADIAL	REMARKS
C822-206	Cal., Rad.	0-2.27	196	270°	184"	Thrust Cone - Aft
C666-206	Cal., Total	0-2.27	140	275°	144"	Thrust Cone - Aft
C688-206	Cal., Total	0-2.27	115	275°		Thrust Cone - Aft
C701-206	Cal., Total	0-2.27	196	270°	180"	Thrust Cone - Aft
C821-208	Cal., Total	0-2.27	170	275°		Thrust Cone - Aft
C671-206	Gas Temp.**	228-339*	72	30°	45"	Engine Compartment
C672-206	Gas Temp.	228-339*	72	210°	45"	Engine Compartment
C673-206	Gas Temp.	255-422*	48 48 48	20° 45° 70°	76" 56" 76"	Heat Shield Curtain (Series Connected Thermocouples)
C674-206	Gas Temp.	255-422*	48 48 48	110° 135° 160°	76" 56" 76"	Heat Shield Curtain (Series Connected Thermocouples)
C675-206	Gas Temp.	255-422*	48 48 48	200° 225° 250°	76" 56" 76"	Heat Shield Curtain (Series Connected Thermocouples)
C676-206	Gas Temp.	255-422*	48 48 48	290° 315° 340°	76" 56" 76"	Heat Shield Curtain (Series Connected Thermocouples)

* °K

TABLE 4-IV. J-2 ENGINE COMPARTMENT AND THRUST CONE INSTRUMENTATION (CONCLUDED)

MEASUREMENT NUMBER	INSTRUMENT TYPE	RANGE	LOCATION			
			STATION	ANGULAR	RADIAL	REMARKS
C677-206	Gas Temp.	255-422°K	48	0 °	45"	Heat Shield Curtain
			48	90°	45"	(Series Connected Thermocouples)
			48	180°	45"	
			48	270°	45"	
D187-206	Pressure	0-0.069 N/cm^2	140	2°	130"	Thrust Cone - Aft

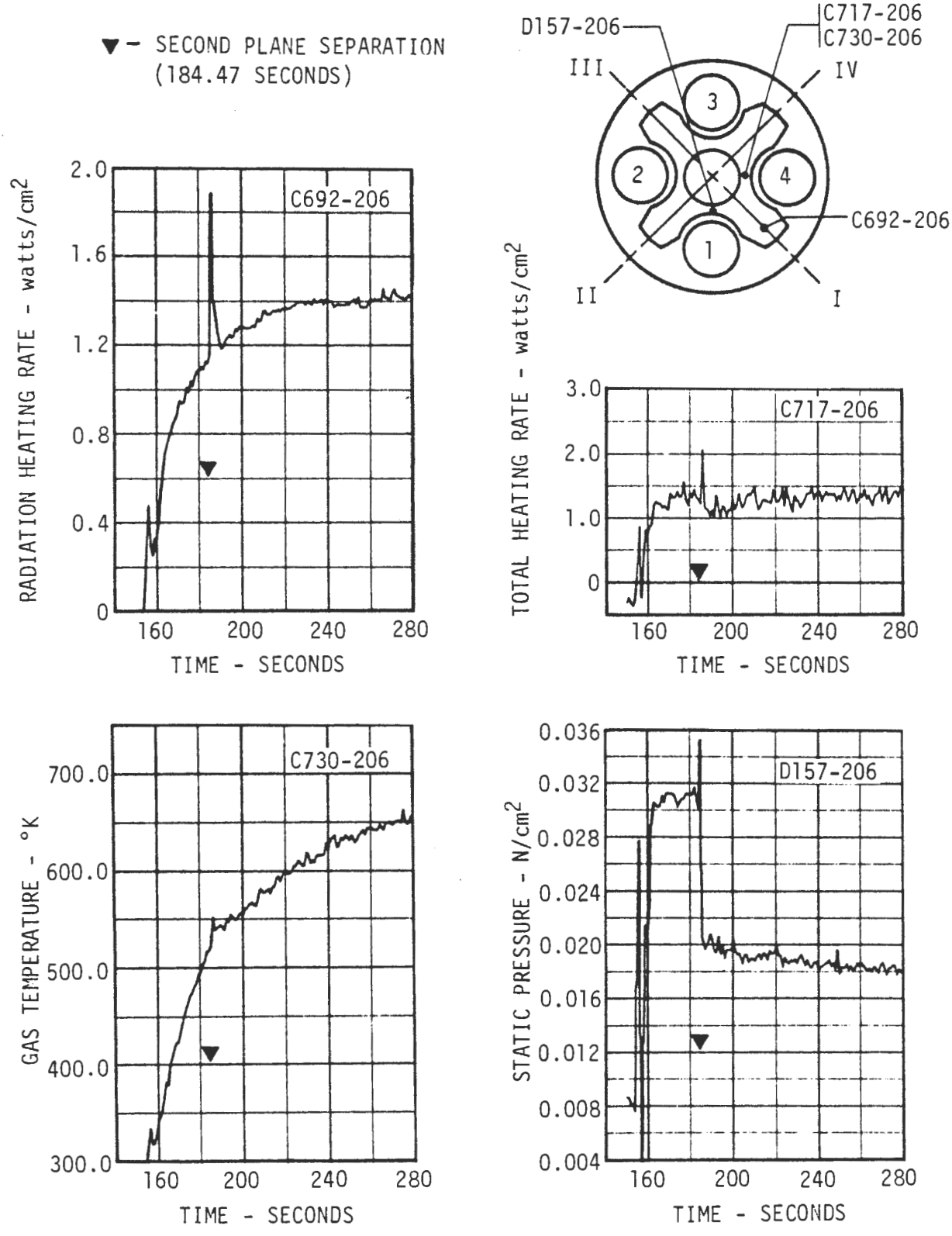

FIGURE 4-54. TYPICAL S-II BASE REGION ENVIRONMENT DURING AS-503 INTERSTAGE SEPARATION

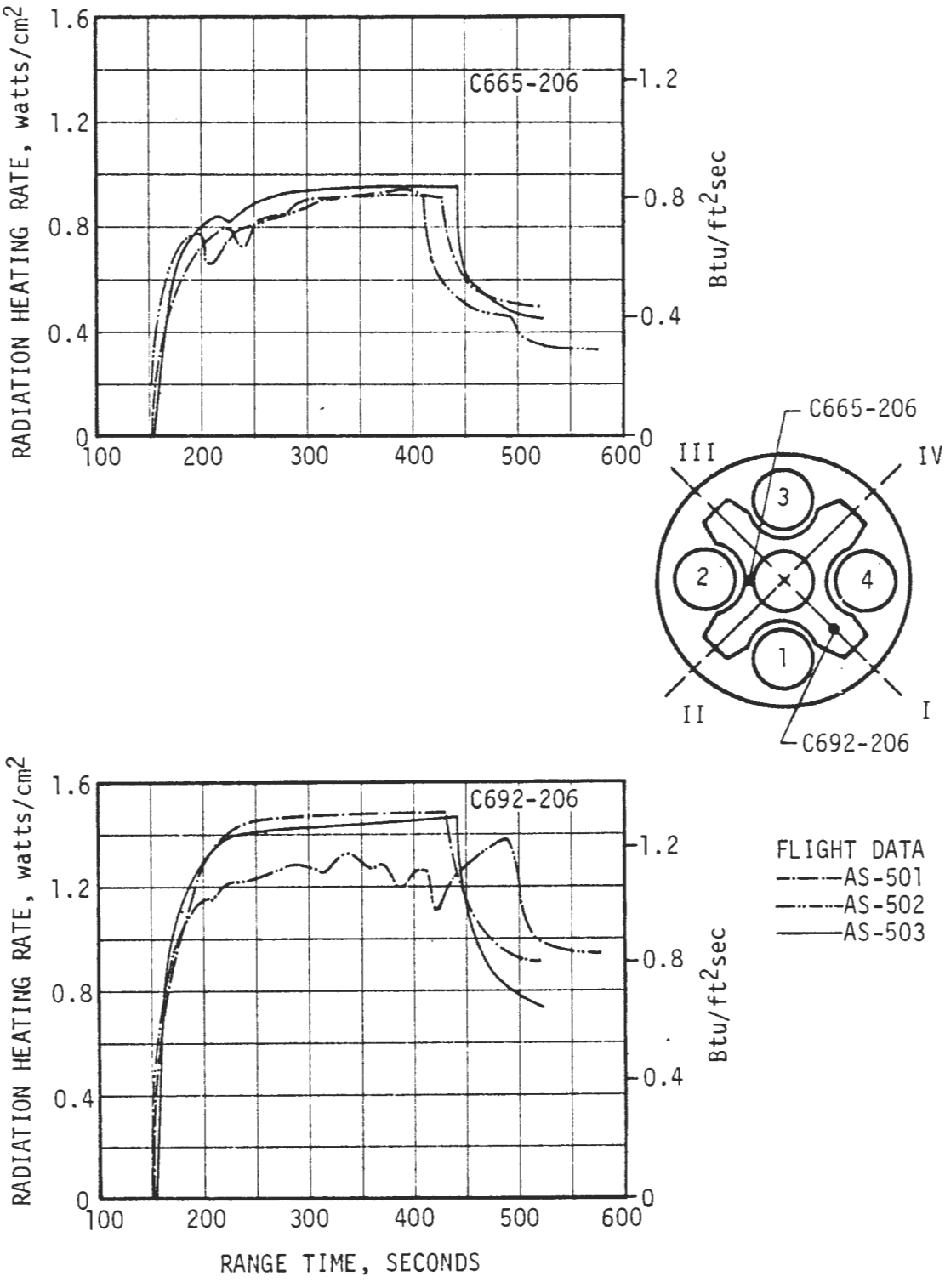

FIGURE 4-55. S-II HEAT SHIELD RADIATION HEATING RATES

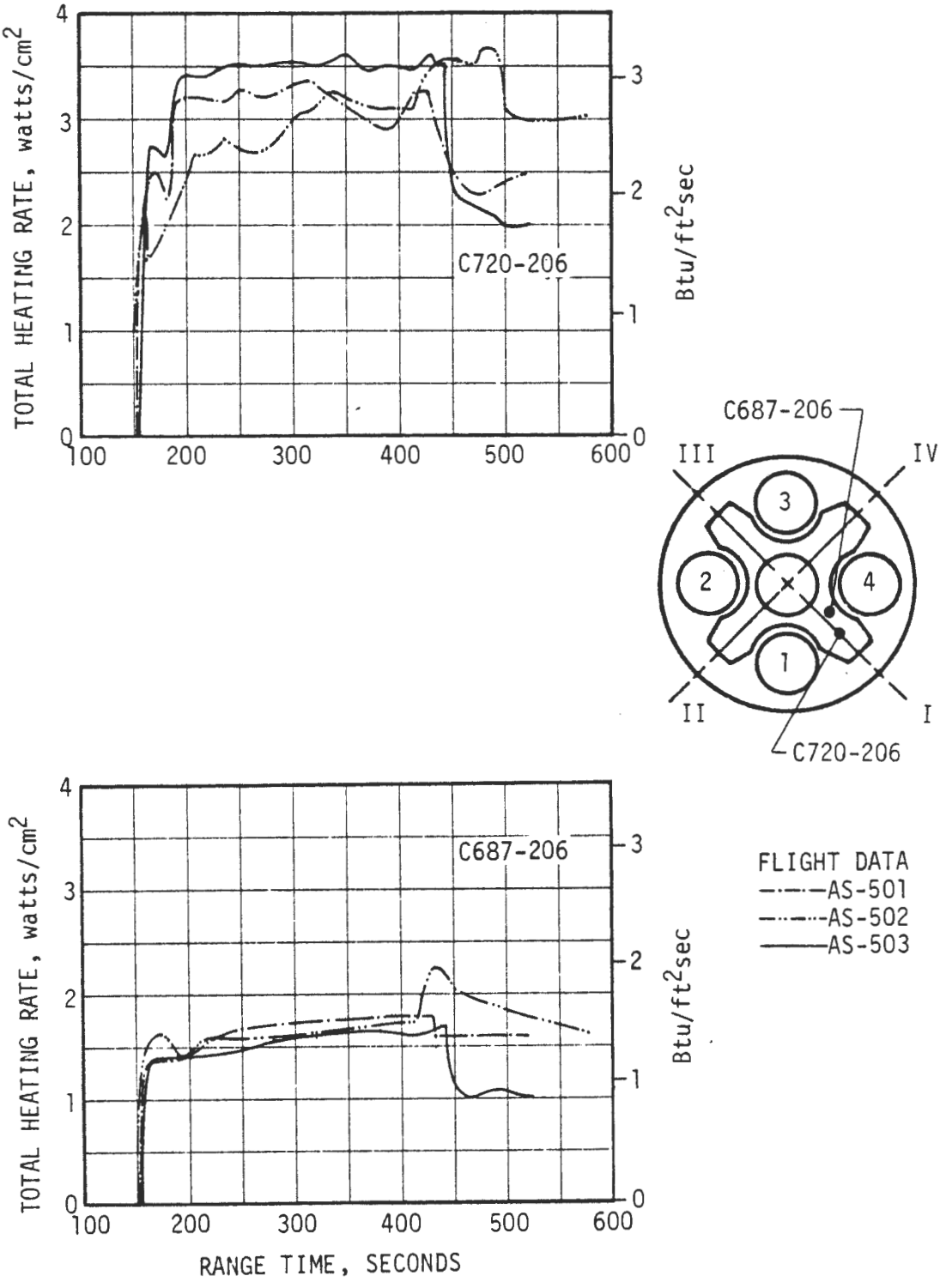

FIGURE 4-56. S-II HEAT SHIELD TOTAL HEATING RATES (CONTINUED ON NEXT PAGE)

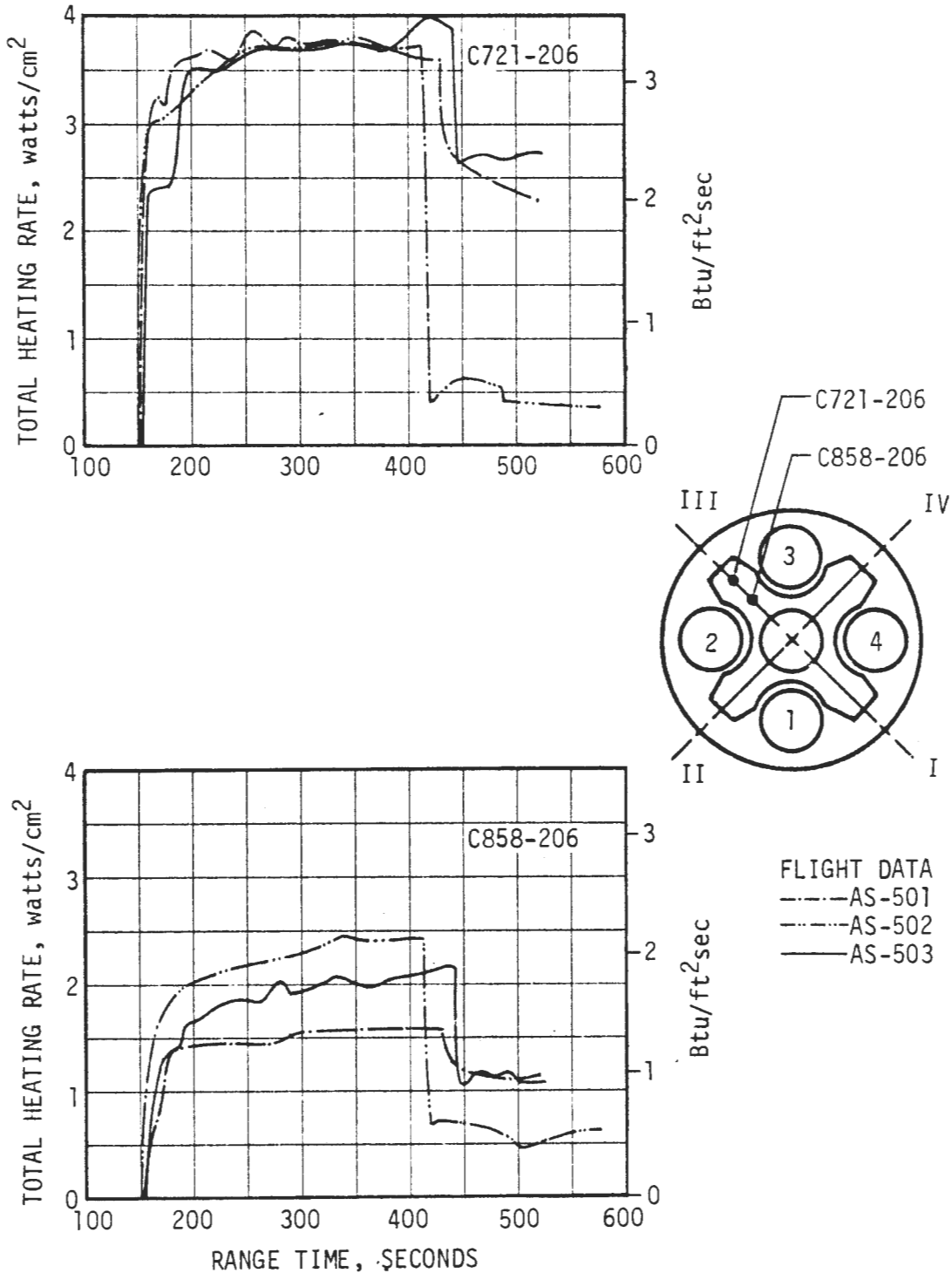

FIGURE 4-56. S-II HEAT SHIELD TOTAL HEATING RATES (CONTINUED ON NEXT PAGE)

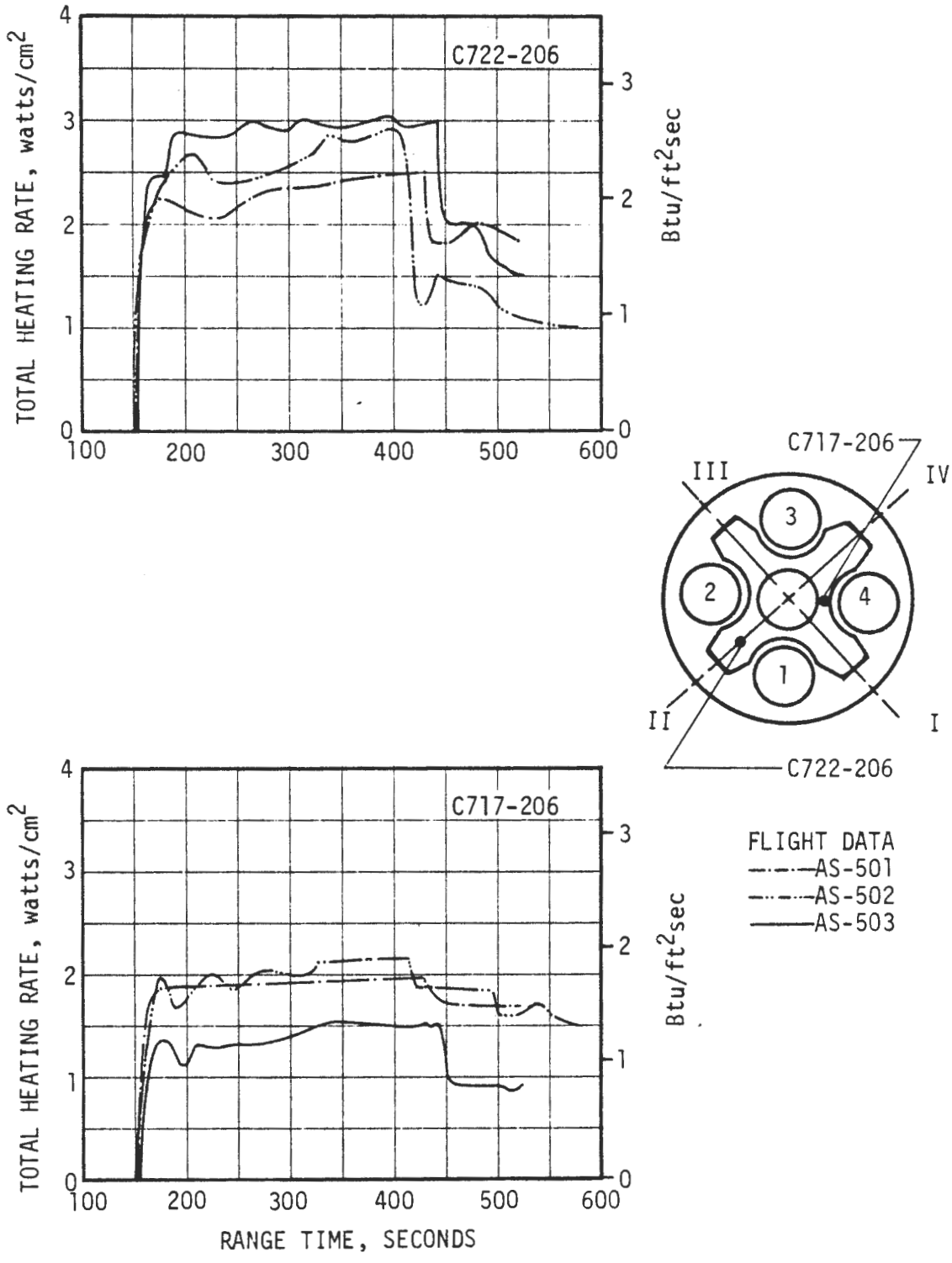

FIGURE 4-56. S-II HEAT SHIELD TOTAL HEATING RATES (CONCLUDED)

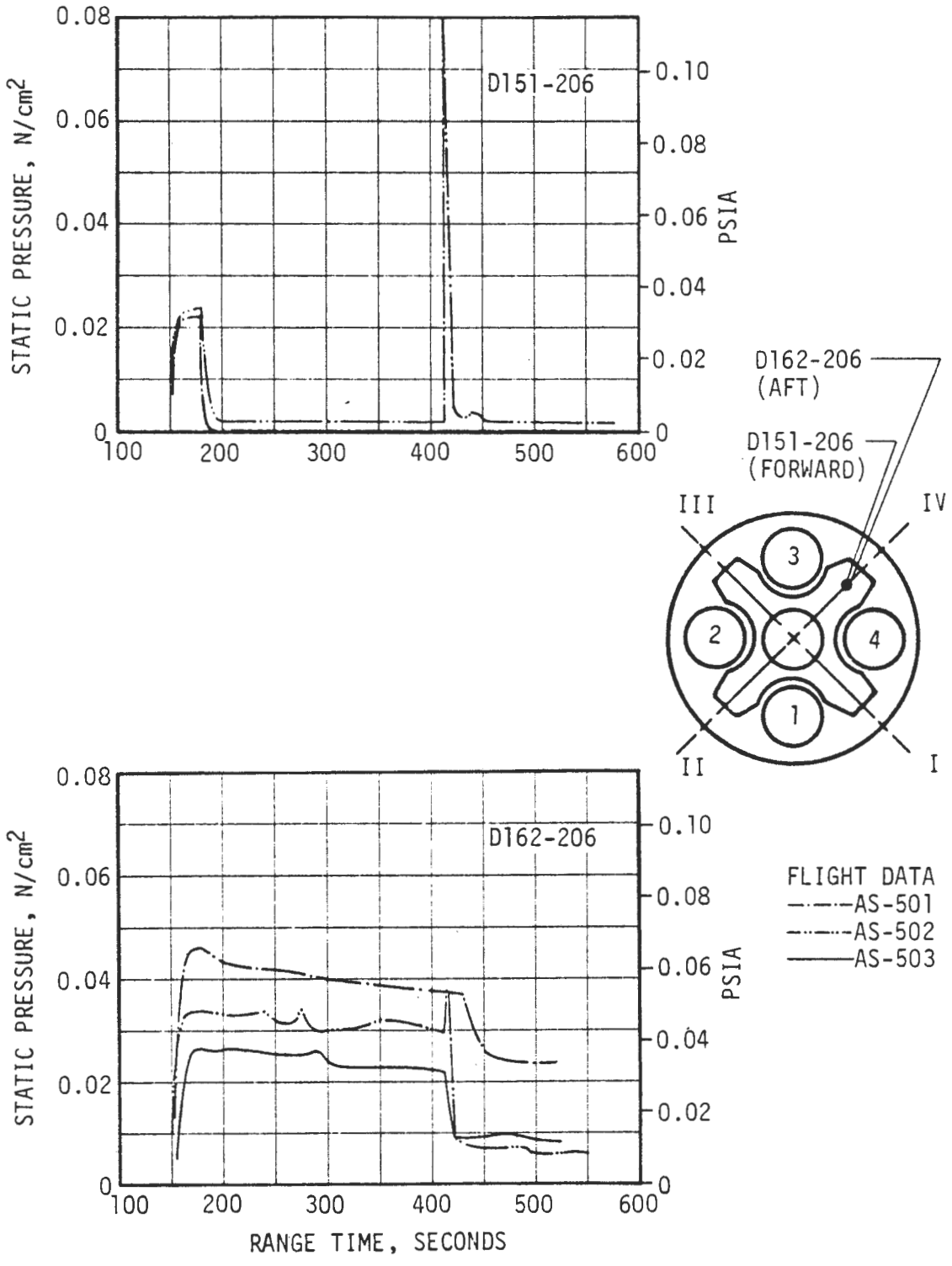

FIGURE 4-57. S-II HEAT SHIELD STATIC PRESSURE - AFT AND FORWARD SURFACES
(CONTINUED ON NEXT PAGE)

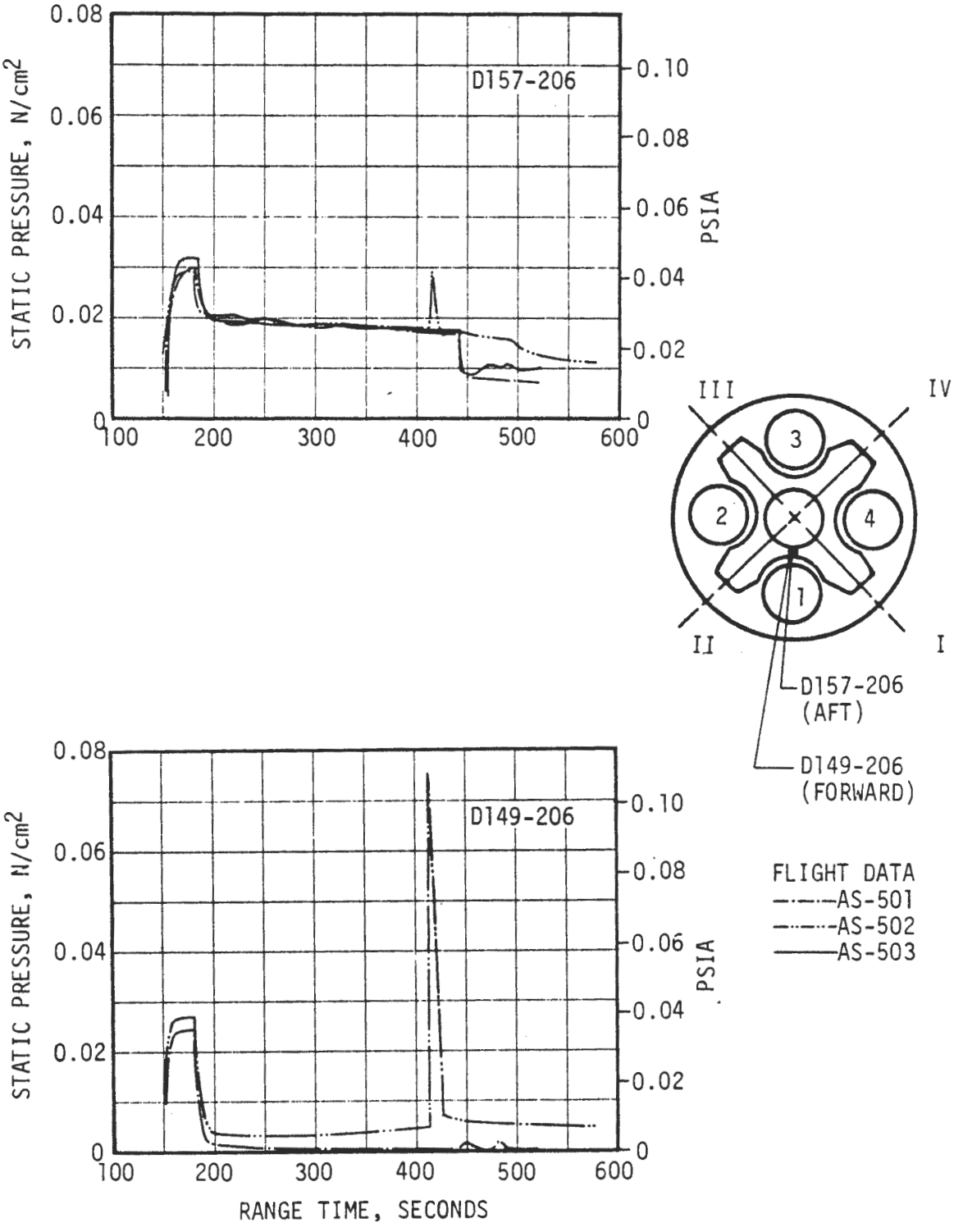

FIGURE 4-57. S-II HEAT SHIELD STATIC PRESSURE - AFT AND FORWARD SURFACES
(CONTINUED ON NEXT PAGE)

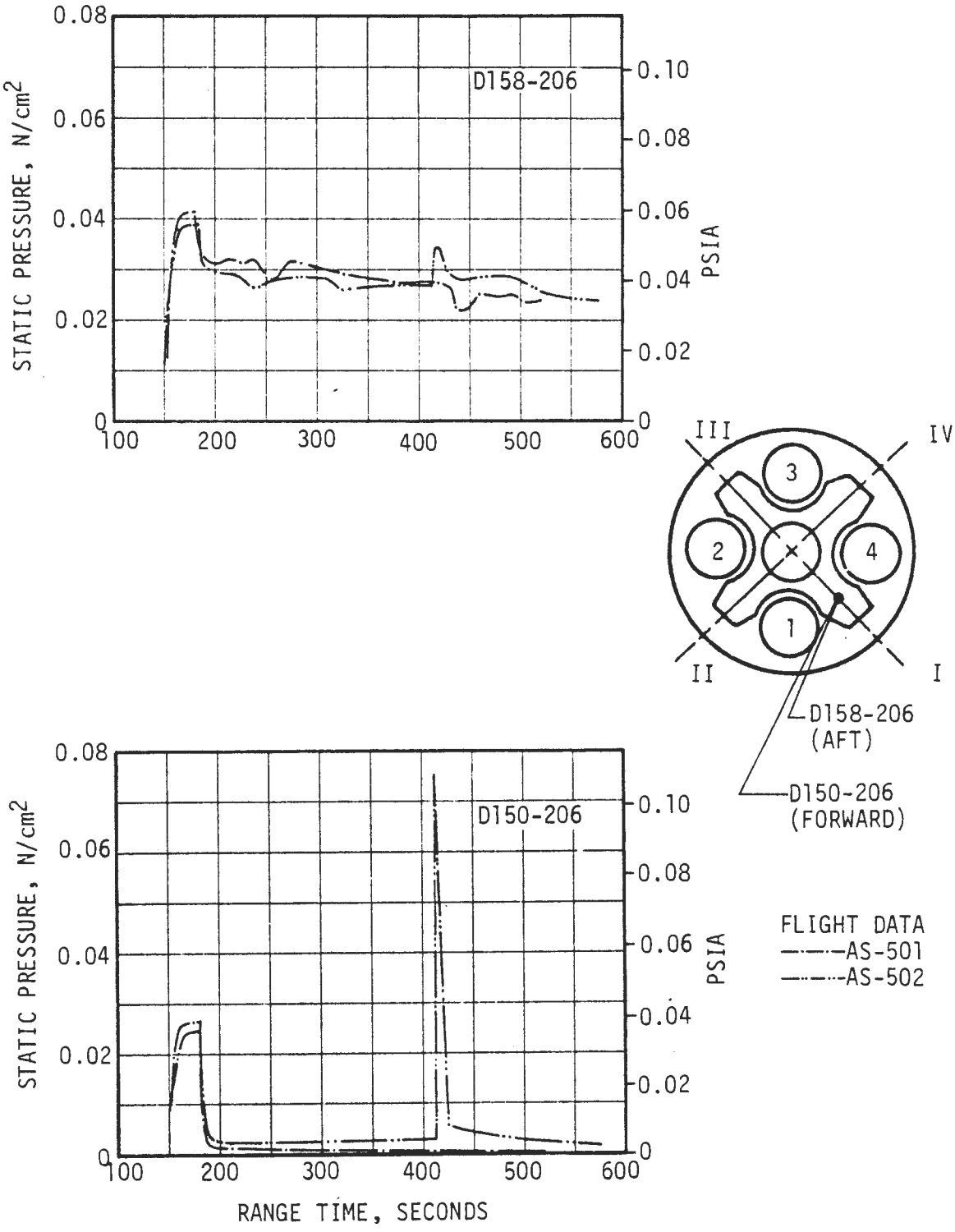

FIGURE 4-57. S-II HEAT SHIELD STATIC PRESSURE - AFT AND FORWARD SURFACES
(CONTINUED ON NEXT PAGE)

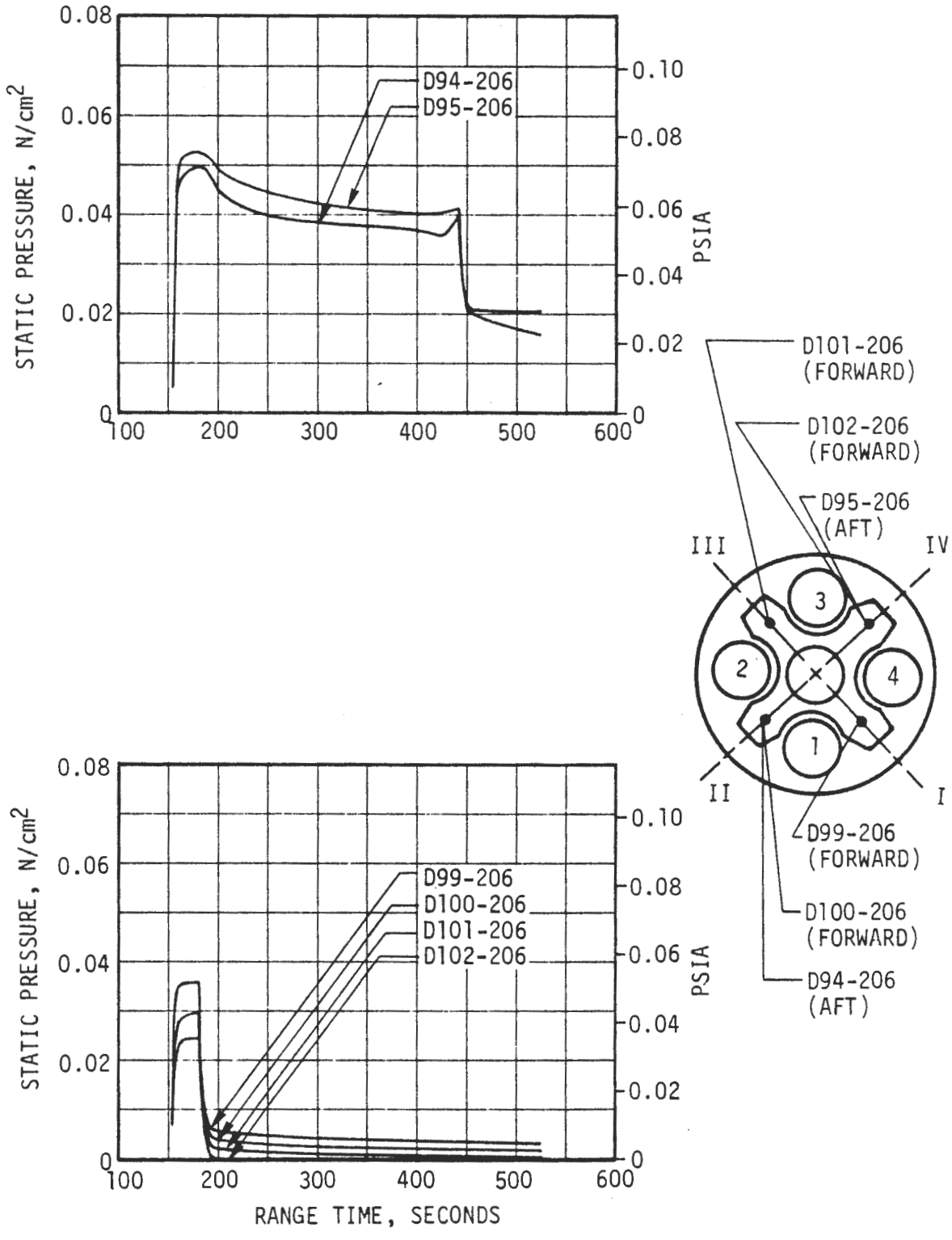

FIGURE 4-57. S-II HEAT SHIELD STATIC PRESSURE - AFT AND FORWARD SURFACES (CONCLUDED)

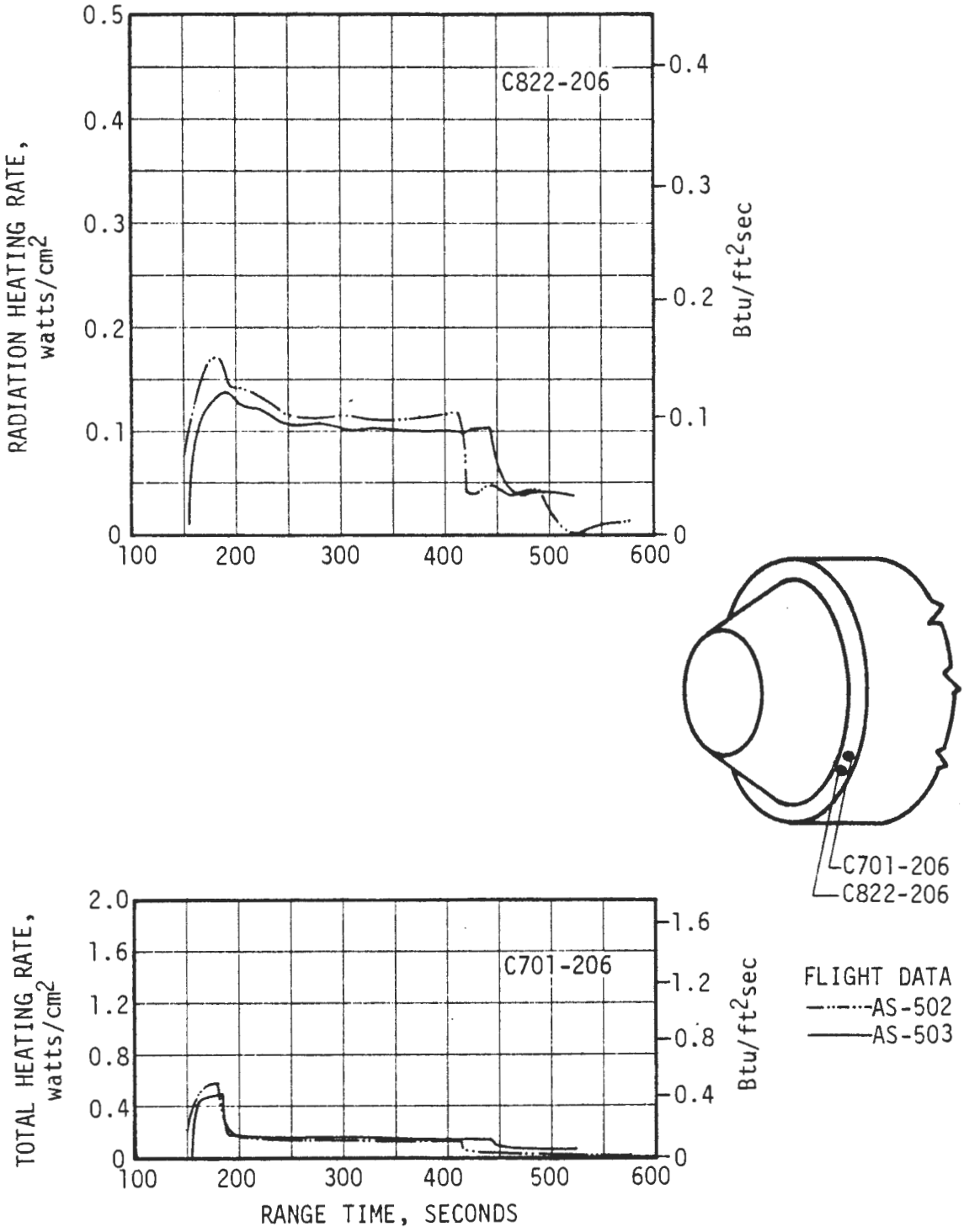

FIGURE 4-58 S-II THRUST CONE RADIATION AND TOTAL HEATING RATES

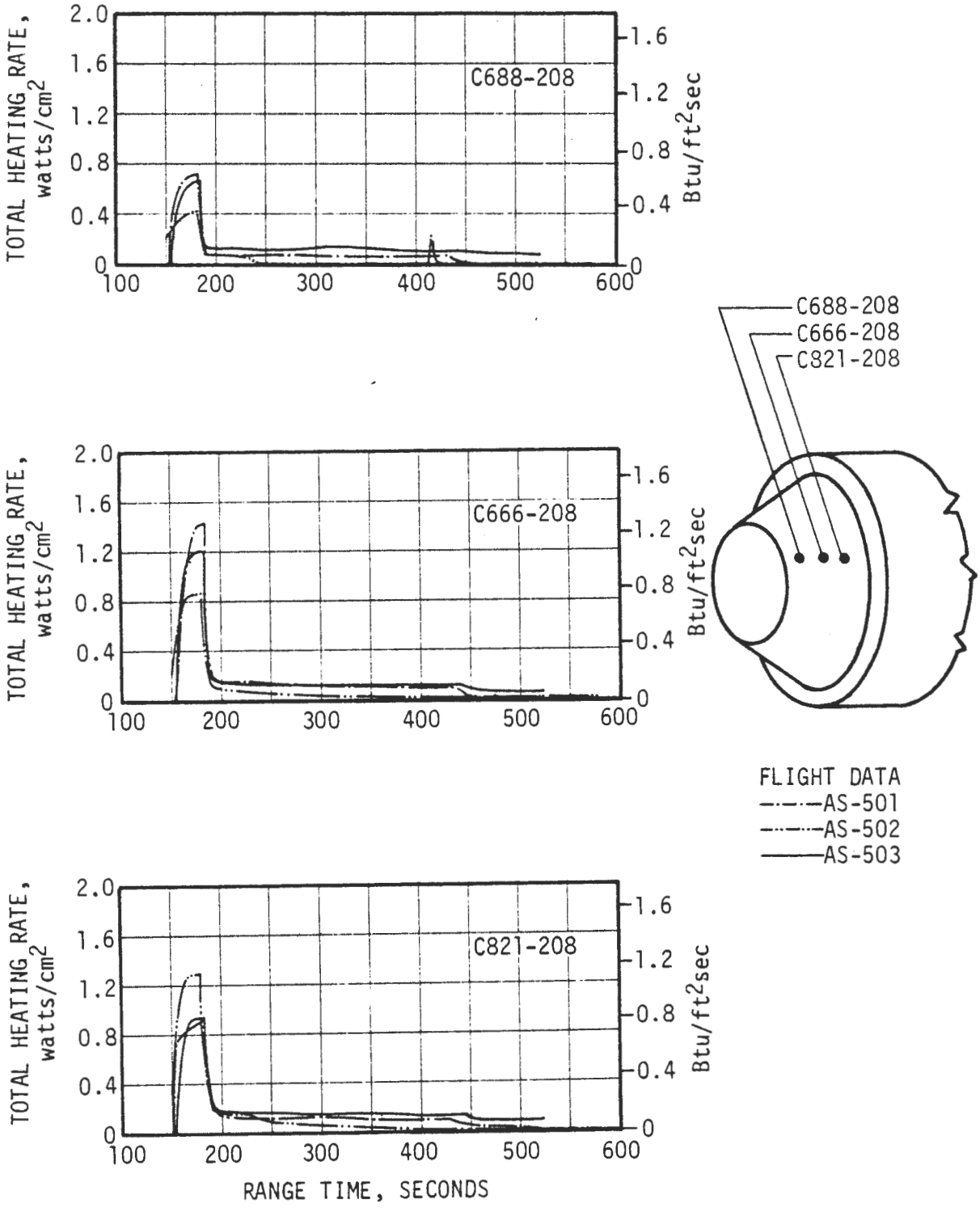

FIGURE 4-59. S-II THRUST CONE TOTAL HEATING RATES

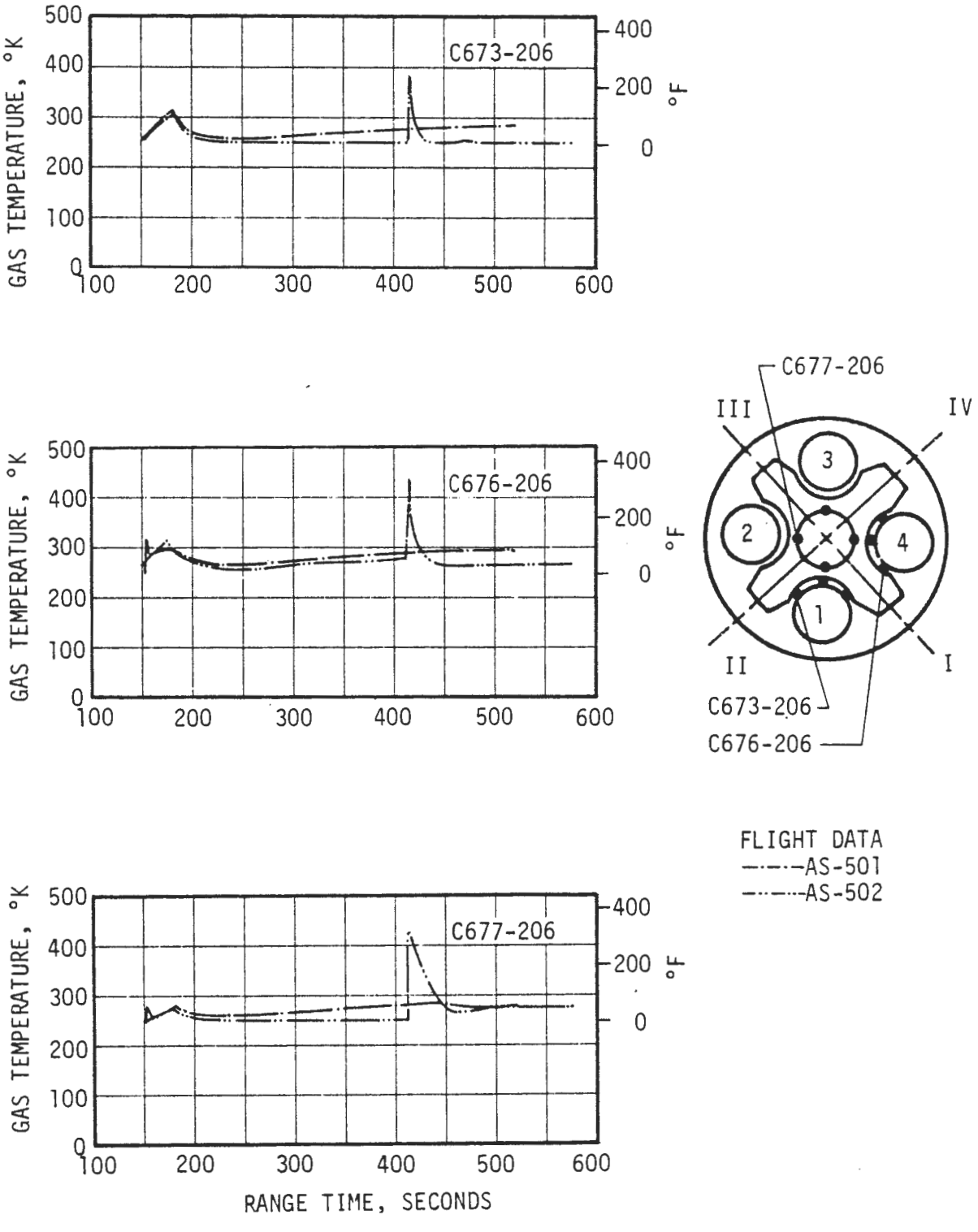

FIGURE 4-60. S-II ENGINE CURTAIN GAS TEMPERATURES (CONTINUED ON NEXT PAGE)

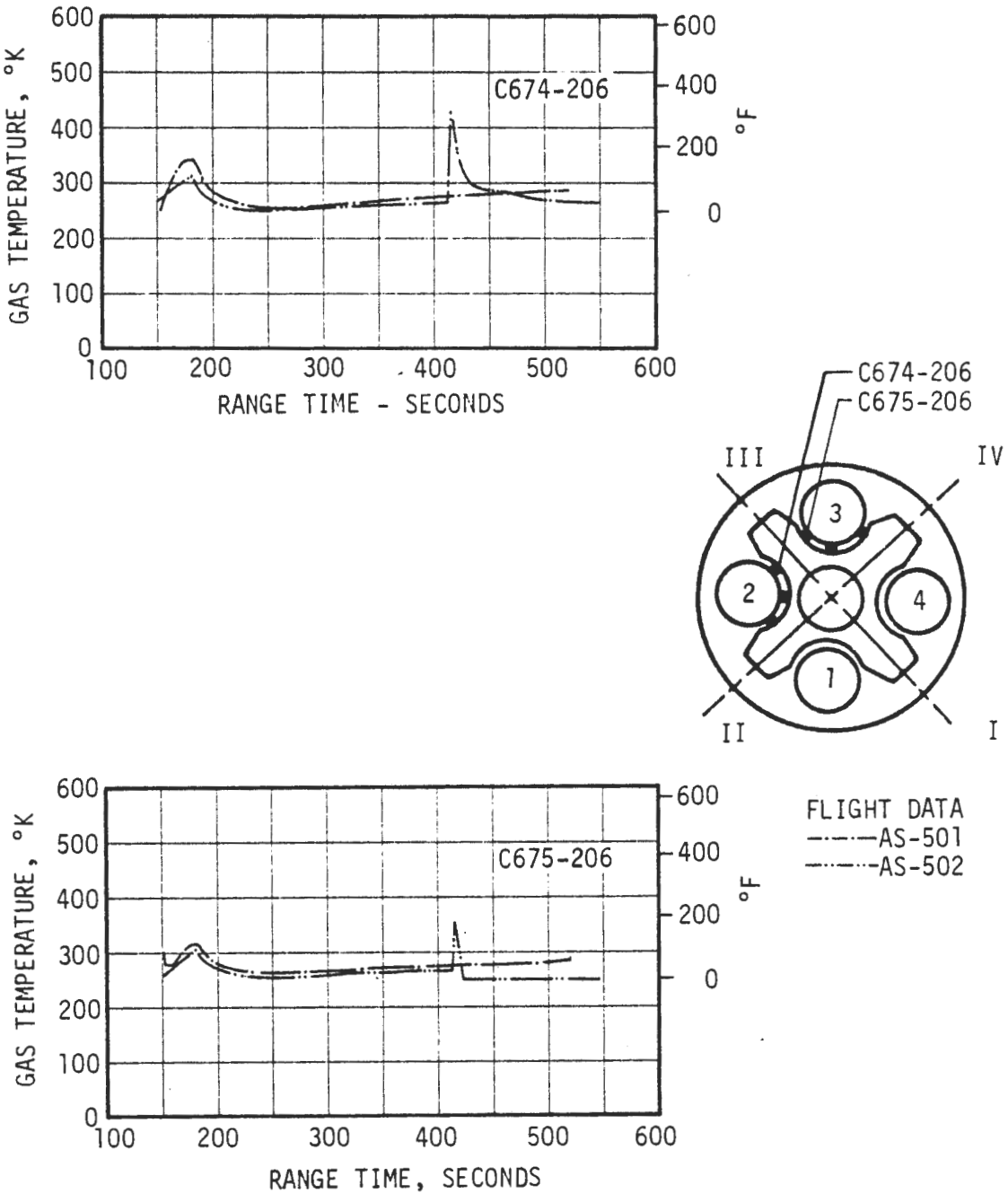

FIGURE 4-60. S-II ENGINE CURTAIN GAS TEMPERATURES (CONCLUDED)

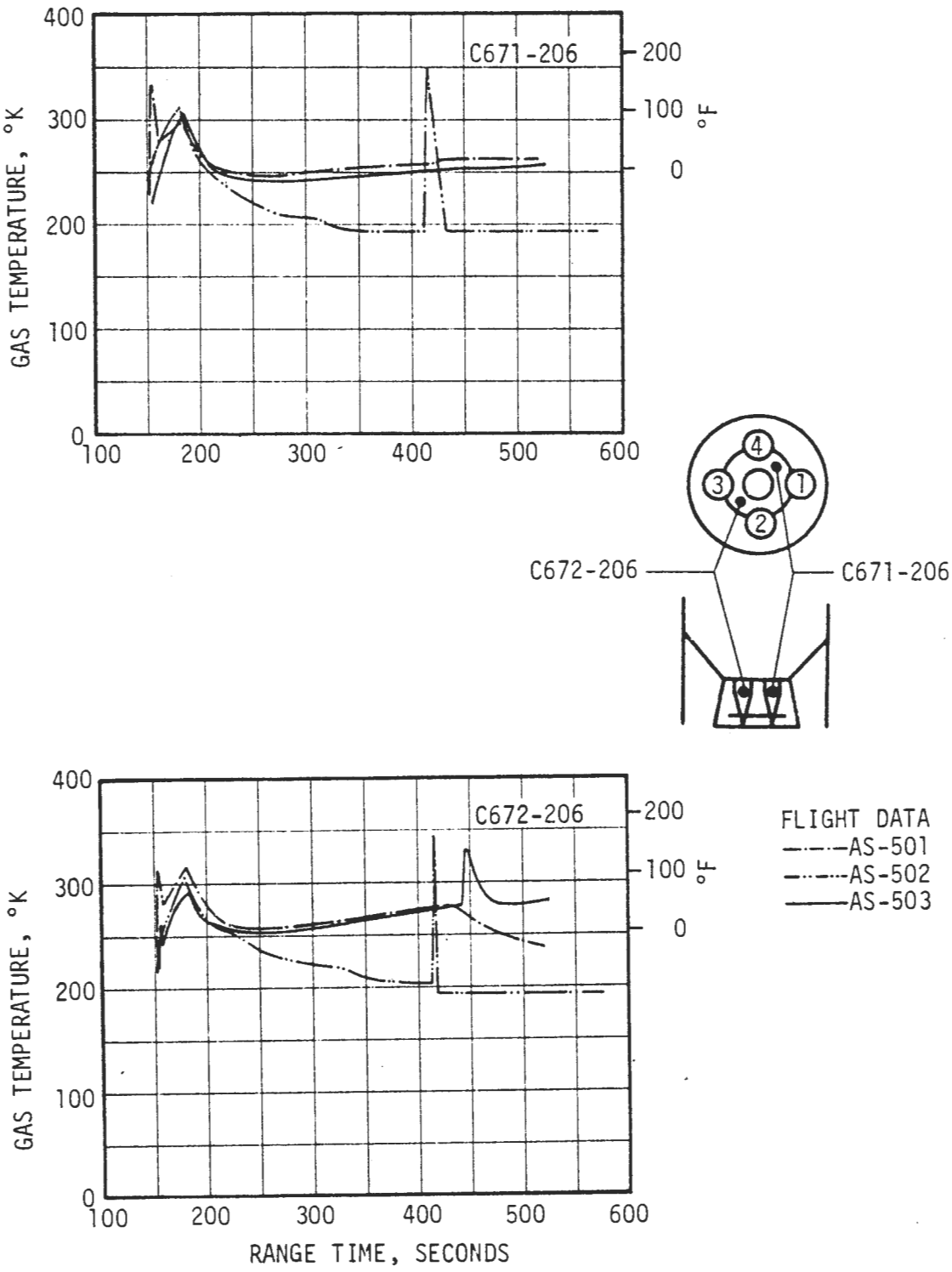

FIGURE 4-61. S-II ENGINE COMPARTMENT GAS TEMPERATURES

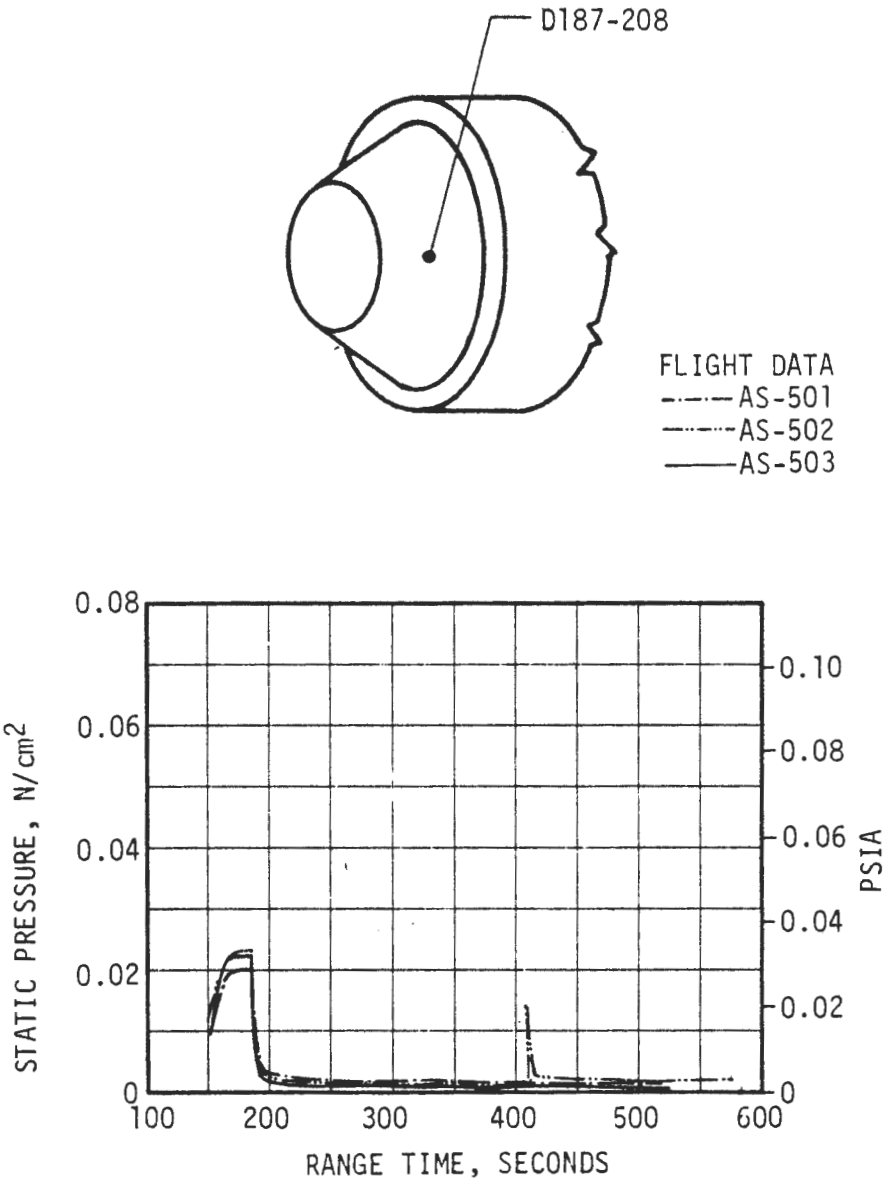

FIGURE 4-62. S-II THRUST CONE STATIC PRESSURE

SECTION 5

STAGE SEPARATION ENVIRONMENTS

5.0 INTRODUCTION

This section contains the flight data analysis of the thermal environment associated with S-IC/S-II and S-II/S-IVB stage separation for AS-501, AS-502 and AS-503. Flight instrumentation is described and locations are given. Flight to flight data comparisons are made and discussions of data variations and trends are included where applicable.

5.1 S-IC/S-II STAGE SEPARATION

5.1.1 Separation Sequence and Flow Fields

S-IC/S-II stage separation utilized a dual plane separation technique wherein the structure between the two stage was severed by linear shaped charges at two different planes as shown in Figure 5-1. First plane separation was accomplished with the aid of eight S-IC retro motors which provided separation thrust after S-IC burnout. Four ullage motors (eight ullage motors were installed on AS-501) located on the S-II interstage were used to provide a small forward acceleration to insure stable flow of propellants into the S-II stage main engines. Second plane (interstage) separation occurred approximately 30 seconds after first plane separation. The combined effects of vehicle acceleration and the reaction caused by the J-2 engine exhaust plume impingement separated the interstage. S-IC/S-II stage separation events and times for AS-501, AS-502 and AS-503 are shown in Table 5-I for first plane separation. Second plane separation is discussed in Section 4.0 because of its influence only on the S-II base region thermal environment.

During stage separation, exhaust gases and solid particles from the retro motor and ullage motor plumes surrounded the vehicle (see Figure 5-2) and severely attenuated radio signals to ground receiving stations. Times of data dropout for the instruments monitoring the S-IC/S-II separation environment are shown in Table 5-II for the AS-501 and AS-502 vehicles. AS-503 flight data from these instruments were stored on the airborne tape recorders for subsequent transmission to ground station with no loss of telemetry data. The AS-502 gas temperature data were also tape recorded.

5.1.2 Instrumentation

Seven static pressure transducers and two gas temperature probes were used to monitor the staging environment on the forward skirt of the S-IC stage for the AS-501, AS-502, and AS-503 flights. These instruments were located as shown in Figures 5-3 and 5-4 and are described and summarized in Table 5-III.

5.1.3 S-IC Thermal Environment

The gas temperatures and impingement pressures monitored on the S-IC forward skirt and LOX dome did not indicate severe heating or pressure environments. The flight data also indicated that the separation rates and attitudes of the S-IC and S-II stage were essentially the same for all three flights. Removal of four S-II ullage motors had little effect on the environment as monitored in the instrumentation locations.

The internal forward skirt gas temperature data recorded during S-IC/S-II staging for the AS-501, AS-502, and AS-503 flights are shown in Figure 5-5. The gas temperature data were approximately the same for all three flights. Maximum gas temperature in the forward skirt compartment was approximately 1300°K and occurred after 90 percent thrust was obtained for the S-II stage J-2 engines.

The impingement pressures in the S-IC forward skirt region monitored during S-IC/S-II staging for the AS-501, AS-502 and AS-503 flights are shown in Figure 5-6. The AS-501 and AS-502 data were not tape recorded and may be inaccurate due to radio signal attenuation during staging. Pressure spikes during AS-503 ullage motor firing were small and did not reach magnitudes equal to AS-501 and AS-502 flight data. The maximum pressure recorded on the AS-503 flight was approximately 1 N/CM^2 which occurred during S-II main engine startup (see Figure 5-6).

Five external pressure measurements were recorded on the S-IC forward skirt for the AS-501, AS-502, and AS-503 flights. All external pressure data recorded during the AS-502 and AS-503 flights were essentially zero and are, consequently, not shown. The maximum external pressure recorded on the AS-501 was 5.78 N/CM^2 at instrument D100-120, which was almost directly under an ullage motor. Four other measurements in similar locations recorded pressures below 1.25 N/CM^2. The pressure measurements on AS-501 are questionable based on AS-502 and AS-503 experience.

5.2 S-II/S-IVB STAGE SEPARATION

5.2.1 Separation Sequence and Flow Field

S-II/S-IVB stage separation occurred at the top of the S-II/S-IVB interstage (see Figure 5-1). The tension strap attaching the S-II/S-IVB interstage at station 2746.5 was severed. At the time of separation, four retro motors mounted on the interstage structure below the separation plane were fired to decelerate the S-II stage. Acceleration was applied to the S-IVB stage by means of two ullage motors to provide stable propellant flow during S-IVB main engine start. S-II/S-IVB stage separation events and times for AS-501, AS-502, and AS-503 are shown on the following page.

5.2.1 (Continued)

EVENT	TIME FROM SEPARATION COMMAND - SECONDS		
	AS-501	AS-502	AS-503
S-II Engine Cutoff	-0.77	-0.74	-0.86
S-IVB Ullage Ignition	-0.11	-0.12	-0.12
S-II/S-IVB Separation Command	0.00	0.00	0.00
S-II Retro Motor Ignition	0.07	0.10	0.08

The S-II/S-IVB separation commands were given at 520.53, 577.08, and 524.90 seconds range time for AS-501, AS-502 and AS-503, respectively.

Immediately after stage separation, the retro motors exhaust plume impinged on the base region of the S-IVB stage. The presence of the S-II/S-IVB interstage and S-IVB ullage motor plumes greatly complicated the flow field surrounding the S-IVB stage. Radio signal attenuations were noted during stage separation, however, the airborne tape recorders performed as required to monitor separation environments on all three flights.

5.2.2 Instrumentation

Thermal environment instrumentation in the base of the S-IVB stage, used to measure staging environment, was limited in number as a consequence of prior successful R&D flights. Two total calorimeters were installed on the S-IVB J-2 engine bell of only the AS-501 and AS-502 vehicles. Figure 5-7 depicts their location. These calorimeters had a range of 0-5.65 watts/cm^2. Also one gas temperature probe located in the engine area is also shown in Figure 5-7.

5.2.3 Thermal Environment

The maximum heating rates and increases in gas temperatures on the S-IVB J-2 engine bell during AS-501 and AS-502 retro motor fire are shown in Figure 5-7.

AS-501 and AS-502 S-IVB structural temperatures and gas temperature rise indicate only small differences in the retro motor plume impingement heating environment between flights. Data from the calorimeters indicate that the heating rates to the J-2 engine were higher on the AS-502 than on the AS-501, but all heating rates were below the maximum value expected. More severe environments were experienced during separation of the AS-202 vehicle.

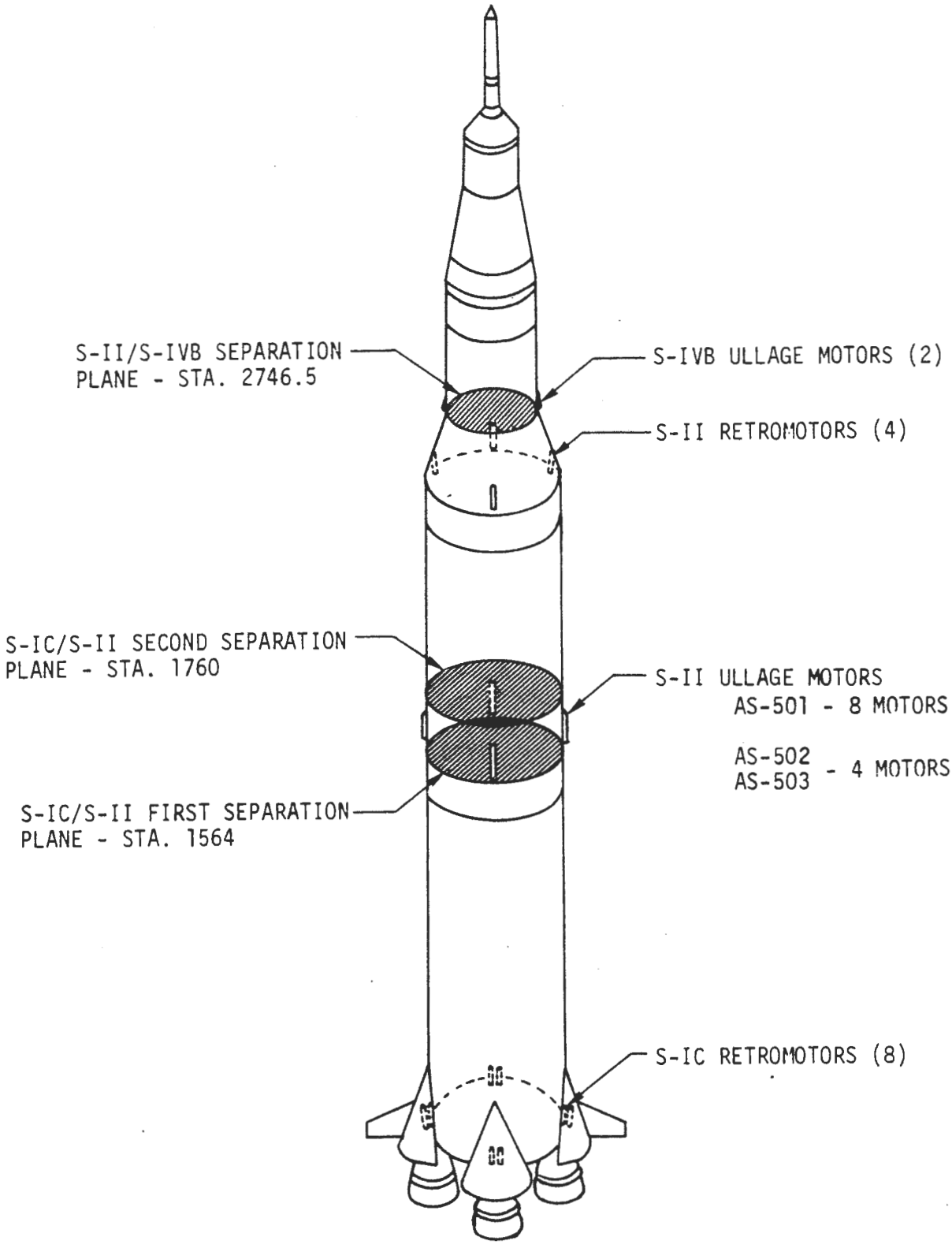

FIGURE 5-1. SATURN V STAGE SEPARATION PLANES

TABLE 5-I

S-IC/S-II STAGING EVENTS

EVENT	TIME FROM SEPARATION (SECONDS)		
	AS-501	AS-502	AS-503
S-IC Outboard Engine Cutoff	-0.81	-0.78	-0.74
S-II Ullage Motor Ignition	-0.32	-0.28	-0.24
S-IC Retro Motor Ignition	-0.12	-0.10	-0.08
S-IC/S-II Physical Separation*	0.00	0.00	0.00
S-IC Retro Motor Burnout	0.64	0.64	0.78
S-II Thrust Buildup Begins	1.97	2.02	2.14
S-II Thrust - 10 Percent	2.50	2.52	2.61
S-II Ullage Motor Burnout	3.42	3.30	3.66
S-II Thrust - 90 Percent	3.75	3.78	3.81

* AS-501 separation occurred at 151.58 seconds range time
AS-502 separation occurred at 149.18 seconds range time
AS-503 separation occurred at 154.56 seconds range time

TABLE 5-II.
S-IC STAGE TELEMETRY DATA DROP-OUT
DURING S-IC/S-II SEPARATION

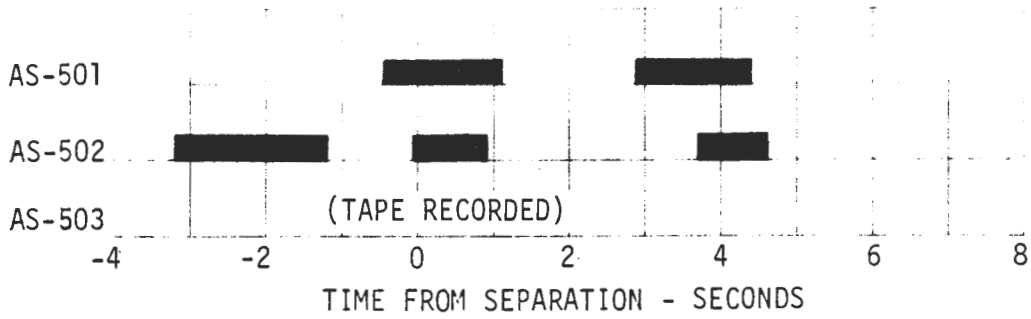

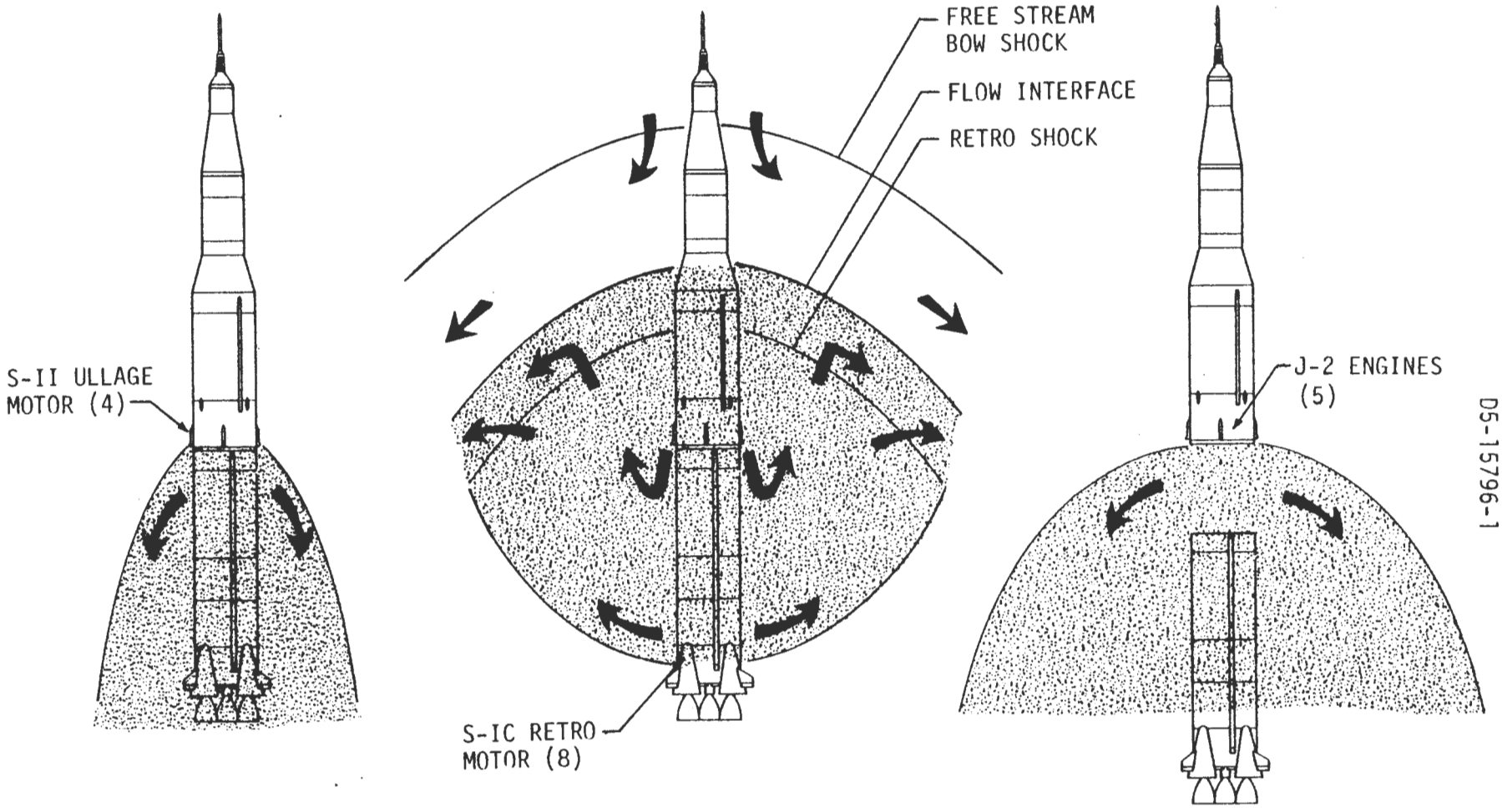

FIGURE 5-2. SCHEMATIC OF S-IC/S-II STAGE SEPARATION FLOW FIELD

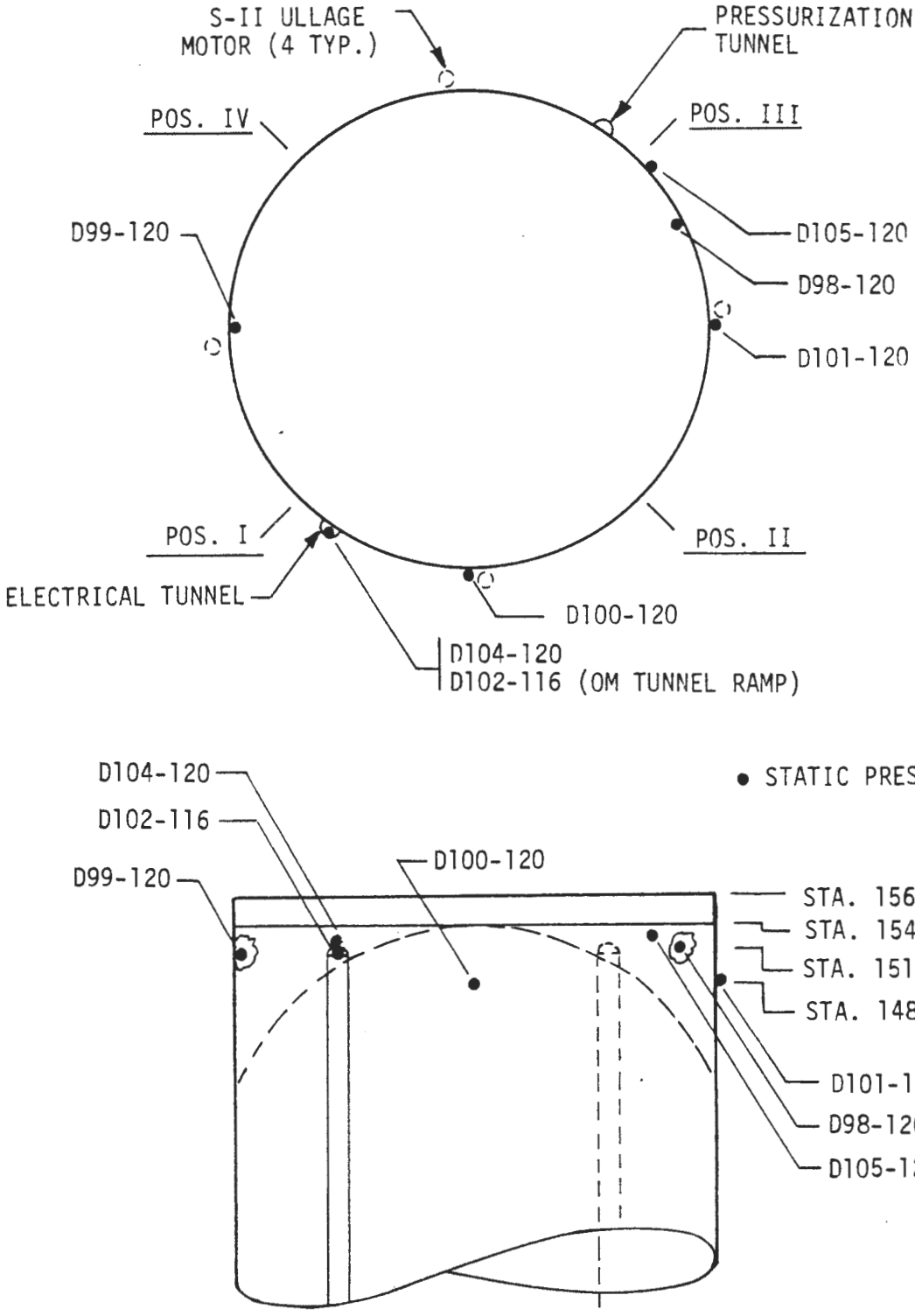

FIGURE 5-3. S-IC FORWARD SKIRT PRESSURE INSTRUMENTATION

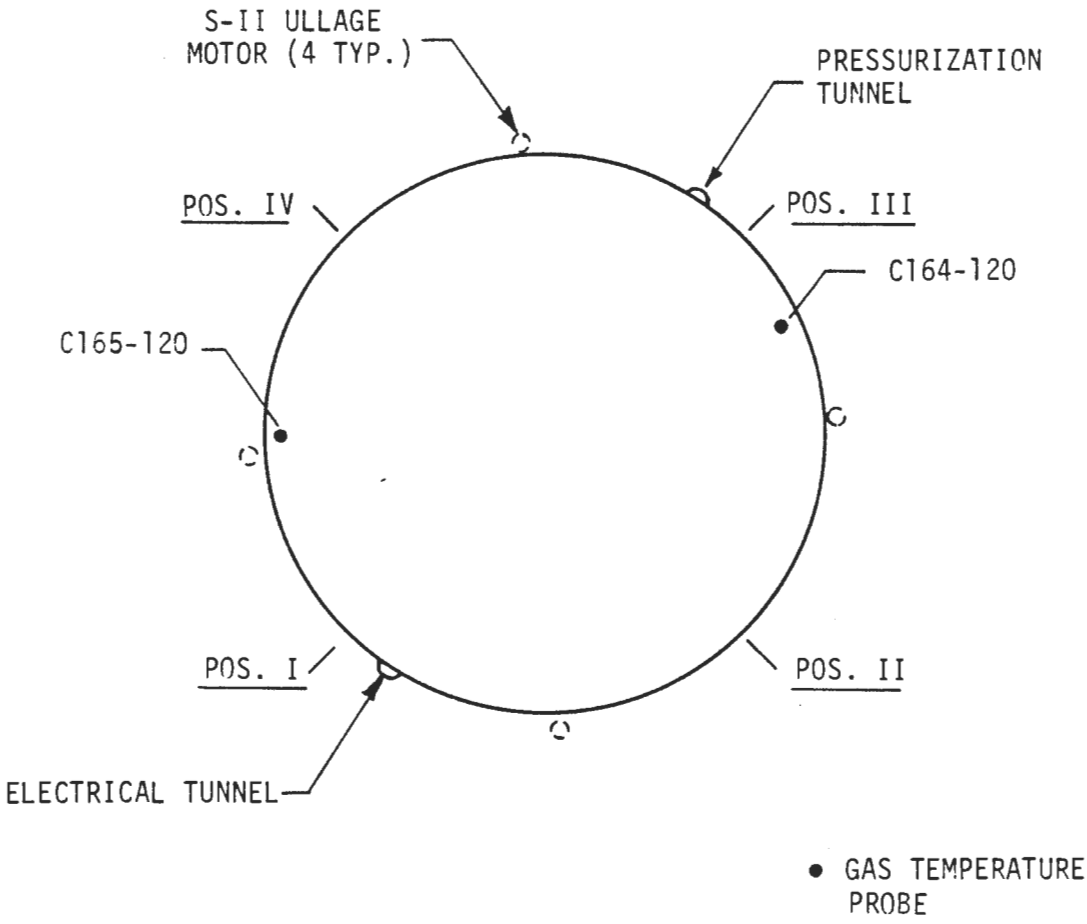

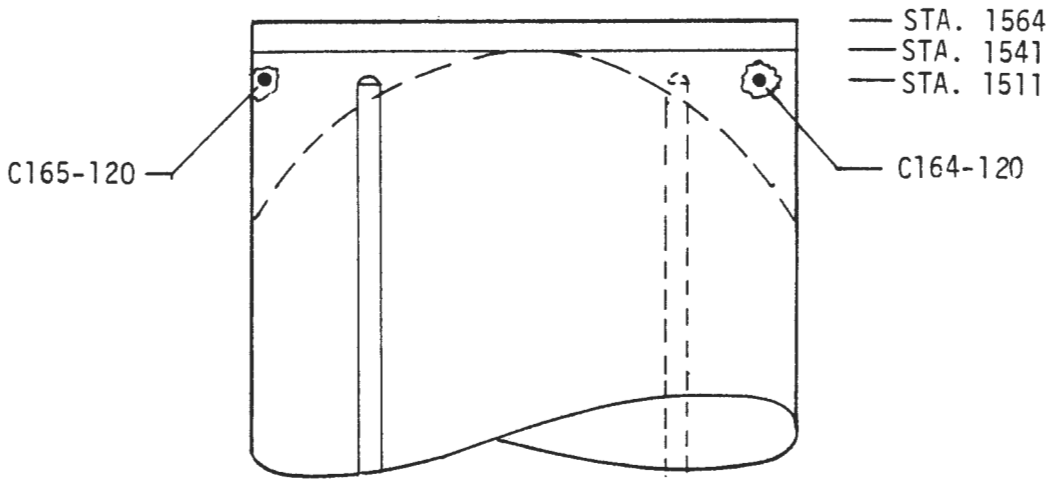

FIGURE 5-4. S-IC FORWARD SKIRT GAS TEMPERATURE INSTRUMENTATION

TABLE 5-III. S-IC/S-II SEPARATION ENVIRONMENT INSTRUMENTATION

MEASUREMENT NUMBER	INSTRUMENT TYPE	RANGE N/cm^2	LOCATION		
			STATION	RADIAL	REMARKS
C164-120	Gas Probe*	373-1253°K	1511.0	65° From Fin C Toward Fin B	Internal
C165-120	Gas Probe*	373-1253°K	1511.0	Fin D Centerline	Internal
D98-120	Static Pressure	0-13.79	1511.0	65° From Fin C Toward Fin B	Internal
D99-120	Static Pressure	0-13.79	1511.0	Fin D Centerline	Internal
D100-120	Static Pressure	0-13.79	1488.0	Fin Line A	External
D101-120	Static Pressure	0-13.79	1491.0	Fin Line B	External
D102-116	Static Pressure	0-13.79	1496.0	Cable Tunnel Forward Ramp	External
D104-120	Static Pressure	0-13.79	1512.0	Conduit Fairing	External
D105-120	Static Pressure	0-13.79	1524.0	50° From Fin C Toward Fin B	External

*Chromel - Alumel Thermocouple

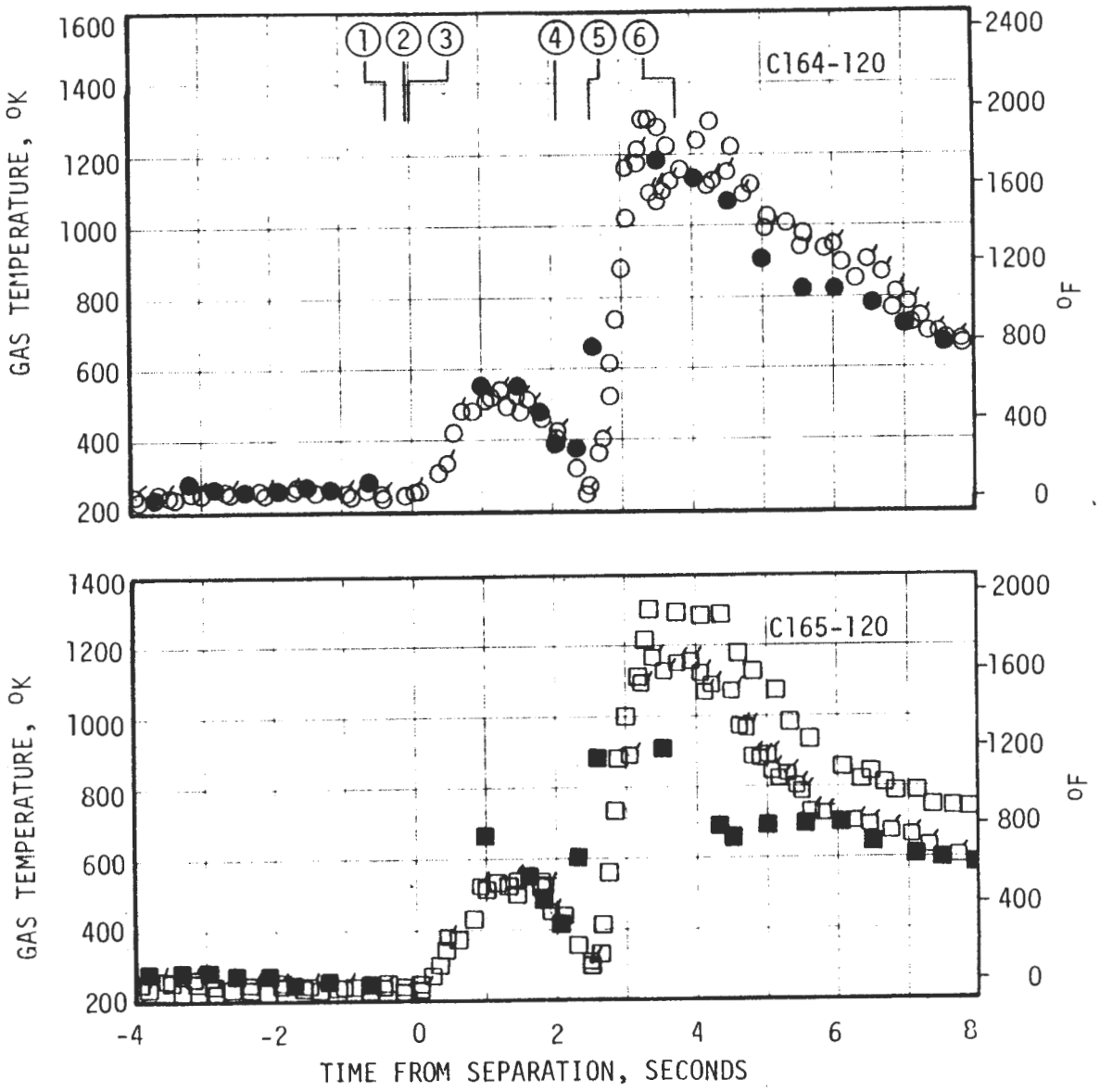

FIGURE 5-5. S-IC FORWARD SKIRT GAS TEMPERATURE DURING SEPARATION

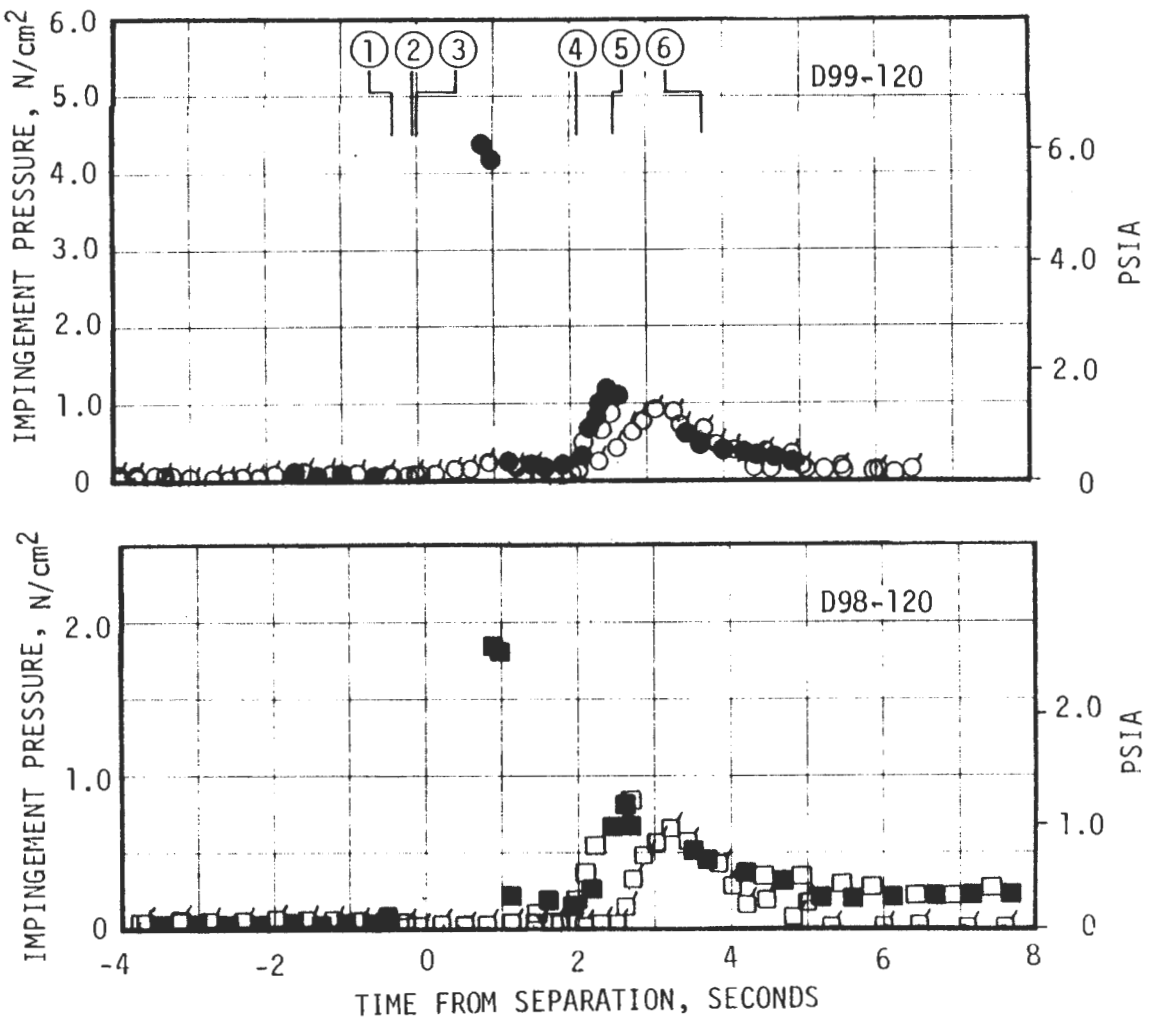

① S-II ULLAGE IGNITION

② S-IC RETRO IGNITION

③ S-IC/S-II SEPARATION

④ S-II THRUST BUILDUP BEGINS

⑤ S-II THRUST - 10%

⑥ S-II THRUST - 90%

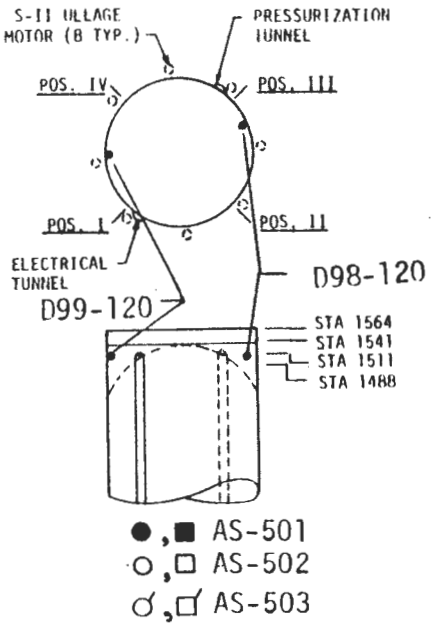

FIGURE 5-6. S-IC FORWARD SKIRT INTERNAL PRESSURE DURING SEPARATION

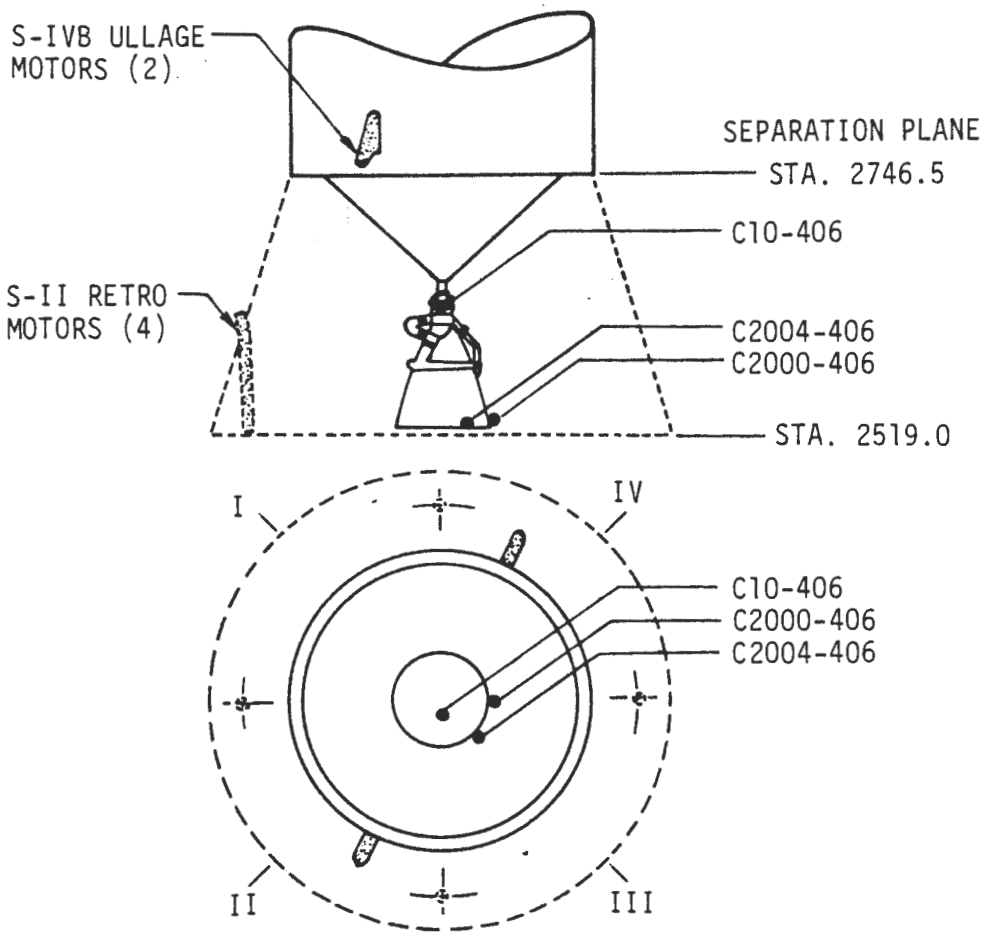

MEASUREMENT NUMBER	INSTRUMENT TYPE	*MAXIMUM MEASURED VALUE	
		AS-501	AS-502
C10-406	Gas Temp.	**262 °K	**264 °K
C2000-406	Cal., Total	0.454 watts/cm^2	0.624 watts/cm^2
C2000-406	Cal., Total	0.397 watts/cm^2	1.24 watts/cm^2

* AS-503 Not Instrumented
** Temperature rise

FIGURE 5-7. S-IVB STAGE THERMAL ENVIRONMENT DURING SEPARATION

SECTION 6

AERODYNAMIC HEATING ENVIRONMENT

6.0 INTRODUCTION

This section presents the analysis of the aerodynamic heating environment monitored on the AS-501, AS-502 and AS-503 vehicles. Environments of the S-IC stage, S-II stage, S-IVB stage and the Instrument Unit (IU) are discussed separately. The relative locations of these stages are shown in Figure 6-1. Flight data from thermocouples, resistance thermometers and calorimeters are presented and discussions of data variation and trends are included where applicable. Flight instrumentation is described and locations are given.

The Aerodynamic Heating Indicators (AHI) for the AS-501, AS-502 and AS-503 post flight trajectories are shown in Figure 6-2. The AHI is qualitatively defined as a time integrated heating potential and serves as a useful comparison of the aerodynamic heating characteristics of different trajectories. The AS-502 vehicle experienced the most severe aerodynamic heating environment. The trajectories are discussed in Section 2.

6.1 S-IC STAGE

6.1.1 Flow Fields

The flow field about the Saturn V vehicle during boost dictated the external thermal environment. This flow field was complicated by protuberances which created corner flow, shock waves and wakes and caused localized increased heating conditions. Also, plume induced free stream boundary layer flow separation resulted at the higher altitudes and changed the primary mechanism of heating from aerodynamic to radiation in the separated flow region. The F-1 engine expanded plumes created an adverse pressure gradient which caused the free stream flow to separate from the surface of the vehicle. Exhaust gases were forced into the separated region from the base region and the plume-separated flow interface. Flow separation was established at approximately 109 seconds on AS-501, 110 seconds on AS-502, and 106 seconds on the AS-503 vehicle. These times correspond to altitudes of 30.0 KM for AS-501, 29.5 KM for AS-502, and 28.0 KM for AS-503. The earlier flow separation on the AS-503 resulted from the 2° outboard engine cant which was not present on the AS-501 and AS-502 vehicles. The forward point of flow separation determined from Airborne Lightweight Optical Tracking System (ALOTS) optical data is presented in Figure 6-3 for the AS-502 and AS-503 flights. The ALOTS data was unavailable for the AS-501 flight.

On the AS-503 vehicle, the inboard engine cutoff (IECO) at 126 seconds altered the exhaust plume shape such that the flow separation heating environment was significantly reduced. This effect of IECO was also indicated by AS-501 and AS-502 flight data, but IECO occurred at later times (135 and 145 seconds, respectively) and the effect was not as

6.1.1 (Continued)

significant as on the AS-503 vehicle.

6.1.2 Instrumentation

The S-IC stage aerodynamic heating environment was monitored by thermocouples installed on the exterior and interior of the vehicle skin. Not all instruments installed on the S-IC stage are discussed, but typical measurements were selected and are shown in Figures 6-4 through 6-6. These instruments are considered representative and are described and summarized in Table 6-I.

Flight data from thermocouples located in clean body areas (i.e., no protuberance or interference heating effects) and areas not covered by insulation were used to determine total heating rates and heat-transfer coefficients.

The heating rates were determined from measured skin temperature data by the equation,

$$q = \rho C p \tau \quad (dT_w/dt)$$

where ρ, Cp, and τ are the skin density, specific heat, and thickness, respectively, and dt_w/dt is the slope of the skin temperature versus time curve. The slope of the skin temperature versus time curve was obtained by the polynomial moving-arc differentiation procedure discussed in Reference 3.

Heat-transfer coefficients can be determined from the equation,

$$h \equiv q/(T_r - T_w)$$

where h is the heat-transfer coefficient, q is the previously determined heating rate, T_r is the air recovery temperature and T_w is the measured skin temperature. The air recovery temperatures for AS-501, AS-502, and AS-503 post flight trajectories are presented in Figure 6-7.

6.1.3 S-IC Aerodynamic Heating

Internal skin temperatures on the forward skirt are shown in Figure 6-8. The forward skirt was insulated with silicone rubber insulation which limited aerodynamic heating effects and does not permit the derivation of heating rates from the measured temperatures obtained from C64-120. However, measurements C315-120, C317-120, C318-120, and C319-120 (installed only on the AS-503 vehicle) were not insulated and provided external skin temperatures from which aerodynamic heating rates were obtained. These measurements were made with thermocouples installed on 0.10 inch thick aluminum plates mounted on top of stringers at various locations on the forward skirt (see Figures 6-4 and 6-5). The silicone rubber insulation was reduced in thickness under the instrumented plates, however, a thin layer of insulation was maintained between the plate and stringer. The

6.1.3 (Continued)

insulation along the top of the stringers was built up around the edge of the plate in order to provide a smooth surface.

External skin temperatures and heating rates derived from measurements C315-120 and C318-120 are presented in Figure 6-9. These measurements were located in areas unaffected by protuberances. External skin temperatures and derived heating rates for areas affected by protuberances are presented in Figure 6-10. A temperature increase of approximately 15°K (27°F) above those measured in unaffected areas is shown in areas affected by the protuberances. Post-flight simulations for the S-IC forward skirt skin temperatures and heating rates are also presented in Figures 6-9 and 6-10. These simulations utilize analytically determined heat-transfer coefficients and recovery temperatures based on the AS-503 post-flight trajectory.

A comparison of internal skin temperature measurements (C64-120, C314-120, and C316-120) are presented in Figure 6-11 for AS-503 only. These measurements were located in an insulated area, therefore, heating rates were not determined.

S-IC intertank skin temperatures and derived heating rates for C62-118 and C63-118 are presented in Figures 6-12 and 6-13, respectively, for AS-501, AS-502, and AS-503. Measurement C63-118 indicated slightly higher temperatures than C62-118, which was located approximately 3 meters forward of C63-118. This trend is attributed to effects of flow separation heating. The AS-503 flight data for measurements C62-118 and C63-118 indicate a decrease in heating after inboard engine cutoff (IECO). The decrease in heating is attributed to the recession of the forward point of the separated flow region after IECO as evidenced by flight optical data (see Figure 6-3).

S-IC aft compartment heating rates and skin temperatures are presented in Figures 6-14 through 6-16. The relatively high heating rate during the first ten seconds of flight is attributed to radiation from the S-IC exhaust flow field. The sharp increase in the heating rate at approximately 110 seconds results from flow separation and subsequent radiation heating from the exhaust gases in the separated flow region. Measurement C117-115 was located in a potential engine fairing interference region on the aft compartment. Skin temperatures and derived heating rates for C117-115 are presented in Figure 6-16. A comparison of results from other aft compartment measurements (Figures 6-14 and 6-15) with C117-115 indicate no apparent interference heating effects.

S-IC fin heating rates and skin temperatures are presented in Figures 6-17 through 6-22. The heating rates presented were derived from flight data which include aerodynamic heating up to the time flow separation occurs and radiation heating after separation occurs. The heating rates indicate a sharp rise at approximately 110 seconds, which is the time flow separation was observed to occur. In some cases, the effect is sufficient to produce a readily noticeable change in the slope of the time-temperature curve. The

6.1.3 (Continued)

skin temperature and heating rate data also show the effect of the decreased heating potential in the separated flow region after IECO.

Post-flight simulations for the S-IC fins (measurements C101-112 and C101-114) are also presented in Figures 6-19 and 6-20. These simulations include aerodynamic heating up to the beginning of flow separation and radiation heating only during the period of flow separation.

Unsummetrical heating to the fins was noted in AS-501, AS-502, and AS-503 flight data. A comparison of AS-503 flight data skin temperatures and heating rates for measurements C99-112 (Fin B) and C99-114 (Fin D) is presented in Figure 6-22. From this data it can be seen that Fin D receives a higher heating rate throughout the latter portion of flight. This is possibly due to unsymmetrical flow separation.

Skin temperature and heating rates for the S-IC engine fairings are shown in Figures 6-23 through 6-26. All data follows the same trend except C114-110 data from AS-501. This instrument is believed to be in error. These instruments reflect the effects of the observed flow separation as evidenced by the distinct increase in heating rates at approximately 110 seconds. The effect of early IECO on the AS-503 flight is also indicated by a sharp change in the temperature curve slope at approximately 130 seconds.

Protuberances on the S-IC stage on which skin temperature measurements were made consisted of the electrical and pressure tunnels. Measurement C66-120 was located on the forward 25° conical ramp of the pressure tunnel and was covered with insulation, therefore, protuberance effects were not evaluated at this location. A comparison of skin temperatures recorded by C66-120 is made in Figure 6-27. Measurement C72-116 was located on the electrical tunnel crest (10.5 inches above the vehicle surface) in the intertank region. Skin temperatures recorded by measurement C72-116 are given in Figure 6-28. The effect of early IECO on the AS-503 flight is also clearly indicated by this instrument.

6.2 S-II STAGE

6.2.1 Instrumentation

The S-II stage aerodynamic heating instrumentation consisted of asymptotic calorimeters and resistance thermometers as shown in Figure 6-29. The location of significant protuberances and thermal instrumentation locations are also shown in Figure 6-29. The instrumentation is described and summarized in Table 6-II.

Since the varying structural surface temperature significantly affects the transient heating rate predictions, comparisons of the calorimeter flight data with analytically predicted heating rates for the structural surfaces are not valid. However, by using flight data from these instruments, direct comparisons of heating rates between flights and between different areas on the vehicle can be accomplished. Indirect comparisons of the heating rates can be made using the measured temperature data.

6.2.2 S-II Aerodynamic Heating

The S-IC/S-II interstage aerodynamic heating rates monitored in clean body areas during AS-501, AS-502, and AS-503 flights are shown in Figure 6-30. Based on protuberance wake areas, instrument C909-200 is located approximately 4 inches inside the predicted bow shock wave of a S-II ullage motor fairing. However, the similarity of flight data between this measurement and measurements C801-200 and C905-200, indicates that instrument C909-200 is not within the significant influence region of the ullage fairing bow wake. Therefore, it is presented in Figure 6-30 as a clean body measurement. Increased heating on the interstage is noted on all three vehicles during IECO and S-IC/S-II stage separation. The increase heating during staging is more evident on the AS-502 and AS-503 vehicles. This increase is believed due to the change in the staging flow field which resulted when four ullage motors were removed from the AS-502 and AS-503 vehicles. The difference in the heating rates indicated early in flight could be due to different initial calorimeter body heat sink temperatures.

The S-IC/S-II interstage had resistance thermometers located in an uninsulated clean body area (C904-200) and in an area affected by the bow shock of an ullage motor fairing (C906-200). The flight data from these instruments are shown in Figures 6-31 and 6-32, respectively, for AS-501 and AS-502 vehicles. These instruments were not installed on the AS-503 vehicle. Measurement C906-200 indicates approximately a 20% increase in heating during the period of maximum aerodynamic heating. This increased heating is attributed to protuberance effects.

Heating rates monitored on the S-IC/S-II ordinance fairing are presented in Figure 6-33. In addition to being on the S-IC/S-II ordinance fairing, they are in the wake area of ullage motors. A heating rate greater than that which a clean body area would experience is expected for this area. Comparison with Figure 6-30, however, indicates the measured peak heating values to be only slightly above those measured in clean body area. The flight data also deviates from the predicted environment in this area.

A comparison of AS-501, AS-502 and AS-503 LH_2 feedline forward fairing heating rates is presented in Figure 6-34. The data bands are produced from the response of calorimeters C848-218 and C850-218 located on the forward fairing of the LH_2 feedline fairings (Figure 6-29). The data indicate the AS-502 vehicle to have received the most severe aerodynamic heating. The probable cause of the recorded heating rates being somewhat different during the first 50 seconds of flight is the difference in the initial temperature of the calorimeter body.

S-II forward skirt measured skin temperatures and post flight simulations are presented in Figure 6-35. Measured skin temperatures on the AS-501 vehicle are indicated to be higher than either AS-502 or AS-503 measured values. This is probably due to the higher initial temperature of the AS-501 S-II forward skirt and does not necessarily indicate a higher heating rate during flight.

6.3 S-IVB STAGE

6.3.1 Instrumentation

The S-IVB stage aerodynamic heating was monitored by resistance thermometers. The instruments chosen for data presentation are described and summarized in Table 6-III. The S-IVB stage is depicted in Figure 6-36. The instrumentation locations are shown in sketches presented with the flight data.

6.3.2 S-IVB Aerodynamic Heating Environment

In general, the S-IVB stage aerodynamic heating environment was lower than design values and good agreement was demonstrated between AS-501 and AS-502 flight data. The flight data show that the AS-502 vehicle had a slightly more severe flight thermal environment than AS-501.

S-IVB aft interstage external skin temperatures monitored during AS-501 and AS-502 flights are shown in Figure 6-37. The thermocouples were covered with an ablative type insulation for the flights.

Representative skin temperatures of the S-IVB aft skirt are shown in Figures 6-38 and 6-39. The skin temperature presented in Figure 6-38 are for an uninsulated area of the aft skirt and indicate similar heating for the AS-501 and AS-502 vehicles during the period of maximum aerodynamic heating. The instruments presented in Figure 6-39 were located in a protuberance-induced wake heating area (in the vicinity of the LH_2 feedline fairing) which was insulated. The data response for the instrumentation located in this area show similar trends to that shown in Figure 6-38 for a clean body area.

Representative S-IVB forward skirt skin temperatures are presented in Figure 6-40 along with instrument locations. Good data agreement was experienced between flights.

The LH_2 feedline fairing forward ramp temperature response is presented in Figure 6-41 for AS-501 and AS-502. The flight data indicates good agreement until approximately 110 seconds after which the AS-502 temperature exceeds the AS-501 temperature This deviation is presently unexplained, but is believed to be caused in part by the more severe AS-502 aerodynamic heating environment.

6.4 INSTRUMENT UNIT

6.4.1 Instrumentation

The Instrument Unit (IU) aerodynamic heating environment was monitored by eight thermocouples mounted on the inner surface of the honeycomb structure. This instrumentation is described and summarized in Table 6-IV. Sketches showing their locations are depicted with the flight data presentations.

6.4.2 IU Aerodynamic Heating Environment

All temperatures monitored on the inner surface of the IU honeycomb structure are shown in Figure 6-42 as flight data bands for AS-501, AS-502, and AS-503. These bands indicate a relatively consistent aerodynamic heating environment between flights. Individual measurements near Position IV showed slight temperature rises during approximately the first 30 seconds of flight. This rise may be the result of internal radiation or convective heating. After 30 seconds all measurements show a small cooling trend until aerodynamic heating begins to increase significantly at approximately 80 seconds flight time.

Analytically predicted aerodynamic heating rates show good agreement with flight data when compared indirectly by means of a thermal model of the instrument installation. Post-flight simulation and the top of the flight data band from Figure 6-42 are presented in Figure 6-43. Solar heating was not considered in the simulation.

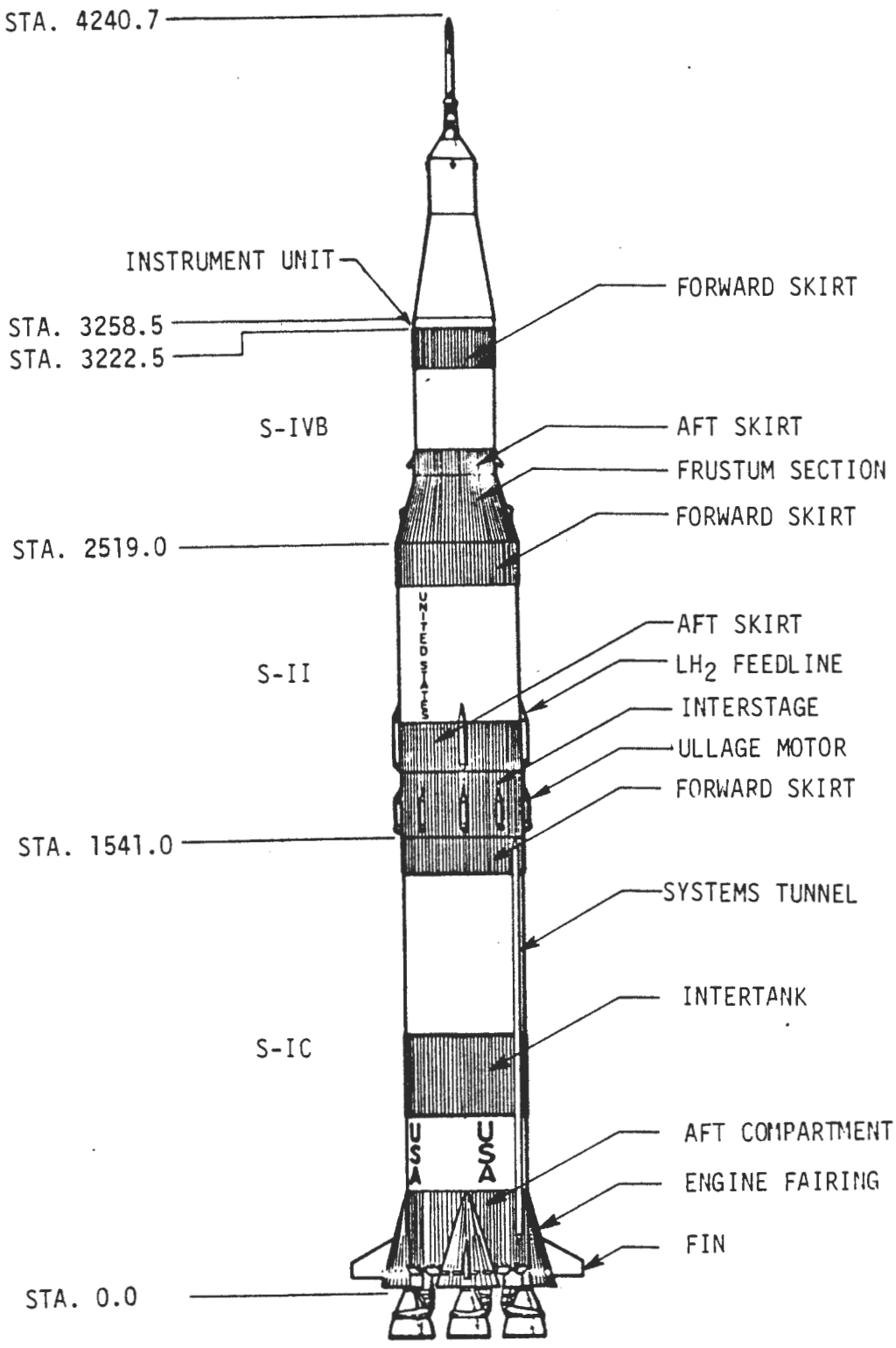

FIGURE 6-1. SATURN V CONFIGURATION

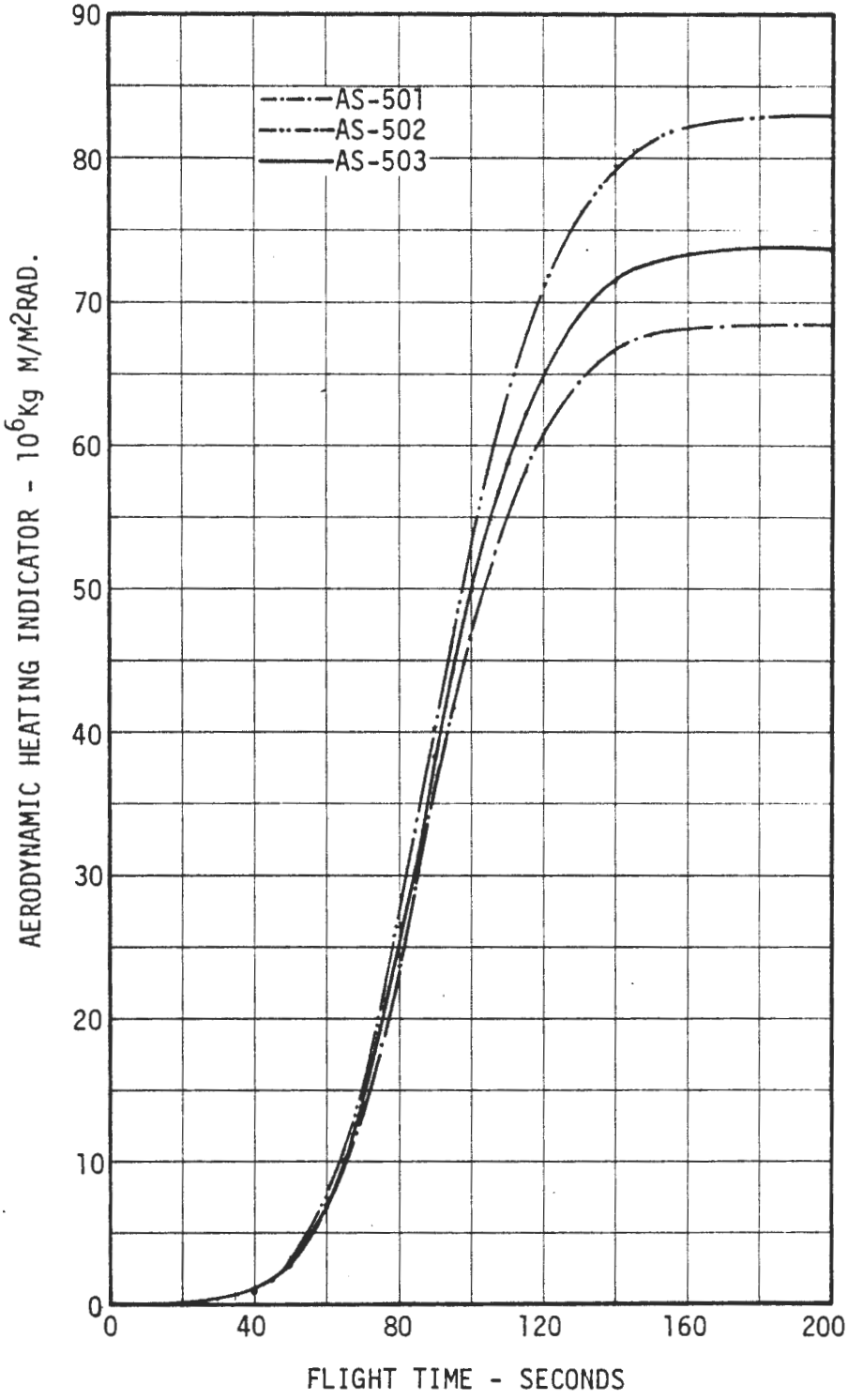

FIGURE 6-2. AERODYNAMIC HEATING INDICATOR FOR AS-501, AS-502, AND AS-503 POST-FLIGHT TRAJECTORIES

FLIGHT TIME =
119 SECONDS

ALTITUDE =
36.6 KILOFEET

OPTICAL FLIGHT DATA
○ AS-502
△ AS-503

NOTE: AS-501 ALOTS FILM
NOT AVAILABLE

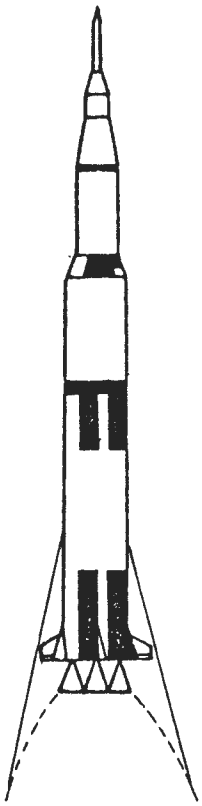

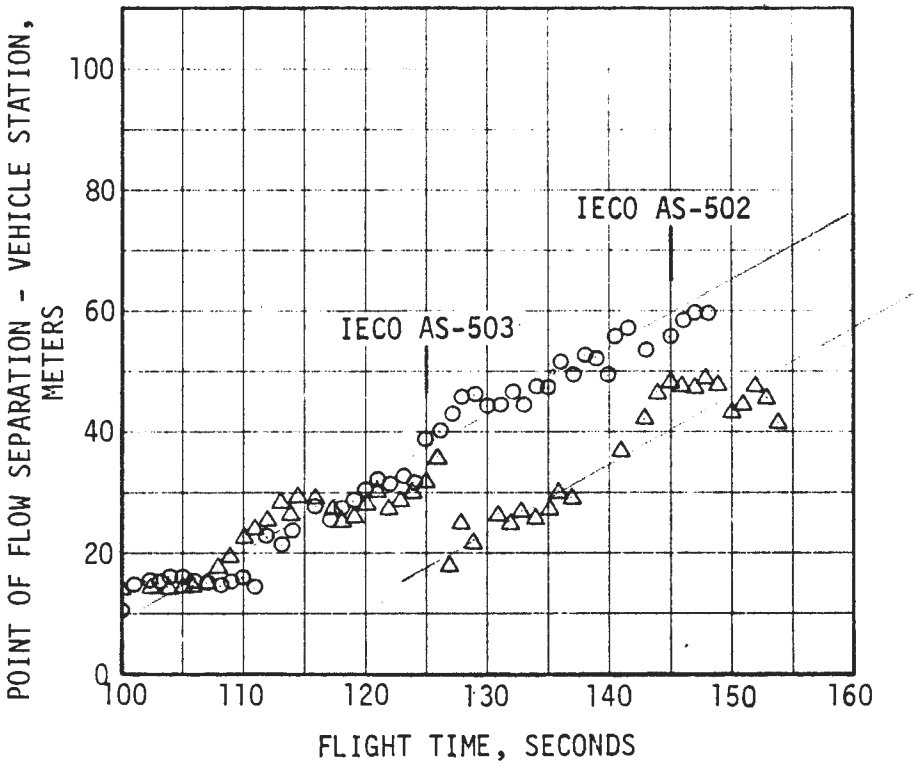

FIGURE 6-3. SEPARATED FLOW FORWARD LOCATION MEASURED FROM ALOTS 70 MM FILM

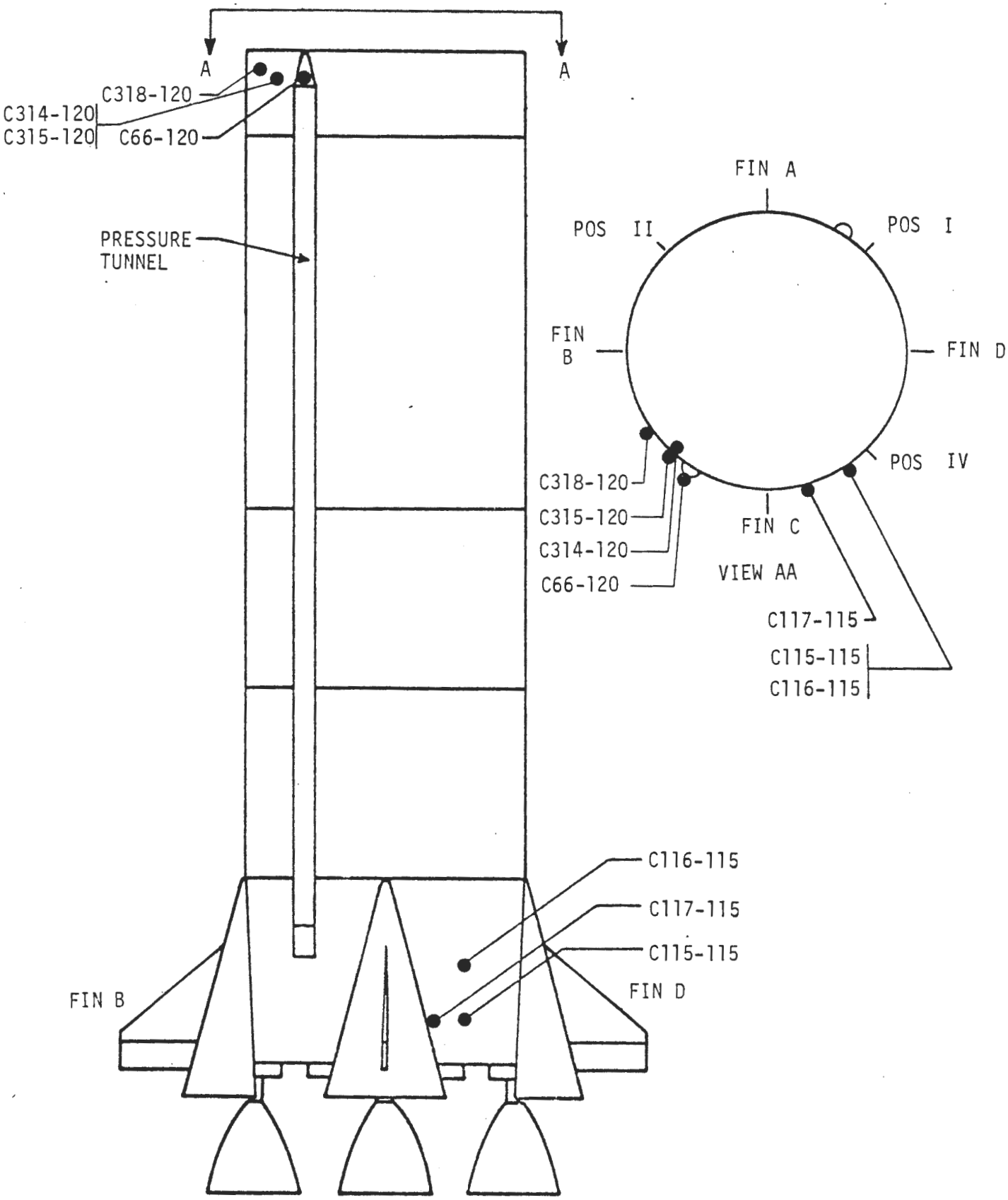

FIGURE 6-4. S-IC STAGE AERODYNAMIC HEATING INSTRUMENTATION - AFT COMPARTMENT, PRESSURE TUNNEL AND FORWARD SKIRT

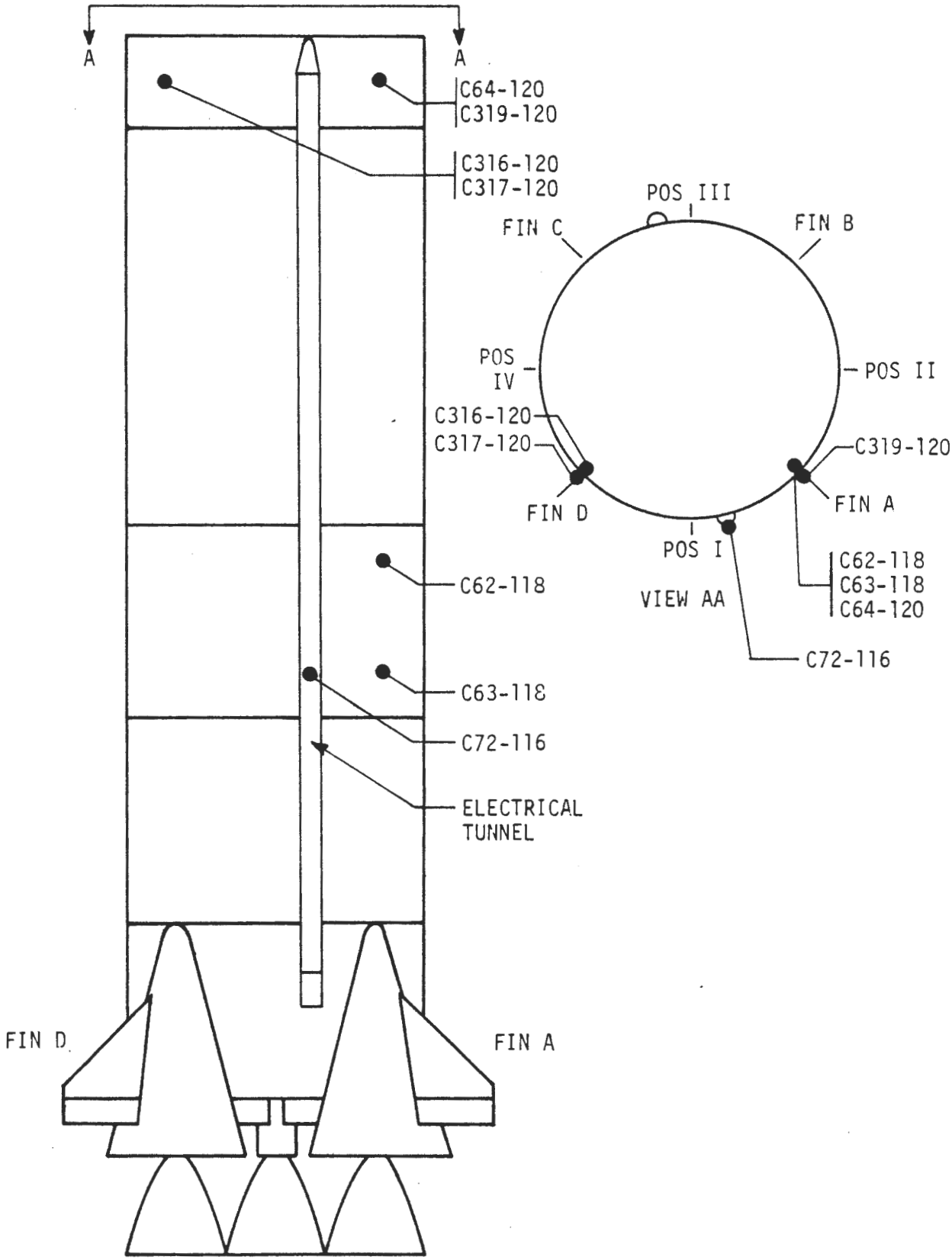

FIGURE 6-5. S-IC STAGE AERODYNAMIC HEATING INSTRUMENTATION - ELECTRICAL TUNNEL, INTERTANK AND FORWARD SKIRT

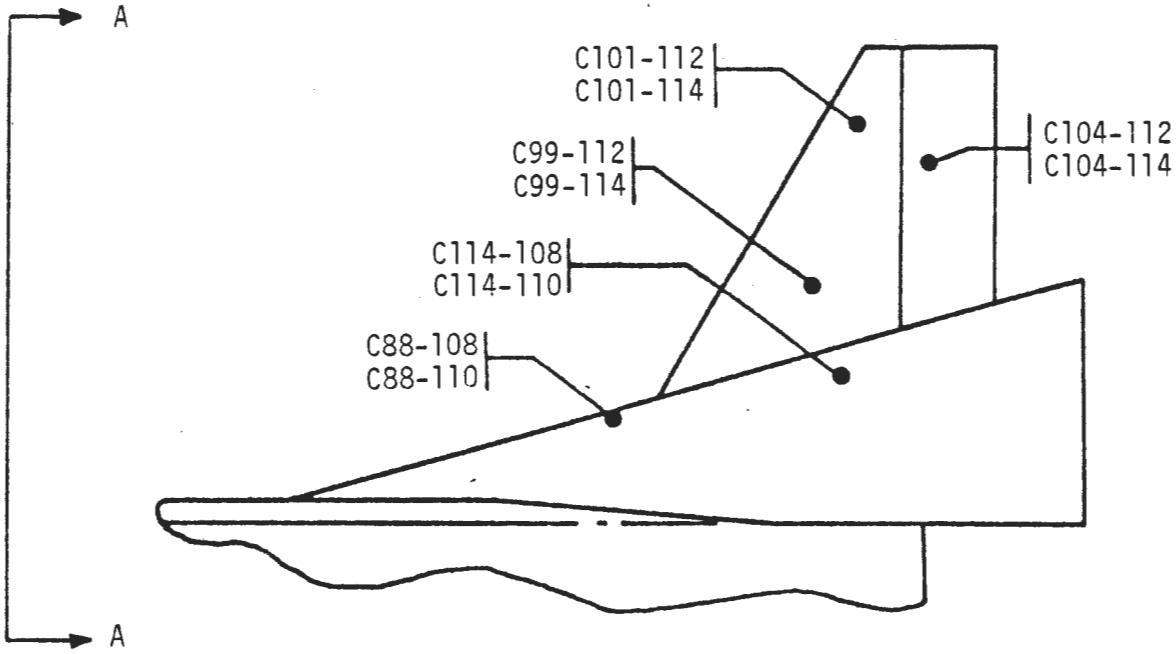

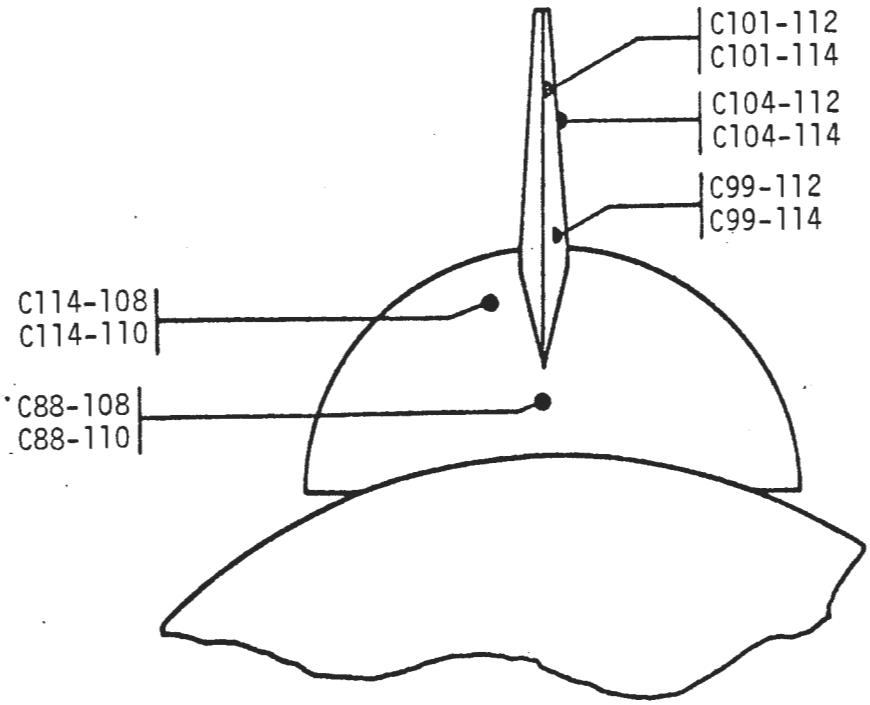

VIEW AA

FIGURE 6-6. S-IC ENGINE FAIRING AND FIN AERODYNAMIC HEATING INSTRUMENTATION

TABLE 6-I. S-IC STAGE AERODYNAMIC HEATING INSTRUMENTATION

(CONTINUED ON NEXT PAGE)

MEASUREMENT NUMBER	INSTRUMENT TYPE*	RANGE °K	INSTALLATION METHOD**	LOCATION
C62-118	Skin Temperature	173-393	1	Station 844, Internal Vehicle Skin, Fin A Centerline
C63-118	Skin Temperature	173-393	1	Station 724, Internal Vehicle Skin, Fin A Centerline
C64-120	Skin Temperature	173-393	1	Station 1491, Internal Vehicle Skin, Fin A Centerline
C66-120	Skin Temperature	223-473	1	Station 1519, Internal Pressurization Tunnel Ramp
C72-116	Skin Temperature	273-623	1	Station 727, Internal Electrical Tunnel Skin
C88-108	Skin Temperature	223-623	2	Station 211, Internal Engine Fairing Skin, 7.2 Inches from Fin B Centerline toward Stringer #9
C88-110	Skin Temperature	223-623	2	Station 218, Internal Engine Fairing Skin, 7.2 Inches from Fin D Centerline toward Position IV

* Chromel-alumel thermocouple

** 1 Bare wire welded to skin internal surface

** 2 Bare wire welded to tab which is bonded and bolted to skin internal surface

TABLE 6-I. S-IC STAGE AERODYNAMIC HEATING INSTRUMENTATION

(CONTINUED ON NEXT PAGE)

MEASUREMENT NUMBER	INSTRUMENT TYPE*	RANGE °K	INSTALLATION METHOD**	LOCATION
C99-112	Skin Temperature	273-823	2	Ramp Section of Fin B at Fin Station 61.9, 24.5 Inches above Datum "B" Measured Parallel to Fin Stations, Internal Fin Skin Toward Fin A
C99-114	Skin Temperature	273-823	2	Ramp Section of Fin D at Fin Station 61.9, 24.5 Inches above Datum "B" Measured Parallel to Fin Stations, Internal Fin Skin Toward Fin A
C101-112	Skin Temperature	273-823	2	Ramp Section of Fin B at Fin Station 122.4, 14.5 Inches above Datum "B" Measured Parallel to Fin Stations, Internal Fin Skin Toward Fin A
C101-114	Skin Temperature	273-823	2	Ramp Section of Fin D at Fin Station 122.7, 12.9 Inches above Datum "B" Meausred Parallel to Fin Stations, Internal Fin Skin Toward Fin C
C104-112	Skin Temperature	273-823	2	Flat Section of Fin B at Fin Station 92.78, 17.2 Inches above Fin Base, Internal Fin Skin Toward Fin A
C104-114	Skin Temperature	273-823	2	Flat Section of Fin D at Fin Station 92.7, 17.05 Inches above Fin Base, Internal Fin Skin Toward Fin C

* Chromel-alumel thermocouple

** 1 Bare wire welded to skin internal surface

** 2 Bare wire welded to a tab which is bonded and bolted to skin internal surface

TABLE 6-I. S-IC STAGE AERODYNAMIC HEATING INSTRUMENTATION

(CONTINUED ON NEXT PAGE)

MEASUREMENT NUMBER	INSTRUMENT TYPE*	RANGE °K	INSTALLATION METHOD**	LOCATION
C114-108	Skin Temperature	223-623	2	Station 137, Internal Engine Fairing Skin, Fin B, 5.8 Inches from Center of Stringer #12 toward Stringer #13
C114-110	Skin Temperature	223-623	2	Station 137, Internal Engine Fairing Skin, Fin D, 5.9 Inches from Center of Stringer #12 toward Stringer #13
C115-115	Skin Temperature	223-393	1	Station 170, Internal Vehicle Skin, 35°9' from Fin C Centerline toward Position IV
C116-115	Skin Temperature	223-393	1	Station 230, Internal Vehicle Skin, 35°9' from Fin C Centerline toward Position IV
C117-115	Skin Temperature	223-393	1	Station 170, Internal Vehicle Skin, 23°45' from Fin C Centerline toward Position IV
C314-120	Skin Temperature	173-393	1	Station 1507, Internal Vehicle Skin, 6°40' from Position III toward Position IV
C315-120	Plate Temperature	223-473	2	Station 1507, Aluminum Plate Mounted on Top of Stringer, 7°30' from Position III toward Position IV

* Chromel-alumel thermocouple

** 1 Bare wire welded to skin internal surface

** 2 Bare wire welded to a tab which is bonded and bolted to skin internal surface

TABLE 6-I. S-IC STAGE AERODYNAMIC HEATING INSTRUMENTATION (CONCLUDED)

MEASUREMENT NUMBER	INSTRUMENT TYPE*	RANGE °K	INSTALLATION METHOD**	LOCATION
C316-120	Skin Temperature	173-393	1	Station 1491.5, Internal Vehicle Skin, Fin D Centerline
C317-120	Plate Temperature	223-473	2	Station 1491.5, Aluminum Plate Mounted on Top of Stringer, 44°10' from Position I toward Position IV
C318-120	Plate Temperature	223-473	2	Station 1519, Aluminum Plate Mounted on Top of Stringer, 9°10' from Position III toward Position II
C319-120	Plate Temperature	223-473	2	Station 1491.5, Aluminum Plate Mounted on Top of Stringer, 45°50' from Position I toward Position II

* Chromel-alumel thermocouple

** 1 Bare wire welded to skin internal surface

** 2 Bare wire welded to a tab which is bonded and bolted to skin internal surface

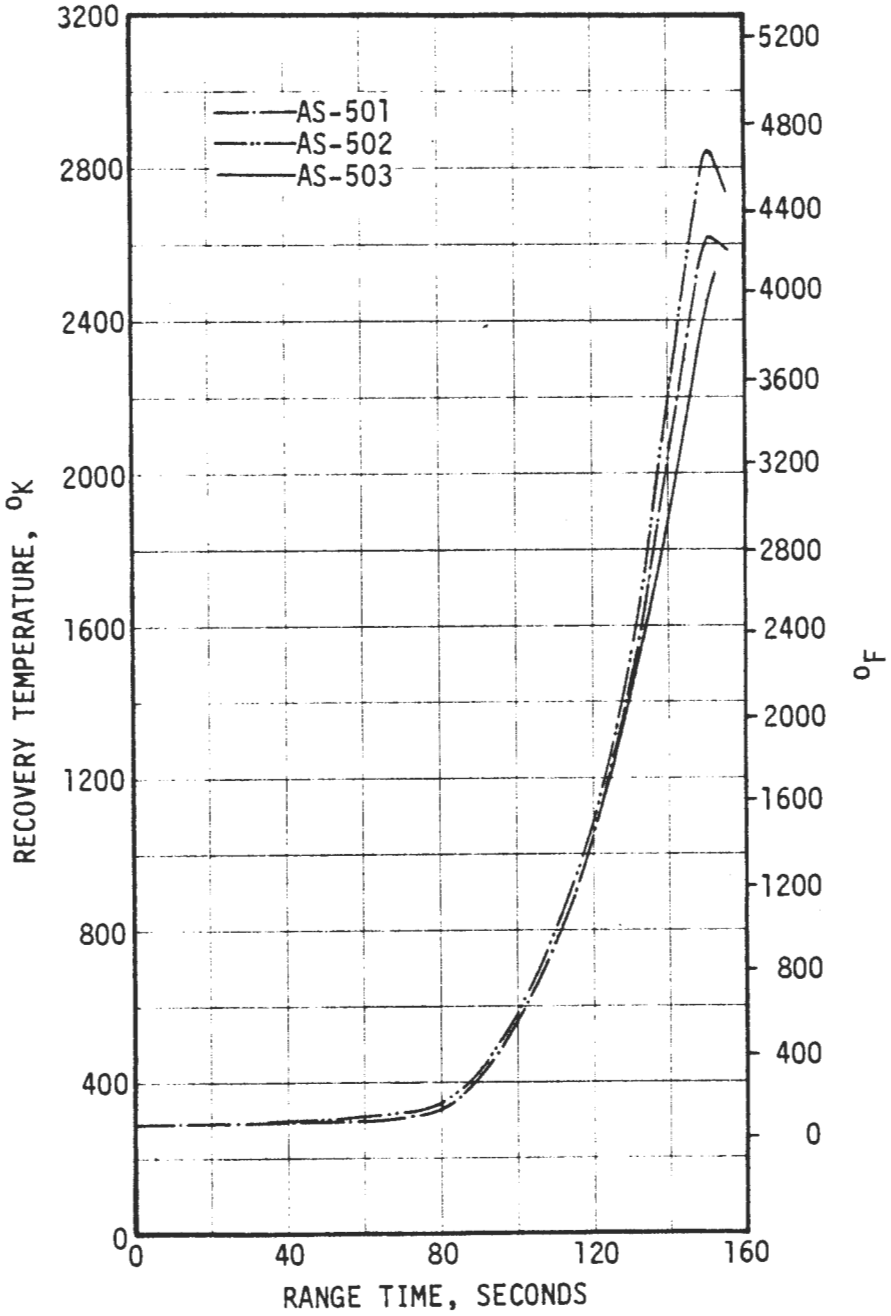

FIGURE 6-7. RECOVERY TEMPERATURE FOR AS-501, AS-502 AND AS-503 TRAJECTORIES

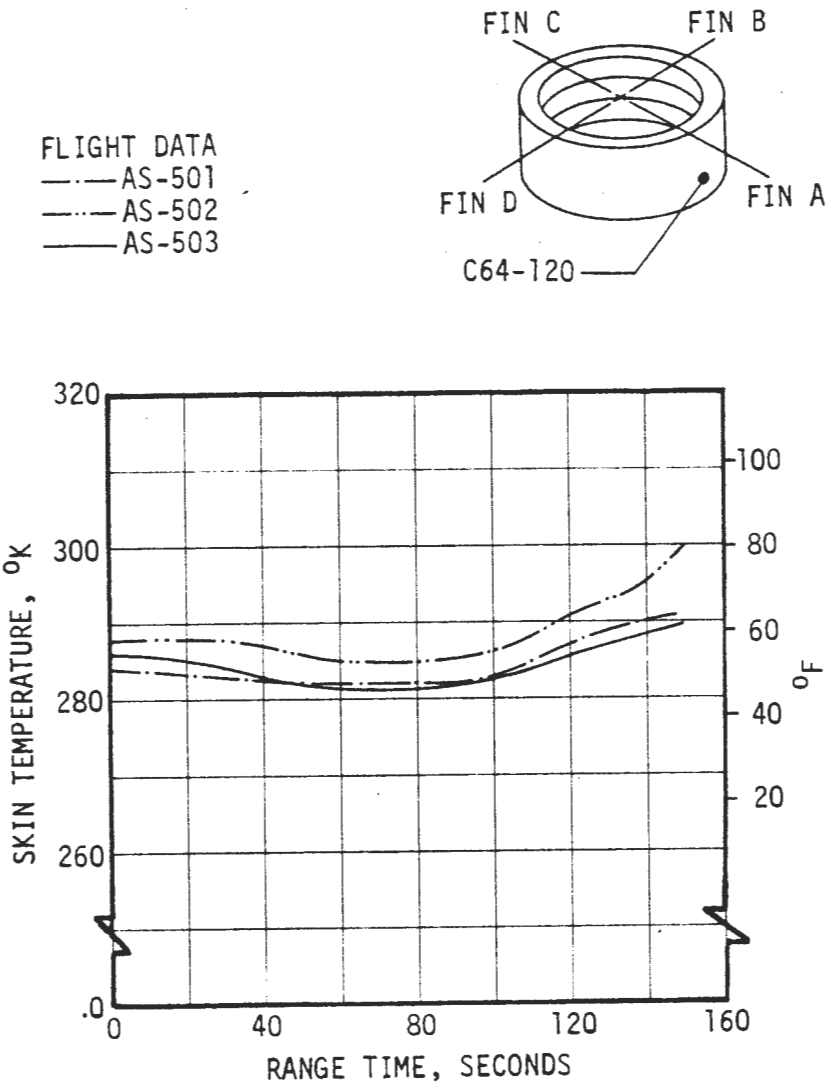

FIGURE 6-8. S-IC FORWARD SKIRT SKIN TEMPERATURE - C64-120

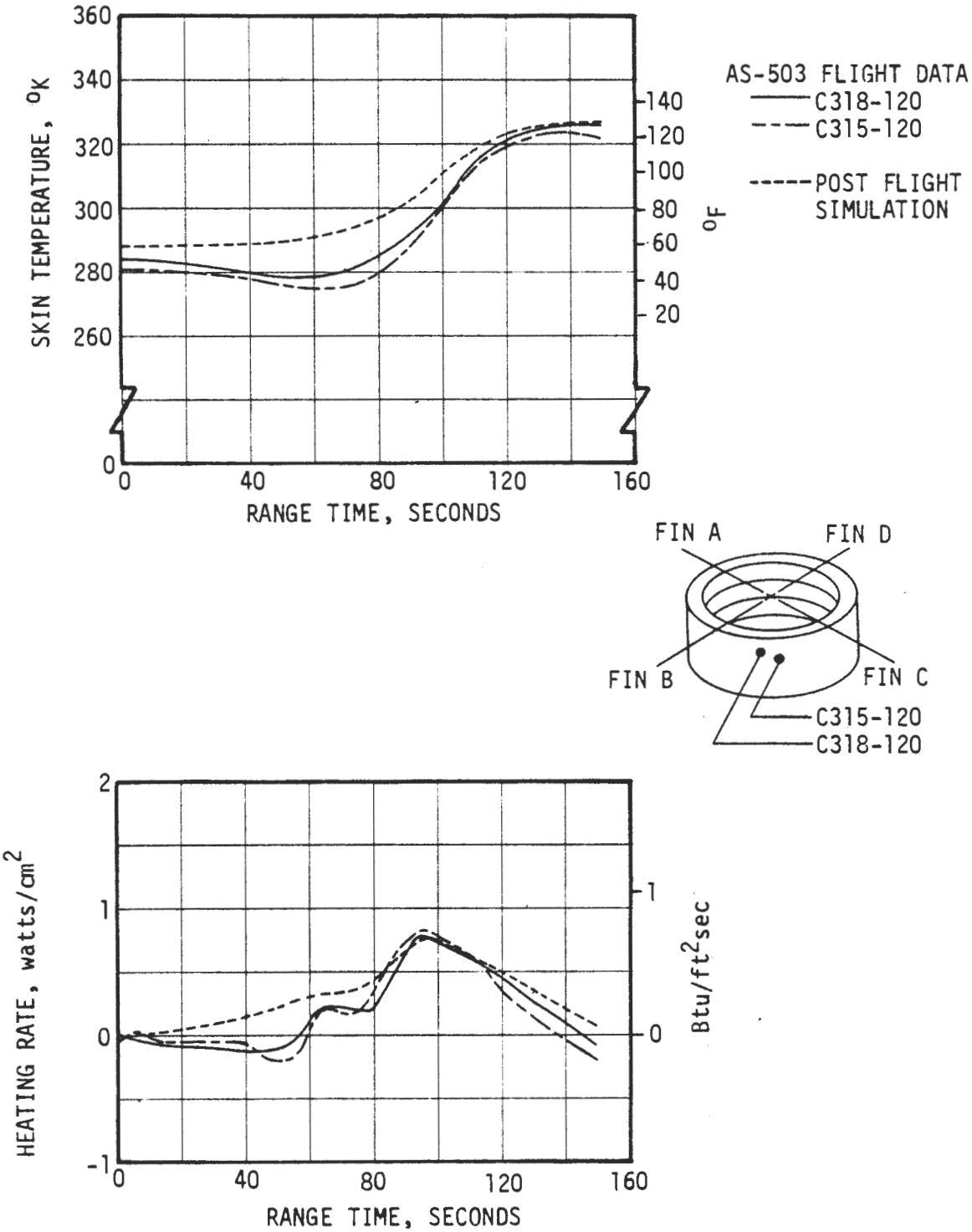

FIGURE 6-9 . S-IC FORWARD SKIRT HEATING RATE AND SKIN TEMPERATURE - C315-120 AND C318-120

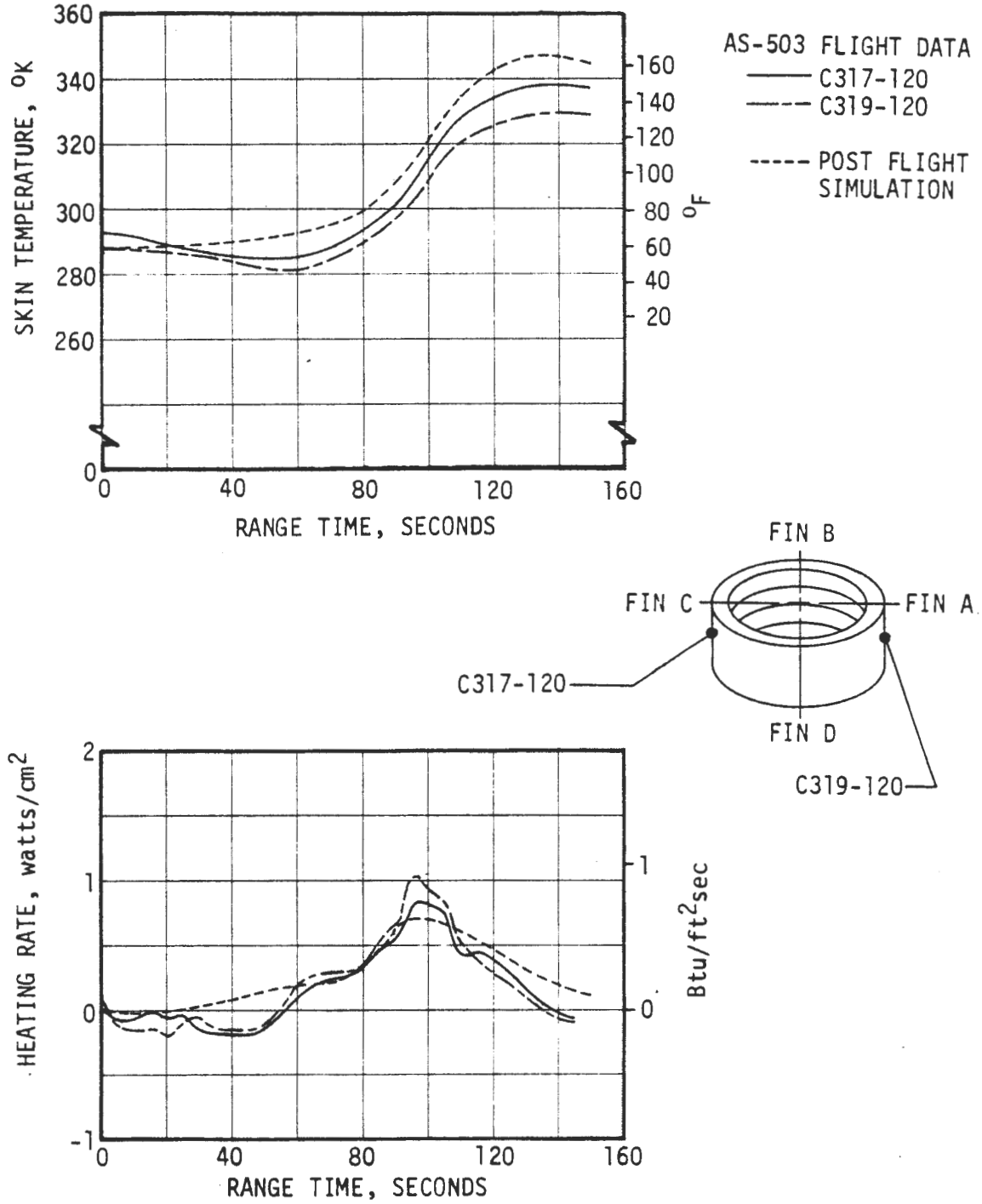

FIGURE 6-10. S-IC FORWARD SKIRT HEATING RATE AND SKIN TEMPERATURE - C317-120 AND C319-120

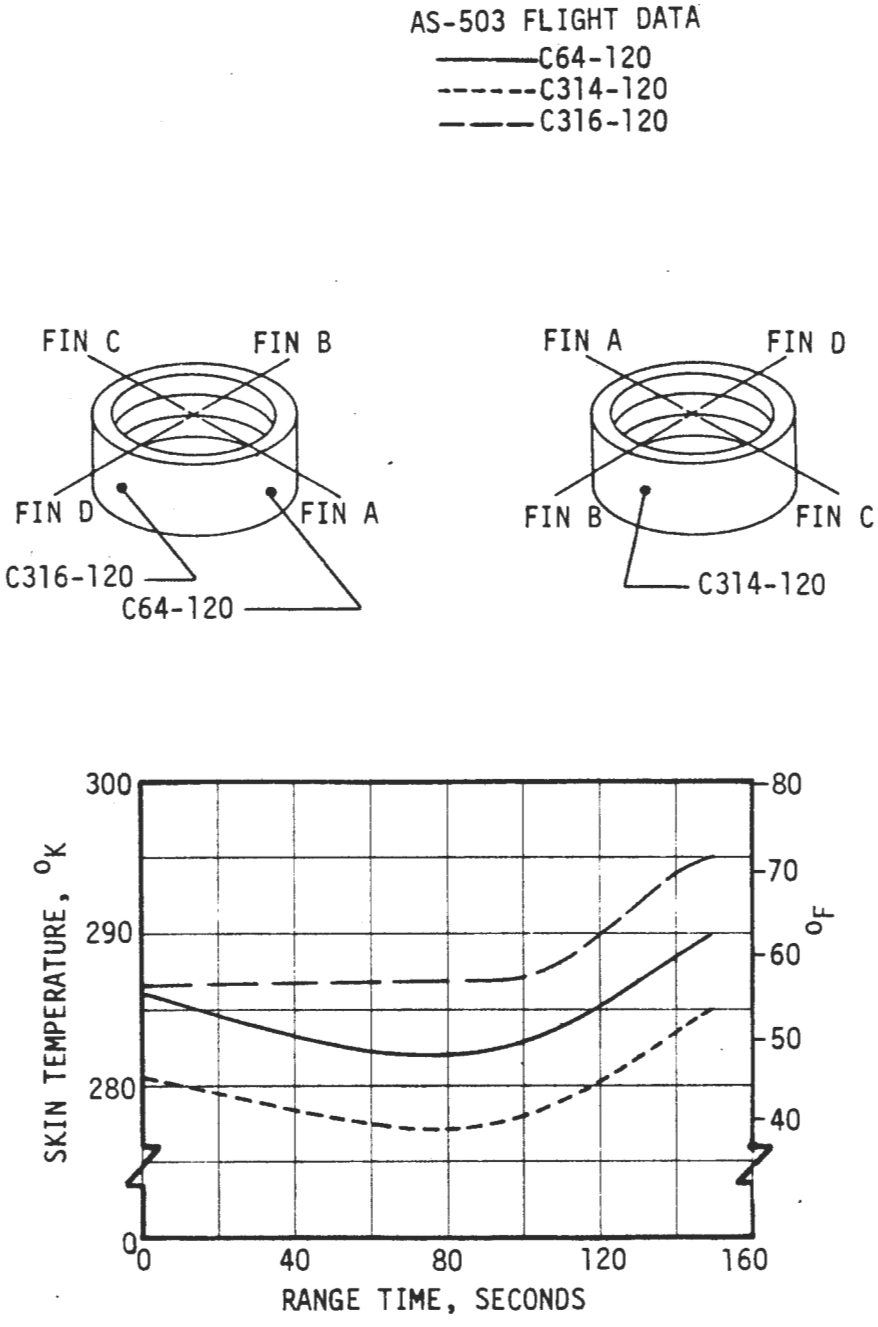

FIGURE 6-11. S-IC FORWARD SKIRT INTERNAL SKIN TEMPERATURES - C64-120, C314-120, AND C316-120

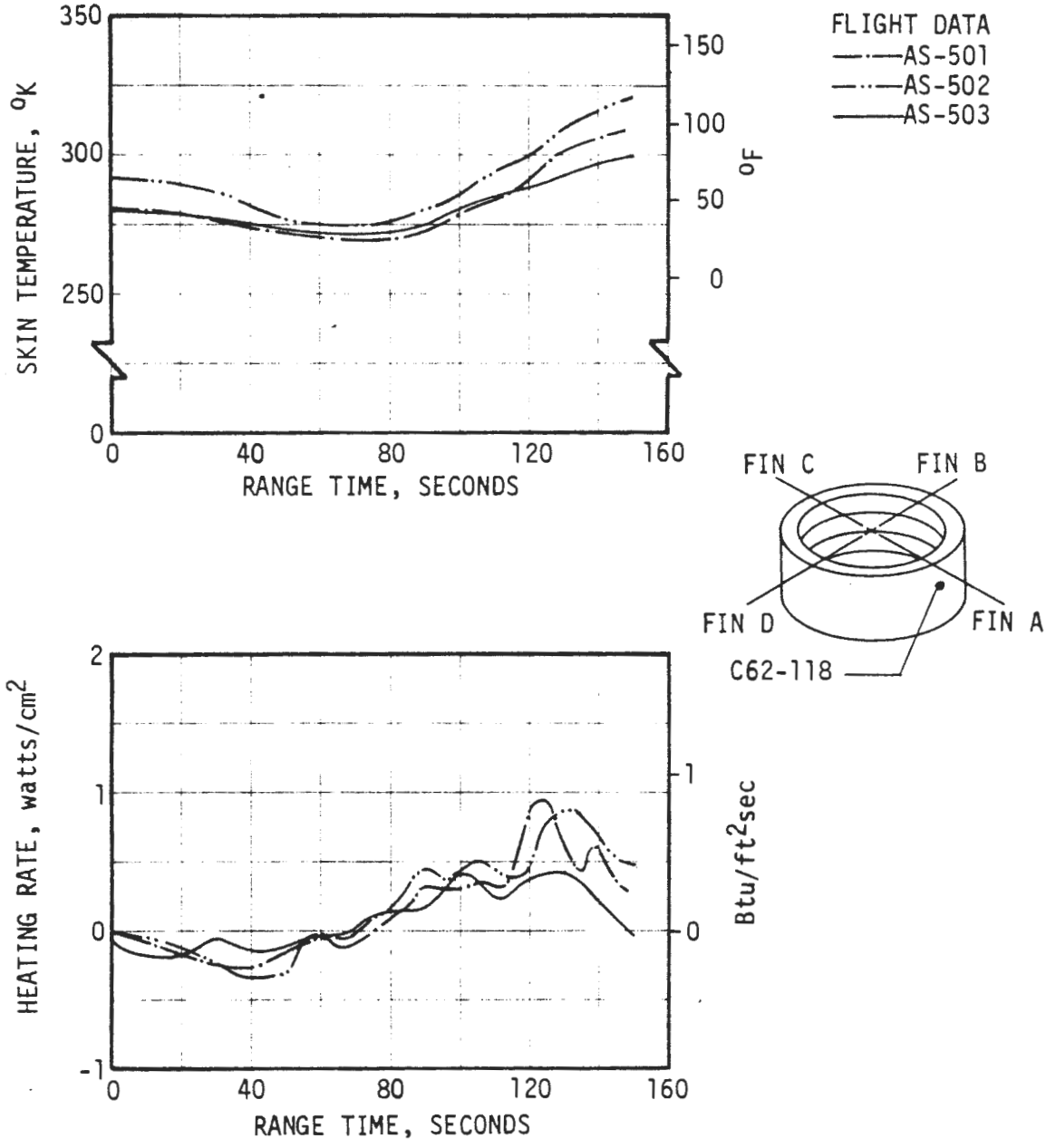

FIGURE 6-12. S-IC INTERTANK HEATING RATE AND SKIN TEMPERATURE - C62-118

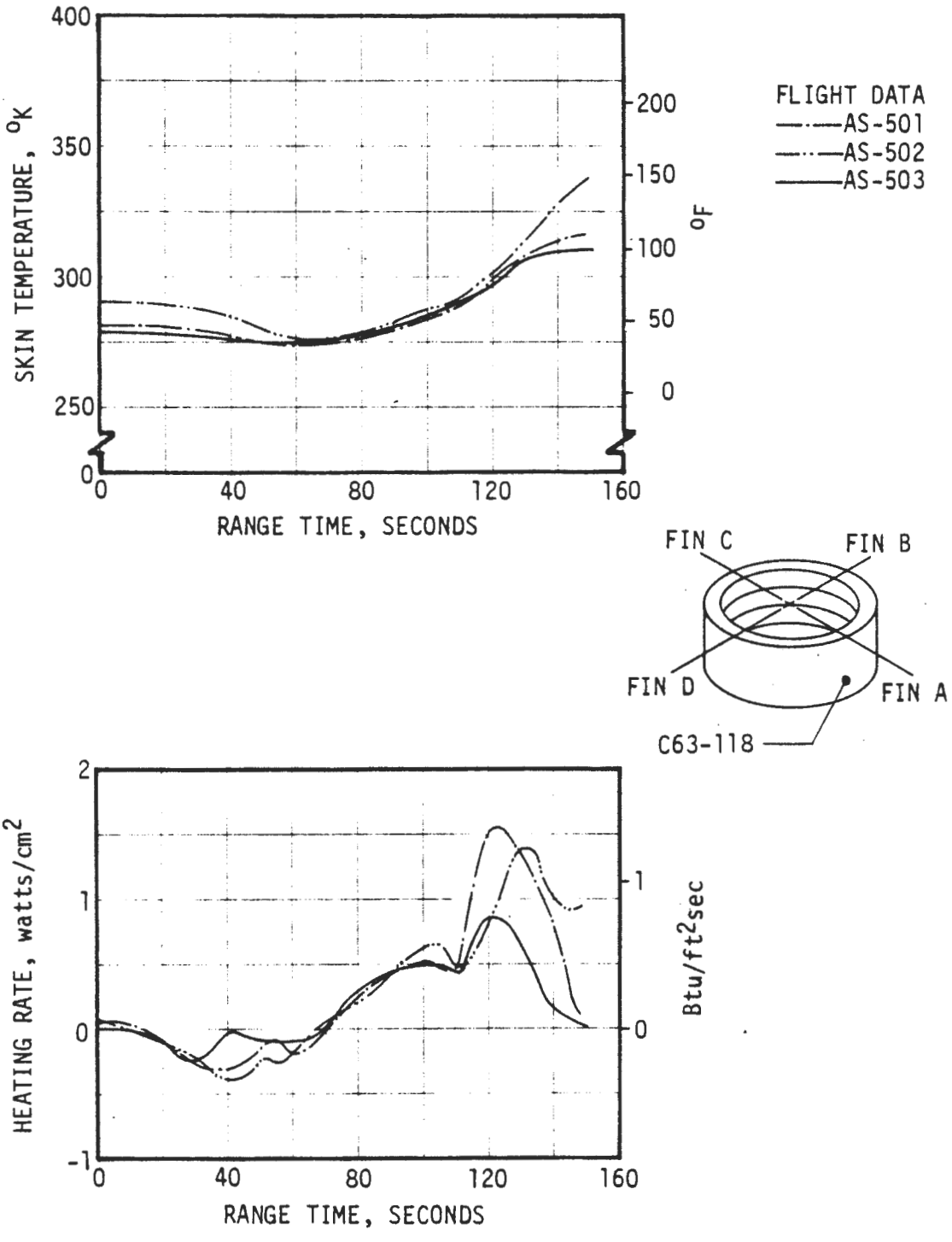

FIGURE 6-13. S-IC INTERTANK HEATING RATE AND SKIN TEMPERATURE - C63-118

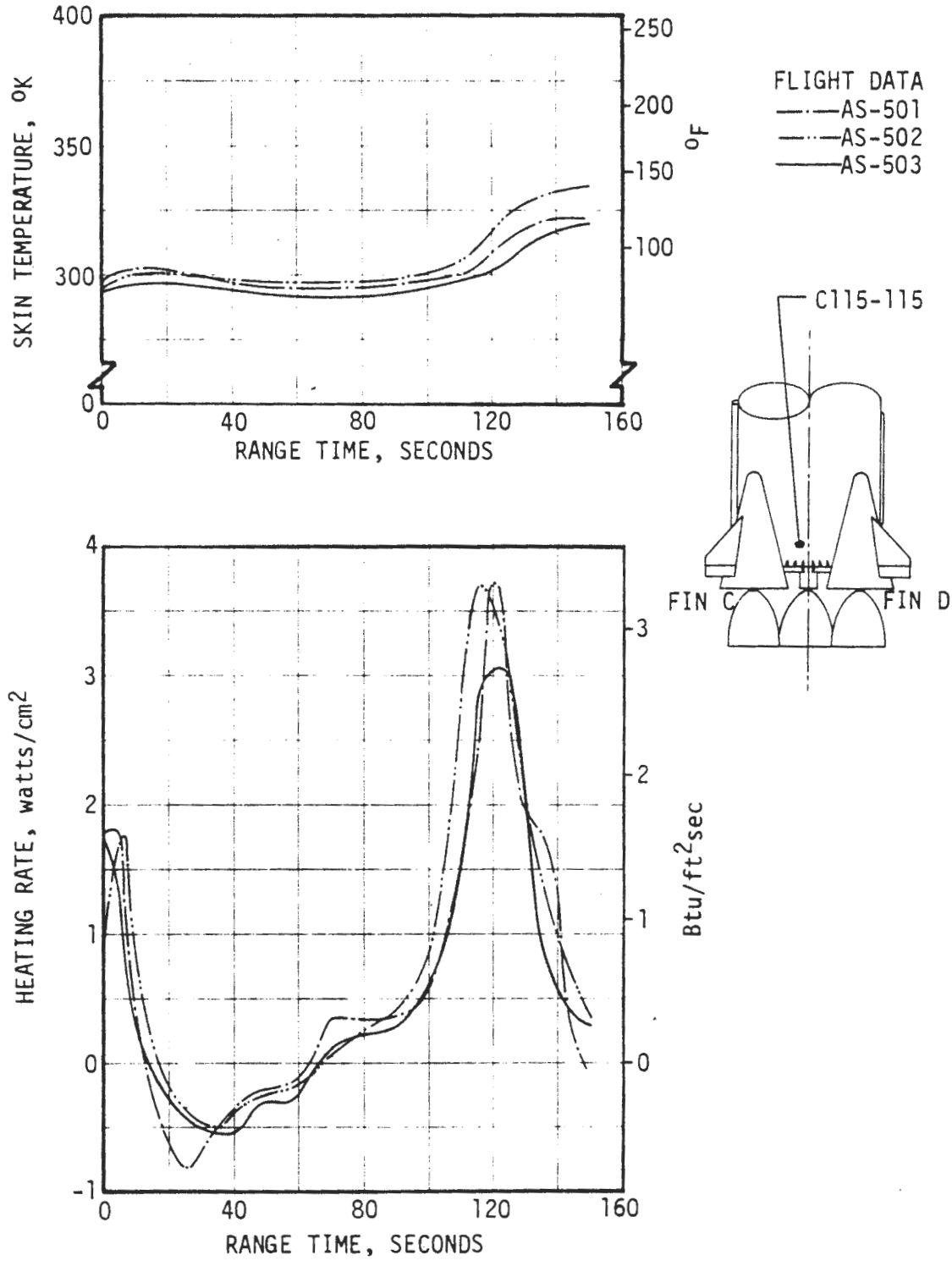

FIGURE 6-14. S-IC AFT COMPARTMENT HEATING RATE AND SKIN TEMPERATURE - C115-115

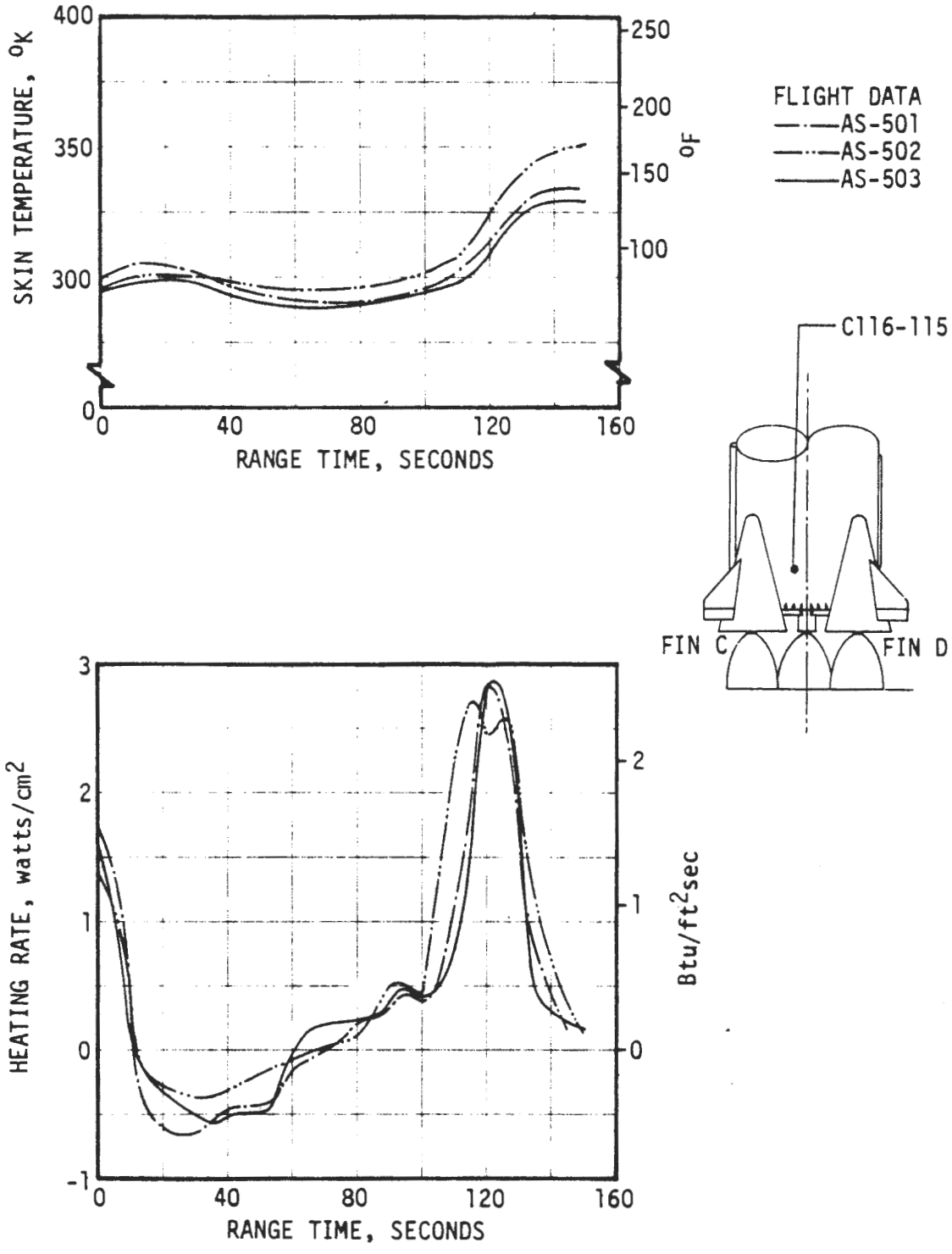

FIGURE 6-15. S-IC AFT COMPARTMENT HEATING RATE AND SKIN TEMPERATURE - C116-115

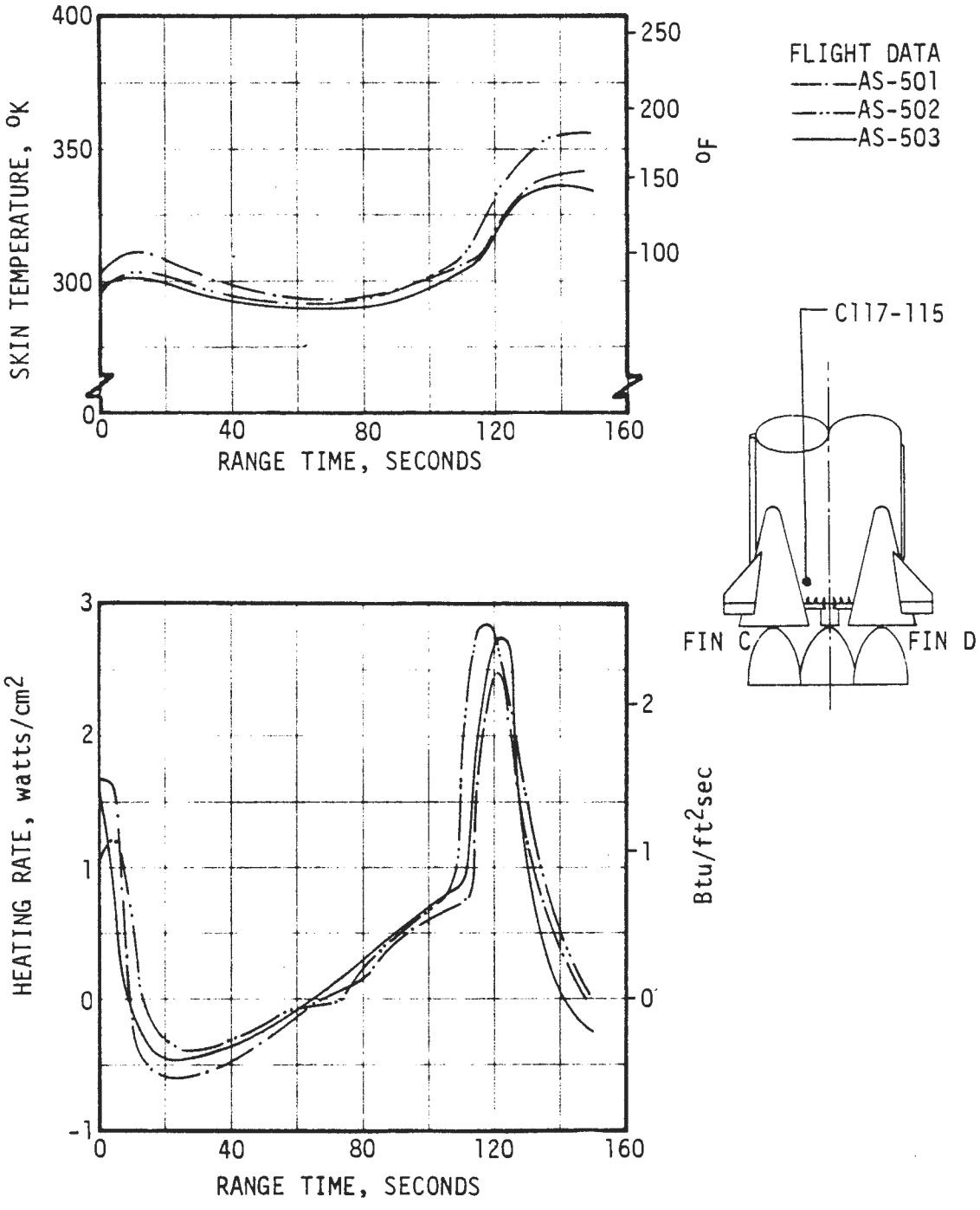

FIGURE 6-16. S-IC AFT COMPARTMENT HEATING RATE AND SKIN TEMPERATURE - C117-115

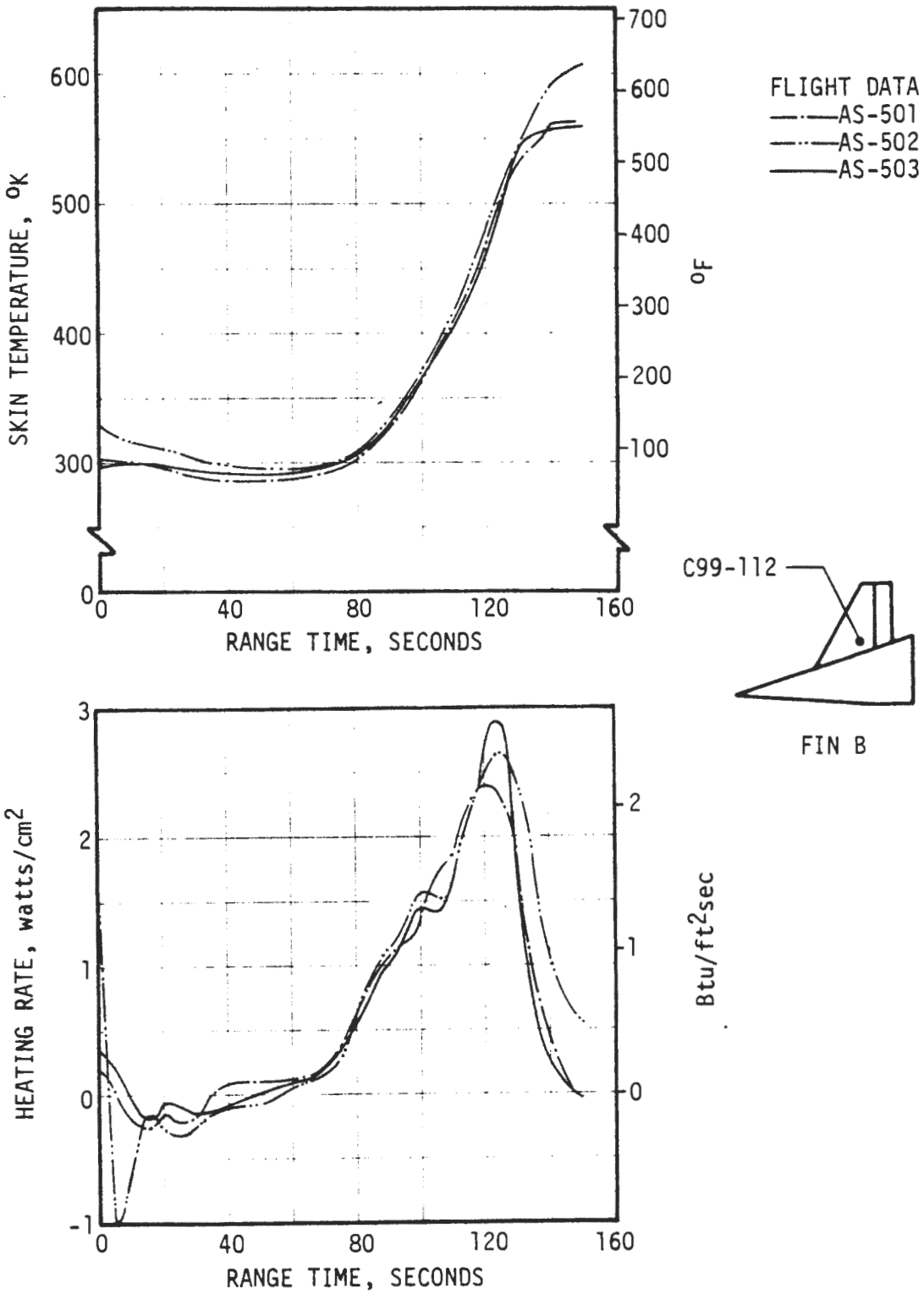

FIGURE 6-17. S-IC FIN HEATING RATE AND SKIN TEMPERATURE - C99-112

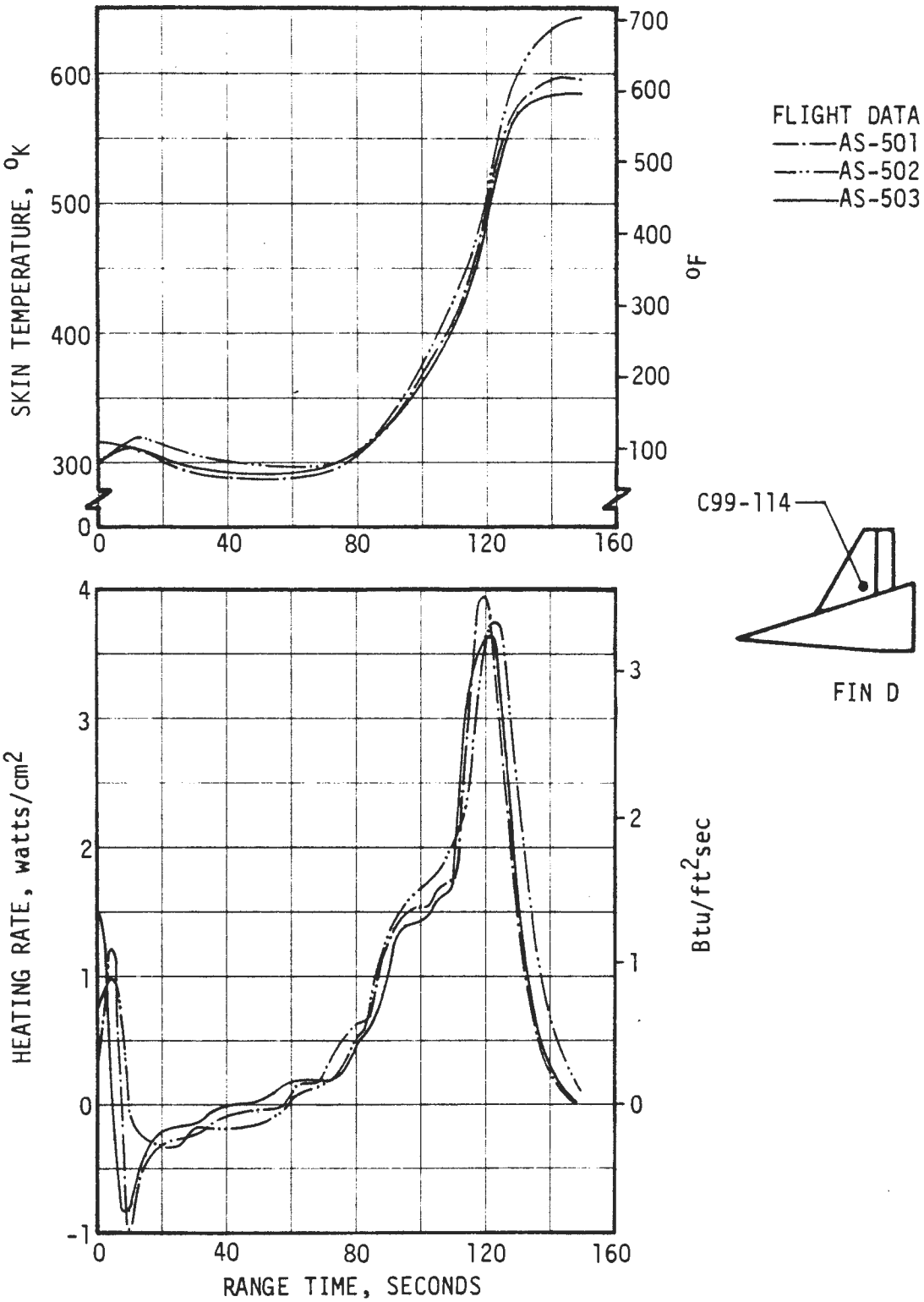

FIGURE 6-18. S-IC FIN HEATING RATE AND SKIN TEMPERATURE - C99-114

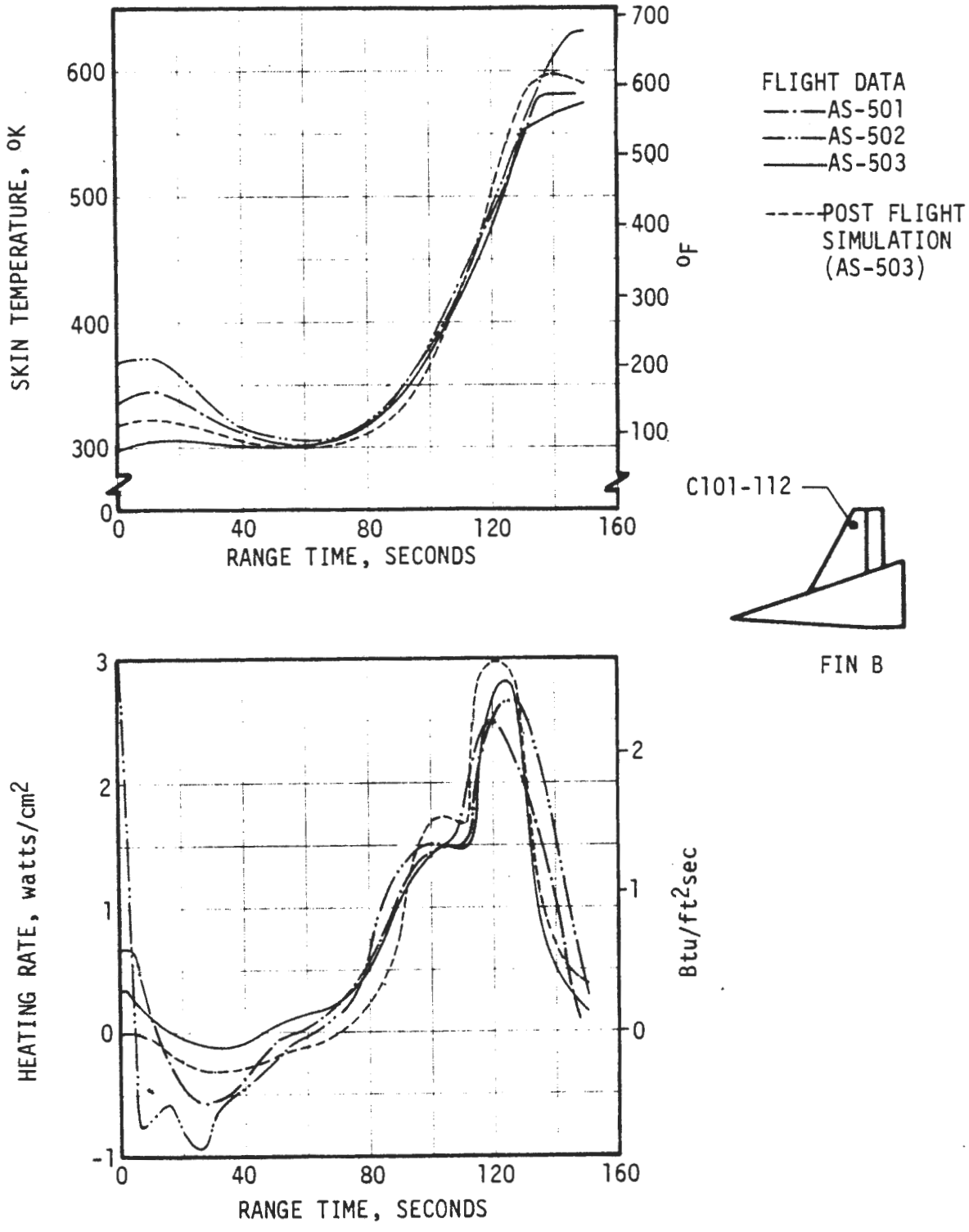

FIGURE 6-19. S-IC FIN HEATING RATE AND SKIN TEMPERATURE - C101-112

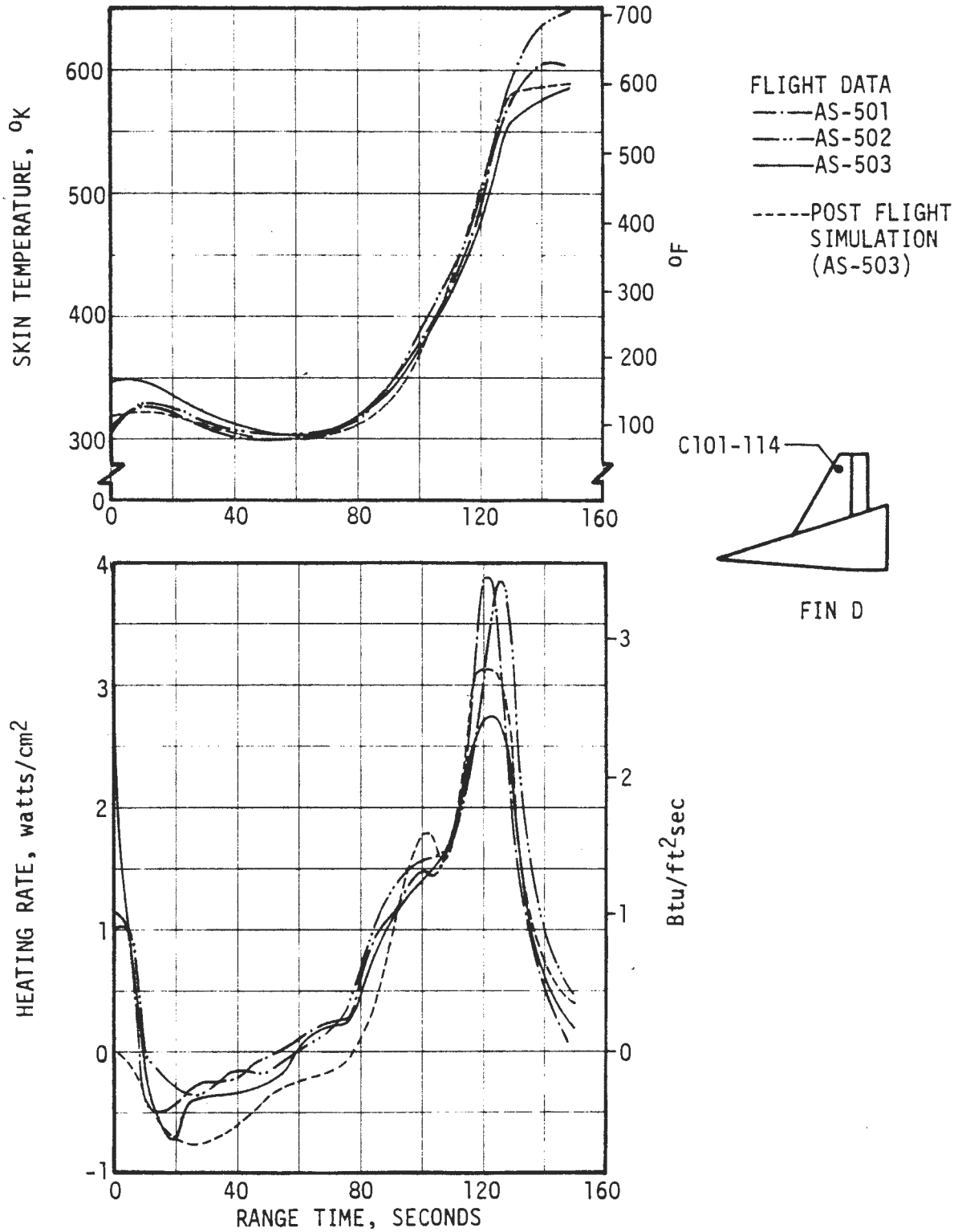

FIGURE 6-20. S-IC FIN HEATING RATE AND SKIN TEMPERATURE - C101-114

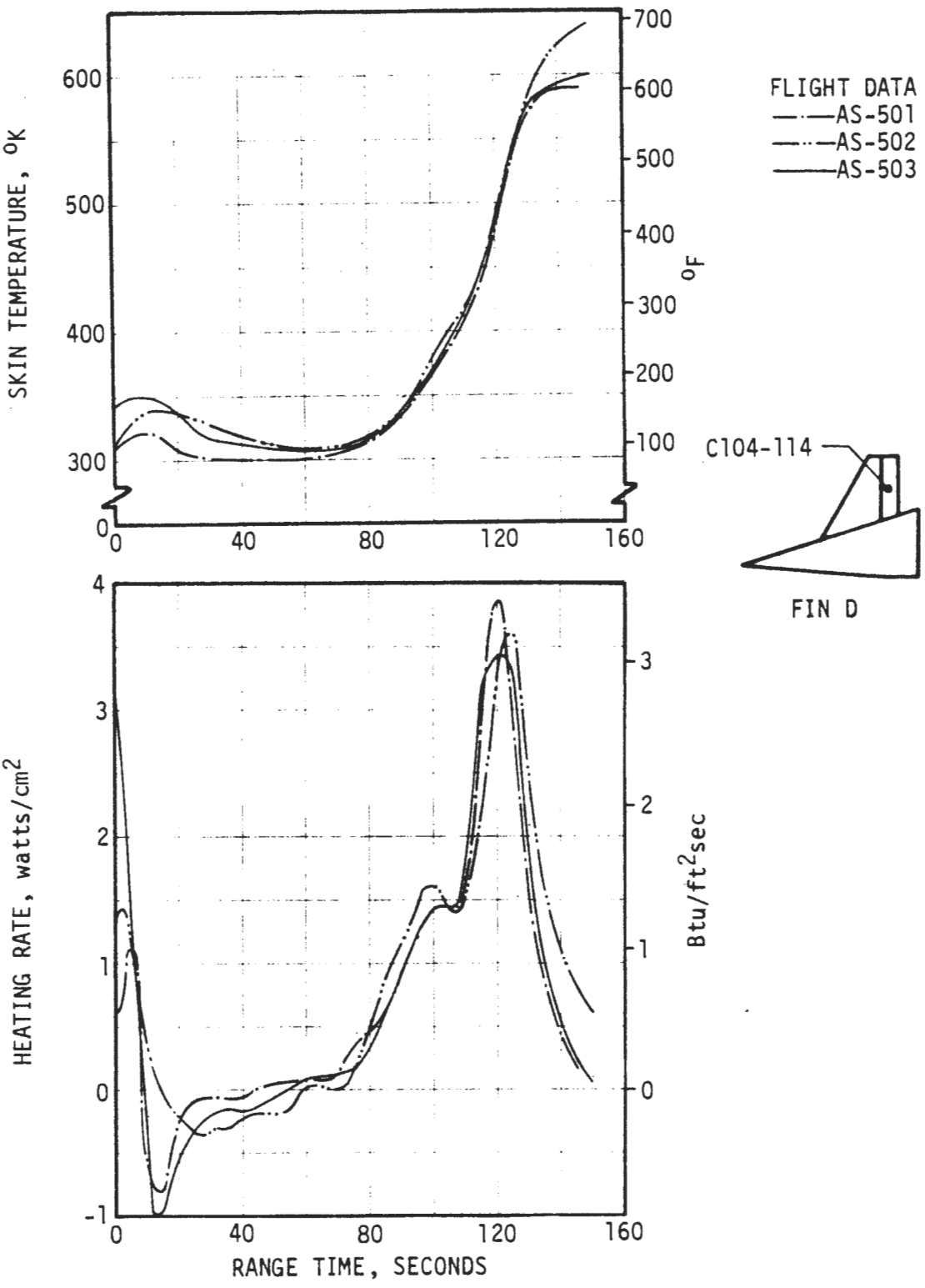

FIGURE 6-21. S-IC FIN HEATING RATE AND SKIN TEMPERATURE - C104-114

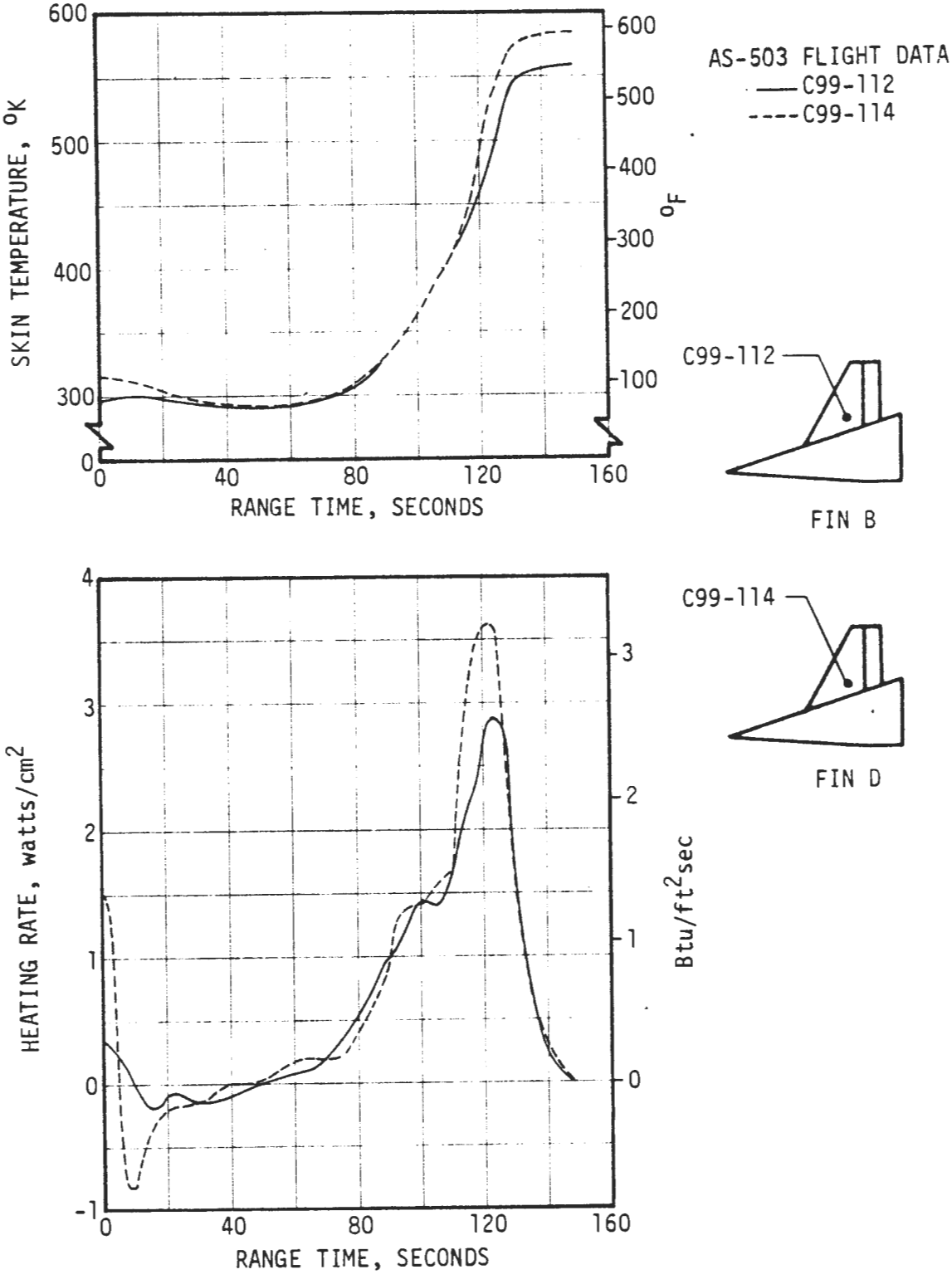

FIGURE 6-22. S-IC FIN HEATING RATES AND SKIN TEMPERATURES - C99-112 AND C99-114

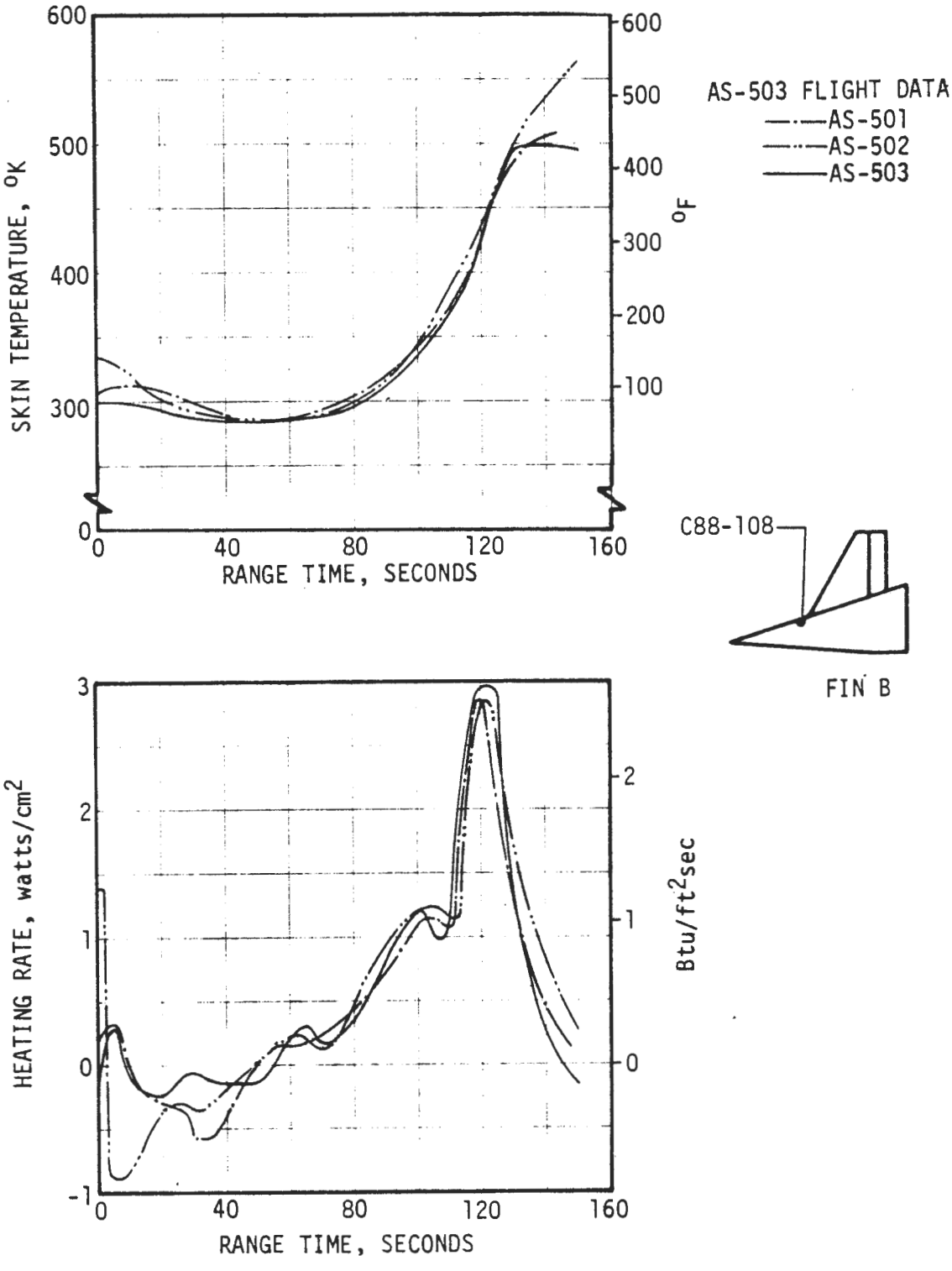

FIGURE 6-23. S-IC ENGINE FAIRING HEATING RATE AND SKIN TEMPERATURE - C88-108

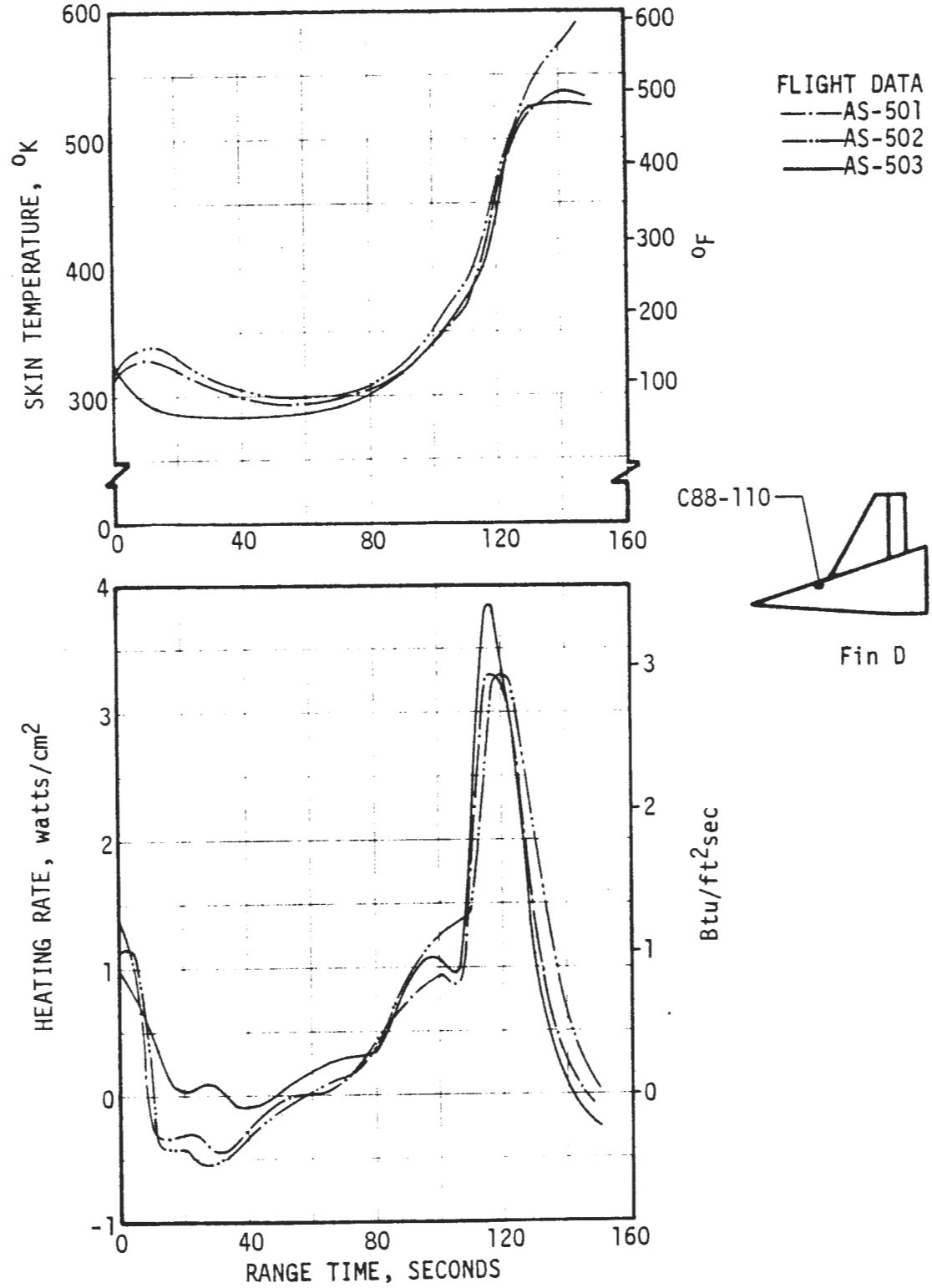

FIGURE 6-24. S-IC ENGINE FAIRING HEATING RATE AND SKIN TEMPERATURE - C88-110

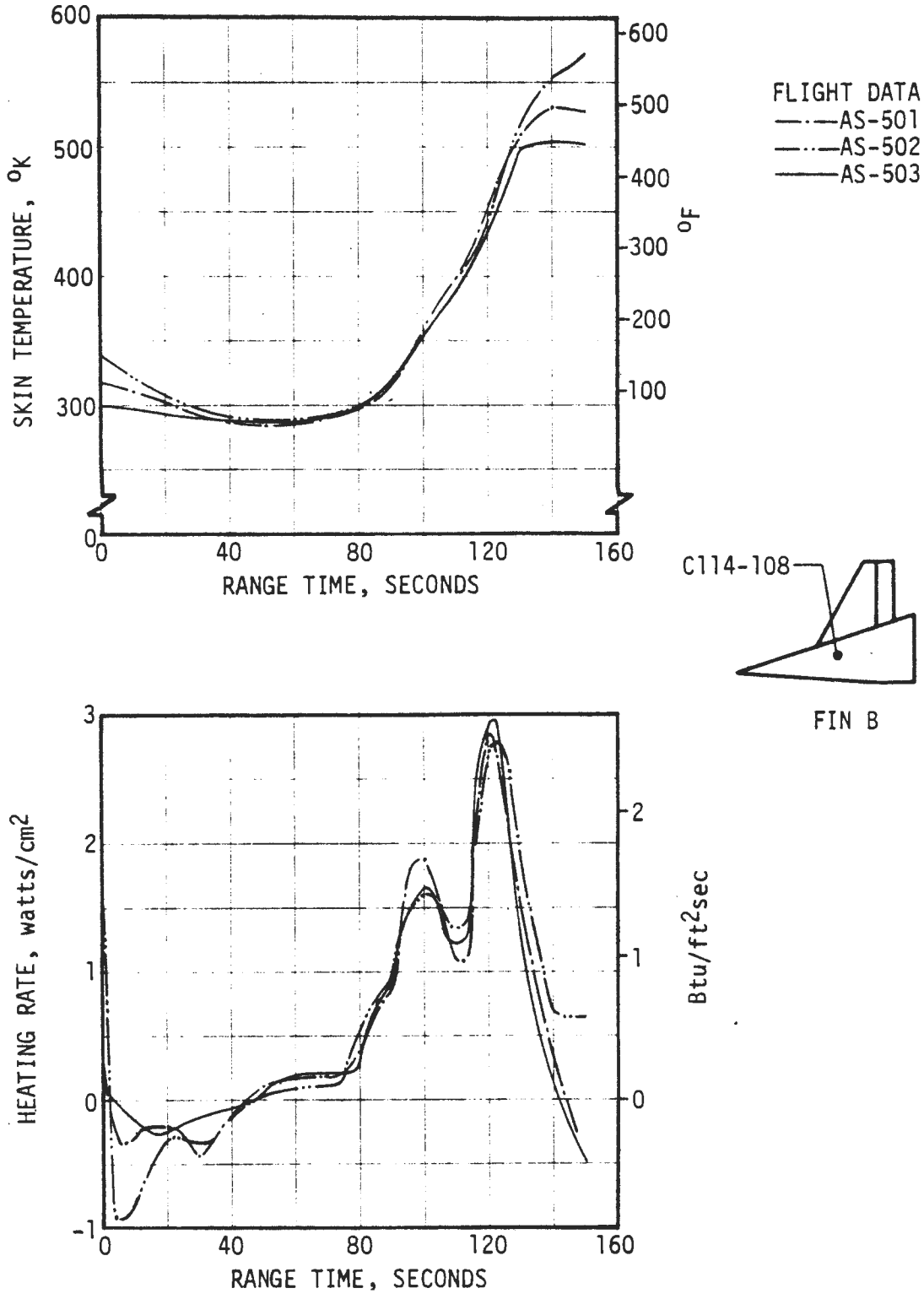

FIGURE 6-25. S-IC ENGINE FAIRING HEATING RATE AND SKIN TEMPERATURE - C114-108

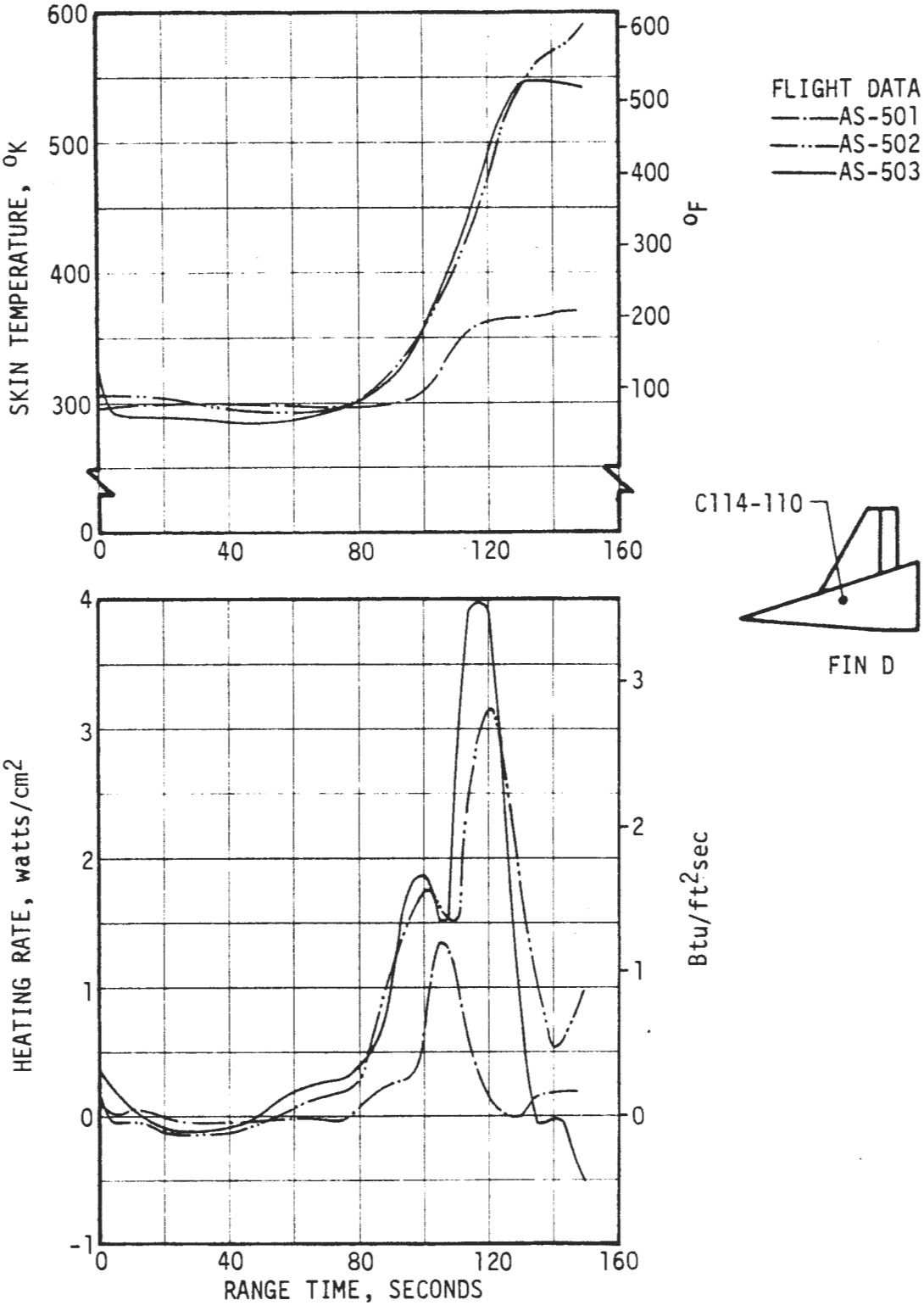

FIGURE 6-26. S-IC ENGINE FAIRING HEATING RATE AND SKIN TEMPERATURE - C114-110

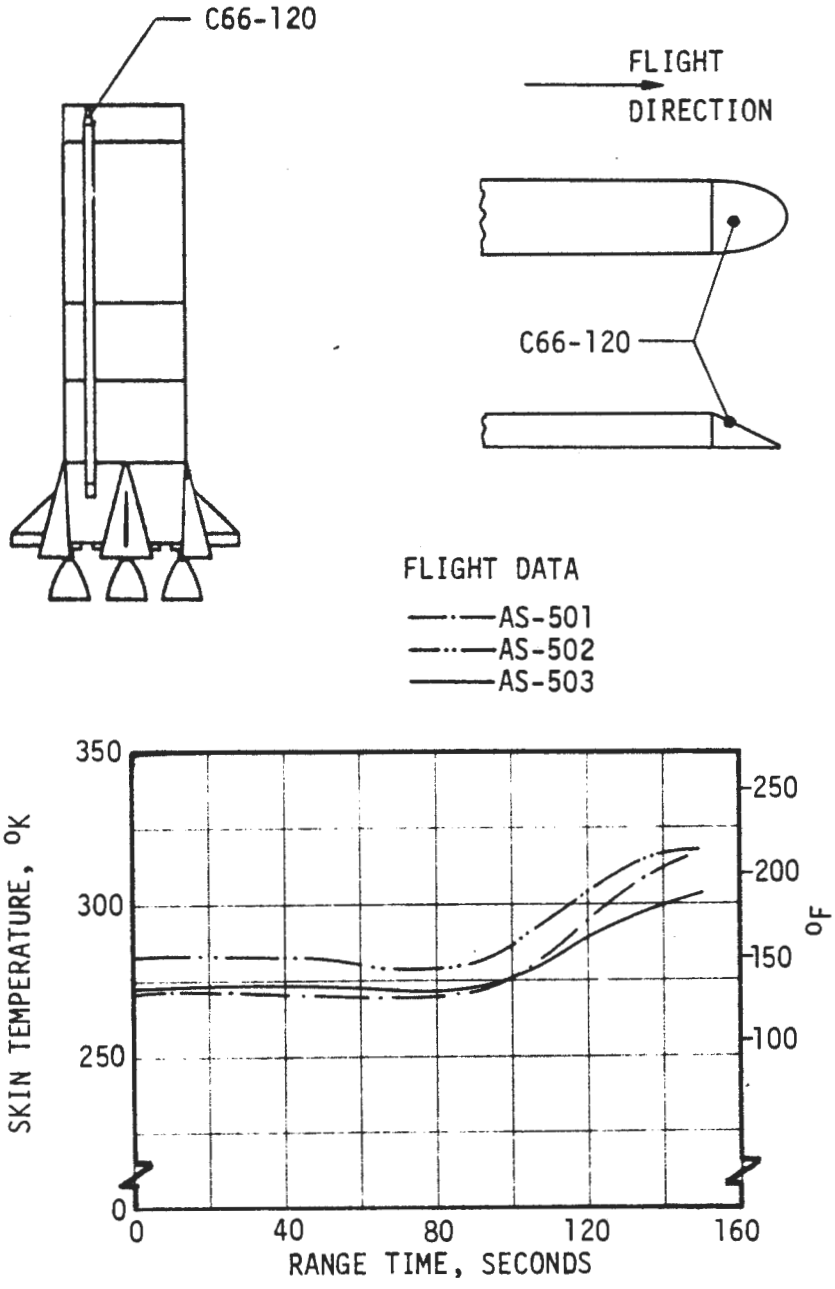

FIGURE 6-27. S-IC PRESSURE TUNNEL FORWARD FAIRING SKIN TEMPERATURE - C66-120

FLIGHT DATA
—·—AS-501
—··—AS-502
———AS-503

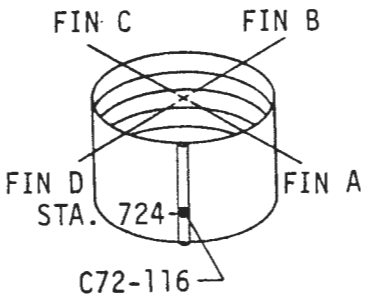

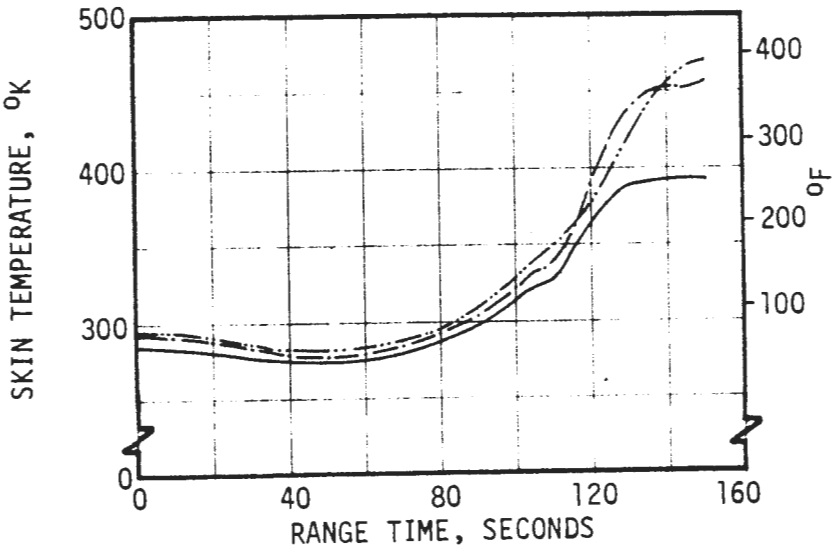

FIGURE 6-28. S-IC ELECTRICAL TUNNEL COVER SKIN TEMPERATURE - C72-116

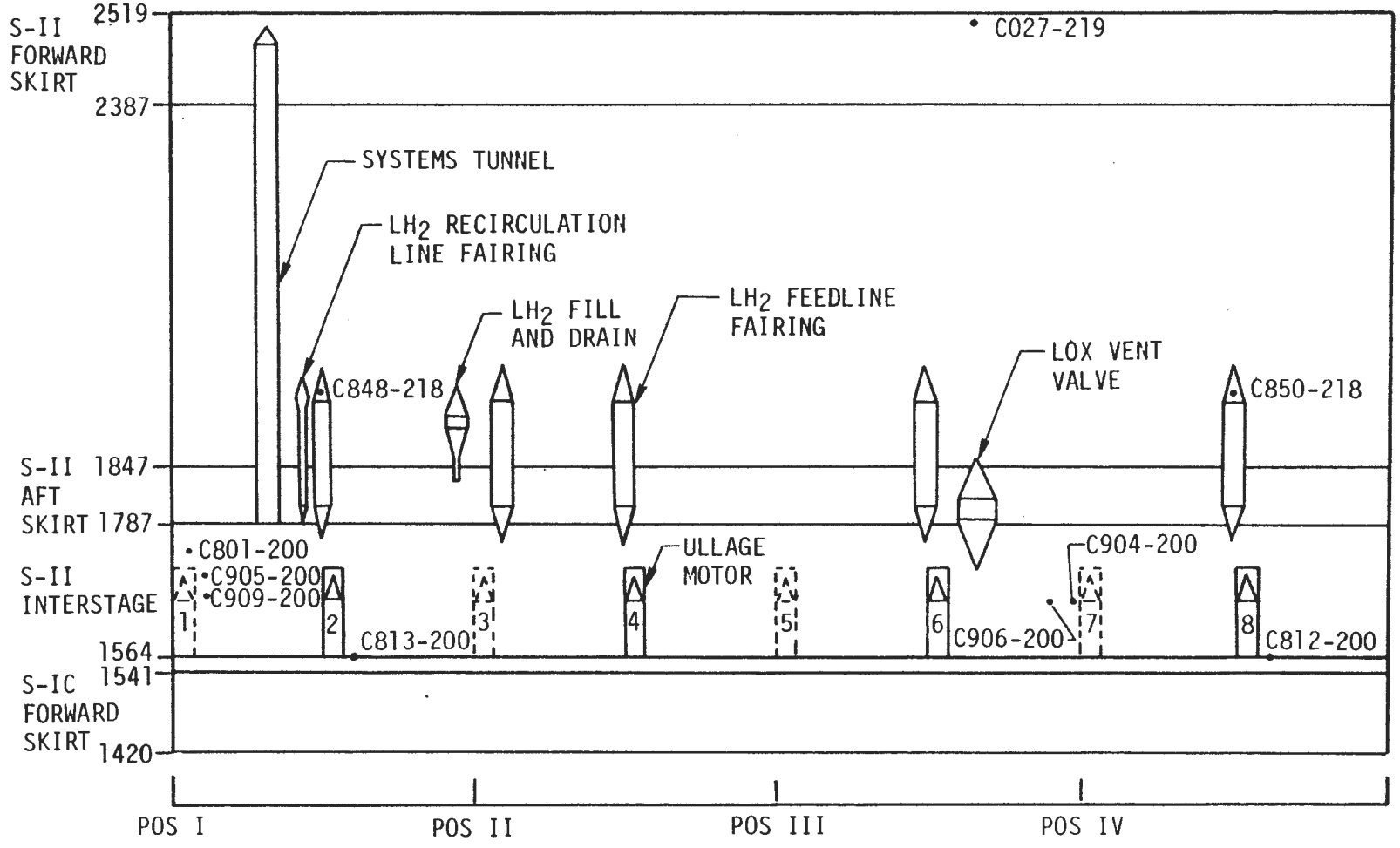

FIGURE 6-29. S-II STAGE STRUCTURAL TEMPERATURE AND HEATING RATE INSTRUMENTATION

TABLE 6-II. S-II STAGE AERODYNAMIC HEATING INSTRUMENTATION

(CONTINUED ON NEXT PAGE)

MEASUREMENT NUMBER	INSTRUMENT TYPE	RANGE	INSTALLATION METHOD**	LOCATION
C027-319	Skin Temperature*	228-477°K	1	Station 2504, Internal Vehicle Skin, 60° from Position III toward Position IV
C801-200	Cal., Total	0-2.83 watts/cm^2	2	Station 1715, Flush with Outer Surface of Interstage, 5° from Position I toward Position II
C812-200	Cal., Total	0-3.4 watts/cm^2	2	Station 1568, Flush with Outer Surface of Ordnance Fairing, 55° from Position III toward Position IV
C813-200	Cal., Total	0-3.4 watts/cm^2	2	Station 1568, Flush with Outer Surface of Ordnance Fairing, 55° from Position I toward Position II
C848-218	Cal., Total	0-5.65 watts/cm^2	2	Station 1947, Flush with Outside Surface of Engine #1 LH_2 Feedline Fairing, 44° from Position I toward Position II
C850-218	Cal., Total	0-5.65 watts/cm^2	2	Station 1947, Flush with Outside Surface of Engine #4 LH_2 Feedline Fairing, 44° from Position IV toward Position I

* Resistance thermometer

** 1 Resistance thermometer bonded to the internal surface of the skin

** 2 Calorimeter body bolted to a brace on the internal side of the skin with the sensing surface protruding through a hole in the skin flush with the outer surface.

** 3 Resistance thermometer bonded to the external surface of the stringer hat section.

TABLE 6-II. S-II STAGE AERODYNAMIC HEATING INSTRUMENTATION (CONCLUDED)

MEASUREMENT NUMBER	INSTRUMENT TYPE	RANGE	INSTALLATION METHOD**	LOCATION
C904-200	Skin Temperature*	228-588°K	3	Station 1649, External Surface of Hat Section of Stringer #211, 82° from Position III toward Position IV
C905-200	Cal., Total	0-2.83 watts/cm^2	2	Station 1701, Flush with Outer Surface of Interstage, 10° from Position I toward Position II
C906-200	Skin Temperature*	228-588°K	3	Station 1649, External Surface of Hat Section of Stringer #215, 89° from Position III toward Position IV
C909-200	Cal., Total	0-2.83 watts/cm^2	2	Station 1654, Flush with Outer Surface of Interstage, 10° from Position I toward Position II

* Resistance thermometer

** 1 Resistance thermometer bonded to the internal surface of the skin

** 2 Calorimeter body bolted to a brace on the internal side of the skin with the sensing surface protruding through a hole in the skin flush with the outer surface.

** 3 Resistance thermometer bonded to the external surface of the stringer hat section.

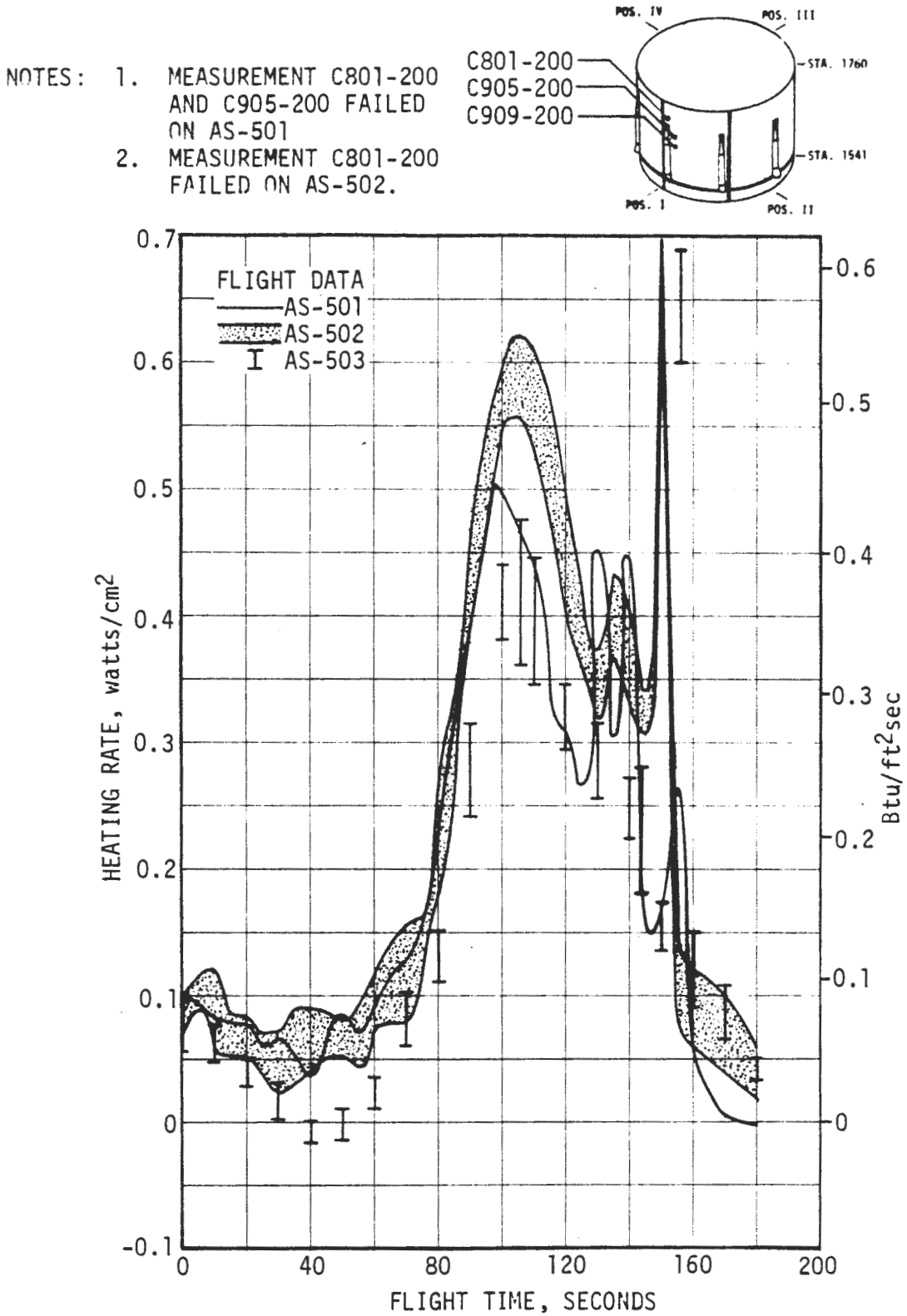

FIGURE 6-30. S-IC/S-II INTERSTAGE CALORIMETER INDICATED HEATING RATES - CLEAN BODY AREA

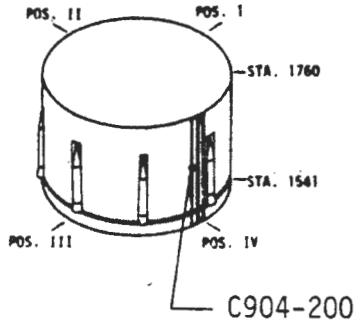

NOT INSTRUMENTED ON AS-503

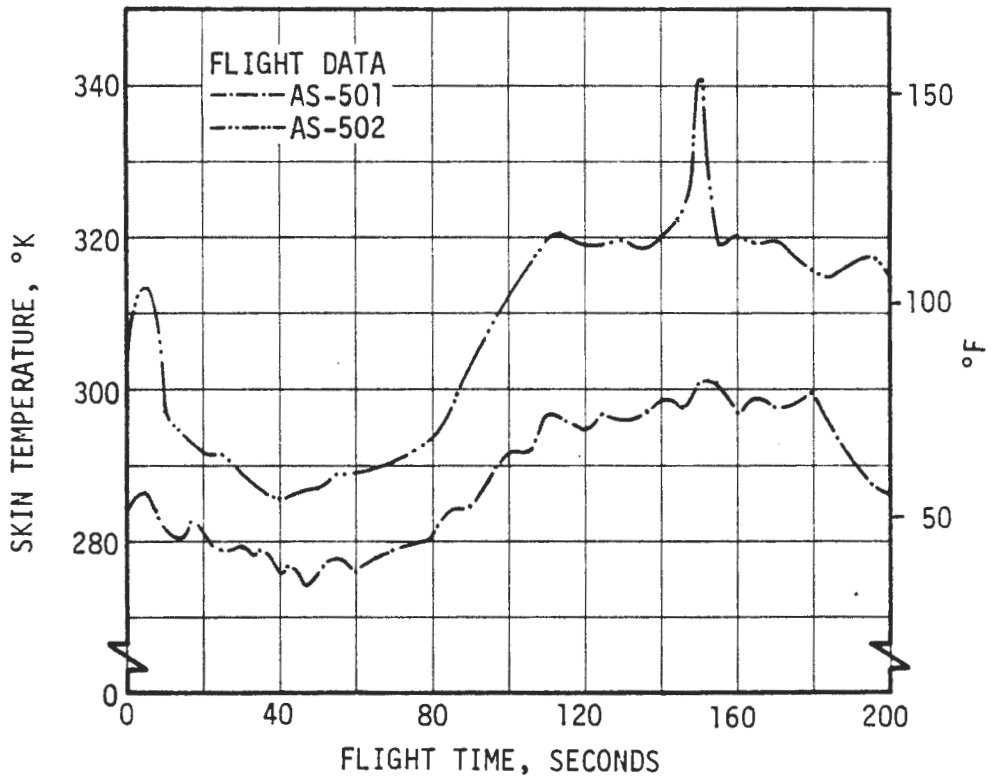

FIGURE 6-31. S-IC/S-II INTERSTAGE TEMPERATURES - CLEAN BODY AREA

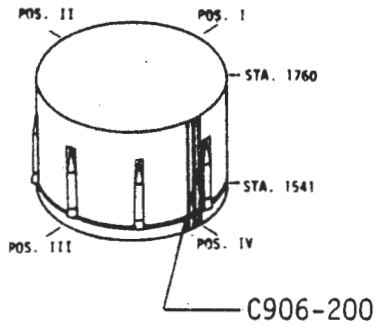

NOT INSTRUMENTED ON AS-503

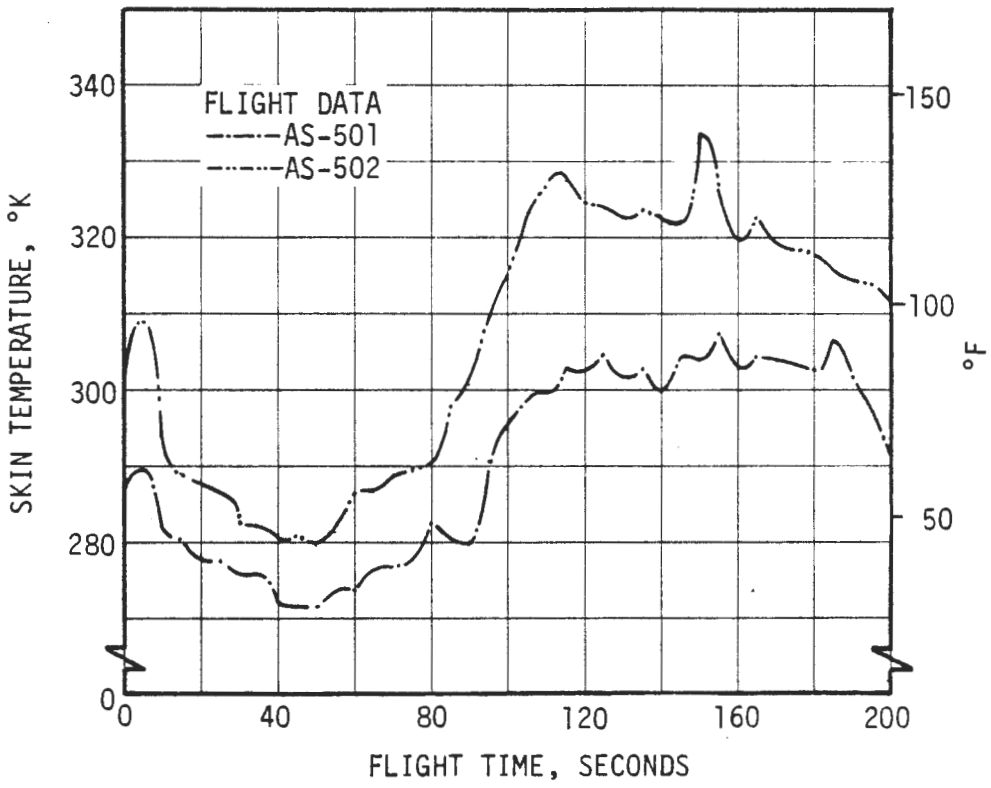

FIGURE 6-32. S-IC/S-II INTERSTAGE TEMPERATURES - PROTUBERANCE AFFECTED AREA

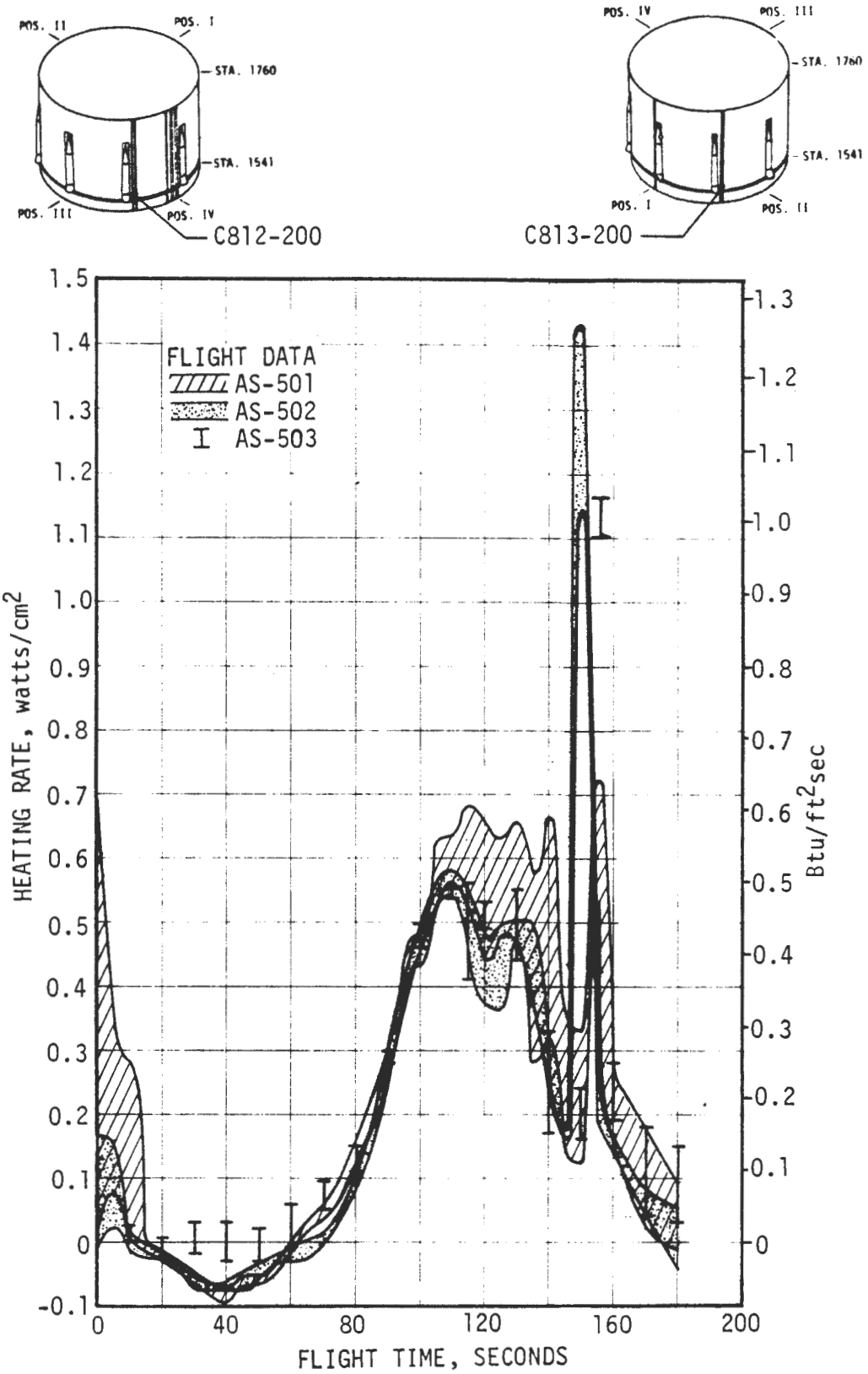

FIGURE 6-33. S-IC/S-II INTERSTAGE STAGING ORDINANCE FAIRING HEATING RATES

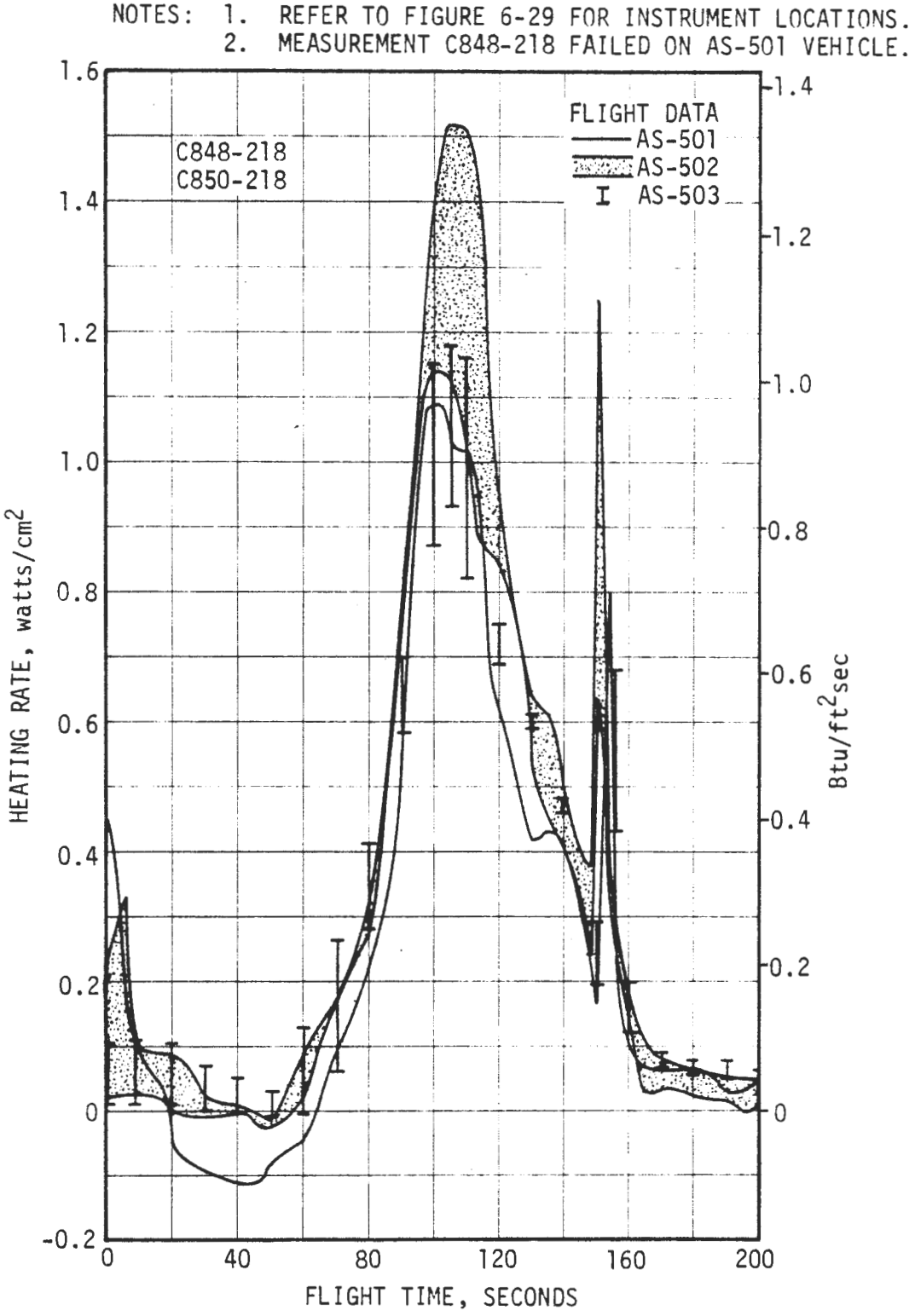

FIGURE 6-34. S-II LH_2 FEEDLINE FORWARD FAIRING HEATING RATES

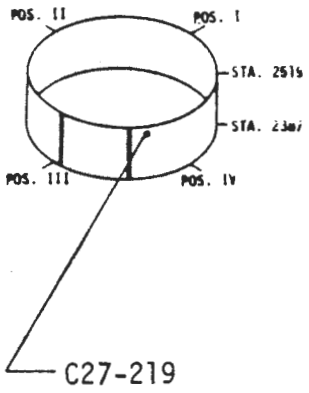

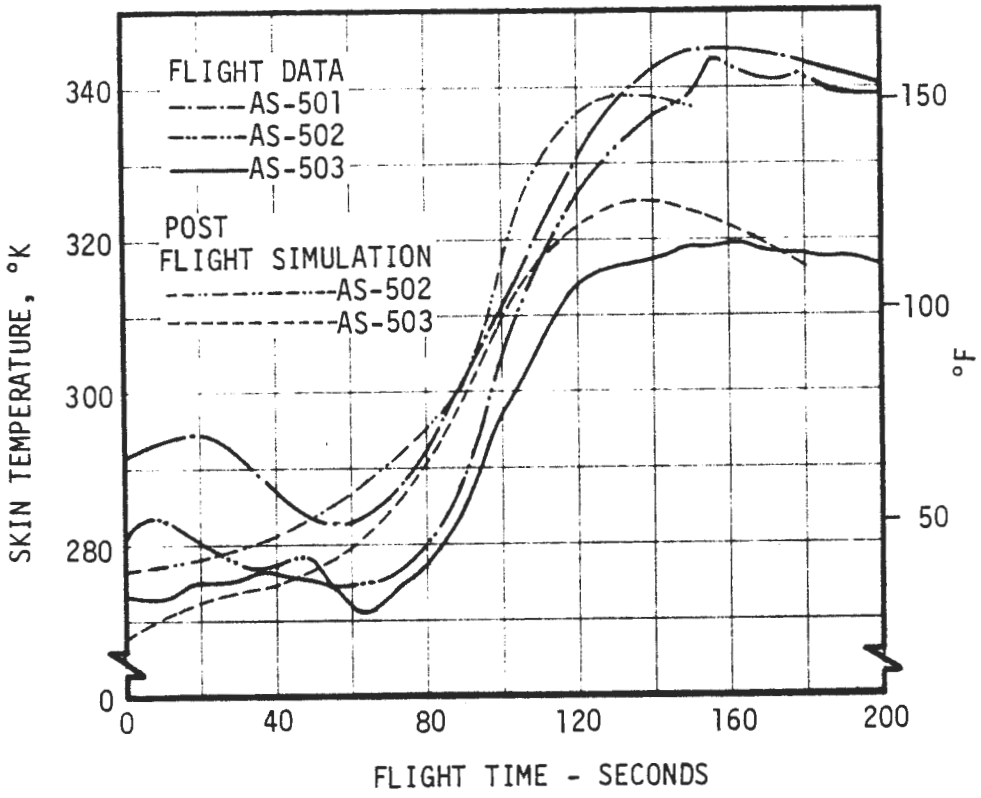

FIGURE 6-35. COMPARISONS OF S-II FORWARD SKIRT SKIN TEMPERATURES WITH ANALYTICAL PREDICTIONS

TABLE 6-III. S-IVB STAGE AERODYNAMIC HEATING INSTRUMENTATION

(CONTINUED ON NEXT PAGE)

MEASUREMENT NUMBER	INSTRUMENT TYPE*	RANGE °K	INSTALLATION METHOD**	LOCATION
C047-427	Skin Temperature	172-491	1	Station 2756, External Vehicle Skin, 30° from Position III toward Position IV
C048-427	Skin Temperature	172-491	1	Station 2756, External Vehicle Skin, 88° from Position I toward Position II
C082-426	Skin Temperature	172-491	1	Station 3217, External Vehicle Skin, 89° from Position III toward Position IV
C083-426	Skin Temperature	172-491	1	Station 3217, External Vehicle Skin, 31° from Position III toward Position IV
C091-427	Skin Temperature	256-547	2	Station 2810, Internal Fuel Line Fairing Skin, 47° from Position IV toward Position I.
C114-427	Skin Temperature	172-491	1	Station 2796, External Vehicle Skin, 60° from Position IV toward Position I
C115-427	Skin Temperature	227-367	1	Station 2796, External Hat Section Skin, 61° from Position IV toward Position I
C119-419	Skin Temperature	256-547	1	Station 2738, External Vehicle Skin, 61° from Position IV toward Position I

* Resistance thermometer

** 1 Bonded to the external surface of the vehicle skin

** 2 Bonded to the internal surface of the vehicle skin

TABLE 6-III. S-IVB STAGE AERODYNAMIC HEATING INSTRUMENTATION (CONCLUDED)

MEASUREMENT NUMBER	INSTRUMENT TYPE*	RANGE °K	INSTALLATION METHOD**	LOCATION
C120-419	Skin Temperature	256-547	1	Station 2701, External Vehicle Skin, 61° from Position IV toward Position I
C121-419	Skin Temperature	256-547	1	Station 2701, External Vehicle Skin, 63° from Position IV toward Position I
C123-419	Skin Temperature	256-547	1	Station 2626, External Vehicle Skin, 61° from Position IV toward Position I
C305-419	Skin Temperature	256-547	1	Station 2626, External Vehicle Skin, 63° from Position V toward Position I
C306-419	Skin Temperature	256-547	1	Station 2738, External Vehicle Skin, 63° from Position IV toward Position I

* Resistance thermometer

** 1 Bonded to the external surface of the vehicle skin

** 2 Bonded to the external surface of the vehicle skin

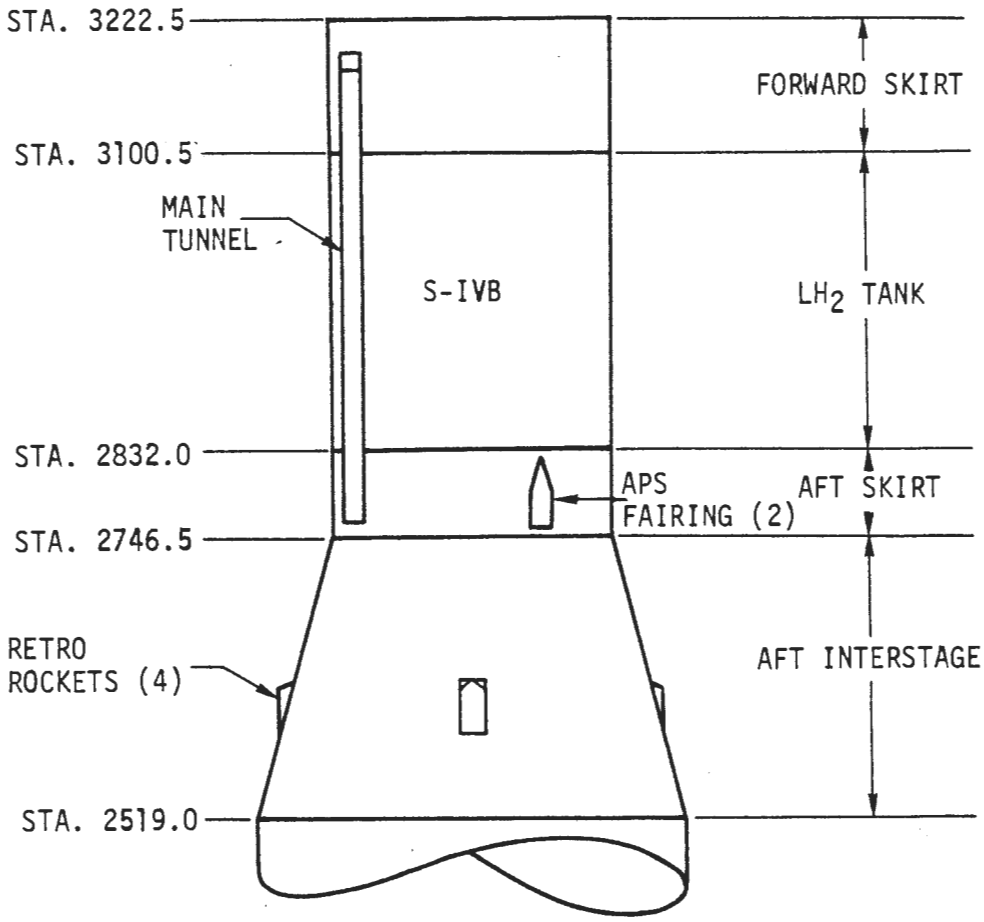

FIGURE 6-36. S-IVB STAGE LAYOUT

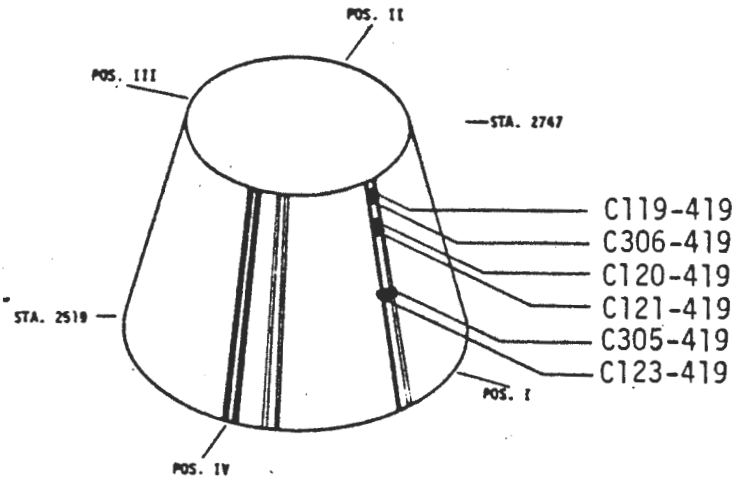

NOTES: 1. MEASUREMENT C121-427 FAILED ON AS-501
2. NOT INSTRUMENTED ON AS-503

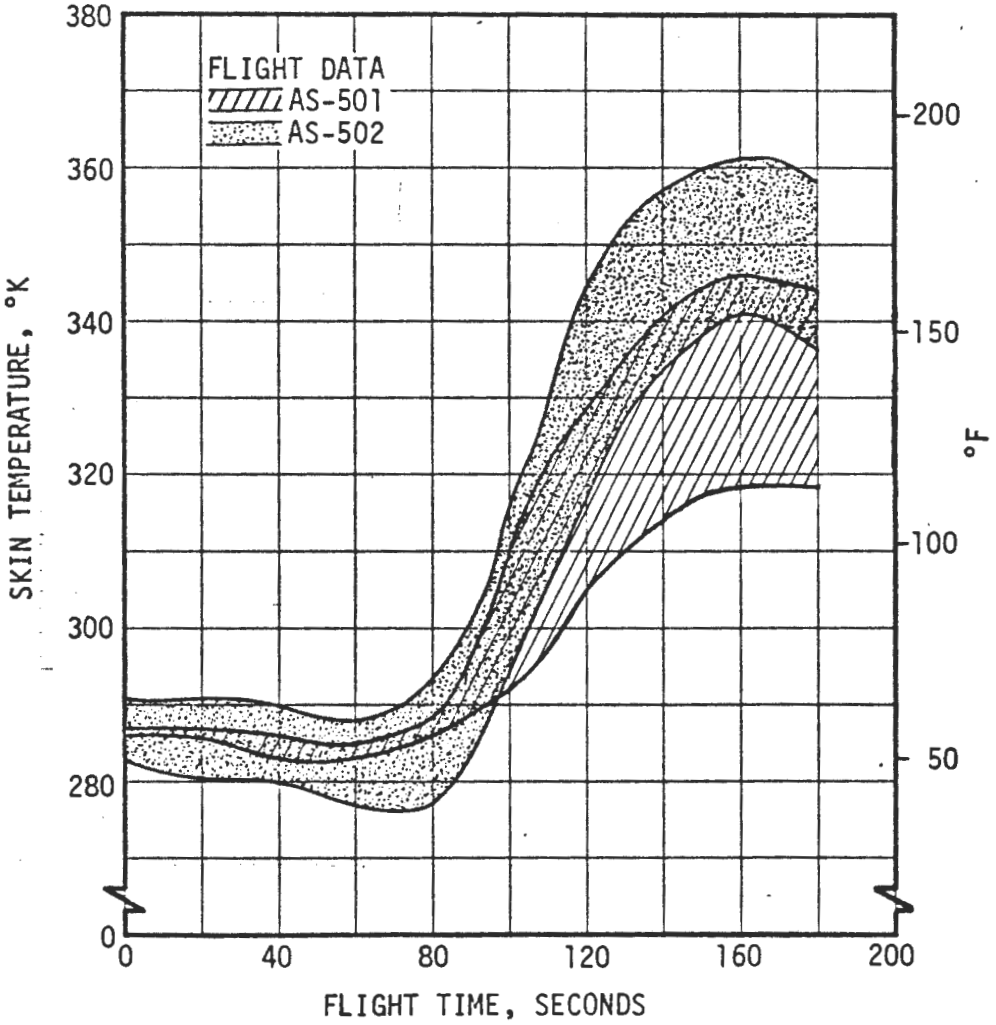

FIGURE 6-37. S-IVB AFT INTERSTAGE SKIN TEMPERATURE - INSULATED AREA

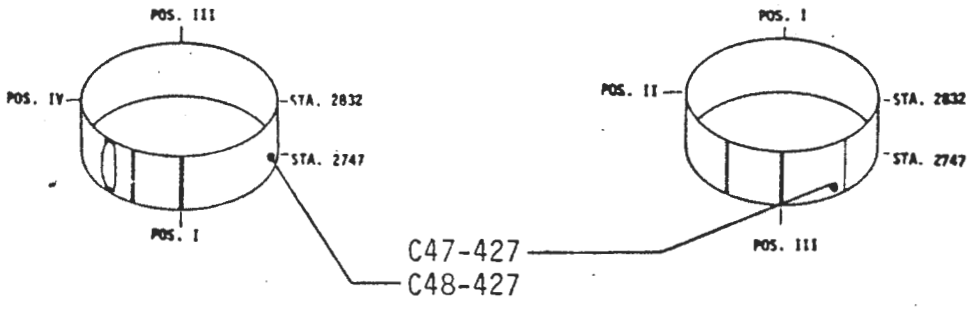

NOT INSTRUMENTED ON AS-503

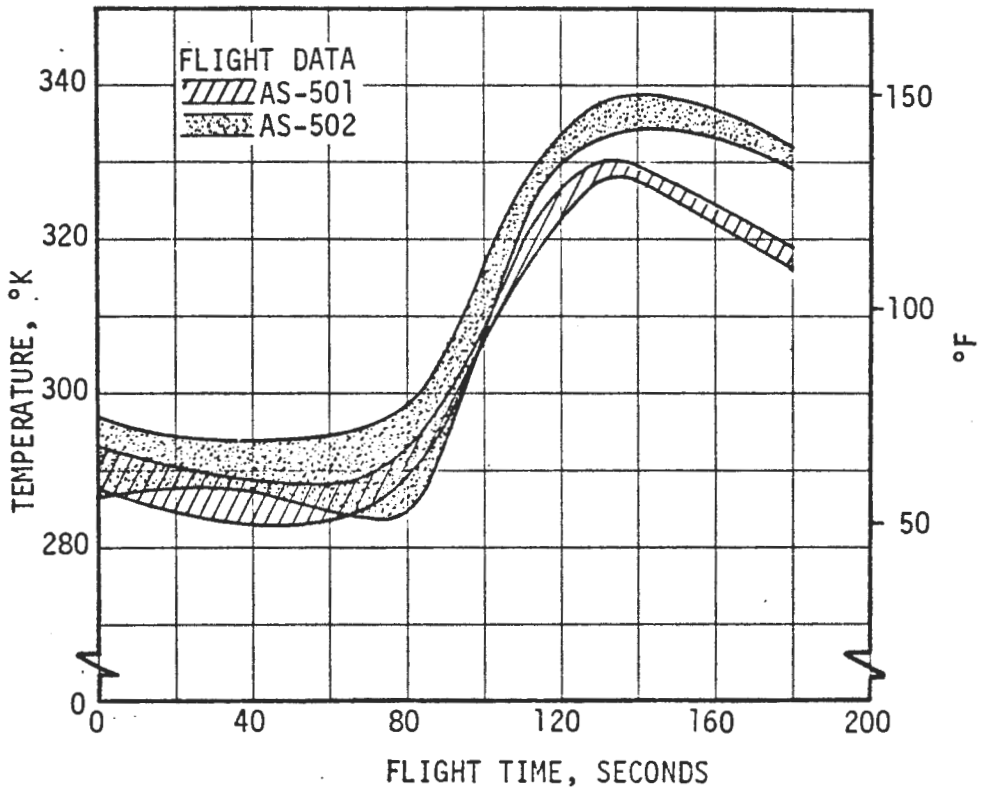

FIGURE 6-38. S-IVB AFT SKIRT SKIN TEMPERATURE - CLEAN BODY AREA

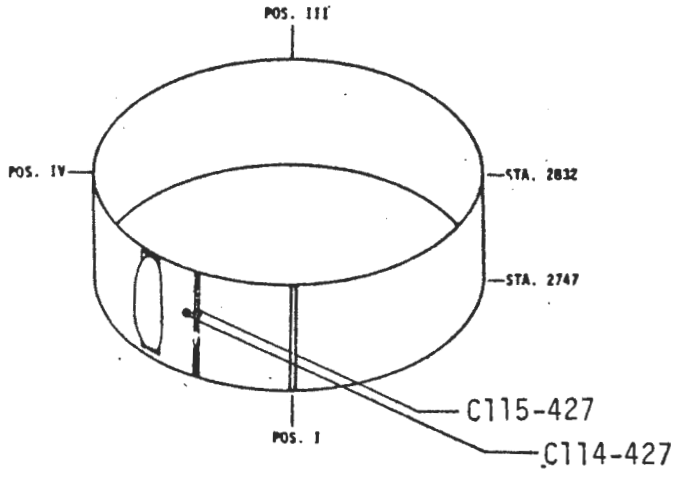

NOT INSTRUMENTED ON AS-503

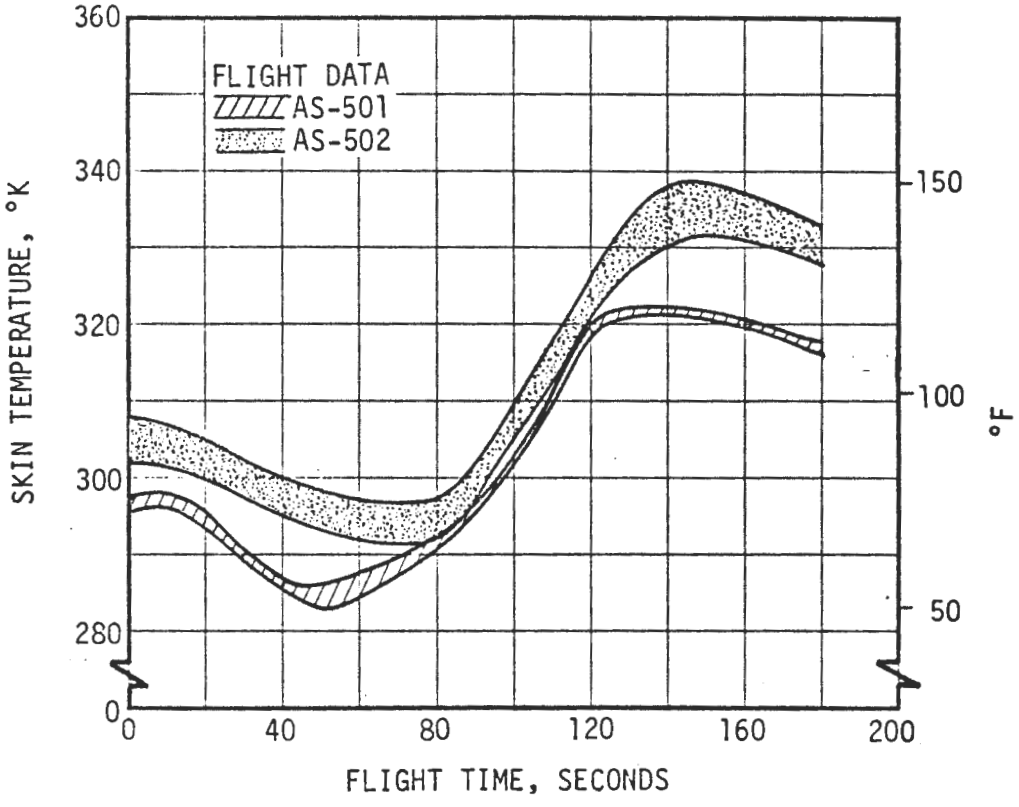

FIGURE 6-39. S-IVB AFT SKIRT SKIN TEMPERATURE IN THE WAKE OF THE LH_2 FEEDLINE FAIRING - INSULATED AREA

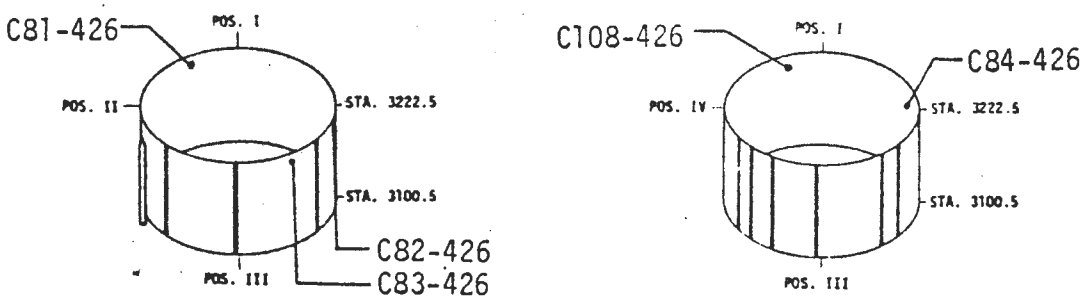

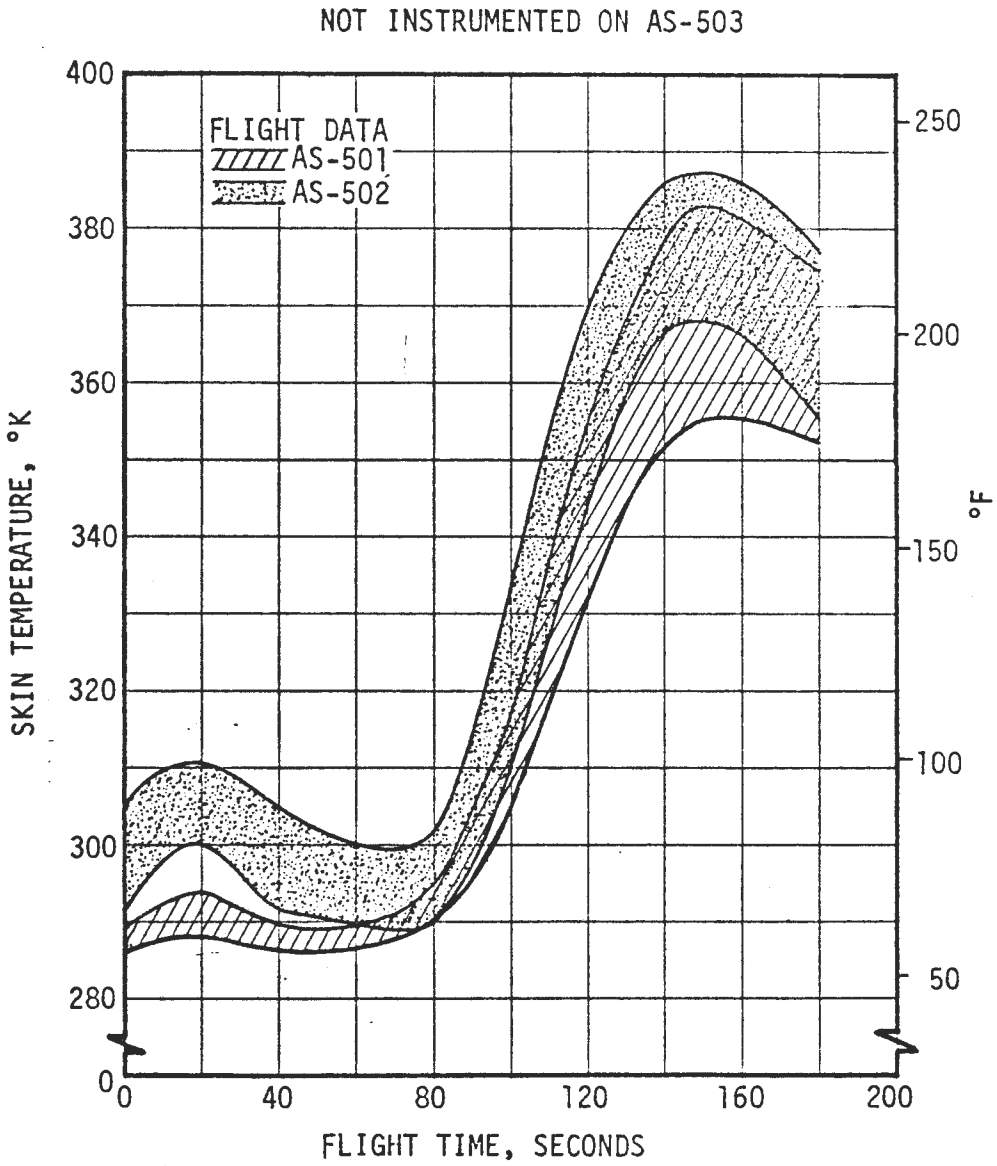

FIGURE 6-40. S-IVB FORWARD SKIRT SKIN TEMPERATURE - CLEAN BODY AREA

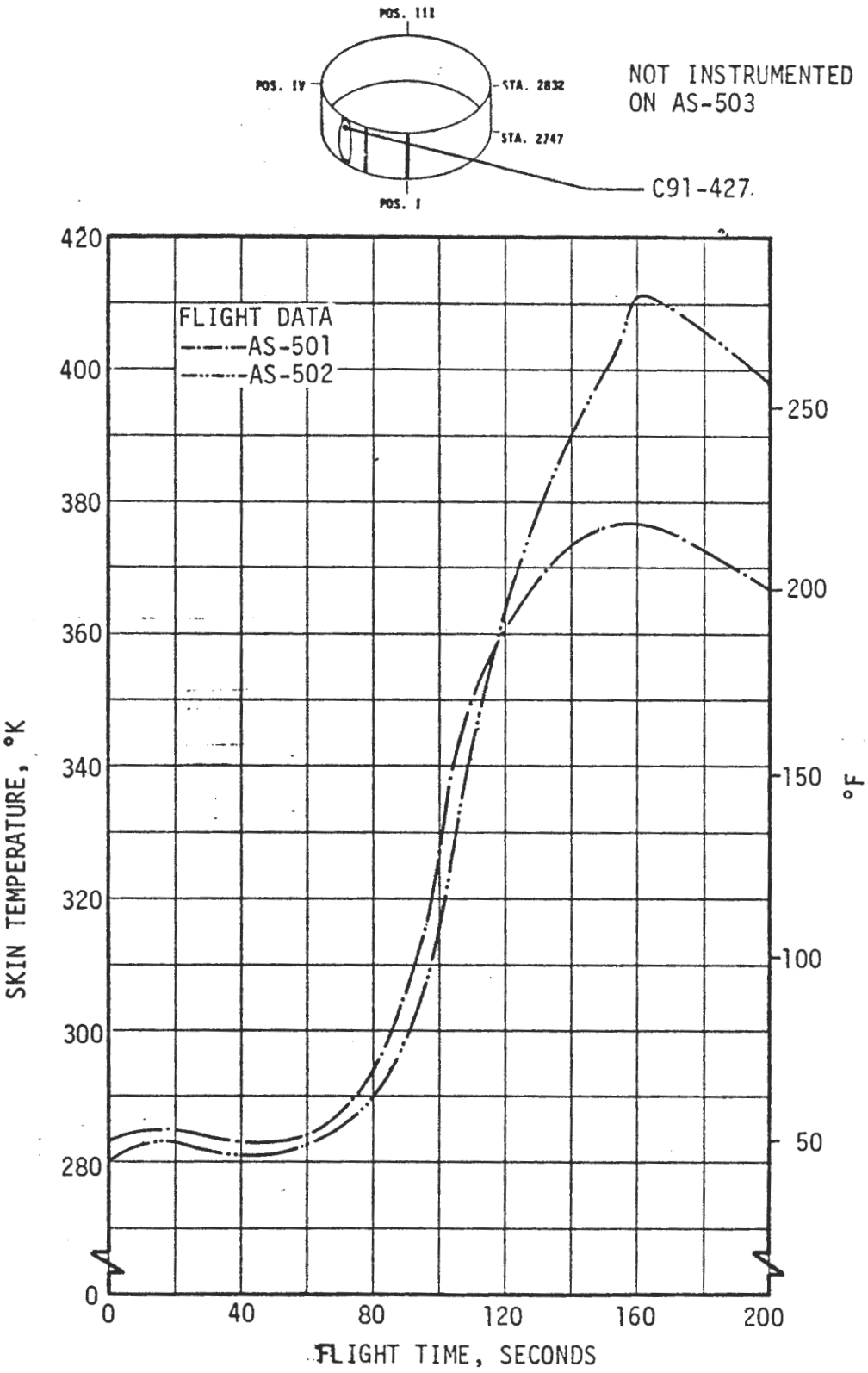

FIGURE 6-41. S-IVB LH_2 FEEDLINE FORWARD FAIRING SKIN TEMPERATURE - INSULATED AREA

TABLE 6-IV. INSTRUMENT UNIT AERODYNAMIC HEATING INSTRUMENTATION

MEASUREMENT NUMBER	INSTRUMENT TYPE*	RANGE °K	INSTALLATION METHOD**	LOCATION
C037-601	Skin Temperature	223-398	1	Station 3246.9, Internal Vehicle Skin, 13° from Position I toward Position II
C038-601	Skin Temperature	223-398	1	Station 3234.3, Internal Vehicle Skin, 74° from Position IV toward Position I
C039-602	Skin Temperature	223-398	1	Station 3246.6, Internal Vehicle Skin, 15° from Position II toward Position III
C040-602	Skin Temperature	223-398	1	Station 3234.3, Internal Vehicle Skin, 1° from Position II toward Position III
C041-602	Skin Temperature	223-398	1	Station 3246.6, Internal Vehicle Skin, 14° from Position III toward Position IV
C042-602	Skin Temperature	223-398	1	Station 3234.6, Internal Vehicle Skin, 75° from Position II toward Position III
C043-603	Skin Temperature	223-398	1	Station 3246.6, Internal Vehicle Skin, Position IV
C044-603	Skin Temperature	223-398	1	Station 3234.6, Internal Vehicle Skin, 74° from Position III toward Position IV

* Resistance thermometer

** 1 Bonded to internal surface of honeycomb skin

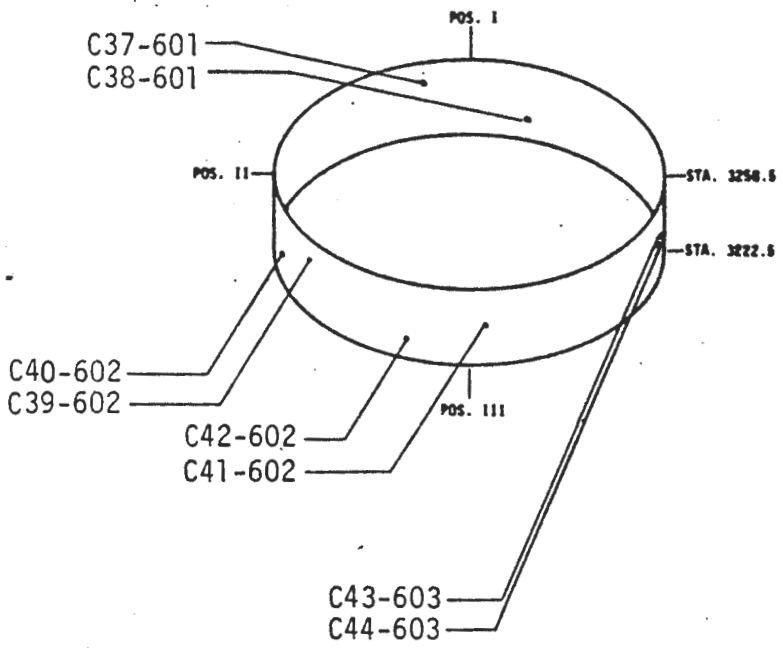

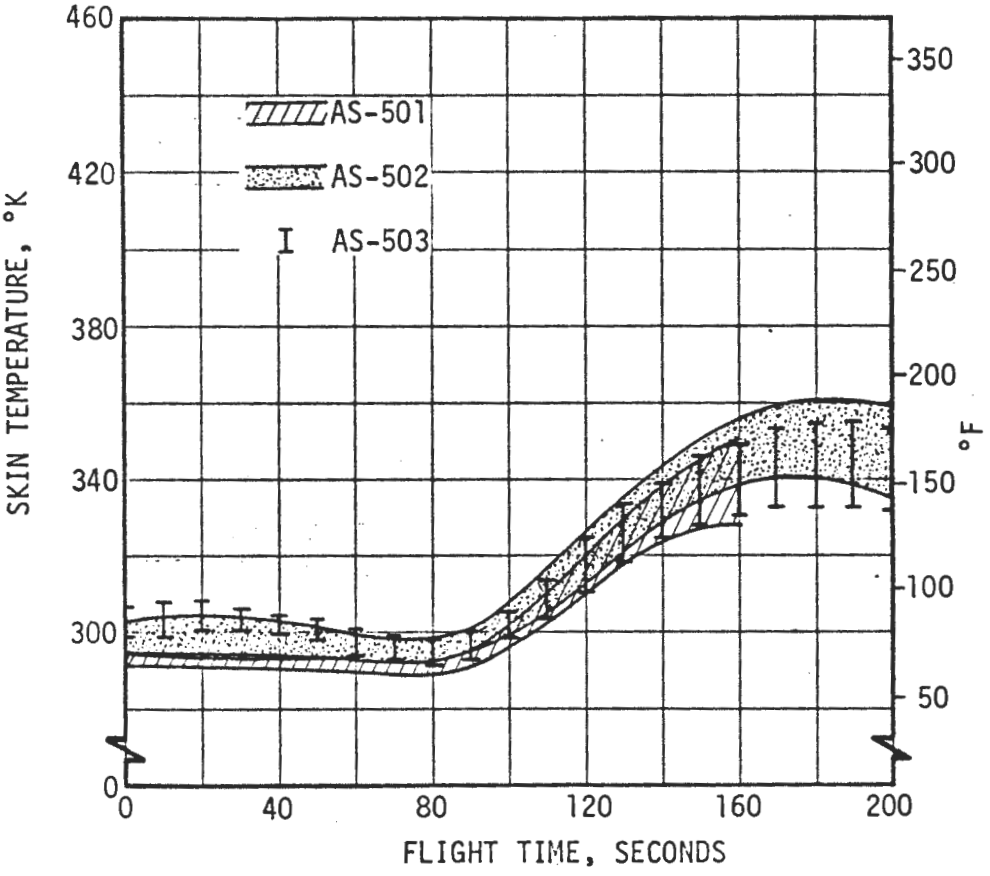

FIGURE 6-42. INSTRUMENT UNIT INTERNAL SKIN TEMPERATURES

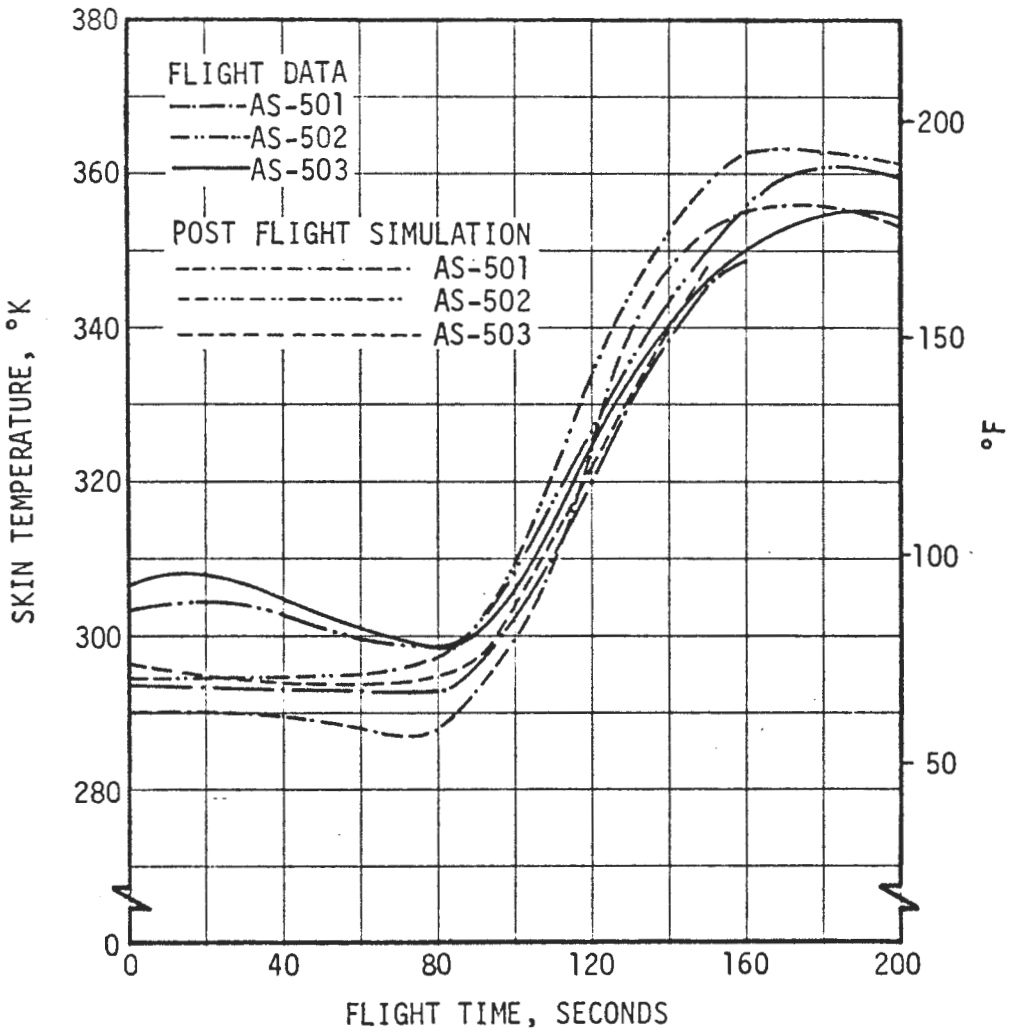

FIGURE 6-43. COMPARISON OF INSTRUMENT UNIT MAXIMUM INTERNAL SKIN TEMPERATURE WITH POST FLIGHT SIMULATIONS

(THIS PAGE INTENTIONALLY LEFT BLANK)

SECTION 7

CONCLUSIONS

AERODYNAMICS

1. The vehicle measured aerodynamic flight environment was below design levels. The repeatability of the data from AS-501, AS-502, and AS-503 was generally good.

2. S-IC base pressures showed good agreement in trend between flights. The differences in magnitudes are attributed to the base flow deflectors on AS-501 and the two degree outboard engine cant on AS-503.

3. The vehicle compartment pressures were below design values.

VEHICLE EXTERNAL ACOUSTICS

1. The vehicle external liftoff and inflight acoustic environments demonstrated good agreement between flights and were below design environments. Maximum measured values during liftoff and inflight were 161.1 db and 160.0 db, respectively.

BASE REGION ENVIRONMENTS

1. The S-IC stage base region total heating rates were, in general, below design values. Maximum heating rates of 25 watts/cm^2 and 37 watts/cm^2 were measured on the heat shield and engines, respectively.

2. The AS-501 base region flow deflectors caused exhaust flow reversal to occur at a higher altitude, and hence, a less severe environment was experienced on AS-501 than on AS-502 or AS-503.

3. The AS-503 F-1 control engines two degree outboard cant did not significantly affect the base region environment.

4. Radiation heating was the principal mode of heat transfer in the base region and demonstrated a middle altitude "hump" which is believed to be caused by exhaust gases recirculated into the base region after exhaust flow reversal.

5. A momentary increase in the base region thermal environment occurred during inboard engine cutoff and is believed to be caused by an increase in the exhaust gas emissivity due to the inboard engine residual exhaust products and carbon particles.

6. The S-II stage base region thermal environment was generally below design values and in good agreement with predicted values. Maximum heating rates of 4 watts/cm^2 was experienced in the base region.

STAGE SEPARATION ENVIRONMENTS

1. S-IC/S-II stage environmental measurements located on the S-IC forward skirt and LOX dome monitored a maximum gas temperature of approximately 1300°K and a maximum tape recorded pressure of 1.25 N/cm^2.

2. S-IVB stage environmental measurements located in the S-IVB base region indicated that the S-II/S-IVB separation environment was well below design values.

AERODYNAMIC HEATING ENVIRONMENT

1. The aerodynamic heating environments measured on AS-501 through AS-503 vehicles were below the design environments. Measured heating in areas of protuberance influence were generally below predicted levels. The lack of properly placed instrumentation and the inconsistencies in the measurements made it difficult to evaluate protuberance influences.

2. Boundary layer flow separation caused exhaust gases to recirculate forward along the side of the vehicle past the S-IC/S-II interstage. Small increases in heating above the normal aerodynamic heating were experienced with flow separation. Early center engine cutoff on AS-503 reduced the area affected by flow separation.